



UNIVERSIDAD DE LA RIOJA

TESIS DOCTORAL

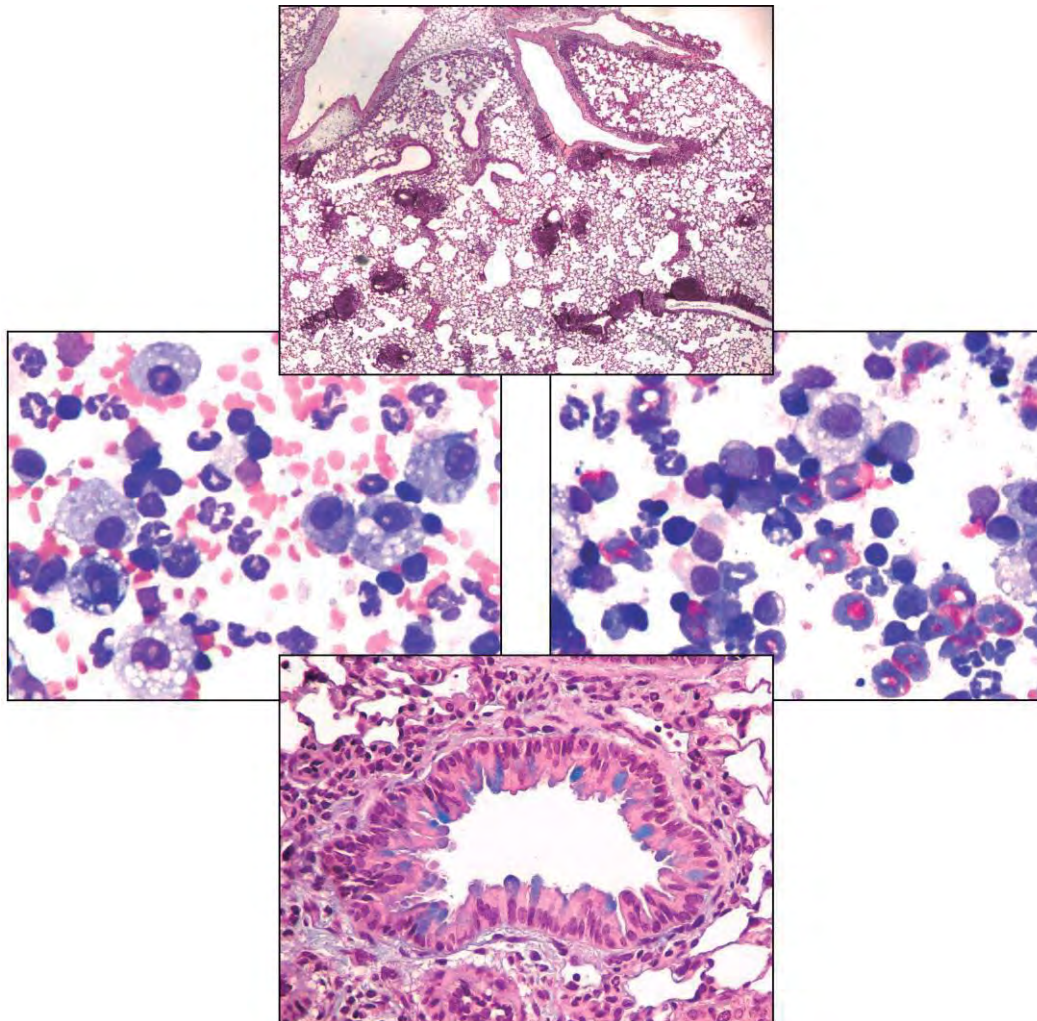
Título
Implication of IGF1R in murine acute lung inflammation and house dust mite-induced allergy
Autor/es
Sergio Piñeiro Hermida
Director/es
José Manuel García Pichel
Facultad
Facultad de Ciencia y Tecnología
Titulación
Departamento
Curso Académico



Implication of IGF1R in murine acute lung inflammation and house dust mite-induced allergy, tesis doctoral de Sergio Piñeiro Hermida, dirigida por José Manuel García Pichel (publicada por la Universidad de La Rioja), se difunde bajo una Licencia Creative Commons Reconocimiento-NoComercial-SinObraDerivada 3.0 Unported. Permisos que vayan más allá de lo cubierto por esta licencia pueden solicitarse a los titulares del copyright.

- © El autor
- © Universidad de La Rioja, Servicio de Publicaciones, 2018
publicaciones.unirioja.es
E-mail: publicaciones@unirioja.es

IMPLICATION OF IGF1R IN MURINE ACUTE LUNG INFLAMMATION AND HOUSE DUST MITE-INDUCED ALLERGY



Sergio Piñeiro Hermida



UNIVERSIDAD
DE LA RIOJA



Universidad
Zaragoza

1542

Center for Biomedical Research of La Rioja (CIBIR)
Lung Cancer and Respiratory Diseases Unit, Logroño, Spain



IMPLICATION OF IGF1R IN MURINE ACUTE LUNG INFLAMMATION AND HOUSE DUST MITE-INDUCED ALLERGY

Sergio Piñeiro Hermida



Logroño 2017

José Manuel García Pichel, Ph.D. in Biological Sciences and head of the Lung Cancer and Respiratory Diseases Unit from the Center of Biomedical Research of La Rioja,

Certify that:

The present thesis entitled "*Implication of IGF1R in murine acute lung inflammation and house dust mite-induced allergy*" undertaken by **Sergio Piñeiro Hermida**, B.Sc. in Biology and M.Sc. in Forensic Sciences, meets the conditions of originality required to qualify for the international doctorate mention from the Universities of La Rioja and Zaragoza.

Logroño, 11 December 2017.

José M. García Pichel, Ph.D.

Head of the Lung Cancer and Respiratory Diseases Unit

Center for Biomedical Research of La Rioja (CIBIR)

26006 Logroño, Spain

Tel.: + (34) 941278855

Email: jgpichel@riojasalud.es

Á miña familia e en especial ó meu pai,

por ensinarme o que é a constancia,

a humildade e a xenorosidade

AGRADECIMIENTOS

Quien lo iba a decir, cuatro años después aquí estoy escribiendo los agradecimientos de mi tesis, algo que ni me imaginaba que ocurriría. Después de terminar mi máster y tras pasar por varios laboratorios sin un proyecto definido ni financiación, estuve a punto de abandonar la investigación. Debido a esto, todas mis esperanzas por encontrar financiación para desarrollar mi carrera investigadora estaban por los suelos. Anteriormente, había estado matriculado en un programa de doctorado en la Universidad de Santiago de Compostela, cuyo proyecto se estaba desarrollando en el “Grupo de Medicina Genómica” del Hospital Clínico. Debido a que estaba en una lista de correos del hospital, todavía me seguían llegando emails de charlas, ofertas de trabajo, etc. y en Octubre de 2013 recibí un email en el que se anunciaba un contrato para la realización de la tesis en la “Unidad de Cáncer de Pulmón y Enfermedades Respiratorias del CIBIR”. Después del proceso de selección, en el que se tuvo en cuenta tanto la experiencia de cada candidato como la entrevista personal, me quedé a las puertas de conseguir el contrato. Pocos días después de la resolución del proceso de selección, recibí una llamada (concretamente el viernes 6 de Diciembre de 2013) en la que se me comunica que el contrato era para mí porque la persona a la que se le había concedido había renunciado. Ese fue uno de los días más felices de mi vida!

En primer lugar me gustaría agradecer a la Consejería de Industria, Innovación y Empleo del Gobierno de la Rioja la aportación económica necesaria para mi incorporación a la Unidad de Cáncer de Pulmón y Enfermedades Respiratorias del CIBIR. También me gustaría dar las gracias a la Fundación Rioja Salud por las maravillosas instalaciones del CIBIR, donde se ha desarrollado la mayor parte de mi tesis. En particular me gustaría dar las gracias a las siguientes personas:

A **José Pichel**, mi director de tesis, por darme la oportunidad de incorporarme a su grupo de investigación, por sus consejos y apoyo durante estos 4 años y por creer en mi “intuición investigadora” cada vez que proponía hacer algo nuevo.

A **Raquel** por su maravilloso trabajo con las histologías, el cual se ve reflejado en las últimas publicaciones del grupo y que son un valor añadido a cualquier trabajo debido a su gran profesionalidad.

A **Icía** por hacerme sentir como en casa cuando llegué al laboratorio y por enseñarme la dinámica de trabajo del grupo, debido a que todo era nuevo para mí, ya que venía de otro ámbito investigador diferente. Muchas gracias por tu apoyo a nivel investigador durante estos 4 años, sobre todo en los momentos más críticos como son las revisiones de los “papers” en las que se pedían experimentos adicionales y también por cuidar de mis ratoncitos.

A **Elvira**, por ser una excepcional compañera de laboratorio y amiga, siempre con una sonrisa en la cara y optimista ante cualquier adversidad, a pesar de estar en una situación similar a la que yo viví antes de llegar al CIBIR. También me gustaría agradecer su apoyo y tiempo invertido en algunos de los experimentos presentados en esta tesis, así como por la atención mostrada siempre que le explicaba alguna de las técnicas en las que me había formado. Espero y deseo que tengas mucha suerte con tu tesis y poder verte en la presentación de la tuya, en la que seguro mostrarás resultados prometedores.

Al resto del personal de la segunda planta del CIBIR: **Alfredo, Álvaro, Ana, Angelina, Bea, Bego, Eva, Iñaki, Josune, Juan, Judith, Laura, Luís, María, Rafa, Rodri y Sonia**. Por el buen ambiente de trabajo y las risas y tertulias de la hora del café que hacían que me olvidase de los problemas cotidianos.

A **Angelina, Chus y Lidia**, por compartir esta experiencia tan bonita del doctorado y nuestras luchas con el "RAPI". Os deseo un todo lo mejor para el futuro!

A **Mikael Adner**, mi supervisor durante la estancia predoctoral realizada en el "Instituto Karolinska" de Estocolmo, por su apoyo y consejos como experto en asma para la realización de proyecto colaborativo entre ambas instituciones fruto del cual ha salido una publicación muy bonita.

A **Josh Gregory**, por introducirme en el campo de la alergia durante la estancia predoctoral realizada en el "Instituto Karolinska" de Estocolmo y por su apoyo a nivel técnico. También me gustaría agradecerle que me haya hecho partícipe de la cultura de su país "EE.UU.", al invitarme a vivir lo que es la "cena de acción de gracias", un acontecimiento muy importante para él.

Por ultimo me gustaría agradecer a mi familia (papa, mama, abuelas y a mi hermano, Rodri), por todo su apoyo a pesar de estar lejos de ellos durante todo este tiempo. A ellos les debo todo lo que soy, los valores que me han enseñado y que me han hecho ser como soy, entre los cuales se encuentran la constancia, la humildad y la generosidad. Durante estos 4 años he tenido momentos muy buenos debido a los buenos resultados obtenidos y a las recientes publicaciones del grupo. Por otro lado, también ha habido momentos muy duros tras la pérdida de mi mejor amigo, mi padre, durante mi segundo año aquí en el CIBIR. Gracias a la ayuda de mis compañeros y familia, he tirado hacia adelante como lo habría hecho él, ya que una de sus grandes lecciones que nunca olvidaré es que nunca hay que rendirse, ya que la constancia es lo que hace conseguir grandes cosas en la vida. Siempre recordaré sus últimas palabras hacia mí, en las que literalmente me dijo "eres auténtico", palabras que para mí significan mucho porque él creía mucho en mí y en que podía conseguir grandes cosas. Por todo ello, le doy las gracias por lo que me ha enseñado y por ser el mejor padre posible. Me gustaría terminar estos agradecimientos diciendo lo mucho que admiro a mi madre, hermano y abuelas por sacar esa fuerza para tirar hacia adelante en los momentos más duros.

LIST OF ABBREVIATIONS

4-OHT	4-hydroxytamoxifen
α-SMA	Alpha-smooth muscle actin
<i>Acta2</i>	Actin, alpha 2, smooth muscle, aorta (gene)
<i>Adgre1</i>	Adhesion G protein-coupled receptor E1 (gene)
AEC1	Alveolar epithelial type 1 cells
AEC2	Alveolar epithelial type 2 cells
AHR	Airway hyperresponsiveness
AKT	AKT serine/threonine kinase 1
ALI	Acute lung inflammation
<i>Aqp5</i>	Aquaporin 5 (gene)
AQP5	Aquaporin 5
ARDS	Acute respiratory distress syndrome
BADJ	Bronchioalveolar duct junction
BAL	Bronchoalveolar lavage
BALF	Bronchoalveolar lavage fluid
BASCs	Bronchioalveolar stem cells
BLM	Bleomycin
BM	Bone marrow
bp	Base pairs
BSA	Bovine serum albumin
BSCs	Basal stem cells
BW	Body weight
<i>Ccl2</i>	Chemokine (C-C motif) ligand 2 (gene)
<i>Ccl5</i>	Chemokine (C-C motif) ligand 5 (gene)
<i>Ccl11</i>	Chemokine (C-C motif) ligand 11 (gene)
CCL11	C-C motif chemokine ligand 11 (eotaxin-1)
<i>Cd209a</i>	CD209a antigen (gene)
CD3	CD3 molecule
<i>Cd4</i>	CD4 antigen (gene)
CD4	CD4 molecule

cDNA	Complementary DNA
Cgrp	Calcitonin/calcitonin-related polypeptide, alpha (Calca)
Col1a1	Collagen, type I, alpha 1 (gene)
COPD	Chronic obstructive pulmonary disease
COX2	Cytochrome c oxidase subunit II
Cre	Cre recombinase
CREBBP	CREB binding protein
Csf1	Colony stimulating factor 1 (macrophage) (gene)
Cxcl1	Chemokine (C-X-C motif) ligand 1 (gene)
Derp1	Derp1 allergen
DNA	Deoxyribonucleic acid
ECL	Enhanced chemiluminescence
EDTA	Ethylenediaminetetraacetic acid
ELISA	Enzyme-linked immunosorbent assay
EP300	E1A binding protein p300
F4/80	Adhesion G protein-coupled receptor (ADGRE1)
FDR	False discovery rate
Foxm1	Forkhead box M1 (gene)
FOXM1	Forkhead box M1
Foxo1	Forkhead box O1 (gene)
FPKM	Fragments per kilobase of exon per million fragments mapped
GFs	Growth factors
GH	Growth hormone
GHRH	Growth hormone releasing hormone
GLUTUB	Glu-tubulin
GMCSF	Colony stimulating factor 2 (CSF2)
Gpx8	Glutathione peroxidase 8 (gene)
HDM	House dust mite
H&E	Hematoxylin and eosin
Hif1a	Hypoxia inducible factor 1, alpha subunit (gene)
HIF1A	Hypoxia inducible factor 1, alpha subunit
HPF	High-power field

HSP90	Heat shock protein 90
Ki67	Antigen identified by monoclonal antibody Ki67
IgE	Immunoglobulin E
IGFs	Insulin-like Growth Factors
IGFBPs	IGF-binding proteins
<i>Igfbp3</i>	Insulin-like growth factor binding protein 3 (gene)
<i>Igfbp5</i>	Insulin-like growth factor binding protein 5 (gene)
<i>Igf1</i>	Insulin-like growth factor 1 (gene)
IGF1	Insulin-like growth factor 1
<i>Igf1r</i>	Insulin-like growth factor 1 receptor (gene)
IGF1R	Insulin-like growth factor 1 receptor
IGF2	Insulin-like growth factor 1
IGF2R	Insulin-like growth factor 2 receptor
<i>Il1b</i>	Interleukin 1 beta (gene)
IL1B	Interleukin 1 beta
IL2	Interleukin 2
<i>Il4</i>	Interleukin 4 (gene)
IL4	Interleukin 4
<i>Il5</i>	Interleukin 5 (gene)
IL5	Interleukin 5
<i>Il6</i>	Interleukin 6 (gene)
IL6	Interleukin 6
<i>Il10</i>	Interleukin 10 (gene)
IL10	Interleukin 10
<i>Il13</i>	Interleukin 13 (gene)
IL13	Interleukin 13
<i>Il25</i>	Interleukin 25 (gene)
IL25	Interleukin 25
<i>Il33</i>	Interleukin 33 (gene)
IL33	Interleukin 33
<i>Insr</i>	Insulin receptor (gene)
INSR	Insulin receptor

loxP	DNA sequence for Cre-mediated recombination
LTs	Leukotrienes
<i>Ly6g</i>	Lymphocyte antigen 6 complex, locus G (gene)
<i>Marco</i>	Macrophage receptor with collagenous structure (gene)
MAPKs	Mitogen-activated protein kinase
MCh	Methacholine
mRNA	Messenger ribonucleic acid
mTOR	Mechanistic target of rapamycin
<i>Muc5ac</i>	Mucin 5, subtypes A and C (gene)
MUC5AC	Mucin 5AC, oligomeric mucus/gel-forming
NE	Neuroendocrine
<i>Nkx2-1</i>	NK2 homeobox 1
NLRP3	NLR family pyrin domain containing 3 (NLRP3 inflammasome)
PAS	Periodic acid-Schiff
PBS	Phosphate buffered saline
PCR	Polymerase chain reaction
<i>Pdpr</i>	Podoplanin
<i>Pecam</i>	Platelet/endothelial cell adhesion molecule 1
PI3K	Phosphoinositide-3 kinase
PMSF	Phenylmethylsulfonyl fluoride
<i>Pre-Sftpc</i>	Surfactant protein C precursor
<i>Prex1</i>	Phosphatidylinositol-3,4,5-trisphosphate dependent Rac exchange factor 1 (gene)
PREX1	Phosphatidylinositol-3,4,5-trisphosphate dependent Rac exchange factor 1
<i>Ptgs2</i>	Prostaglandin-endoperoxide synthase 2 (gene)
qRT-PCR	Quantitative real-time PCR
RFU	Relative fluorescence units
<i>Rn18s</i>	18S ribosomal RNA (gene)
RNS	Reactive nitrogen species
ROS	Reactive oxygen species
SAL	Saline
<i>Scgb1a1</i>	Secretoglobin, family 1A, member 1 (uteroglobin) (gene)
SCGB1A1	Secretoglobin, family 1A, member 1 (uteroglobin)

<i>Sftpa1</i>	Surfactant associated protein A1 (gene)
<i>Sftpb</i>	Surfactant associated protein B (gene)
<i>Sftpc</i>	Surfactant-associated protein C (gene)
SFTPC	Surfactant-associated protein C
<i>Sftpd</i>	Surfactant-associated protein D (gene)
<i>Spdef</i>	SAM pointed domain containing ets transcription factor (gene)
SMS	Somatostatin
SPDEF	SAM pointed domain containing ets transcription factor
STATs	Signal transducers and activators of transcription
Th0	T helper type 0 lymphocytes
Th1	T helper type 1 lymphocytes
Th2	T helper type 2 lymphocytes
TMX	Tamoxifen
<i>Tnf</i>	Tumor necrosis factor (gene)
TNF	Tumor necrosis factor
<i>Tslp</i>	Thymic stromal lymphopoietin (gene)
TSLP	Thymic stromal lymphopoietin
TUNEL	TdT-mediated dUTP Nick-End Labeling
wt	Wild type

ABSTRACT

Background: IGF1R (Insulin-like Growth Factor 1 Receptor) is a ubiquitous tyrosine kinase that modulates multiple cellular functions including proliferation, growth, differentiation and survival. Since prenatal *Igf1r* knockout mice die shortly after birth, the generation of *Igf1r* conditional mutant mice would allow to avoid postnatal mortality. IGFs were reported to play a role in chronic lung pathologies including cancer, ARDS, COPD, pulmonary fibrosis and asthma, in which inflammation is a relevant component.

Methods: *Igf1r* deficiency was induced in four-week-old *UBC-CreERT2; Igf1r^{fl/fl}* mice by five consecutive intraperitoneal tamoxifen (TMX) injections to generate *UBC-CreERT2; Igf1r^{Δ/Δ} (CreERT2)* mice. Then, six-week-old *CreERT2* male or female mice were intra-tracheally administered with a single dose of bleomycin (BLM) to study the implication of IGF1R in acute lung inflammation. In addition, eight- to 10-week-old female *CreERT2* mice were intranasally challenged with house dust mite (HDM) five days per week for four weeks to study the implication of IGF1R in chronic asthma pathobiology. On the other hand, inbred C57BL/6 and *CreERT2* mice were given daily consecutive doses of HDM extract to study the acute allergic profile and the implication of IGF1R in acute asthma pathobiology. Finally, IGF1R deficiency was therapeutically induced in mice to evaluate the resolution of allergic airway inflammation.

Results: Unchallenged eight-week-old *CreERT2* male mice showed a significant reduction of *Igf1r* expression in all organs analyzed, reflected in delayed body growth and reduced size of testes. Testes revealed halted spermatogenesis and liver and alveolar lung parenchyma showed increased cell proliferation rates. In addition, the lung transcriptome analysis of *CreERT2* mice identified differentially expressed genes with potentially protective roles. After bleomycin-induced lung injury, *CreERT2* mice demonstrated improved survival, reduced expression of pro-inflammatory markers, up-regulation of resolution indicators, decreased vascular fragility and permeability and reduced inflammatory cell presence in BALF and lungs and alveolar damage. Following chronic HDM exposure, *CreERT2* mice exhibited increased expression of surfactant genes, no AHR, and a selective decrease in blood and BALF eosinophils, lung IL13 levels, airway collagen and smooth muscle thickness, as well as a significant depletion of goblet cell metaplasia and mucus secretion markers. Moreover, acute HDM exposure in inbred C57BL/6 mice led to a progressive increase in inflammatory cells in BALF, airway remodeling and mRNA expression of allergic airway inflammation and remodeling markers and preventively-induced *Igf1r*-deficiency in mice demonstrated reduced neutrophil and eosinophil numbers in BALF and bone marrow, decreased airway remodeling and depleted levels of associated molecular indicators. Additionally, therapeutic targeting of *Igf1r* in mice, promoted the resolution of allergic airway inflammation and remodeling.

Conclusions: These findings support that IGF1R function is highly dependent on cell, tissue and organ type, and identify IGF1R as an important player in murine acute lung inflammation and HDM-driven allergic airway inflammation. Thus, IGF1R is suggested to be a promising candidate for future therapeutic approaches for the treatment of respiratory diseases with persistent damage and inflammation.

LIST OF PUBLICATIONS

This thesis is based on the following publications:

- I. López IP, Rodríguez-de la Rosa L, Pais RS, **Piñeiro-Hermida S**, Torrens R, Contreras J, Varela-Nieto I, Pichel JG. Differential organ phenotypes after postnatal *Igf1r* gene conditional deletion induced by tamoxifen in *UBC-CreERT2; Igf1r^{fl/fl}* double transgenic mice. *Transgenic Res* 2015; 24(2):279-294.
- II. **Piñeiro-Hermida S**, López IP, Alfaro-Arnedo E, Torrens R, Iñiguez M, Alvarez-Erviti L, Ruíz-Martínez C, Pichel JG. IGF1R deficiency attenuates acute inflammatory response in a bleomycin-induced lung injury mouse model. *Sci Rep* 2017; 7(1):4290.
- III. **Piñeiro-Hermida S**, Gregory JA, López IP, Torrens R, Ruíz-Martínez C, Adner M, Pichel JG. Attenuated airway hyperresponsiveness and mucus secretion in HDM-exposed IGF1R-deficient mice. *Allergy* 2017; 72(9):1317-1326.
- IV. **Piñeiro-Hermida S**, Alfaro-Arnedo E, Gregory JA, Torrens R, Ruíz-Martínez C, Adner M, López IP, Pichel JG. Characterization of the acute inflammatory profile and resolution of airway inflammation after *Igf1r*-gene targeting in a murine model of HDM-induced asthma. *PLoS One* (Manuscript under review).

I also contributed to five additional publications that were not included within the body of this thesis:

Berenguer JR, Pichel JG, Giménez N, Lalinde E, Moreno MT, **Piñeiro-Hermida S**. Luminescent pentafluorophenyl-cycloplatinated complexes: synthesis, characterization, photophysics, cytotoxicity and cellular imaging. *Dalton Trans* 2015; 44(43):18839-18855.

López IP, **Piñeiro-Hermida S**, Pais RS, Torrens R, Hoeflich A, Pichel JG. Involvement of *Igf1r* in bronchiolar epithelial regeneration: role during repair kinetics after selective club cell ablation. *PLoS One* 2016; 11(11):e0166388.

Lalinde E, Moreno MT, Lara R, López IP, Alfaro-Arnedo E, Pichel JG, **Piñeiro-Hermida S**. Benzothiazole based cycloplatinated chromophores: synthesis, optical and biological studies. *Chem Eur J* (Manuscript accepted for publication).

Martínez-López D, García-Irrepa C, **Piñeiro-Hermida S**, López IP, Alfaro-Arnedo E, Pichel JG, Campos PJ, Sampedro D. Photocontrol of cytotoxic activity in metronidazole derivatives. *J Org Chem* (Manuscript submitted).

Kolmert J, **Piñeiro-Hermida S**, Gregory JA, López IP, Fauland A, Wheelock CE, Dahlén SE, Pichel JG, Adner M. Prominent global LOX activation in a murine house dust mite-induced asthma model. *Prostag Oth Lipid M* (Manuscript submitted).

CONTENTS

1 INTRODUCTION	1
1.1 The mouse respiratory system	1
1.1.1 Structure and function.....	1
1.1.2 Cellular composition.....	2
1.1.3 Lung epithelial stem cell niches.....	3
1.2 Acute lung inflammation.....	4
1.2.1 Bleomycin-induced lung injury.....	4
1.2.2 Biological mechanisms of acute lung inflammation.....	4
1.3 Asthma.....	6
1.3.1 Background.....	6
1.3.2 House dust mite allergy.....	7
1.3.3 Pathogenesis of allergic asthma.....	7
1.4 Insulin-like growth factors (IGFs).....	9
1.4.1 The IGF/Insulin system: signaling and function in the lung.....	9
1.4.2 Regulation of circulating and tissue levels of IGFs.....	10
1.4.3 IGFs in human pathology.....	10
1.4.4 IGFs in mouse development.....	11
1.4.5 Expression of IGF1R in the mouse lung and implication in airway epithelial regeneration.....	11
1.5 Role of IGFs in inflammation and allergy.....	13
1.6 The Cre/lox site-specific recombination system.....	13
2 AIMS OF THE THESIS	15
3 MATERIALS AND METHODS	16
3.1 Ethics statement.....	16
3.2 Generation of the <i>UBC-CreERT2; Igf1r^{fl/β}</i> mice.....	16
3.3 Mouse genotyping.....	17
3.4 Generation of the BLM-induced acute lung injury mouse model.....	18
3.5 Establishment of the murine models of experimental asthma.....	19

3.6 In vivo measurement of lung function.....	19
3.7 Tissue collection and preparation.....	21
3.8 Histopathological analyses and immunostaining.....	21
3.8.1 Hematoxylin and eosin (H&E) staining.....	21
3.8.2 Periodic acid-Schiff (PAS) and Masson's trichrome staining.....	22
3.8.3 May-Grünwald/Giemsa staining.....	23
3.8.4 TUNEL detection of apoptotic cells.....	23
3.8.5 Immunohistochemical staining.....	23
3.8.6 Fluorescent immunostaining.....	24
3.9 RNA isolation, reverse transcription and qRT-PCR.....	25
3.9.1 Unchallenged <i>CreERT2</i> and <i>Igf1r^{fl/fl}</i> mice.....	25
3.9.2 BLM- or HDM-challenged <i>CreERT2</i> and <i>Igf1r^{fl/fl}</i> mice.....	25
3.10 Lung transcriptome analysis.....	27
3.11 Western blot analysis.....	27
3.12 ELISAS.....	28
3.13 Statistical analysis.....	28
4 RESULTS.....	29
4.1 Differential organ phenotypes after postnatal <i>Igf1r</i> gene conditional deletion induced by tamoxifen in <i>UBC-CreERT2; Igf1r^{fl/fl}</i> double transgenic mice (Paper I).....	29
4.1.1 Generation and genotyping of <i>UBC-CreERT2; Igf1r^{fl/fl}</i> double transgenic mice.....	29
4.1.2 Prepuberal TMX treatment of <i>UBC-CreERT2; Igf1r^{fl/fl}</i> mice causes somatic growth retardation with differential effects on organ weights.....	29
4.1.3 TMX treatment of <i>UBC-CreERT2; Igf1r^{fl/fl}</i> induces mice to efficiently delete <i>Igf1r</i> floxed sequences and significantly reduce IGF1R expression in different organs.....	31
4.1.4 Conditional deletion of <i>Igf1r</i> has a tissue-dependent phenotypic impact on different organs.....	34
4.1.5 Increased proliferation and normal apoptotic levels in liver and pulmonary alveolar parenchyma of <i>CreERT2</i> mice.....	35

4.2 IGF1R deficiency attenuates acute inflammatory response in a BLM-induced lung injury mouse model (Paper II).....	37
4.2.1 Postnatal IGF1R deficiency in CreERT2 mice causes a general inhibition of differentially expressed genes in the prepuberal lung.....	37
4.2.2 IGF1R deficiency improves mouse survival and alters IGF system gene expression in early stages after BLM-mediated pulmonary injury.....	40
4.2.3 IGF1R depletion protects against lung vascular fragility and permeability, and reduces inflammatory cell presence in BALF after BLM treatment.....	41
4.2.4 IGF1R deficiency reduces proliferation and attenuates acute lung inflammation and bone marrow neutrophilopoiesis after BLM-challenge.....	43
4.2.5 IGF1R deficiency reduces alveolar damage and HIF1A expression in BLM-challenged lungs.....	46
4.3 Attenuated airway hyperresponsiveness and mucus secretion in HDM exposed IGF1R-deficient mice (Paper III).....	48
4.3.1 Depletion of IGF1R in CreERT2 mutant mice and changes in expression of IGF system genes after the HDM challenge.....	48
4.3.2 IGF1R deficiency improves lung function and counteracts allergic airway inflammation and airway remodeling in HDM-treated mice.....	49
4.3.3 IGF1R depletion attenuates airway hyperreactivity and enhances surfactant expression.....	51
4.4 Characterization of the acute inflammatory profile and resolution of airway inflammation after <i>Igf1r</i> -gene targeting in a murine model of HDM-induced asthma (Paper IV)	54
4.4.1 Characterization of the murine acute allergic profile.....	54
4.4.2 Decreased HDM-induced neutrophilopoiesis and eosinophilopoiesis, and IL13, CCL11 and IgE serum levels after preventively-induced <i>Igf1r</i> deficiency.....	56
4.4.3 Preventively-induced <i>Igf1r</i> deficiency reduces inflammation and remodeling features.....	58
4.4.4 Preventively-induced <i>Igf1r</i> deficiency involves changes in expression of IGF system genes and reduces allergy-related marker levels.....	59
4.4.5 Therapeutic <i>Igf1r</i> -gene targeting reduces circulating IL33, CCL11 and IgE levels, inflammation and remodeling features.....	61

4.4.6 Therapeutic targeting of <i>Igf1r</i> diminishes expression of allergic inflammation and remodeling-related markers, and circulating IL33 and CCL11 levels.....	63
5 DISCUSSION	65
5.1 Differential organ phenotypes after postnatal <i>Igf1r</i> gene conditional deletion induced by tamoxifen in <i>UBC-CreERT2; Igf1r^{fl/fl}</i> double transgenic mice (Paper I).....	65
5.2 IGF1R deficiency attenuates acute inflammatory response in a BLM-induced lung injury mouse model (Paper II).....	68
5.3 Attenuated airway hyperresponsiveness and mucus secretion in HDM-exposed IGF1R-deficient mice(Paper III).....	70
5.4 Characterization of the acute inflammatory profile and resolution of airway inflammation after <i>Igf1r</i> -gene targeting in a murine model of HDM-induced asthma (Paper IV).....	72
6 CONCLUSIONS	77
7 REFERENCES	78
8 APPENDICES	90

1 INTRODUCTION

1.1 The mouse respiratory system

1.1.1 Structure and function

The mouse respiratory system is composed of a set of branched tubes organized in three anatomical regions: trachea and main stem bronchi, intrapulmonary airways and the alveoli. In the proximal lung, a branched tubular network of conducting airways transports gases to and from the alveoli. In the distal part of the lung, the surface available for gas exchange is maximized by septation into hundreds of millions of alveoli, surrounded by a dense capillary network. In this region, the vital function of gas exchange depends on both the proper specification and 3D organization of epithelial cells and their close opposition to a dense capillary network.

The basic design of the respiratory system is conserved among vertebrates, but there are important differences between mouse and human lungs (**Figure 1**). In mice, the largest airway, the trachea, has an internal diameter of ~1.5 mm, equivalent to the diameter of the small peripheral airways in the human lung. In mice, cartilage rings are only present in the extrapulmonary airways but, in humans, cartilage extends for several bronchial generations into the lung. Submucosal glands, which produce mucins and other factors, are restricted to only the proximal lung in the mouse but penetrate deep into the human lung. In addition, in the human lung there are more generations of intrapulmonary branches than in the mouse (Herriges and Morrisey 2014; Hogan *et al.*, 2014; Rock *et al.*, 2010; Rock and Hogan 2011; Volckaert and De Langhe 2014).

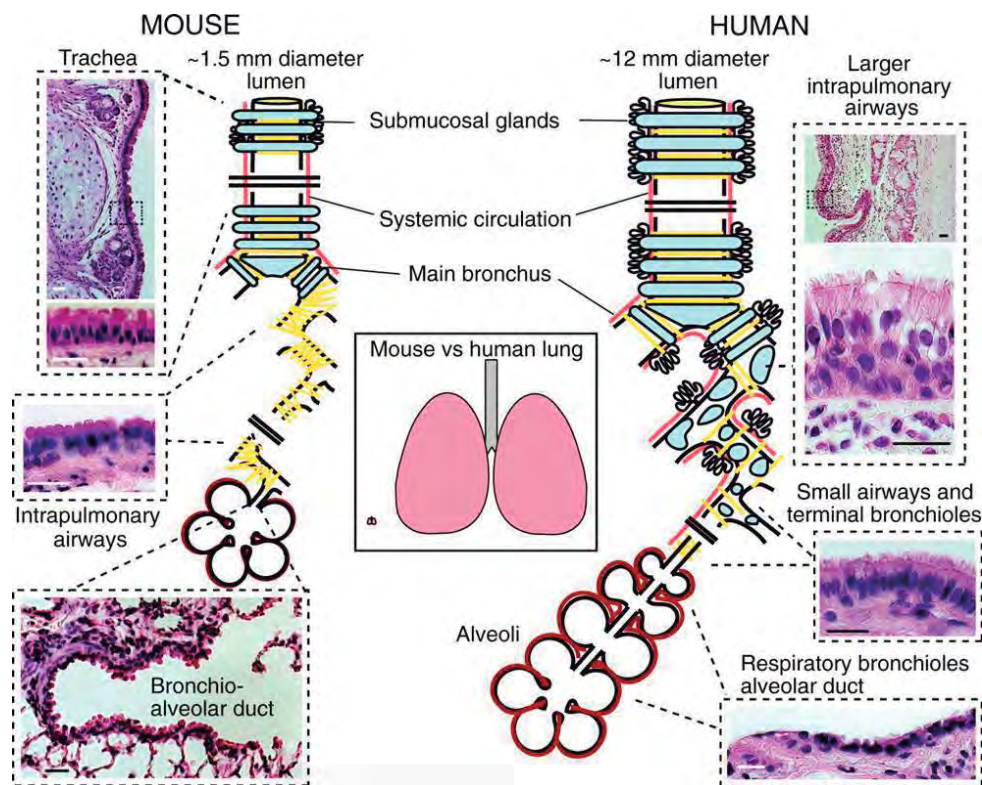


Figure 1. Schematic comparison of the structure of mouse and human lungs (Rock *et al.*, 2010)

1.1.2 Cellular composition

The cellular composition and 3D organization of the mouse lung vary along its proximodistal axis, consisting of a large variety of morphologically and functionally different cell types, whose roles include facilitating gas exchange, balancing fluids in the lung, detoxifying and clearing foreign agents, and the activation of inflammation due to injury (**Figure 2**) (Herriges and Morrissey 2014; Rock and Hogan 2011; Sullivan *et al.*, 2010).

The adult mouse trachea and primary bronchi are lined by a pseudostratified columnar epithelium containing basal, ciliated and club cells and a small number of neuroendocrine (NE) cells. In the intralobar or intrapulmonary bronchioles, the epithelium is simple columnar containing ciliated cells (GLUTUB⁺), secretory cells including club (SCGB1A1⁺) and goblet (MUC5AC⁺) cells and a higher number of NE cells than in the trachea. In this region, club cells predominate over ciliated cells and both ciliated and secretory cells drive mucociliary clearance, the process by which inhaled microorganisms and particulates are cleared from the lung. In addition, the transitional region between the terminal bronchioles and the alveoli or bronchioalveolar duct junction (BADJ) contains a few cells proposed as putative bronchioalveolar stem cells (BASCs) that coexpress SCGB1A1 and surfactant-associated protein C (SFTPC) proteins. On the other hand, the most distal region of the lung is organized into a complex system of alveoli lined by squamous alveolar epithelial type 1 cells (AEC1) and cuboidal alveolar epithelial type 2 cells (AEC2). AEC1 are the primary sites of gas exchange and fluid homeostasis regulation due to their high membrane to cytoplasm ratio, close apposition to the alveolar capillary network, and expression of ion channels and pores including AQP5. AEC2 cells are the main source of SFTPC and other components of pulmonary surfactant, a mix of extracellular proteins and lipids that decreases alveolar surface tension and contributes to host defense and alveolar homeostasis (Hogan *et al.*, 2014; Rawlins and Hogan 2006; Rock and Hogan 2011).

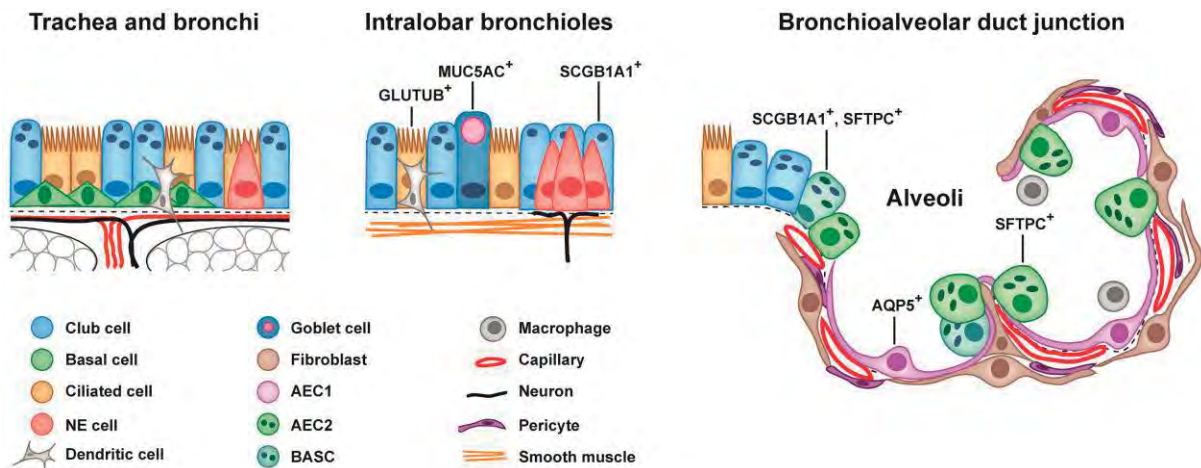


Figure 2. Cellular composition of the adult mouse lung epithelium (Modified from Rock and Hogan 2011).

1.1.3 Lung epithelial stem cell niches

Adult resident stem or progenitor cells are implicated in both homeostatic tissue maintenance and functional restoration after injury in many organs, including the lung. Following postnatal growth, the lung reaches a steady state in which epithelial turnover is low. However, airway epithelial cells are constantly exposed to and damaged by potential toxic agents and pathogens in the environment, and their subsequent regeneration is a vital process in helping maintain the function and integrity of the lungs. Furthermore, many respiratory disorders such as asthma, COPD and pulmonary fibrosis, are the consequence of inefficient repair of respiratory epithelial injury and inadequate resolution of airway inflammation (Hogan *et al.*, 2014).

The lung epithelium is maintained by different stem cell populations along the proximo-distal axis (**Figure 3**). In proximal airways, basal stem cells (BSCs) are responsible for self-renewal or regeneration after injury but in more distal airways, altogether club cells, NE cells, BASCs and AEC2 cells are the main stem cell populations responsible for maintaining the lung epithelium integrity. In particular, BSCs can regenerate both club and ciliated cells of the trachea and proximal bronchi. In the bronchiolar region, club cells can regenerate themselves, goblet cells and ciliated cells and on the other hand, NE cells can regenerate both club and ciliated cells. The transitional part between the terminal bronchioles and the alveoli is known as the BADJ, a region known to harbor variant club cells that coexpress markers of both the secretory epithelium (SCGB1A1) and AEC2 (SFTPC) lineages, which have been referred to as BASCs. Within the alveolar region, alveolar progenitors can regenerate AEC2 cells that have been shown to self-renew and differentiate into AEC1 cells after injury and during normal homeostasis (Herriges and Morrisey 2014; Hogan *et al.*, 2014; Kotton and Morrisey 2014; Morrisey and Hogan 2010; Sullivan *et al.*, 2010; Volckaert and De Langhe 2014).

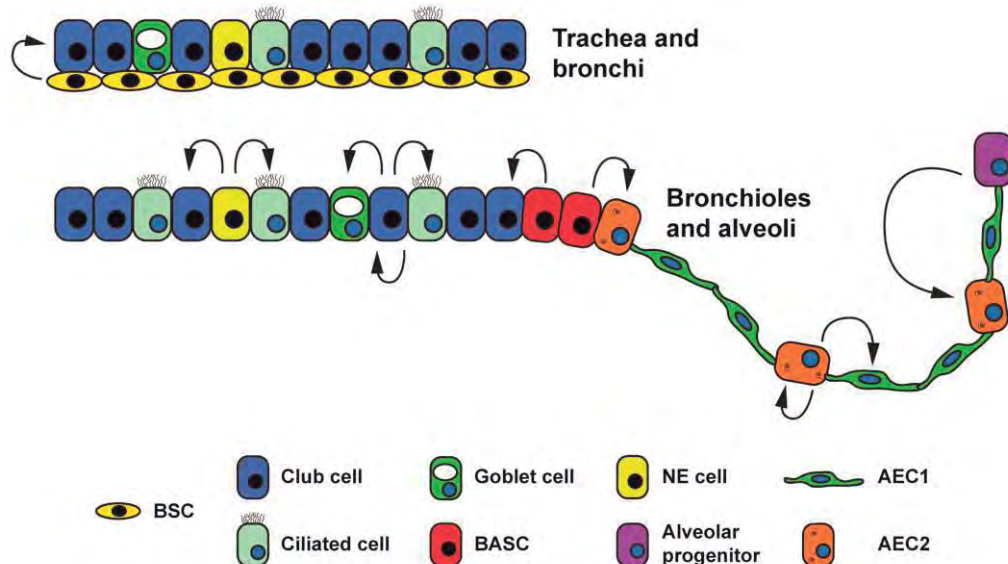


Figure 3. Epithelial stem cell niches in the adult mouse lung (Modified from Herriges and Morrisey 2014).

1.2 Acute lung inflammation

1.2.1 Bleomycin-induced lung injury

Bleomycin (BLM) is a glycopeptide with antitumor activity, first isolated from the fungus *Streptomyces verticillus* by Umezawa and colleagues in 1966. It contains a DNA-binding region but also an iron-binding region at the opposite ends of the molecule. Iron is an essential cofactor for free radical generation and the cytotoxic activity of bleomycin. In the lung, BLM simultaneously binds DNA and Fe (II), which is oxidized to Fe (III) in the presence of oxygen, resulting in the reduction of oxygen to free radicals and subsequent single- and double-strand DNA breaks (**Figure 4**). This oxidative stress ultimately leads to cell death with higher reactive oxygen (ROS) and nitrogen (RNS) species production by activated inflammatory cells recruited into the injured lung (Chen and Stubbe 2005; Della Latta *et al.*, 2015, Reinert *et al.*, 2013).

BLM can be inactivated by the enzyme bleomycin hydrolase but mice and specifically the strain C57BL/6 are more sensitive to BLM-induced toxicity because of the low expression of this enzyme in their lungs. It should be noted that differences in mouse strain susceptibility are also related to differential expression of genes involved in apoptosis or oxidative stress. Early inflammatory stages of lung injury have been experimentally studied using the intratracheal BLM mouse model because of its low complexity and high reproducibility. In mice, BLM has the ability to cause alveolar damage and pulmonary inflammation leading to acute lung inflammation (ALI) within a week. It is believed that initial damage to alveolar cells allows the drug access to the lung interstitium where subsequent epithelial damage occurs. BLM exposure induces an inflammatory response with an initial elevation of pro-inflammatory cytokines such as IL1B, TNF, and IL-6. BLM injury includes classical signs of ALI including damage to the alveolar epithelium and endothelial cells following accumulation of inflammatory cells in the alveolar interstitium and leakage of fluid and plasma proteins into the alveolar space (Chen and Stubbe 2005; Della Latta *et al.*, 2015; Foskett *et al.*, 2014; Matute-Bello *et al.*, 2008; Moeller *et al.*, 2008; Moore and Hogaboam 2008; Mouratis and Aidinis 2011; Walkin *et al.*, 2013).

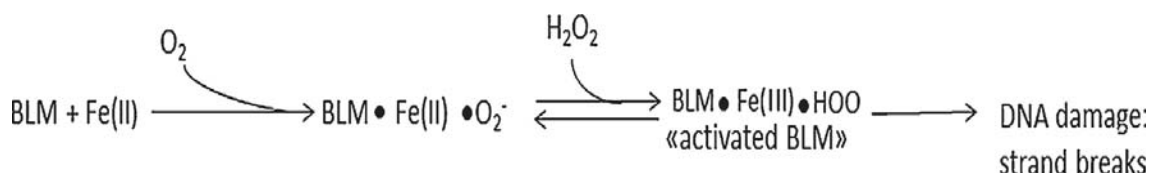


Figure 4. Activation of BLM by oxygen and iron (Della Latta *et al.*, 2015).

1.2.2 Biological mechanisms of acute lung inflammation

Inflammation is a relevant component of many lung diseases including cancer, ARDS, COPD, pulmonary fibrosis and asthma (Conway *et al.*, 2016; Johnson and Matthay 2010; Moldoveanu *et al.*, 2009; Postma and Rabe 2015; Wynn 2011). In ALI, external agents such as BLM interact with both alveolar epithelial cells and macrophages. Alveolar macrophages release early-response pro-inflammatory cytokines at sites of injury, upregulating the expression of cell adhesion molecules and stimulating the endothelium to produce chemokines, which promote chemotactic migration of neutrophils into alveolar spaces through the alveolar-capillary membrane. Activated neutrophils along with activated macrophages,

release several pro-inflammatory mediators including ROS and RNS and proteolytic enzymes inducing apoptosis or necrosis of alveolar type I cells thus, denuding the alveolar side of the basement membrane. Both activated neutrophils and products of its own activation can alter endothelial barrier function by acting on cytoskeletal and junctional proteins and endothelial glycocalyx promoting migration of inflammatory cells across the barrier. Altogether, these events further exacerbate the pathological process by recruiting additional inflammatory cells that in turn produce more cytotoxic mediators and endothelial injury after ALI induction resulting in intercellular gaps. Finally, the increased permeability of the alveolar-capillary barrier permits the efflux of protein rich edema, which inactivates surfactant production (Figure 5) (Chow *et al.*, 2003; Grommes and Soehnlein 2011; Johnson and Matthay 2010; Laskin *et al.*, 2011; Rodrigues and Granger 2015).

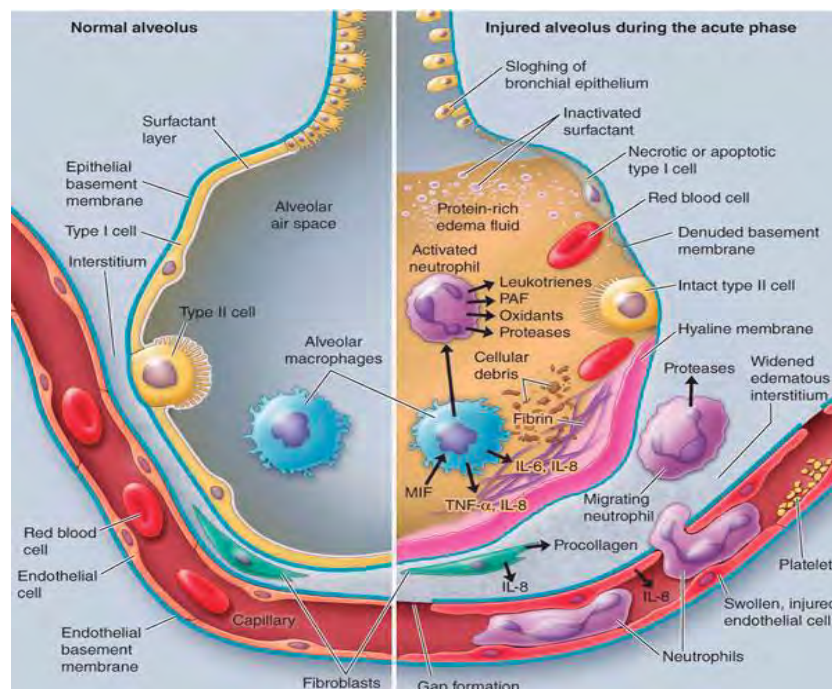


Figure 5. Biological mechanisms of acute lung inflammation (Kasper *et al.*, 2015).

It is noteworthy that oxidative and nitrosative stress are closely linked to lung injury. Although at physiological concentrations ROS/RNS mediate cellular functions including proliferation, differentiation, adhesion, migration, senescence and apoptosis, excess amounts can be toxic. Both oxidative and nitrosative stress in ALI occurs when ROS/RNS production is excessive, cellular antioxidant machinery function is reduced or when both situations occur simultaneously. Due to their strong oxidative capacity, ROS/RNS can induce damage at multiples levels in the lung including to nucleic acids, proteins, lipids, carbohydrates, cells membranes and mitochondria (Bargagli *et al.*, 2009; Cheresh *et al.*, 2013; Mittal *et al.*, 2014; Todd *et al.*, 2011).

1.3 Asthma

1.3.1 Background

Approximately 300 million people worldwide suffer from asthma and in affluent societies 1 in 10 children and 1 in 12 adults are affected with at least 250000 deaths attributed to the disease each year, which results in substantial morbidity and annual healthcare expenditure. Regarding to the prevalence in young teenagers, most people affected with asthma are in low- and middle income countries such as Latin America and English-speaking countries, and it seems that the prevalence continues to rise on these countries. It should be noted that asthma is currently considered as the most common chronic lung pathology (Fahy 2015; Global Asthma Report 2014; Lambrecht and Hammad 2012, Lambrecht and Hammad 2015, Masoli *et al.*, 2004).

Asthma is a chronic inflammatory disease of conducting airways characterized by recurring symptoms of reversible airflow obstruction, bronchial hyperresponsiveness and airway inflammation. Asthma exacerbations lead to repeated periods of shortness of breath, wheezing, cough and sputum production. Exacerbations can range from mild to severe and can result in near-fatal or fatal episodes of respiratory failure. Airway narrowing during asthma exacerbations results not only from concentric smooth muscle contraction but also from mucosal edema and the formation of pathological intraluminal mucus. The pathological changes that occur in the airway epithelium and submucosa are collectively called as airway remodeling, among them increased number of blood vessels and submucosal glands, subepithelial fibrosis and smooth muscle and goblet cell hyperplasia (**Figure 6**). Regarding the treatment of asthma, both inhaled β 2-adrenergic receptor agonists and glucocorticoids continue to be the main treatment for individuals with asthma, although leukotriene receptor antagonists and IgE-directed therapies are now available as additional treatment options (Fahy 2015; Lambrecht and Hammad 2015).

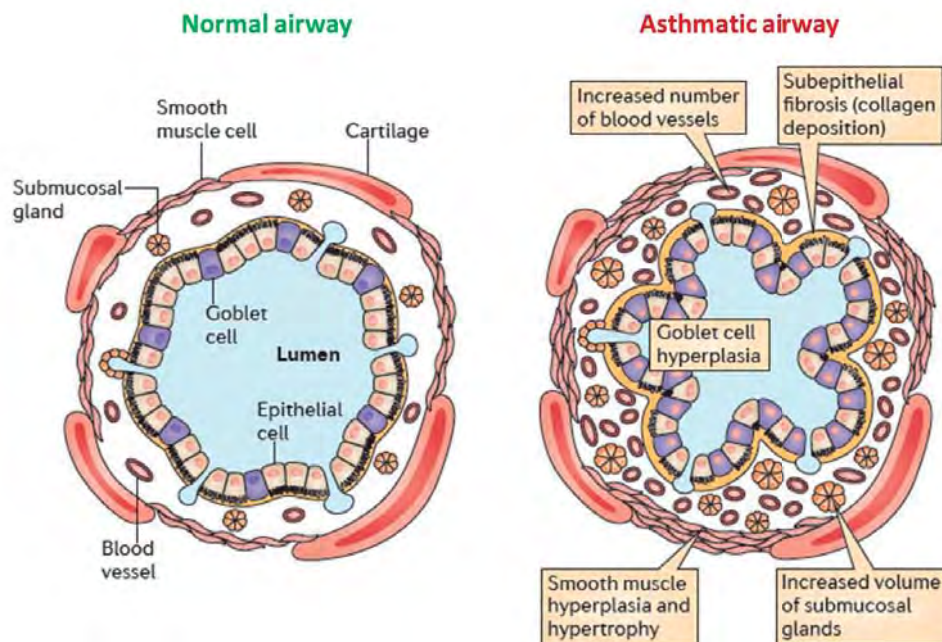


Figure 6. Schematic representation of a normal (left) versus an asthmatic airway (right) (Fahy 2015).

1.3.2 House dust mite allergy

The house dust mite (HDM) is globally ubiquitous in human habitats and a significant factor underlying allergic asthma. Geographical variations notwithstanding, the majority of allergic asthmatic individuals are sensitive to HDM. A comprehensive thesis of HDM allergy suggests that 1% to 2% of the world's population might be affected, which is equivalent to 65 to 130 million persons. Dust provides a detrital habitat with 3 key macromolecules derived from organic debris which are the main food staple of HDM: keratin (human skin scales), cellulose (textile fibers), and chitin (fungal hyphae and mite cuticles). HDM diet also extends to fibers, bacteria, pollen, fungal mycelia, and the spores of microorganisms. During digestion, disassociated digestive cells containing allergenic enzymes bind to ingested food, which are then excreted in the HDM fecal pellets (**Figure 7**). The main source of HDM allergens are *Dematophagoides pteronyssinus* species, whose allergenic potential rests with the mites themselves and with their fecal pellets which contains Derp1 allergens with cysteine protease activity. Derp1 allergens exhibits a complex mixture of molecules including proteases, allergen epitopes, and activators of the innate immune system serving as adjuvants to disrupt intercellular tight junctions leading to cytokine, chemokine, and growth factor production and cellular influx, as well as airway remodeling and mucus hypersecretion (Buday and Plevkova 2014; Calderón *et al.*, 2015; Gregory and Lloyd 2011).

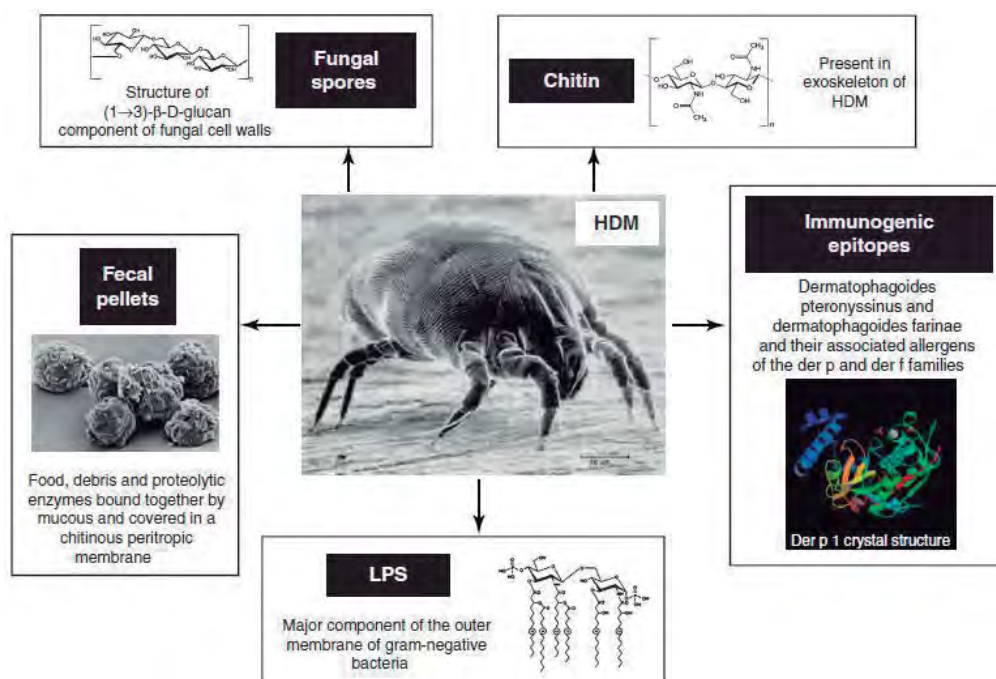


Figure 7. Components of HDM and their associated fecal pellets and dust (Gregory and Lloyd 2011).

1.3.3 Pathogenesis of allergic asthma

It is widely considered that the airway epithelium is an essential controller of inflammatory, immune, and regenerative responses in asthma. In the case of HDM-induced asthma, airway epithelial cells secrete cytokines and chemokines in response to proteolytic allergens such as Derp1 through activation of protease-activated receptor 2 that secretes endogenous danger signals, thereby activating dendritic cells and bridging innate and adaptive immunity. The powerful allergenic effects of HDM are thought to be orchestrated through 2 main routes: Th2 CD4⁺ T lymphocytes that induce and drive the

IgE-dependent allergic response and the innate immune system (**Figure 8**) (Calderón *et al.*, 2015, Lambrecht and Hammad 2012; Whitsett and Alenghat 2015).

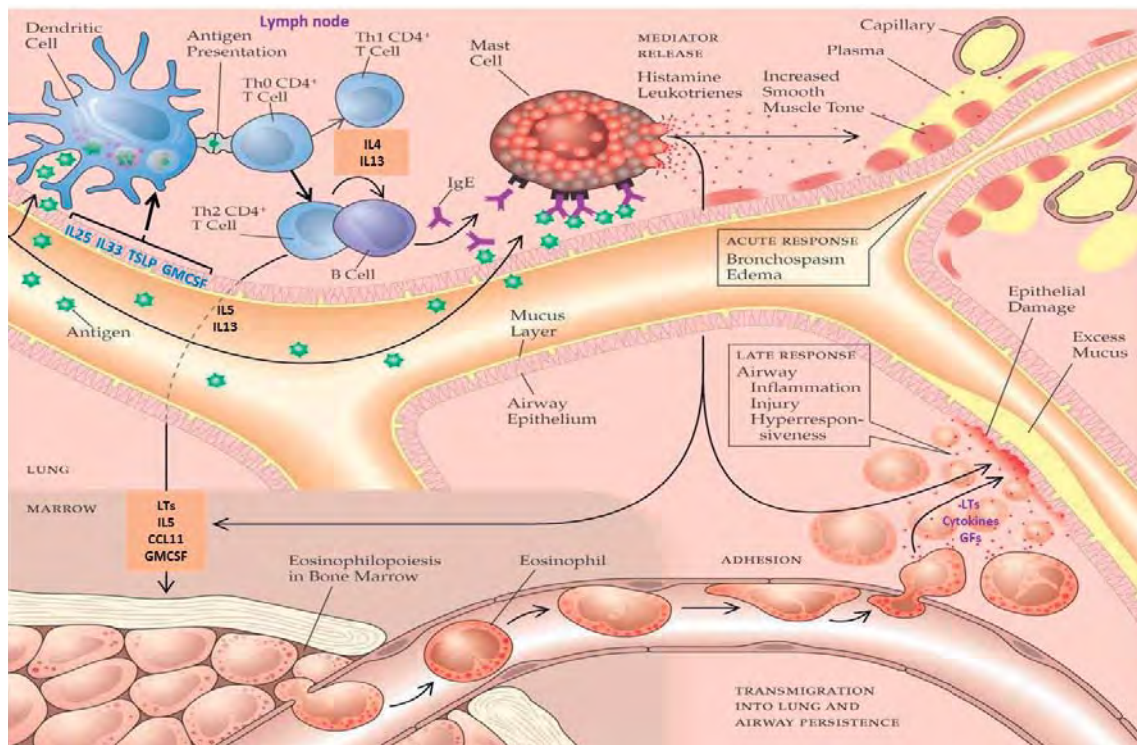


Figure 8. Pathogenesis of allergic asthma (<http://what-when-how.com/acp-medicine/asthma-part-1>).

When the allergen is inhaled into the airway, it is taken up and processed by dendritic cells. Then, dendritic cells are stimulated to migrate from the airway mucosa to regional lymph nodes by the epithelial cytokines IL25, IL33, TSLP and GM-CSF. Upon arrival at the lymph nodes, dendritic cells present the processed antigenic peptides to Th0 CD4⁺ T lymphocytes, which begin to proliferate. Simultaneously, dendritic cells attempt to skew the cytokine profile of the developing T lymphocytes to cause them to become Th1 or Th2 cells. Release of IL4 and IL13 by Th2 cells, stimulates B cells to produce IgE, which binds to the surface of mast cells and basophils. Inhaled antigen binds to IgE, stimulating the mast cells to degranulate, which in turn leads to the release of mediators of both the acute and late responses, including histamine and leukotrienes (LTs), but also inflammatory cytokines which serve to perpetuate inflammatory events in the airway. Allergen specific IgE also facilitates allergen uptake by dendritic cells. Specifically, during the acute response, histamine and leukotrienes produce the increase of smooth muscle tone resulting in bronchospasm and airway edema. Simultaneously, Th2 cells migrate to subepithelial mucosa from the bloodstream and produce mainly IL5 and IL13 to mediate the inflammatory and remodeling changes. The release of eosinophils from bone marrow is dependent on leukotrienes derived from mast cells and epithelial-derived chemokines including CCL11 (eotaxin-1) and IL5 derived from both mast cell activation and Th2 CD4⁺ T lymphocytes. Specifically, IL4 and IL13 act on IL-5 and CCL11, which selectively stimulate eosinophil and mast cell recruitment and activation. Locally generated IL-4 and IL-13 promote the increase of eosinophil adhesion to lung vasculature and the cytokines IL-5 and GM-CSF promote the local survival of eosinophils. During the late response, the eosinophils reach the airways

through the vasculature, releasing high inflammatory granule-associated proteins with cytotoxic, immunological, and remodeling properties in the lung. Specifically, eosinophils are a rich source for leukotrienes, inflammatory cytokines and growth factors (GFs). Upon entry into airway tissue, both eosinophils and Th2 cells secrete their products, which, in addition to the mast cell products, are thought to lead to mucous cell metaplasia and smooth muscle hyperplasia/hypertrophy which are the basis for the hyperresponsiveness and airflow obstruction. Other structural changes are subepithelial fibrosis, increased vascularity and airway injury and inflammation (**Figure 8**) (Calderón *et al.*, 2015; Erle and Sheppard 2014; Gregory and Lloyd 2011; Hammad and Lambrecht 2008; Lambrecht and Hammad 2015; Lemanske and Busse 2010; Lukacs 2001; Possa *et al.*, 2013).

1.4 Insulin-like growth factors (IGFs)

1.4.1 The IGF/Insulin system: signaling and function in the lung

The insulin-like growth factor 1 receptor (IGF1R) is a ubiquitously expressed membrane-bound tyrosine kinase receptor formed by two β subunits with the intracellular tyrosine kinase signaling domain and two extracellular α subunits that recognize its two major ligands, IGF1 and IGF2 (**Figure 9**).

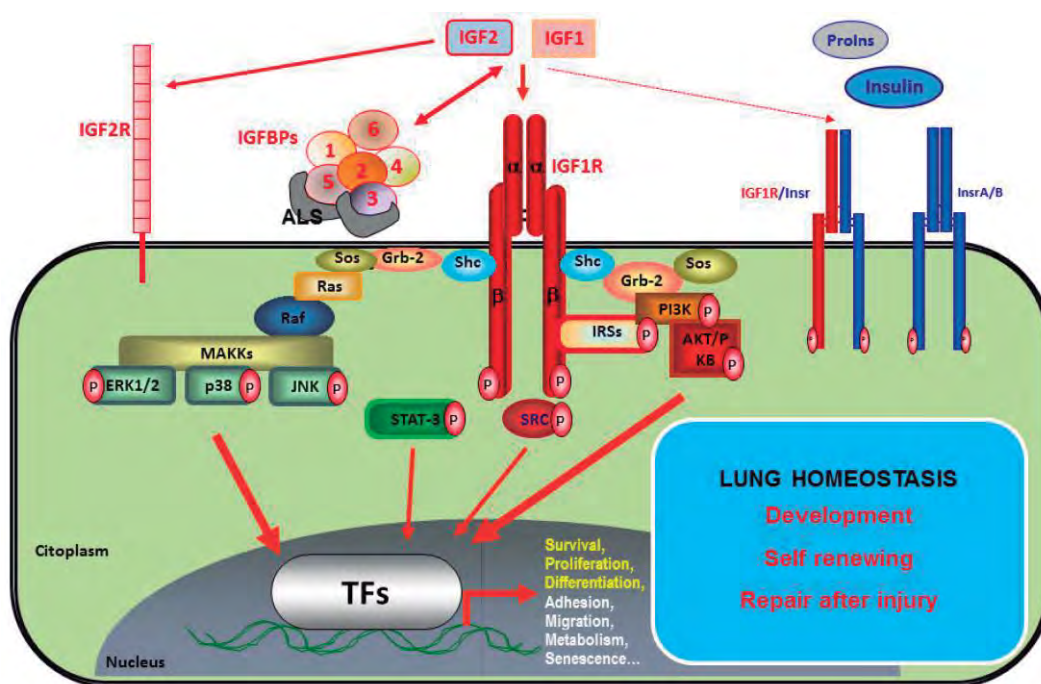


Figure 9. The IGF/Insulin system: signaling and function in the lung.

IGF2 also interacts with a second receptor (IGF2R) that reduces IGF2 signaling through lysosomal degradation. Homology between IGF1R and the insulin receptor (INSR) allows IGF signaling through INSR, although with lower affinity; and *vice versa*, insulin (and pro-insulin) can activate IGF1R. Furthermore, IGF1R and INSR can form hybrid receptors, which have a high binding affinity for IGF1, thereby functioning as IGF1R. Noteworthy, IGF activity and availability are modulated by six high-affinity IGF binding proteins (IGFBPs 1-6). Although IGF1R expression has been found in almost all tissues and cell types during pre- and postnatal development and in adults, IGF1R and ligand expression is tightly regulated in a cell type-specific and spatiotemporal manner. Binding of ligands to IGF1R causes activation

of various signaling pathways, including mitogen-activated protein kinases (MAPKs), involved in cell proliferation and differentiation, PI3K/Akt, with proven cell survival activity and signal transducers and activators of transcription proteins (STATs). IGF1R function is pleiotropic: it controls cell and body growth and tissue homeostasis of endocrine, paracrine and autocrine action of IGFs, playing important roles in regulation of cell survival, proliferation, differentiation, adhesion, migration, metabolism and senescence. These actions keep lung homeostasis, with implications in lung development, self-renewing and repair after injury (Annunziata *et al.*, 2011; Girnita *et al.*, 2014; Crudden *et al.*, 2015; LeRoith and Roberts 2003; Pollak 2008).

1.4.2 Regulation of circulating and tissue levels of IGFs

At the whole organism level, most circulating insulin-like growth factors are produced in the liver, whereas insulin is produced by the pancreatic β cells (Figure 10). In particular, the Growth Hormone (GH), which is produced in the pituitary gland under control of the hypothalamic factors growth hormone releasing hormone (GHRH) and somatostatin (SMS), is a key stimulator of IGF1 production. Various IGF-binding proteins (IGFBPs) are also produced in the liver. Noteworthy, IGF2 is also expressed both in the liver and in extrahepatic sites, but it is not tightly regulated by GH. In IGF responsive tissues, the ligands IGF1 and IGF2 as well as IGFBPs can be delivered through the circulation from the liver (an 'endocrine' source), but IGFs and IGFBPs can also be locally produced through autocrine or paracrine mechanisms (Pollak *et al.*, 2004; Pollak 2008).

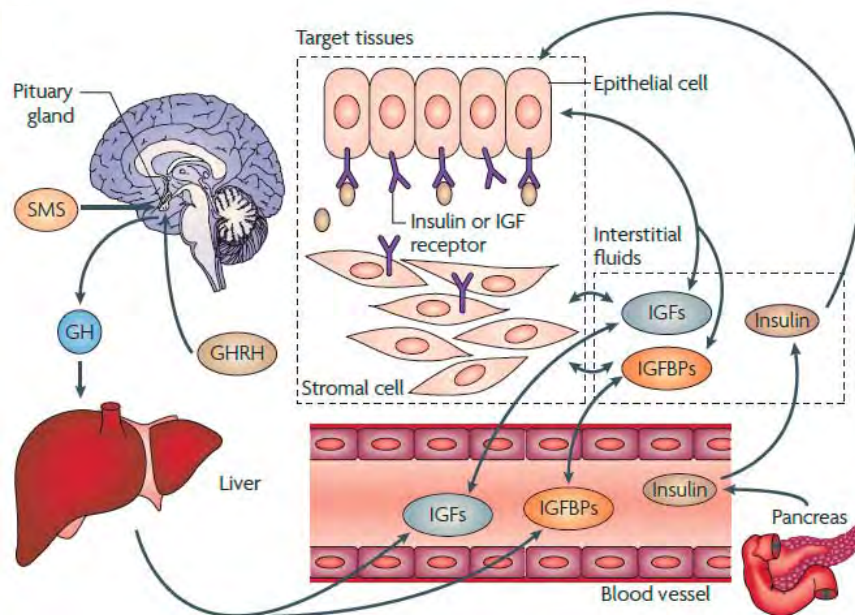


Figure 10. Regulation of circulating and tissue levels of IGFs (Pollak 2008).

1.4.3 IGFs in human pathology

IGF1/IGF1R signaling is implicated in multiple human pathologies, including intrauterine and postnatal growth failure, microcephaly, mental retardation and deafness (Abuzzahab *et al.*, 2003; Raile *et al.*, 2006; Varela-Nieto *et al.*, 2013; Walenkamp *et al.*, 2005; Walenkamp *et al.*, 2008). Furthermore, IGF1R is overexpressed in multiple tumors and targeting its activity is being considered a promising therapy for cancer (Corvaia *et al.*, 2013; Iams and Lovly 2015; Pollak 2008; Werner and Bruchim 2009).

Particularly, IGF activity was extensively reported in maintaining human lung homeostasis, as it seems to be highly relevant in chronic lung pathologies including cancer, ARDS, COPD, pulmonary fibrosis and asthma (Agulló-Ortuño *et al.*, 2015; Ahasic *et al.*, 2014; Esnault *et al.*, 2013; Hoshino *et al.*, 1998; Hsu and Feghali-Bostwick 2008; Pala *et al.*, 2001; Ruan and Ying 2010; Takasaka *et al.*, 2014; Veraldi *et al.*, 2009; Ye *et al.*, 2014). In addition, IGF1R mutations have been identified in humans presenting lung anomalies such as lung hypoplasia and pulmonary hypertension (Gannage-Yared *et al.*, 2013, Roback *et al.*, 1991).

1.4.4 IGFs in mouse development

Targeted mutations of IGF genes in the mouse indicate that IGF signaling is relevant for lung tissue development, homeostasis and repair. In this sense, classical *Igf1r*-deficient mice die at birth presumably due to respiratory failure and exhibit a 55% decrease in body weight compared to wild type controls. Prenatal *Igf1r* knockout embryos exhibit growth retardation and generalized developmental abnormalities, comprising altered central nervous system, abnormal skin formation, delayed bone development, reduced pancreatic beta-cells, failure of testicular determination, cochlear defects and lung immaturity (Bonnette and Hadsell 2001; Epaud *et al.*, 2012; Liu *et al.*, 1993; Nef *et al.*, 2003; Okano *et al.*, 2011; Scolnick *et al.*, 2008; Withers *et al.*, 1999). In particular, *Igf1r* knockout embryos die at birth as they show lungs with strong hypoplasia, atelectasis, increased cell proliferation and apoptotic rates, vascular abnormalities, and altered alveolar differentiation (Epaud *et al.*, 2012; Holzenberger *et al.*, 2000; Liu *et al.*, 1993). Accordingly, prenatal *Igf1*^{-/-} mice die shortly after birth due to respiratory failure showing lungs with severe hypoplasia, increased cell proliferation rates and altered alveolar differentiation and vasculogenesis, among other abnormalities (Moreno-Barriuso *et al.*, 2006; Pais *et al.*, 2013). Remarkably, an inflammatory component is present in several chronic lung pathologies including cancer, ARDS, COPD, pulmonary fibrosis and asthma. On this basis, the generation of *Igf1r* conditional mutant mice to avoid the postnatal mortality observed in knockout mice, would allow the generation of mouse models for the study of implication of IGF1R in these pathologies.

1.4.5 Expression of IGF1R in the mouse lung and implication in airway epithelial regeneration

The adult mouse lung display the highest level of IGF1R activation of any organ upon challenge with IGF1 (Moody *et al.*, 2014). Expression profiles of IGF1R performed in the mouse lung support their functional implication in pulmonary ontogeny. Although IGF1R is present throughout the entire lung, the highest expression levels were found in epithelial cells, alveolar macrophages, and the smooth muscle (**Figure 11**) (López *et al.*, 2016). Specifically, IGF1R expression in smooth muscle and endothelial cells of pulmonary blood vessels also indicates a role of this receptor in lung vasculature, as described elsewhere (Abbas *et al.*, 2011; Engberding *et al.*, 2009). Notably, similar expression patterns have been also described in both the prenatal mouse lung and the adult human lung (Pais *et al.*, 2013; Uhlen *et al.*, 2015).

Regeneration of lung epithelium is vital for maintaining airway function and integrity. Thus, an imbalance between epithelial damage and repair is at the basis of numerous chronic lung diseases such as asthma, COPD and pulmonary fibrosis (Hogan *et al.*, 2014). Little was known about the role of IGF1R in bronchiolar epithelial regeneration. In this regard, it was recently reported that the conditional deletion of *Igf1r* in the murine pulmonary epithelium followed by selective club cell ablation, altered the bronchiolar

epithelium homeostasis, causing increased proliferation and delayed differentiation of club and ciliated cells. This findings support the implication of IGF1R in maintaining control of bronchiolar epithelial regeneration after injury, by keeping an adequate balance between proliferation and differentiation in basal progenitor cells (López *et al.*, 2016).

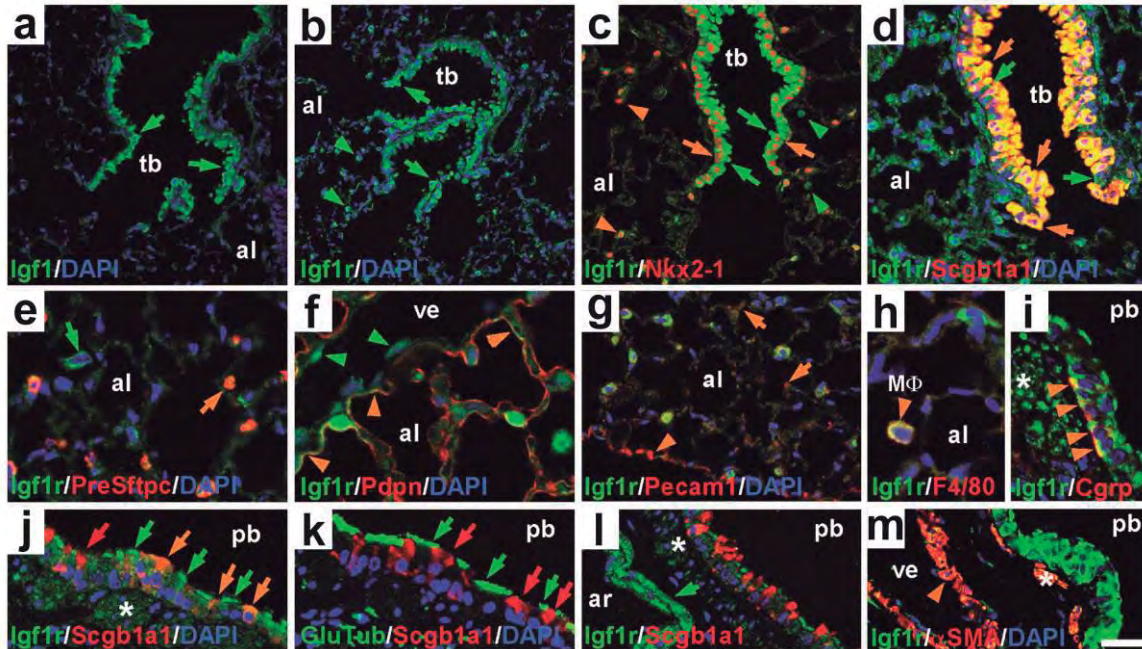


Figure 11. (a-b) Immuno-staining for IGF1 (a) and IGF1R (b) (green labeling) in six-month-old lungs. Distal bronchiolar epithelium showed strong staining for both proteins (green arrows). Note that IGF1R was also found scattered throughout the alveolar parenchyma (green arrowheads in b). (c-m) Immuno-staining for IGF1R (green labeling), counterstained in red with lung cell-type specific markers and blue with DAPI to visualize nuclei, in three-month-old lungs. (c) All bronchiolar epithelial cells showed co-localization of IGF1R (green arrows) with nuclear Nkx2-1 (orange arrows), and also co-localized with Nkx2-1⁺ AEC2 cells in the alveoli (orange arrowheads). There were Nkx2-1⁻ alveolar cells that additionally stained for IGF1R (green arrowheads). (d) IGF1R strongly stained abundant Scgb1a1⁺ club cells in terminal bronchioles (orange arrows), and in apical cilia of scarce ciliated cells (green arrows). (e) IGF1R stained the cytoplasm of Pre-Sftpc⁺ AEC2 cells (orange arrows), and additional cells in alveolar spaces (green arrow). (f) IGF1R co-stained with Pdpn in areas of the apical membrane in AEC1 cells (orange arrowheads). Note the light staining of IGF1R in vein endothelial cells (green arrowheads). (g) IGF1R co-localized with endothelial Pecam1⁺ cells (orange arrows), more abundantly in capillaries under the pleura (orange arrowhead). (h) IGF1R co-localization with the F4/80⁺ alveolar macrophage marker in cells located in alveolar spaces (orange arrowhead). (i) IGF1R stained Cgrp⁺ neuroendocrine cells (orange arrowheads) in proximal bronchioles. (j) IGF1R staining in Scgb1a1⁺ proximal bronchiole club cells is faint (orange and red arrows), but strong in apical membranes (cilia) of ciliated cells (green arrows). In an adjacent section (k), the Glu-Tubulin (GluTub, a cilium specific marker) stained the same ciliated cells (green arrows) as in K, whereas Scgb1a1 stained club cells (red arrows). (l) Pulmonary artery smooth muscle showed strong staining for IGF1R (green arrow), whereas para-bronchiolar smooth muscle stained fainter (asterisk). (m) α-SMA⁺ smooth muscle cells in veins also co-express IGF1R (orange arrowhead), as does the para-bronchiolar smooth muscle (asterisk). al, alveolus; ar, artery; MΦ, macrophage; pb, proximal bronchiole; tb, terminal bronchiole; ve, vein. Scale bar in N: 32 μm in B; 50 μm in C; 34 μm in D-E; 16.6 μm in F; 12,5 μm in G, I, J; 18 μm in K-L; and 25 μm in M-N (López *et al.*, 2016).

1.5 Role of IGFs in inflammation and allergy

IGFs seem to play an important role in the inflammatory process as they appear to modify several aspects of inflammation by influencing the actions of cytokines and other inflammatory mediators (Smith 2010). Specifically, both IGF1R and IGF1 could play an important role in the proliferation of alveolar macrophages taking place during inflammation (Rom and Pääkkö 1991). In this regard, ablation of the macrophage IGF1-IGF1R axis in mice inhibits the NLRP3 inflammasome, a protein complex that is activated in response to lung injury, which indicates that IGF1R plays an important role in initiation of the inflammatory process (Spadaro *et al.*, 2016). In addition, oxidative stress is a key process in the onset of the inflammatory response. In this sense, it was reported that IGF1R plays a critical role in the regulation of pulmonary resistance to oxidative stress, since mice with compromised IGF1R signaling displayed oxidative stress resistance (Ahamed *et al.*, 2005; Kim *et al.*, 2012a).

Although little is known about the role of IGFs in human asthma, IGF1 and IGFBP3 were suggested to be involved in allergic airway inflammation and remodeling and IGF1R was found to be upregulated in BAL cells of asthmatic patients (Esnault *et al.*, 2013; Hoshino *et al.*, 1998; Veraldi *et al.*, 2009). In mice, IGF1 was reported to be a relevant mediator of allergic airway inflammation and remodeling, and that IGFBP3 blocks specific physiological consequences of asthma (Kim *et al.*, 2012b, Lee *et al.*, 2011, Yamashita *et al.*, 2005).

On the basis that an inflammatory component is present in several chronic lung pathologies including cancer, ARDS, COPD, pulmonary fibrosis and asthma, the study of implication of IGF1R in acute lung inflammation and allergic airway inflammation using *Igf1r* conditional mutant mice would allow the development of future therapeutic approaches for these pathologies.

1.6 The Cre/lox site-specific recombination system

The Cre/lox site-specific recombination system is an important tool for generating conditional somatic mouse mutants. This method allows gene activity to be controlled in both space and time in almost any mouse tissue, and thus sophisticated animal models of human diseases can be created. This approach takes advantage of the properties of P1 phage Cre recombinase, a 38 kDa enzyme that recognizes a 34 bp DNA sequence called loxP. The basic strategy for Cre/lox-directed gene knockout experiments is to flank, or “flox”, an essential sequence of the gene of interest. Introduction of loxP sites flanking a DNA target sequence enables binding by Cre-recombinase and either inversion or excision of the sequence, depending on the respective orientation of the loxP sites, thus generating a null allele in all cells where Cre is active (**Figure 12**) (Feil *et al.*, 1997; Feil 2007; Feil *et al.*, 2009; Hayashi and McMahon 2002, Metzger and Chambon 2001; Ruzankina *et al.*, 2007).

The *UBC-CreERT2* transgene consist of an Ubiquitin C gene promoter which drives generalized Cre-recombinase expression and the *CreERT2* fusion protein consisting of the Cre recombinase fused to a triple mutant form of the human estrogen receptor. *CreERT2* is insensitive to the natural ligand (17 β -estradiol) but functions as a specific receptor for the synthetic ligand 4-hydroxytamoxifen (4-OHT) (Danielian *et al.*, 1993). In the absence of 4-OHT, *CreERT2* is sequestered in the cytoplasm, complexed with the heat shock protein 90 (HSP90) (Mattioni *et al.*, 1994). Binding to 4-OHT disrupts the interaction with

HSP90 and permits the translocation of *CreERT2* to the nucleus wherein it catalyzes loxP-specific recombination events, resulting in deletion of flanked sequences in widespread cells/tissues (Hayashi and McMahon 2002) (Figure 12).

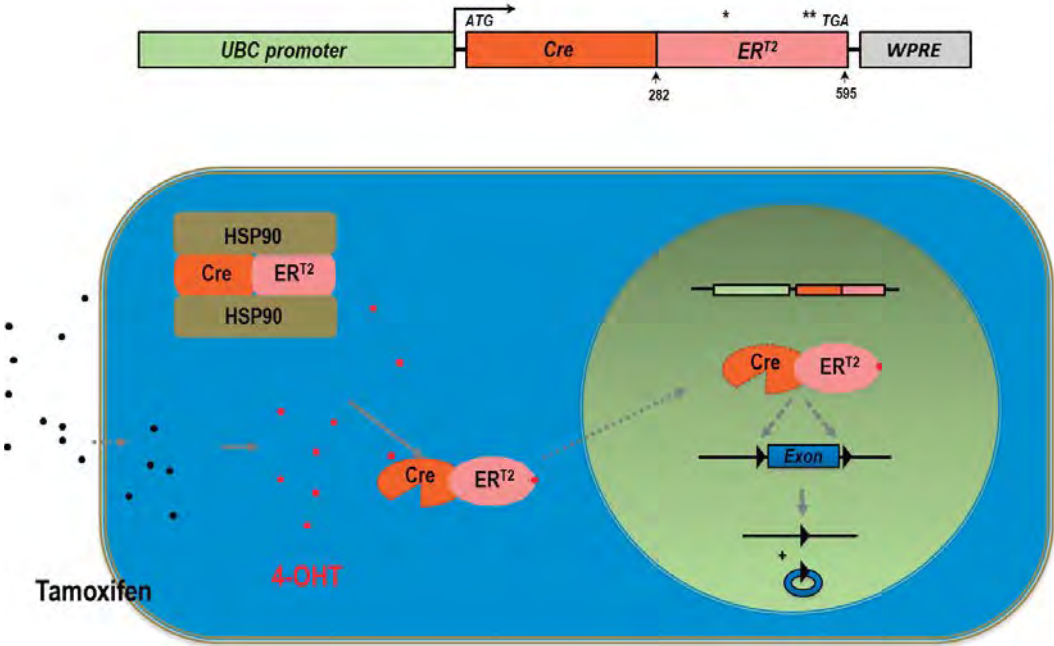


Figure 12. TMX-inducible Cre/lox site-specific recombination system.

2 AIMS OF THE THESIS

The overall aim of this thesis was to investigate the implication of IGF1R in acute lung inflammation and HDM-induced allergy. The following specific aims were proposed:

1. To analyze the differential organ phenotypes after postnatal *Igf1r* gene conditional deletion in mice (**Paper I**).
2. To investigate the implication of IGF1R on the inflammatory process that occurs during BLM-induced acute lung injury in mice (**Paper II**).
3. To study the implication of IGF1R on airway hyperreactivity and mucus secretion in a chronic HDM model of asthma (**Paper III**).
4. To evaluate the implication of IGF1R in murine acute asthma pathobiology and resolution of allergic airway inflammation following HDM exposure (**Paper IV**).

3 MATERIALS AND METHODS

3.1 Ethics statement

All experiments and animal procedures were carried out following the guidelines laid down by the European Communities Council Directive of 24 November 1986 (86/609/EEC) and were revised and approved by the CIBIR Bioethics Committee (refs 03/12, 13/12, JGP02_1 and JGP02_2). On the other hand, the experimentation conducted in Sweden, were carried out in accordance with ethical permit N152/15 approved by the Regional Committee of Animal Experimentation Ethics (Stockholm, Sweden).

3.2 Generation of *UBC-CreERT2; Igf1r^{A/Δ}* mice

UBC-CreERT2; Igf1r^{fl/fl} mice were created in two generations by mating hemizygous *UBC-CreERT2* transgenics (*Tg(UBC-cre/ERT2)1Ejb*; MGI:3707333) with a 129SvEv/C57BL/6 mixed genetic background (Ruzankina *et al.*, 2007), with homozygous *Igf1r^{fl/fl}* mutants (*Igf1^{rtm1}cbcr*; MGI:3818453) that had a C57BL/6 background (Kloting *et al.*, 2008) (F0). *UBC-CreERT2; Igf1r^{fl/+}* heterozygous mice generated in F1 were backcrossed with *Igf1r^{fl/fl}* to yield an F2 with equal proportions of four genotypes, among them mice of the new *UBC-CreERT2; Igf1r^{fl/fl}* double transgenics and the *Igf1r^{fl/fl}* mice, both with a 129SvEv/C57BL/6 mixed genetic background. *UBC-CreERT2; Igf1r^{fl/fl}* double transgenic mice were crossed with *Igf1r^{fl/fl}* mutants to directly generate descendants with equal proportions of both parental genotypes, which were used in experiments to study the differential organ phenotypes after postnatal *Igf1r* gene conditional deletion and to determine the role if *Igf1r* in acute lung inflammation and HDM-induced allergy (Figure 13).

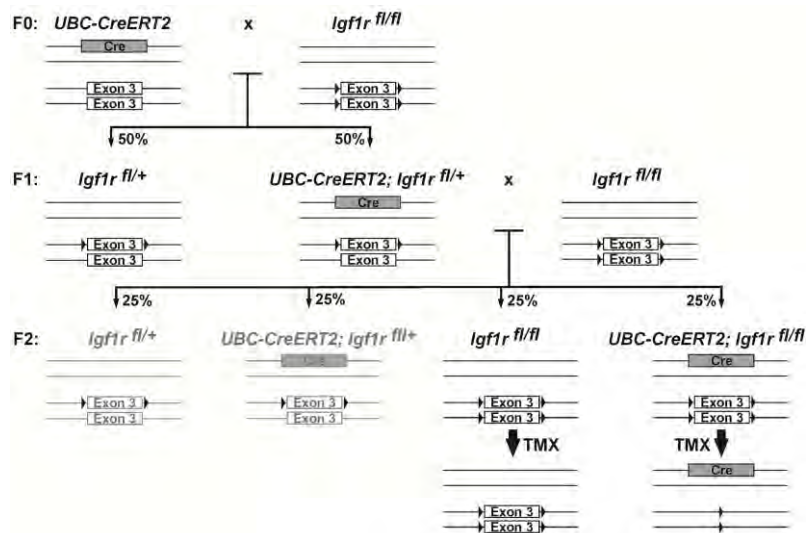


Figure 13. Strategy to achieve TMX-induced *Igf1r* gene deletion in *UBC-CreERT2; Igf1r^{fl/fl}* double mutant mice in two generations (F2), by mating hemizygous *UBC-CreERT2* transgenics with homozygous *Igf1r^{fl/fl}* mutants (F0), followed by a backcross mating in F1. Proportion of genotypes is given in percentages according to Mendelian inheritance. The diagram represents the genomic organization on each locus in the different genotypes. Black arrowheads denote location of loxP sites flanking exon 3 in *Igf1r* gene. Postnatal TMX administration to F2 mice activates Cre recombinase to promote *Igf1r* exon 3 deletion exclusively in *UBC-CreERT2; Igf1r^{fl/fl}* mice, but not in *Igf1r^{fl/fl}* (controls) mice. TMX, tamoxifen.

It should be noted that both *UBC-Cre-ERT2; Igf1^{fl/fl}* and *Igf1^{fl/fl}* mice were never employed for breeding purposes. To induce a postnatal *Igf1r* gene conditional deletion, 4 week-old male or female *UBC-CreERT2; Igf1^{fl/fl}* double transgenics were injected intraperitoneally with tamoxifen (TMX) solution (Sigma-Aldrich, St. Louis, MO) (75 mg/kg) dissolved in corn oil (Sigma-Aldrich) at a concentration of 20 mg/ml for five consecutive days (D0–D4) to obtain the *Igf1r*-deficient *UBC-CreERT2; Igf1^{Δ/Δ}* (*CreERT2*) mice (**Figure 14**) (López *et al.*, 2015). *Igf1^{fl/fl}* mice were also injected with TMX as TMX-experimental controls. Animals were monitored for adverse effects, and if these become apparent, treatment was stopped.

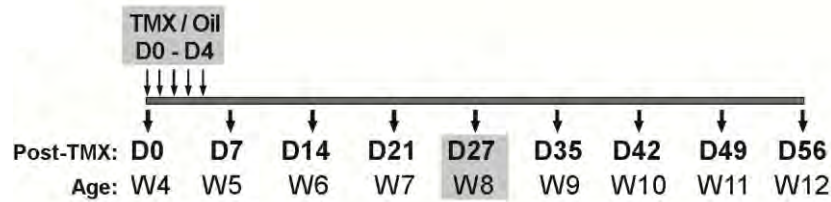


Figure 14. Schematic representation of the experimental protocol designed to generate *UBC-CreERT2; Igf1^{Δ/Δ}* (*CreERT2*) mice and for the study of the differential organ phenotypes. TMX or vehicle (oil) administration was performed daily for 5 days, from D0 to D4, on 4 week-old mice (W4). Their weights were measured weekly up to D56 (W12). For molecular and histological analysis of different organs, some mice were sacrificed at D27 (W8). TMX, tamoxifen.

3.3 Mouse genotyping

Mice were genotyped by standard PCR analysis of tail DNA obtained as described (Pais *et al.*, 2013), and using specific primers for each gene designed as shown in (**Figure 15a-b**). Presence of *UBC-CreERT2* transgene was detected using primers F (5'-TGAAGCTCCGGTTTTGAACT-3') and R (5'-TGGTGTACGGTCAGTAAATTGG-3'), in combination with two additional primers for the IL2 gene, IL2F (5'-CTAGGCCACAGAATTGAAAGATCT-3') and IL2R (5'-GTAGGTGAAAATTCTAGCATCATCC-3'), used as an internal PCR positive control. They rendered 255 and 325 bp-long amplicons, respectively (**Figure 15a, c**). To identify *Igf1r* wild type (wt) or flox (fl) alleles, both the forward F1 (5'-TCCCTCAGGCTTCATCCGCAA-3') and the reverse R1 (5'-CTTCAGCTTTGCAGGTGCACG-3') primers were used, which generated a 300 and/or 380 bp amplicon for each allele, respectively (Kloting *et al.*, 2008) (**Figure 15b-c**). *Igf1r* deletion was detected using the following primers: F3 (5'-TTATGCCTCCTCTCTTCATC-3') and R1 (5'-CTTCAGCTTTGCAGGTGCACG-3') which can generate three products of 1300, 1220 and 491 bp (**Figure 15b-c**). The PCR conditions were as follows: (1) For *UBC-CreERT2* and IL2 genes: 94 °C for 3 min; 30 cycles of 94 °C for 30 s, 60 °C for 30 s, and 72 °C for 30 s; finally 72 °C for 7 min. (2) For *Igf1r* wt/fl alleles: 94 °C for 3 min; 35 cycles of 94 °C for 30 s, 56 °C for 30 s, and 72 °C for 30 s; finally 72 °C for 7 min. And lastly (3) for *Igf1r* deletion: 95 °C for 4 min; 30 cycles of 95 °C for 45 s, 58 °C for 45 s, and 72 °C for 80 s, and finally 72 °C for 10 min.

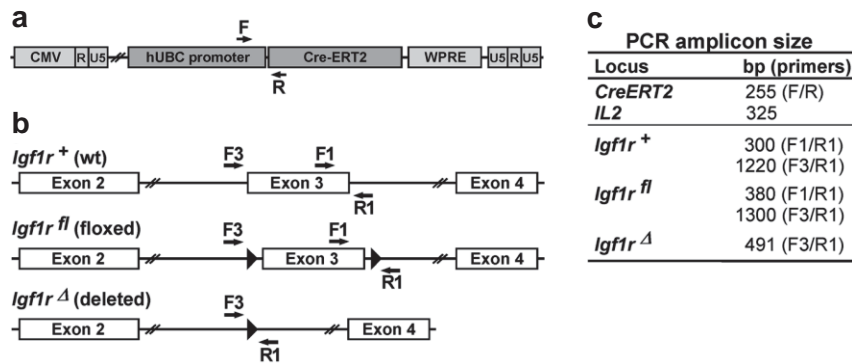


Figure 15. Primers and amplicon sizes to identify presence of the *UBC-CreERT2* transgene and the different *Igf1r* allelic forms by standard PCR analysis. (a) *UBC-CreERT2* transgene elements and location of F/R primers for PCR genotyping. (b) Genomic DNA organization in alternative allelic forms of the *Igf1r* locus (wt, floxed and deleted), and specific primers (F1, F3 and R1) used for *Igf1r* locus analysis by PCR. (c) Expected amplicon sizes in PCR assays to identify presence of the *UBC-CreERT2* transgene and the different *Igf1r* allelic forms. *IL2* primers were used as constitutive positive controls when genotyping hemizygous *UBC-CreERT2* mice.

3.4 Generation of the BLM-induced acute lung injury mouse model

Tamoxifen (TMX) was administered daily for five consecutive days to four-week-old *UBC-Cre-ERT2*; *Igf1r^{fl/fl}* and *Igf1r^{fl/fl}* mice to induce a postnatal *Igf1r* gene conditional deletion in *UBC-Cre-ERT2*; *Igf1r^{fl/fl}* mice (López *et al.*, 2015). Then, six-week-old *CreERT2* and *Igf1r^{fl/fl}* male or female mice (equal sex proportions) were intra-tracheally instilled with either a single dose of 2.5 μ l/g body weight of BLM sulfate (5 U/kg) (EMD Millipore, Billerica, MA) in saline (2 U/ml) or saline (SAL) at D0, under a ketamine-xylazine anesthetic combination in saline (100:10 mg/kg respectively; 10 μ l/g). Animals were monitored for 21 days to determine survival rates of both *CreERT2* and *Igf1r^{fl/fl}* mice after BLM challenge. Those animals that reached the human endpoint, as specified by the CIBIR Bioethics Committee protocol ref. 13/12, were also considered to be dead animals at each time point. The human endpoint criteria were applied when there was severe involvement of one of the specific (body weight, respiratory pattern and bleeding), or moderate involvement of two or more of the general (appearance, natural behavior) or specific parameters occurred. For acute lung injury studies, animals were sacrificed and tissues were collected at D3 (**Figure 16**).

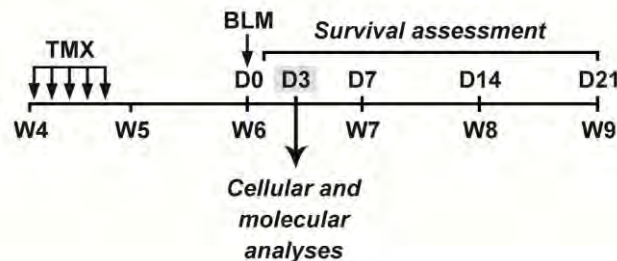


Figure 16. Establishment of the BLM-mediated acute lung injury model. TMX was administered daily for five consecutive days to four-week-old *UBC-CreERT2*; *Igf1r^{fl/fl}* mice to induce a postnatal *Igf1r* gene conditional deletion using *Igf1r^{fl/fl}* mice as experimental controls. Then, six-week-old *CreERT2* and *Igf1r^{fl/fl}* mice were intra-tracheally instilled with 2.5 μ l/g BLM (2 U/ml) or saline using a ketamine-xylazine anesthetic combination. Cellular and molecular analyses were assessed on day (D) 3, based on survival curves. TMX, tamoxifen; BLM, bleomycin.

3.5 Establishment of the murine models of experimental asthma

Eight- to 10-week-old female mice were intranasally (i.n.) challenged with daily consecutive doses of 40 µg of HDM extract (Greer Laboratories Inc, Lenoir, NC) in 20 µl of PBS (2 mg/ml) or equal volume of PBS under light isoflurane anesthesia. Females were used due to their reported higher susceptibility to allergic airway inflammation (Melgert *et al.*, 2005). Four different protocols of HDM exposure were used: 1) *CreERT2* and *Igf1r^{fl/fl}* mice were administered HDM extract five days a week during four weeks and lung function assessment and bronchoalveolar lavage fluid (BALF), serum and lungs were collected 24 h after the last exposure on day 28 (chronic HDM model) (**Figure 17**); 2) inbred C57Bl/6 mice were given seven doses of HDM extract or PBS and BALF and lungs were collected 24 h after the last exposure on days (D) 3, D5 or D7 (acute HDM protocol) (**Figure 18a**); 3) *UBC-CreERT2*; *Igf1r^{fl/fl}* and *Igf1r^{fl/fl}* mice were treated with tamoxifen (TMX) for five consecutive days at four weeks of age to induce a postnatal *Igf1r* gene deletion in *UBC-CreERT2*; *Igf1r^{fl/fl}* mice (López *et al.*, 2015). After TMX treatment, *CreERT2* and *Igf1r^{fl/fl}* mice were administered with seven doses of HDM extract or PBS and bone marrow, serum, BALF and lungs were harvested 24 h after last dose on D7 (prophylactic protocol) (**Figure 18b**); and 4) *UBC-CreERT2*; *Igf1r^{fl/fl}* and *Igf1r^{fl/fl}* mice were challenged with seven (first set of animals non-treated with TMX and sacrificed at D7) or fourteen doses of HDM extract or PBS (second set of animals receiving five consecutive intraperitoneal TMX injections between D7 and D11 to induce *Igf1r* deletion in *UBC-CreERT2*; *Igf1r^{fl/fl}* mice, to generate *CreERT2* mice), followed by serum, BALF and lung tissue collection 24 h after the last exposure (therapeutic protocol) (**Figure 18c**). All animals were bred and maintained under specific pathogen-free conditions in laminar flow caging at CIBIR and Karolinska Institutet animal facilities.

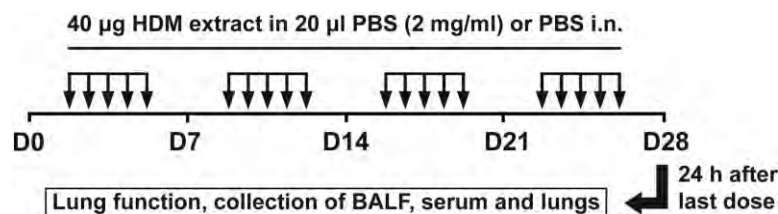


Figure 17. Protocol for chronic exposure to HDM. Eight- to 10-week-old female *CreERT2* mice and their controls (*Igf1r^{fl/fl}*) were challenged by intranasal administration of 40 µg of house dust mite (HDM) extract in 20 µl of phosphate buffered saline (PBS) (2 mg/ml) or equal volume of PBS under inhaled isoflurane anesthesia, five days a week during four weeks. Lung function assessment and BALF, serum, and lungs were collected 24 h after the last exposure on day (D) 28.

3.6 In vivo measurement of lung function

After chronic exposure to HDM *CreERT2* and *Igf1r^{fl/fl}* mice were deeply anesthetized with a combination of 2.5 µl/g of hypnorm (VetaPharma Ltd, Leeds, UK) and 12.5 µg/g of midazolam (Hameln Pharmaceuticals GmbH, Hameln, Germany). Lung function following exposure to increasing concentrations of aerosolized methacholine (0, 15, 65 and 250 mg/ml) was evaluated using the flexiVent system (Scireq, Montreal, QC, Canada). Newtonian resistance (Rn), tissue damping (G), and tissue elastance (H) were determined by assuming a constant-phase model.

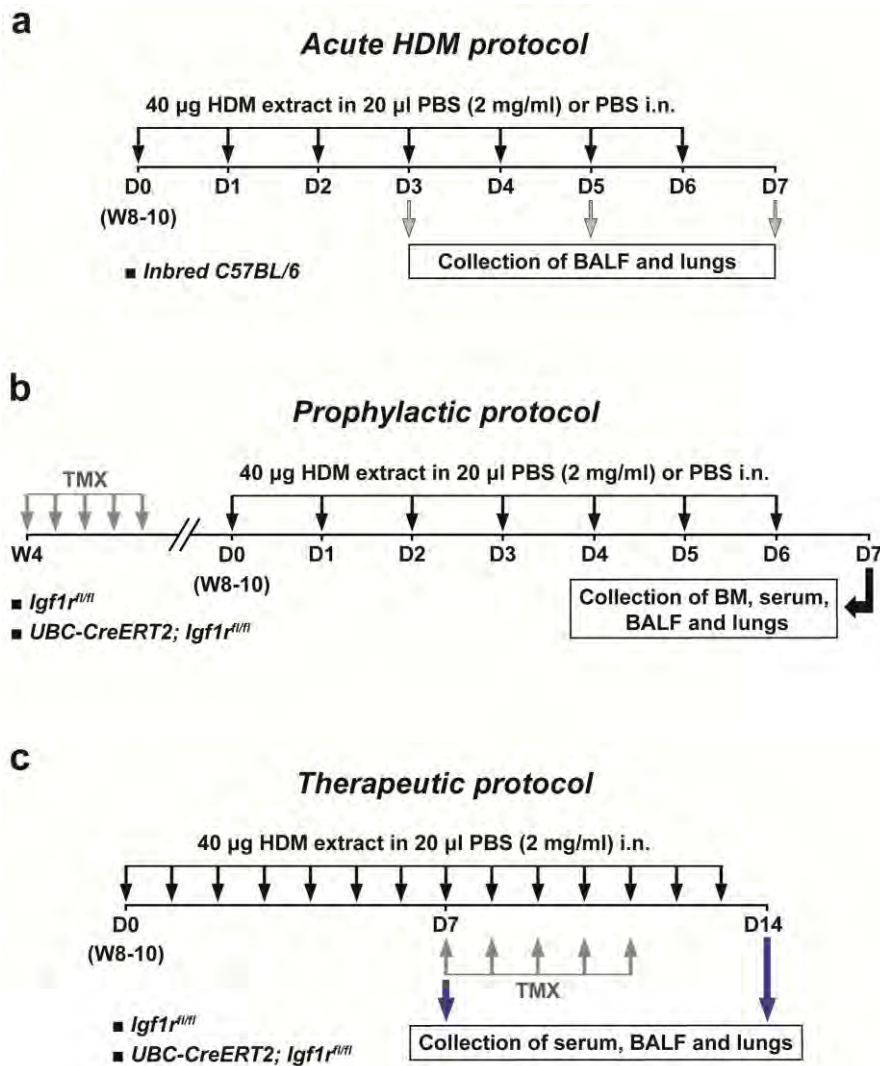


Figure 18. Experimental protocols for acute exposure to HDM and prophylactic and therapeutic induction of *Igf1r* deficiency. Eight- to 10-week-old (W8-10) female mice were intranasally challenged with daily consecutive doses of 40 µg of HDM extract in 20 µl of PBS (2 mg/ml) or equal volume of PBS. (a) Inbred C57BL/6 mice were given seven doses of HDM extract or PBS, and BALF and lungs were collected 24 h after the last exposure on days [D] 3, D5 or D7 (acute HDM protocol). (b) *UBC-CreERT2; Igf1r^{fl/fl}* and *Igf1r^{fl/fl}* mice were treated with tamoxifen (TMX) for five consecutive days at four weeks of age (W4) to induce a postnatal *Igf1r* gene deletion in *UBC-CreERT2; Igf1r^{fl/fl}* mice, and were administered later with seven doses of HDM extract or PBS and bone marrow, serum, BALF and lungs were harvested 24 h after last dose on D7 (prophylactic protocol). (c) *UBC-CreERT2; Igf1r^{fl/fl}* and *Igf1r^{fl/fl}* mice were challenged with seven (first set of animals non-treated with TMX and sacrificed at D7) or fourteen doses of HDM extract or PBS (second set of animals receiving five consecutive intraperitoneal TMX injections between D7 and D11 to induce *Igf1r* deletion in *UBC-CreERT2; Igf1r^{fl/fl}* mice, to generate *CreERT2* mice). Serum, BALF and lungs were collected 24 h after the last exposure (therapeutic protocol). HDM, house dust mite; PBS, phosphate buffered saline; TMX, tamoxifen.

3.7 Tissue collection and preparation

Before tissue collection, animals were euthanized by intraperitoneal injection of 10 μ l/g of a ketamine-xylazine anesthetic combination in saline (300:30 mg/kg respectively). Blood was then collected by cardiac puncture, and serum was obtained by centrifugation at 3000 \times g and stored at -80°C until further usage.

Bone marrow (BM) was isolated (only from *CreERT2* and *Igf1r^{fl/fl}* mice after BLM treatment or acute HDM exposure), from one single femur per animal. After dissection, the femoral heads were incised and femurs were positioned in bottom perforated 0.5 ml tubes placed inside 1.5 ml tubes. After centrifugation at 10000 \times g for 15 seconds, BM was suspended in 500 μ l PBS and centrifuged at 300 \times g for 5 min at 4 °C. Following aspiration of the supernatant, BM pellets were resuspended in 500 μ l of ACK lysing buffer (Thermo Fisher Scientific, Waltham, MA). After 10 minutes of incubation, tubes were centrifuged at 300 \times g for 5 min at 4 °C and following aspiration of the supernatant, 1 ml of PBS was added. Total cell number in BM (cells/ml) was counted in a cell counting chamber (Biosigma S.r.l., Venice, Italy) following manufacturer's guidelines and 250000 cells were used for cytospin preparations which were obtained by centrifugation of the slides at 1500 rpm for 5 min.

On the other hand, lungs from BLM- or HDM-challenged *CreERT2* and *Igf1r^{fl/fl}* mice were lavaged twice with 0.8 ml cold 1X PBS (Thermo Fisher Scientific) to obtain approximately 1 ml of BALF. Then, BALF was centrifuged at 13000 rpm for 5 min at 4 °C and the supernatant was stored at -80 °C to subsequently assess total protein concentration in BALF using the Pierce BCA Protein Assay Kit (Thermo Fisher Scientific). Hereafter, the pellet was resuspended in 500 μ l of ACK lysing buffer (Thermo Fisher Scientific) and after 10 minutes of incubation, tubes were centrifuged at 13000 rpm for 5 min at 4 °C, the supernatant was discarded and 1 ml of PBS was added to the pellet. Cytospin preparations were obtained by centrifugation of slides at 1500 rpm for 5 min. Total cell number in BALF (cells/ml) was counted in a cell counting chamber (Biosigma S.r.l., Venice, Italy) following manufacturer's guidelines and 50000 cells were used for cytospin preparations which were obtained by centrifugation of the slides at 1500 rpm for 5 min.

Organs (including left lungs) were harvested, formalin-fixed, embedded in paraffin and cut into 3 μ m sections for histopathological evaluation or immunohistochemistry. Right lung lobes were separated and snap-frozen in liquid nitrogen for quantitative real-time PCR (qRT-PCR), RNAseq, Western Blot (WB) and ELISA analyses. The rest of organs were snap-frozen in liquid nitrogen for qRT-PCR analysis.

3.8 Histopathological analyses and immunostaining

3.8.1 Hematoxylin and eosin (H&E) staining

H&E staining was performed for the quantification of hepatocyte number, diameter of seminiferous tubules and bronchiolar epithelium thickness in unchallenged *CreERT2* and *Igf1r^{fl/fl}* mice; for the determination of neutrophil infiltration grade into the lung and quantification of inflamed lung areas in BLM-challenged *CreERT2* and *Igf1r^{fl/fl}* mice and for the quantification of inflamed lung areas and airway thickness in HDM-exposed inbred C57BL/6, *CreERT2* and *Igf1r^{fl/fl}* mice. Quantification of both the hepatocyte number and diameter of seminiferous tubules was performed in at least 5 fields per section

per animal. Determination of neutrophil infiltration grade was assessed in lung perivascular areas and expressed as the number of neutrophils to total cell infiltrates, evaluating 5 different fields per animal. Quantification of inflammation was expressed as the percentage of inflamed lung area to total section surface, defining “inflamed lung areas” as darker stained foci, where inflammatory cells accumulate massively. Airway thickness was assessed by means of three different measurements per airway. Diameter of seminiferous tubules was measured using the Fiji open-source image processing software package v1.48r (<https://fiji.sc>). Fiji was also used to delimitate inflamed lung areas, but also to quantify airway thickness and epithelium length.

Paraffin-embedded tissue sections were dewaxed at 60 °C for 30 min, incubated in xylene for 14 min, transferred sequentially into 100% EtOH, 96% EtOH, 70% EtOH and deionized water for 4 minutes. Sections were then stained with Harris hematoxylin (Panreac, Barcelona, Spain) for 1-2 min. After washing with abundant tap water, differentiation was performed by submerging the sections in 1% acid alcohol (1% HCl in 70% EtOH) for 3 secs. Sections were washed again with tap water for 2 min and stained with an alcoholic solution of eosin (Panreac) for 1 min. Finally, after a last wash, sections were dehydrated sequentially in 96% EtOH and 100% EtOH for 1 min, incubated in xylene for 5 min, mounted with Eukitt mounting medium (O. Kindler GmbH & Co, Freiburg, Germany) and photo-documented under a light microscope (Nikon Instruments, Inc, Tokyo, Japan).

3.8.2 Periodic acid-Schiff (PAS) and Masson’s trichrome staining

Periodic acid-Schiff (PAS) and Masson’s trichrome staining protocols served to assess the airway epithelial goblet cell abundance and collagen deposition in the murine models of experimental asthma. Quantification of PAS-positive cells was expressed as the number of positive cells per epithelium length (mm). Both the goblet cell abundance and collagen deposition were performed evaluating a minimum of 4 airways per animal. Fiji open-source image processing software package v1.48r was used to quantify the percentage of collagen area as well as for epithelium length measurements.

Paraffin-embedded lung sections were dewaxed at 60 °C for 30 min, incubated in xylene for 14 min, transferred sequentially into 100% EtOH, 96% EtOH, 70% EtOH and deionized water for 4 minutes. Sections were then placed in a humidity chamber prior to start with Periodic acid-Schiff (PAS) and Masson’s trichrome staining protocols.

Periodic acid-Schiff (PAS): Lung sections were incubated in alcian blue (pH 2.5) for 20 min, washed with distilled water, incubated in 0.5% periodic acid for 5 min and washed again with distilled water. Then, sections were stained with Schiff reactive for 20 min, washed with distilled water and stained with Harris hematoxylin (Panreac). After a last wash with tap water, sections were dehydrated sequentially in 96% EtOH and 100% EtOH for 1 min, incubated in xylene for 5 min, mounted with Eukitt mounting medium (O. Kindler GmbH & Co) and photo-documented under a light microscope (Nikon Instruments, Inc).

Masson’s trichrome staining: Masson’s trichrome staining was carried out using a masson trichrome kit with aniline blue (Bio-Optica, Milan, Italy) following the manufacturer’s instructions. Finally, after a last wash with tap water, sections were dehydrated, mounted and photo-documented in the same way as in the Periodic acid-Schiff protocol.

3.8.3 May-Grünwald/Giemsa staining

May-Grünwald/Giemsa staining was carried out on BALF cytospin preparations obtained from BLM-challenged *CreERT2* and *Igf1r^{fl/fl}* mice and from the murine models of experimental asthma. In addition, May-Grünwald/Giemsa staining was also performed on BM cytospin preparations obtained from *CreERT2* and *Igf1r^{fl/fl}* mice after BLM treatment or acute HDM exposure.

Following air-drying, BALF and BM cytospin preparations were stained with a solution composed by methanol (EMD Millipore, Billerica, MA) and May-Grünwald (Sigma-Aldrich) (1:5 dilution of methanol in May-Grünwald solution) for 10 min. Then, slides were washed three times with distilled water for 1 min and stained with a solution composed by Giemsa (Sigma-Aldrich) and distilled water (1:10 dilution of Giemsa in distilled water). Finally, after three washes in distilled water for 1 min, slides were allowed to air-dry and mounted with Eukitt mounting medium (O. Kindler GmbH & Co). Differential cell counts were performed counting a minimum of 300 cells per slide or 5 fields per slide in a blinded fashion in BALF and BM cytospins, respectively. Cells were distinguished into macrophages, lymphocytes, neutrophils, and eosinophils by standard morphology criteria and cytospin preparations were photo-documented under a light microscope (Nikon Instruments, Inc). Additionally, the average number of red blood cells per high-power field was obtained by evaluating 5 different fields per slide on BALF cytospin preparations.

3.8.4 TUNEL detection of apoptotic cells

Hepatic and lung cells undergoing apoptosis were identified in unchallenged *CreERT2* and *Igf1r^{fl/fl}* mice using a TUNEL (TdT-mediated dUTP Nick-End Labeling) assay kit (DeadEnd Colorimetric System, Promega, Madison, WI) following the manufacturer's instructions. At least 2 slides per animal were counted and density of cells per 10⁵ μm² (liver) or per cm² (lung) was quantified using the Fiji open-source image processing software package v1.48r. Apoptotic nuclei stained dark brown were counted using a light microscope (Nikon Instruments, Inc).

3.8.5 Immunohistochemical staining

Streptavidin-biotinylated immunoperoxidase method was used for visualization of the Ki67 antigen in liver and lungs of unchallenged *CreERT2* and *Igf1r^{fl/fl}* lungs and in perivascular and alveolar areas of BLM-challenged *CreERT2* and *Igf1r^{fl/fl}* lungs. Streptavidin-biotinylated immunoperoxidase method was also used for visualization of CD3 antigen in perivascular areas of BLM-challenged *CreERT2* and *Igf1r^{fl/fl}* lungs to determine the lymphocyte infiltration grade. Both the proliferation indices and lymphocyte infiltration grade were expressed as the number of Ki67⁺ or CD3⁺ cells to total cell numbers, evaluating at least 5 fields per animal.

Paraffin-embedded sections were dewaxed at 60 °C for 30 min, incubated in xylene for 14 min, transferred sequentially into 100% EtOH, 96% EtOH, 70% EtOH and deionized water for 4 minutes. Antigen retrieval for Ki67 was performed immersing the slides in a boiling solution of 1 mM EDTA (pH 9.0) for 25 min, and followed by a 15 min cool down in the same buffer and for CD3, slides were immersed in a boiling solution of 10 mM Citrate (pH 6.0) for 25 minutes, and followed by a 15 min cool down in the same buffer. Then, sections were washed in 1X PBS for 10 minutes and twice in PBS-Triton (0.1%) and Glycine (10 mM) for 5 min. Endogenous peroxide was blocked by 0.2% H₂O₂ for 15 min, and sections were

washed three times with PBS-Triton (0.1%) for 5 min and blocked with 4% goat serum in PBS-Triton (0.1%) and BSA (2%) for 1 h at room temperature. Hereafter, slides were incubated at 4°C overnight with primary antibodies anti-Ki67 (Clone SP6, 1:200 Master Diagnostica SL, Granada, Spain) and CD3 (ab5690 1:200, Abcam, Cambridge, UK) diluted in the appropriate blocking solution, and then washed three times with PBS-Triton (0.1%) for 5 min. Sections were treated with biotinylated goat anti-rabbit antibody (BA-1000, 1:300, Vector Laboratories, Inc, Burlingame, CA) diluted in 1X PBS, washed three times with PBS-Triton (0.1%) for 5 min and visualized with avidin-biotin-peroxidase complex (Vector Elite ABC kit; Vector Laboratories) and 3,3'-diaminobenzidine substrate (Sigma-Aldrich). Finally, sections were stained with Harris haematoxylin (Panreac) for 1-2 min, washed with distilled water, differentiated in 1% acid alcohol (1% HCl in 70% EtOH) for 3 secs, dehydrated sequentially in 50% EtOH, 70% EtOH, 90% EtOH and 100% EtOH for 5 min, incubated in xylene for 5 min and mounted with Eukitt mounting medium (O. Kindler GmbH & Co). Sections were photo-documented under a light microscope (Nikon Instrumentns, Inc).

3.8.6 Fluorescent immunostaining

Expression of IGF1R was evaluated in kidneys, liver and testis of unchallenged *CreERT2* and *Igf1^{fl/fl}* mice. In addition, assessment of macrophages and alveolar type 2 cell numbers and HIF1A relative fluorescence were evaluated in BLM-challenged *CreERT2* and *Igf1^{fl/fl}* lungs. Quantification of macrophages and alveolar type 2 cells using F4/80 and SFTPC antibodies, respectively, was assessed in 5 different alveolar areas and expressed per unit area. Macrophage diameters were measured and volumes were extrapolated using the sphere volume formula. HIF1A expression was evaluated in 5 different alveolar fields using the Fiji open-source image processing software package v1.48r as previously described (McCloy *et al.*, 2014). On the other hand, fluorescent immunostaining for GLUTUB, MUC5AC, SGB1A1 and α -SMA in chronically HDM-exposed *CreERT2* and *Igf1^{fl/fl}* mice was evaluated in four airways per animal. Quantification of SCGB1A1, GLUTUB, and MUC5AC-positive cells was expressed as the number of positive cells per epithelium length (mm). Smooth muscle (α -SMA) thickness was assessed by means of three different measurements per airway using the using the Fiji open-source image processing software package v1.48r.

Paraffin-embedded sections were dewaxed at 60 °C for 30 min, incubated in xylene for 14 min, transferred sequentially into 100% EtOH, 96% EtOH, 70% EtOH and deionized water for 4 minutes. Then, sections were subjected to an antigen retrieval procedure: antigen retrieval for α -SMA and IGF1R was performed immersing the slides in a boiling solution of 1 mM EDTA (pH 9.0) for 25 min, and followed by a 15 min cool down in the same buffer; for F4/80 and SFTPC slides were immersed in 10 mM TE buffer with Proteinase K (Roche, Basel, Switzerland) (20 mg/ml) for 15 min at 37°C and followed by a 15 min cool down and for GLUTUB, HIF1A, MUC5AC and SCGB1A1, slides were immersed in a boiling solution of 10 mM Citrate (pH 6.0) for 25 minutes, and followed by a 15 min cool down in the same buffer. Then, sections were washed in 1X PBS for 10 minutes and twice in PBS-Triton (0.1%) and Glycine (10 mM) for 5 min and blocked with 10% normal goat serum (Jackson ImmunoResearch Laboratories, Inc., Baltimore, PA) (α -SMA, IGF1R and MUC5AC) or with 10% normal donkey serum (Jackson ImmunoResearch Laboratories, Inc., Baltimore, PA) (F4/80, GLUTUB, HIF1A, SCGB1A1 and SFTPC) in PBS-Triton (0.1%) and Glycine (10 mM) for 1 h at RT. Slides were then incubated at 4 °C overnight with primary antibodies diluted in the

appropriate blocking solution: anti- α -SMA (Clone 1A4 1:100 and 1:500, Sigma-Aldrich), anti-F4/80 (Clone MCA497GA 1:100, Bio-Rad, Langford, UK), anti-GLUTUB (Clone TU-20 1:300, EMD Millipore, Billerica, MA), HIF1A antibody (ab2185 1:100, Abcam), anti-IGF1Rb (C-20, sc-713 1:100, Santa Cruz Biotech Inc, Dallas, TX), MUC5AC (Clone 45M1 1:50, Thermo Fisher Scientific), anti-SCGB1A1 (Clone T18 1:400, Santa Cruz Biotech Inc) and anti-SFTPC (AB3786 1:1500, EMD Millipore, Billerica, MA). After three washes in PBS-Triton (0.1%) and Glycine (10 mM) for 5 min, sections were incubated for 1 h with the following secondary antibodies diluted in 1X PBS: Alexa Fluor 488® chicken anti-rat (1:1000, Thermo Fisher Scientific) for F4/80; Alexa Fluor 546® donkey anti-rabbit (1:500, Thermo Fisher Scientific) for GLUTUB, HIF1A and SFTPC; Alexa Fluor 546® goat anti-rabbit (1:500, Thermo Fisher Scientific) for IGF1R; Alexa Fluor 633® donkey anti-goat (1:400, Thermo Fisher Scientific) for SCGB1A1 and MUC5AC and Alexa Fluor 633® goat anti-mouse (1:500, Thermo Fisher Scientific) for α -SMA. Finally sections were washed three times with 1X PBS for 5 min and mounted with ProLong Gold Antifade Reagent with DAPI (Life technologies) to be examined under a confocal microscope (Leica Microsystems, Wetzlar, Germany).

3.9 RNA isolation, reverse transcription and qRT-PCR

Mechanical disruption of tissues from unchallenged *CreERT2* and *Igf1r^{f/f}* mice and BLM- or HDM-challenged *CreERT2* and *Igf1r^{f/f}* mice was performed using a tissue homogenizer T8 Ultra Turrax (IKA Works Inc, Staufen, Germany).

3.9.1 Unchallenged *CreERT2* and *Igf1r^{f/f}* mice

Kidneys, heart, liver, testes and cochlea were homogenized in a Tissue Lyser (Qiagen, Hilden, Germany). Total RNA was subsequently isolated using RNeasy Plus Mini Kit in a QIAcube (Qiagen) according to the manufacturer's instructions. Total RNA obtained from spleen and lung was isolated using TRIzol Reagent (Invitrogen, Carlsbad, CA), treated with 2.72 KU/ μ l RNase-free DNase (Qiagen) and purified through RNeasy columns (Qiagen) following the manufacturer's instructions. The quantity and quality of total RNA were assessed on a NanoDrop Spectrophotometer (Thermo Fisher Scientific), respectively. Total RNA obtained from individual mice was reverse-transcribed to cDNA using the High-Capacity cDNA Reverse Transcription Kit (Applied Biosystems, Foster City, CA) and qRT-PCR was conducted on Applied Biosystems 7900HT. The expression level of *Igf1r* TaqMan® probe (Mm00802831_m1; Applied Biosystems) was studied in the different tissues and two housekeeping genes were used as endogenous controls to normalize results: mouse ribosomal phospho-protein P0 (*Rplp0*) and 18S ribosomal RNA (*Rn18s*). *Igf1r* quantitative real-time PCR of D56 lung samples was carried out with SYBR Green Technology (Power SYBR® in a 7300 Real Time PCR System, Applied Biosystems, Carlsbad, CA) using the following pair of primers: 5'-CCAGAGCAAAGGGGACATAA-3' and 5'-TGATTCCGGTTCTTCCAGGTC-3'.

3.9.2 BLM- or HDM-challenged *CreERT2* and *Igf1r^{f/f}* mice

Total RNA obtained from inferior lung lobes was isolated using TRIzol Reagent (Invitrogen), treated with 2.72 KU/ μ l RNase-free DNase (Qiagen) and purified through RNeasy columns (Qiagen) following the manufacturer's instructions. The quantity and quality of total RNA was assessed on a NanoDrop

Spectrophotometer (Thermo Fisher Scientific). cDNA was generated using SuperScript II First-Strand Synthesis System (Invitrogen) according to manufacturer guidelines.

Table 1. Primer sets used for qRT-PCR.

Gene	Accession No.	Forward primer (5'-3')	Reverse primer (5'-3')
<i>Acta2</i>	NM_007392.3	AATGGCTCTGGGCTCTGTAA	CTCTTGCTCTGGGCTTCATC
<i>Adgre1</i>	NM_010130.4	ATACCCTCCAGCACATCCAG	CTCCCATCCTCCACATCAGT
<i>Aqp5</i>	NM_009701	GGTGGTCATGAATCGGTTTCAGC	GTCCCTCCTCTGGCTCATATGTG
<i>Ccl2</i>	NM_011333.3	CACCAGCCAACCTCTCACTGA	CGTAACTGCATCTGGGCTGA
<i>Ccl5</i>	NM_013653.3	CCAACCCAGAGAAGAAGTGG	AGCAAGCAATGACAGGGAAG
<i>Ccl11</i>	NM_011330.3	GAGAGCCTACAGAGCCCAGA	ACCGTGAGCAGCAGGAATAG
<i>Cd4</i>	NM_013488.2	ATGTGGAAGGCAGAGAAGGA	TGGGGTATCTTGAGGGTGAG
<i>Cd209a</i>	NM_133238.5	GAGATGACGGCTGGAATGAC	AGATGGTGGAGGGAGTTGG
<i>Col1a1</i>	NM_007742.4	CGGAGAAGAAGGAAAAACGAG	CAGGGAAACCACGGCTAC
<i>Csf1</i>	NM_007778.4	CGAGTCAAACAGAGCAACCAA	TGCTTCTGGGTCAAAAATC
<i>Cxcl1</i>	NM_008176.3	ATCCAGAGCTTGAAGGTGTTG	GTCTGTCTTCTTCTCCGTTACTT
<i>Foxm1</i>	NM_008021.4	CCTGCTTACTGCCCTTTCTCT	CACACCCATCTCCCTACACC
<i>Foxo1</i>	NM_019739.3	TTCTCTCGTCCCAACATCT	TGCTGTCTGAAGTGTCTGC
<i>Gpx8</i>	NM_027127.2	ACATTCCCCATCTTCCACAA	ATTCACCTTGCTCCTTCT
<i>Hif1a</i>	NM_010431.2	TTGGAAGTGGTGGAAAACTG	ACTTGGAGGGCTTGAGAAAT
<i>Igfbp3</i>	NM_008343.2	GCCCTCTGCCTTCTTGATTT	TCACTCGGTTATGGGTTTCC
<i>Igfbp5</i>	NM_010518.2	GATGAGACAGGAATCCGAACAAG	AATCCT TTGCGGTACAGTTG
<i>Igf1</i>	NM_010512	CAGAAGCGATGGGAAAAAT	GTGAAGGTGAGCAAGCAGAG
<i>Igf1r</i>	NM_010513	ATGGCTTCGTTATCCACGAC	AATGGCGGATCTTCACGTAG
<i>Il1b</i>	NM_008361.3	GCAACTGTTCTGAACTCAACT	ATCTTTTGGGGTCCGTCAACT
<i>Il4</i>	NM_021283.2	CCTCACAGCAACGAAGAACA	CGAAAAGCCGAAAGAGTC
<i>Il5</i>	NM_010558.1	GAAGTGCTGGAGATGGAACC	GGATGAGGGGGAGGGAGTAT
<i>Il6</i>	NM_031168.1	ACGGCCTTCCCTACTTCACA	CATTTCCACGATTTCCAGAG
<i>Il10</i>	NM_010548.2	GCACTACCAAAGCCACAAGG	TAAGAGCAGGCAGCATAGCA
<i>Il13</i>	NM_008355.3	GCCTCCCCGATACCAAAAT	CTTCTCCTCAACCTCCTC
<i>Il25</i>	NM_080729.3	AAGCCCTCAAAGCCCTAC	TCTCCCAAGTCTCCATC
<i>Il33</i>	NM_133775.2	GCCTTGCTCTTTCTTTTCTC	TCGGTTGTTTCTTGTTTTCG
<i>Insr</i>	NM_010568.2	TCCTGAAGGAGCTGGAGGAGT	CTTTCGGGATGGCCTGG
<i>Ly6g</i>	NM_001310438.1	CCTGGTTTCAGTCCTTCTGC	CACACACTACCCCAACTCA
<i>Marco</i>	NM_010766.2	TCCCTGTGATGGAGACCTTC	GTGAGCAGGATCAGGTGGAT
<i>Muc5ac</i>	NM_010844.1	CACACACAACCACTCAACCA	TCTCTCTCCGCTCCTCTCAA
<i>Ptgs2</i>	NM_011198.4	GGAGGCCAAGTGGGTTTTA	TGATGGTGGCTGTTTTGGTA
<i>Rn18s</i>	NR_003278.3	ATGCTCTTAGCTGAGTGTCCCG	ATTCTTAGCTGCGGTATCCAGG
<i>Scgb1a1</i>	NM_011681	ATGAAGATCGCCATCACAATCAC	GGATGCCACATAACCAGACTCT
<i>Sftpa1</i>	NM_023134.4	CCATCGCAAGCATTACAAAG	CACAGAAGCCCCATCCAG
<i>Sftpb</i>	NM_147779.2	CTGCTGCTTCTACCTCTG	ATCCTCACACTCTTGGCACA
<i>Sftpc</i>	NM_011359	GAAGATGGCTCCAGAGGCATC	GGACTCGGAACCAAGTATCATGC
<i>Sftpd</i>	NM_009160.2	TGAGAATGCTGCCATACAGC	GAATAGACCAGGGGCTCTCC
<i>Tnf</i>	NM_013693.3	GCCTCTTCTATTCTGCTTG	CTGATGAGAGGGAGGCCATT
<i>Spdef</i>	NM_013891.4	GGCCAGCCATGAACTATGAT	GGTAGACAAGGCCTGAGAG
<i>Tslp</i>	NM_021367.2	AAATGGGAAATGAGCAATAGAC	GCAGGGGAGGTGAGAAAGAC

Then, cDNA samples were amplified by qRT-PCR in triplicate reactions for each primer pair assayed (**Table 1**) on a 7300 Real-Time PCR Instrument (Applied Biosystems, Foster City, CA), using SYBR green master mix (Applied Biosystems) (HDM-challenged *CreERT2* and *Igf1r^{fl/fl}* lungs) and SYBR Premix Ex Taq (Takara Bio Inc., Kusatsu, Japan) (BLM-challenged *CreERT2* and *Igf1r^{fl/fl}* lungs). Results were normalized using 18S rRNA gene as endogenous control. The qRT-PCR conditions were as follows: 95 °C for 10 min; 40 cycles of 95 °C for 15 s, 60 °C for 1 min, 72 °C for 30 s and 95 °C for 15 s, 60 °C for 1 min, 95 °C for 15 s, 60 °C for 15 s (SYBR green master mix) (BLM-challenged lungs); and 95 °C for 2 min; 40 cycles of 95 °C for 30 s, 60 °C for 30 s and 95 °C for 15 s, 60 °C for 1 min, 95 °C for 15 s, 60 °C for 15 s (Premix Ex Taq) (HDM-challenged lungs).

3.10 Lung transcriptome analysis

RNAseq analysis was performed on eight-week-old unchallenged *CreERT2* and *Igf1r^{fl/fl}* lungs (n = 3 per genotype). Approximately, 1 µg of total RNA from each sample was submitted to the CIBIR Genomics Core Facility for sequencing. Briefly, after verifying RNA quality in an Experion Bioanalyzer (Bio-Rad Laboratories, Hercules, CA), TruSeq total RNA libraries were generated according to the manufacturer's instructions (Illumina Inc, San Diego, CA). The libraries were sequenced in a Genome Analyzer Iix (Illumina Inc) to generate 150 single-end reads. *Mus musculus* GRCm38.71 (FASTA) from the Ensemble database was used as the reference genome. After removing adapter sequences with the Cutadapt software (Martin 2011), mapping to the reference genome was performed with TopHat2 (version 2.5) (Trapnell *et al.*, 2012). Gene expression quantification, normalization, and statistical analyses were performed with SeqSolve (Integromics, Granada, Spain). Expression data were normalized by calculating the fragments per kilobase of exon per million fragments mapped (FPKM) reads for each gene. *Igf1r*-transcriptionally regulated genes involved in biological processes were classified according to GO and Keyword annotations. Additionally, a PubMed search, and the Genecards and OMIM tools were used to help assign biological functions.

3.11 Western blot analysis

Superior lung lobes from BLM-exposed and chronically HDM-exposed *CreERT2* and *Igf1r^{fl/fl}* mice were solubilized in a 10 mM Tris/HCl (pH 7.4) buffer containing 0.1% sodium dodecyl sulfate, a protease inhibitor mixture, and DNase (Promega) using a tissue homogenizer T8 Ultra Turrax (IKA Works Inc). Total protein concentration was determined using the Pierce BCA Protein Assay Kit (Thermo Fisher Scientific) following manufacturer's instructions in a POLARstar Omega (Biogen Idec, Cambridge, MA).

Samples were separated in NuPAGE Novex 4–12% Bis-Tris Gel (Invitrogen) and transferred to a polyvinylidene difluoride membrane (EMD Millipore, Burlington, MA). Membranes were incubated with primary antibodies for IGF1R (#3027 Cell Signalling Inc., Danvers, MA) and beta-Actin (ab6276 Abcam, Cambridge, UK) at 1:1000 and 1:30000 dilutions respectively, and then incubated with horseradish peroxidase-conjugated anti-rabbit or anti-mouse antibodies (DAKO, Agilent technologies, Santa Clara, CA) for IGF1R and beta-Actin respectively, at a 3:10 dilution. Signals were detected using ECL Western Blot Substrate (Thermo Fisher Scientific) and Hyperfilm ECL (GE Healthcare, Little Chalfont, UK). Films were

scanned and signals in the linear range were quantified using the Fiji open-source image processing software package v1.48r and normalized to beta-Actin levels.

3.12 ELISAS

Lung tissues were homogenized in a solution composed by a protease inhibitor cocktail containing PMSF 1 mM, aprotinin 1µg/ml, leupeptin 1µg/ml and pepstatin 1µg/ml (Roche) and a tissue protein extraction reagent (20 ml/g tissue) (Thermo Fisher Scientific), using a tissue homogenizer T8 Ultra Turrax (IKA Works Inc). Lung homogenates were incubated in ice for 30 min and then centrifuged at 14000 xg for 10 min. Supernatants were then collected and stored at -80°C for assessment of cytokine levels. Total protein concentration was determined using the Pierce BCA Protein Assay Kit (Thermo Fisher Scientific) following manufacturer's instructions in a POLARstar Omega (Biogen).

TNF and IL13 levels were determined in homogenized lung lysates from *CreERT2* and *Igf1^{fl/fl}* BLM-exposed mice using left lungs with the help of mouse TNF-alpha Quantikine and IL-13 DuoSet ELISA Kits (R&D Systems, Minneapolis, MN). After chronic exposure to HDM, serum total IgE levels were assessed in *CreERT2* and *Igf1^{fl/fl}* mice with an IgE mouse ELISA kit (Abcam), and IL13 levels were determined in homogenized lung lysates from middle lung lobes with a mouse IL-13 DuoSet ELISA Kit (R&D Systems). In addition, IL10, IL13, IL33 and CCL11 levels were assessed using mouse IL13 DuoSet and IL10, IL33 and CCL11 Quantikine ELISA Kits (R&D systems) in serum and tissue homogenate supernatants from middle lung lobes in inbred C57BL7/6 mice after acute HDM exposure, and after the prophylactic and therapeutic induction of *Igf1r* deficiency in HDM exposed mice. In addition, serum total IgE levels were also assessed using an IgE mouse ELISA kit (Abcam). ELISAS were performed according to manufacturer's guidelines and determination of optical density of each well was performed at 450 nm in a POLARstar Omega (Biogen).

3.13 Statistical analysis

Statistical analyses were performed using SPSS Statistics Software v21 for Windows (IBM, Armonk, NY). Differences between experimental groups were evaluated for significance using the non-parametric Mann-Whitney U test or the Dunn-Sidak test for multiple comparisons. Results are shown as mean values ± standard error of the mean (SEM). For all analyses, a p value < 0.05 was considered statistically significant.

4 RESULTS

4.1 Differential organ phenotypes after postnatal *Igf1r* gene conditional deletion induced by tamoxifen in *UBC-CreERT2; Igf1r^{fl/fl}* double transgenic mice (Paper I)

4.1.1 Generation and genotyping of *UBC-CreERT2; Igf1r^{fl/fl}* double transgenic mice

To determine the effect of IGF1R loss on adult mice, while avoiding the neonatal lethality shown in *Igf1r^{-/-}* mice, *UBC-CreERT2; Igf1r^{fl/fl}* double transgenic mice were generated, which were used to induce postnatal *Igf1r* gene deletion after TMX administration. These mice were generated in two generations by mating *UBC-CreERT2* transgenics (Ruzankina *et al.*, 2007), with *Igf1r^{fl/fl}* mutants (Kloting *et al.*, 2008) (**Figure 13**). *UBC-CreERT2* mice express a CreERT2 fusion protein composed of Cre recombinase and a mutant form of the estrogen receptor with a G400V/M543A/L544A triple mutation, which is selectively activated only in the presence of TMX, but not estrogen (Feil *et al.*, 1997) (**Figure 15a-b**). *Igf1r^{fl/fl}* mice contain loxP sites flanking exon 3 of the *Igf1r* gene (Kloting *et al.*, 2008). *UBC-CreERT2; Igf1r^{fl/fl}* double mutant mice were apparently normal and fertile, and even occasionally used to generate both groups of experimental animals when mated with *Igf1r^{fl/fl}* mice, but only for a unique additional generation. The expected size of PCR products obtained from different alleles, using specific primers for each locus and designed as depicted in **Figure 15a-b**, is shown in **Figure 15c**. Genotyping of extracted tail DNA from the progeny revealed a band of 255 bp exclusively in animals bearing the *UBC-CreERT2* recombinase gene (**Figure 19a**). PCR products for the *Igf1r* locus when using F1/R1 primers resulted in bands at 380 and 300 bp for heterozygous floxed animals (*Igf1r^{fl/+}*) or a single band at 380 bp for *Igf1r^{fl/fl}* homozygous mice (**Figure 19b**). CreERT2 recombinase expression induced after TMX administration in *UBC-CreERT2; Igf1r^{fl/fl}* mice was expected to result in excision of the floxed exon of the *Igf1r* to generate an *Igf1r* deleted allele (**Figure 13** and **Figure 15b**), which results in a complete *Igf1r* gene knockout (Kloting *et al.*, 2008). The expected size of PCR products when using F3/R1 primers was 491 bp for the *Igf1r^Δ* allele and 1,300 bp for the *Igf1r^{fl}* form (**Figure 15c**).

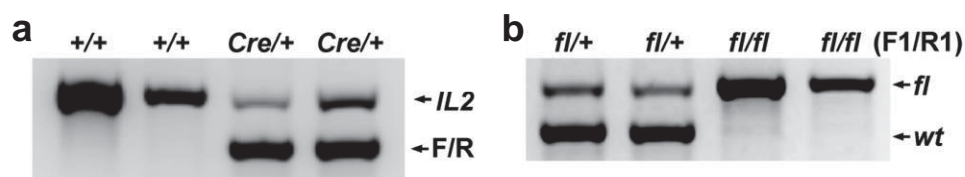


Figure 19. PCR assays for *UBC-CreERT2* using F/R primers and IL2 primers (a) and to genotype *Igf1r* floxed mice using F1/R1 primers (b) in mouse tail DNA.

4.1.2 Prepuberal TMX treatment of *UBC-CreERT2; Igf1r^{fl/fl}* mice causes somatic growth retardation with differential effects on organ weights

To generate and analyze *Igf1r* conditional mutants, *Igf1r^{fl/fl}* (controls) and the newly generated *UBC-CreERT2; Igf1r^{fl/fl}* double mutant mice were treated for 5 days with intra-peritoneal injections of TMX at 4 weeks of age (D0) and weighed weekly until they were 12 weeks old (D56) (**Figure 14**). To prevent sex

effects due to endogenous estrogen present in females, all data presented in this report refer to male TMX-treated mice. Growth curves for each genotype of TMX-treated males were represented as animal body weight gain from D0 to D56 in order to avoid initial weight differences at D0 (**Figure 20**). *UBC-CreERT2; Igf1r^{Δ/Δ} (CreERT2)* mice readily showed a significant growth deficiency at D7. *Igf1r* conditional mutants continue to grow at a slower pace than *Igf1r^{fl/fl}* controls until D35, with their maximal weight gain at D27 (3.22 g mean difference). Interestingly, this effect gradually decreased after this time point, and did not become significant between D42 and the final check at D56 (**Figure 20**).

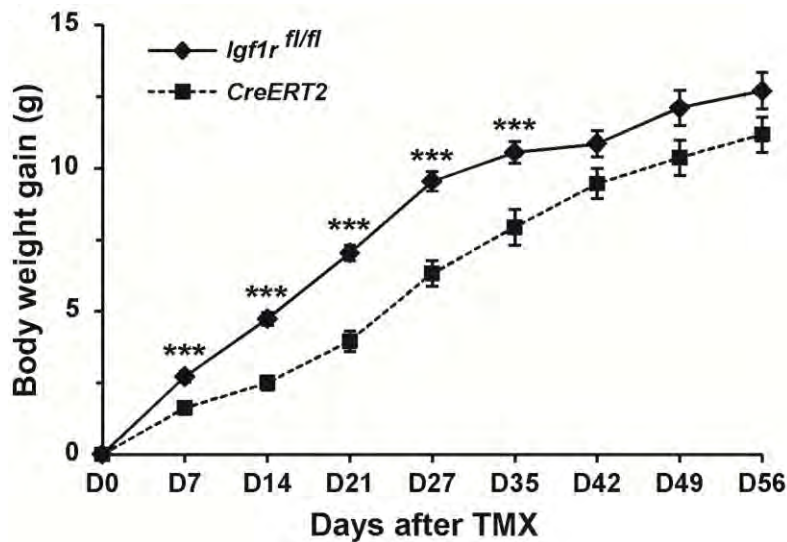


Figure 20. Postnatal growth curves of *Igf1r^{fl/fl}* and *CreERT2* males after TMX treatment. Curves represent the weekly mean of body weight gains of males from each genotype. Body weight gains for each animal were obtained by deducting the weight at a specific time point from its weight at D0. Values are mean \pm SEM. $n = 23$ from D0 to D27 and $n = 16$ from D35 to D56, in *Igf1r^{fl/fl}* mice. $n = 20$ from D0 to D27 and $n = 13$ from D35 to D56, in *CreERT2* mice. TMX, tamoxifen. *** $p < 0.001$; NS, not significant.

Since maximum somatic growth retardation in *CreERT2* males was observed four weeks later, at D27, seven of these mice from each genotype were sacrificed at this stage for further analyses. As expected, these *CreERT2* males also showed significant differences in diminished total body weight and body weight gain with respect to *Igf1r^{fl/fl}* controls (88 and 70%, respectively) (**Table 2**). In order to determine how different organs were contributing to the body growth deficit in TMX-treated *UBC-CreERT2; Igf1r^{fl/fl}* mice, the mean weight of kidney, spleen, heart, brain, liver, lung and testis was determined in *Igf1r^{fl/fl}* and *CreERT2* males (**Table 2**). Surprisingly, only the weight of the brain, and more prominently, the testes, were significantly lower in *CreERT2* than in *Igf1r^{fl/fl}* mice (86 and 47% of controls, respectively). When corrected and expressed as organ to body weight ratios, kidney, liver, lung and brain showed no differences, whereas these ratios were significantly increased in spleen and heart, and strongly decreased in testes (**Table 2**). Altogether these results demonstrate that TMX treatment of prepuberal *UBC-CreERT2; Igf1r^{fl/fl}* mice causes somatic growth retardation with differential effects on organ weights, particularly reducing testis size.

Table 2. Body and organ weight, and ratio of organ to body weight in *Igf1r^{fl/fl}* and *CreERT2* male mice sacrificed at D27 after TMX treatment in 8 week-old mice.

	<i>Igf1r^{fl/fl}</i>	<i>CreERT2</i>	Ratio ^c
Body weight (g)	21.86 ± 0,6	19.21 ± 1,10 *	0.88
Body weight gain (g) ^a	10.55 ± 0,4	7.35 ± 0,54 **	0.70
Kidney (mg)	237.83 ± 7,97	208.60 ± 10,18	0.88
Spleen (mg)	94.44 ± 6,93	103.71 ± 7,78	1.10
Heart (mg)	110.10 ± 3,67	104.20 ± 4,26	0.95
Brain (mg)	444.01 ± 4,91	382.23 ± 26,27 *	0.86
Liver (mg)	1200.59 ± 60,25	1116.50 ± 95,55	0.93
Lung (mg) ^b	166.79 ± 8,61	149.99 ± 7	0.90
Testis (mg)	129.63 ± 12,46	60.86 ± 9,87 **	0.47
Kidney / BW (%)	1.09 ± 0,02	1.10 ± 0,07	-
Spleen / BW (%)	0.43 ± 0,03	0.54 ± 0,02 *	-
Heart / BW (%)	0.50 ± 0,01	0.55 ± 0,02 *	-
Brain / BW (%)	2.04 ± 0,06	1.98 ± 0,05	-
Liver / BW (%)	5.51 ± 0,3	5.77 ± 0,29	-
Lung / BW (%) ^b	0.76 ± 0,03	0.78 ± 0,02	-
Testis / BW (%)	0.59 ± 0,04	0.31 ± 0,03 **	-

Values are mean ± SEM (n = 7)

BW, Body weight

*p<0.05; **p<0.01. Mann-Whitney U test (two tailed)

a Mouse weight gain between D0 and D27 of TMX treatment

b Lung weight includes trachea

c Ratio is expressed as *CreERT2* to *Igf1r^{fl/fl}* values

4.1.3 TMX treatment of UBC-CreERT2; *Igf1r^{fl/fl}* induces mice to efficiently delete *Igf1r* floxed sequences and significantly reduce IGF1R expression in different organs

Genomic DNA obtained on D27 from a variety of tissues from *Igf1r^{fl/fl}* and *CreERT2* mice, either treated with TMX or the control vehicle (corn oil), was analyzed by PCR using specific primers to determine the extension of recombination in exon 3 floxed sequences of the *Igf1r* locus to render a deleted allele (*Igf1r^d*) (**Figure 15b**), and therefore a non-functional *Igf1r* gene (Kloting *et al.*, 2008). DNA from all organs analyzed, including kidney, spleen, liver, lung, testis and cochlea obtained in vehicle-treated *UBC-CreERT2; Igf1r^{fl/fl}* or TMX-treated *Igf1r^{fl/fl}* mice only rendered the presence of the floxed undeleted PCR fragment of 1300 bp (**Figure 21a**). As expected, PCR analysis of DNA obtained from all tissues of TMX-treated *UBC-CreERT2; Igf1r^{fl/fl}* animals resulted in a prominent band of 491 bp (**Figure 21a**). However, the presence of variable residual amounts of the 1300 bp PCR product in these mice indicated that the floxed allele remained unrecombined in a variable and undetermined small percentage of cells in all tissues. Although the PCR assay cannot be considered quantitative, it is interesting to note that the ratio of the

undeleted band varies among different organs and between individuals when analyzing the same organ. Thus, the *UBC-CreERT2* mouse line provides a system to conditionally activate Cre recombinase in a wide range of tissues upon TMX treatment, and therefore to mediate deletion of floxed sequences in the *Igf1r* locus. However, since the floxed allele remained undeleted in some cells of all organs, this system allowed production of mice that are mosaic for *Igf1r^f* recombination. To quantify the extent to which the *Igf1r* deletion affected *Igf1r* transcription levels, qRT-PCR in RNA obtained from organs of TMX-treated mice was performed at D27. A significant reduction was found in all conditional mutant tissues examined when compared to controls, with maximal depletion of *Igf1r* mRNA levels in kidney (19% of controls), followed by liver and lung (38%), cochlea (40%), heart (48%) and testis (50%); the spleen was the least affected (63%) (**Figure 21b**). To some extent these data correlate with the PCR test, where the faintest intensity of the 1300 bp undeleted floxed bands correspond to kidney, liver and lung, and the darkest one to spleen (**Figure 21a**). Although IGF1R expression levels were not followed up at later developmental stages in other tissues, an additional qRT-PCR analysis performed on lungs obtained from mice at D56, 8 weeks after TMX treatment, revealed that mRNA reduced expression was maintained significantly lower in *CreERT2* mice as compared to controls (45%) (0.71 ± 0.009 vs. 1.58 ± 0.21 , respectively; $**p = 0.006$, two tailed Mann-Whitney U test). IGF1R immuno-staining in tissues obtained from TMX-treated mice at D27, allowed visualization of IGF1R protein expression at the cellular level. Results obtained in tissue sections of kidney cortex, liver and testis are shown in **Figure 21c-e**. IGF1R was found ubiquitously expressed in control tissues, with a uniform pattern in liver parenchyma and variable levels of intensity in kidney cortex and testis. Thus, whilst kidney glomeruli showed weak staining, IGF1R staining intensity in cells of conducting tubules was heterogeneous. In a similar way, in testis, a positive stain was found in both germ cells and somatic Leydig cells although with uneven levels in both cell types (**Figure 21c-e**, top panel). In *CreERT2* mutants, IGF1R staining is absent in most cells, almost undetected in liver parenchyma, but with some residual cells immuno-stained for IGF1R in conducting tubules of kidney cortex and in both germ cells and Leydig cells in testis (**Figure 21c-e**, bottom panels). All together qRT-PCR and immuno-staining results on IGF1R expression demonstrate that TMX efficiently mediates *Igf1r* deletion in organs of *CreERT2* mice, but this occurs in mosaic form. Moreover, these results show that recombination efficiency varies among animals and tissues, and even among different cell types in the same tissue.

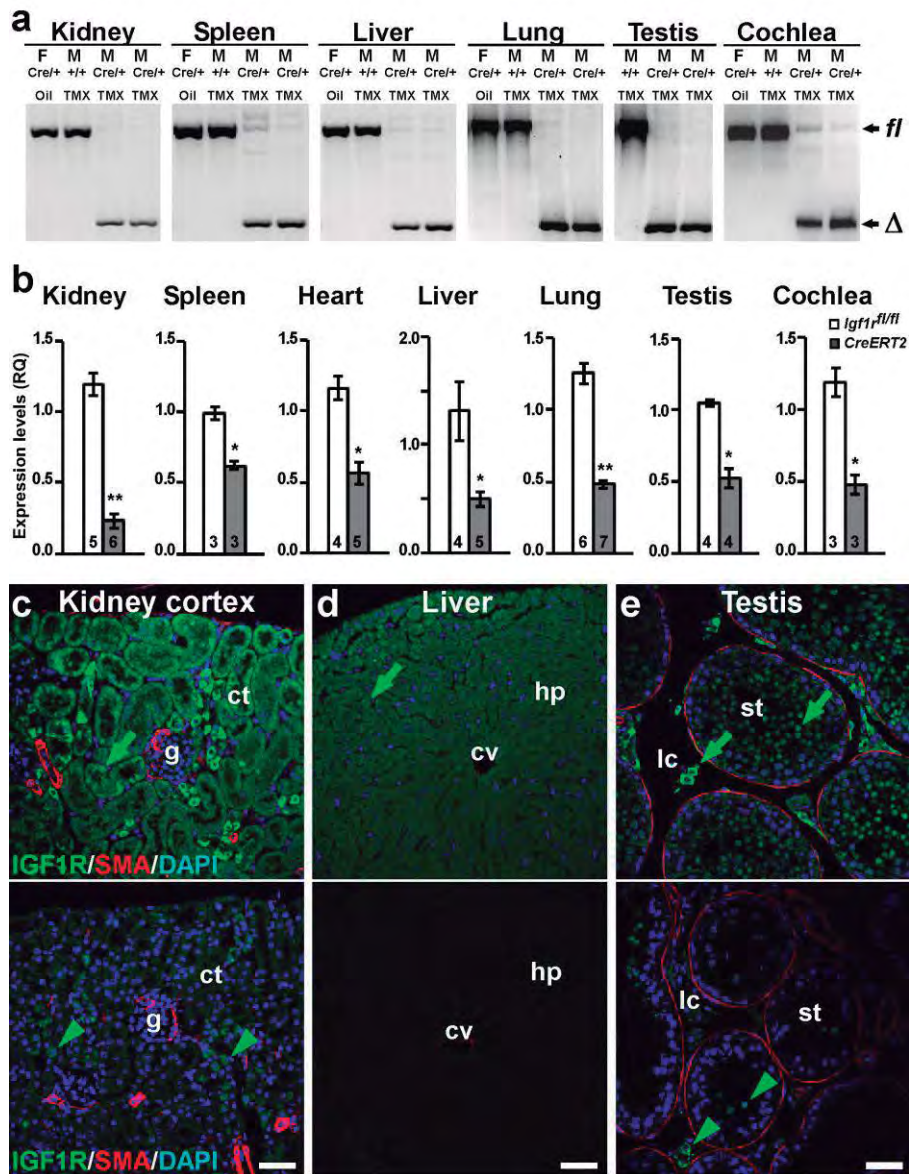


Figure 21. TMX treatment causes *Igf1r* exon 3 deletion and reduces levels of IGF1R mRNA and protein in organs of D27 *CreERT2* mutant mice. **(a)** PCR assays to determine the presence of the deleted allele (Δ) using F3/R1 primers on genomic DNA obtained from different organs of *Igf1r^{fl/fl}* (+/+) and *UBC-CreERT2; Igf1r^{fl/fl}* (*Cre/+*) male (M) and female (F) mice, either treated with vehicle (oil) or TMX. The 491 bp fragment of the deleted form (Δ) is clearly predominant in *Cre/+* TMX-treated animals in detriment to the 1300 bp floxed (*fl*) allele. Note the presence of undeleted *Igf1r* allele (*fl*) in organs of TMX-treated *UBC-CreERT2; Igf1r^{fl/fl}* mice, indicating a mosaic inactivation. **(b)** *Igf1r* mRNA expression levels analyzed by qRT-PCR in different organs of *Igf1r^{fl/fl}* and *CreERT2* male mice. Numbers in bars indicate mice analyzed and percentages show the proportion of *Igf1r* mRNA in mutants with respect to controls. * $p < 0.05$; ** $p < 0.01$. **(c-e)** Immuno-staining for IGF1R (green labeling; green arrows) and SMA (smooth muscle actin; red labeling) counterstained in blue with DAPI in kidney cortex **(c)**, liver **(d)** and testis **(e)** of *Igf1r^{fl/fl}* (upper panels) and *UBC-CreERT2; Igf1r^{fl/fl}* (lower panels) TMX-treated male mice. Note the presence of remaining IGF1R staining in kidney collecting tubules, and in testis germ cells and Leydig cells (green arrowheads) of *UBC-CreERT2; Igf1r^{fl/fl}* TMX-treated mice. g, Glomerulus; ct, collecting tubules; cv, central vein; hp, hepatic parenchyme; st, seminiferous tubules; lc, Leydig cells; TMX, tamoxifen. Scale bars 50 μ m.

4.1.4 Conditional deletion of *Igf1r* has a tissue-dependent phenotypic impact on different organs

Phenotypic consequences of *Igf1r* deletion in kidney, spleen, cochlea, liver, lung and testis were analyzed by histological analysis. H&E staining of kidney and spleen sections did not reveal gross histological alterations (**Figure 22a-b**).

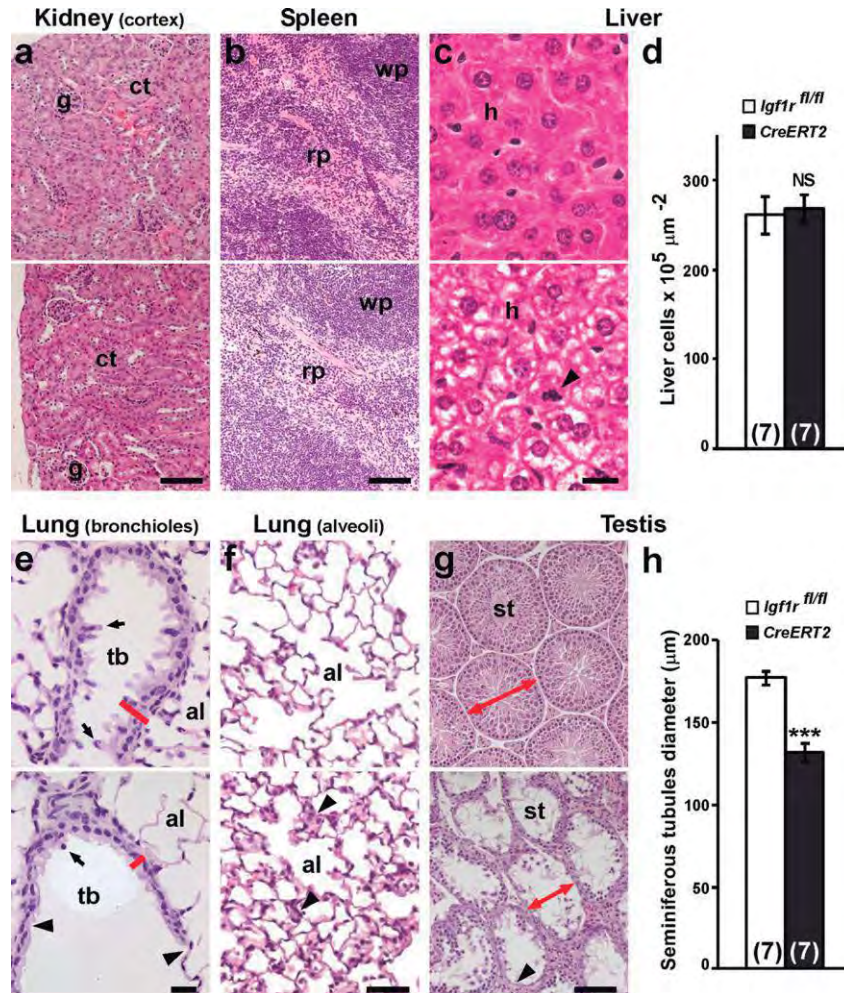


Figure 22. Histological analysis in organs of TMX-treated *UBC-CreERT2; Igf1r^{fl/fl}* mutant male mice at D27. (**a-c**) and (**e-g**) Representative H&E staining of kidney cortex, spleen, liver, lung bronchiole, lung alveoli and testis sections obtained from *Igf1r^{fl/fl}* (upper panels) and *UBC-CreERT2; Igf1r^{fl/fl}* (lower panels) of TMX-treated male mice. Note the following alterations in *CreERT2* organs: (i) presence of mitotic figures in the liver (arrowhead in **c**, lower panel), (ii) presence of flat cells (arrowheads in **e**, lower panel), and reduction of protruding cells (arrows in **e**) and bronchiolar epithelium thickening in lung bronchioles (red segments in **e**), (iii) presence of cell cumuli in the alveolar parenchyma (arrowheads in **f**, lower panel), and (iv) reduction in seminiferous tubule diameter (red double arrows in **g**) and germ cells (arrowhead in **g**, lower panel) in testes. g Glomerulus, ct collecting tubules, rp red pulp, wp white pulp, h hepatic parenchyma, tb terminal bronchiole, al alveolar area, st seminiferous tubules. Scale bars 100 μm in **a**, **b** and **g**; 20 μm in **c** and **e**; 50 μm in **f**. (**d**) Graphical representation of liver cells density. (**h**) Representation of seminiferous tubules diameter in testes of both genotypes. In parentheses, number of mice evaluated. Values in graphs shown mean ± SEM. ****p*<0.001; NS, not significant.

Analysis of liver, lung and testis from TMX-treated *UBC-CreERT2; Igf1r^{fl/fl}* animals showed readily distinguishable pathologies (**Figure 22c, e-g**). Histology of liver parenchyma of conditional mutants unveiled a heterochromatic cell staining pattern and an abundance of mitotic figures, in clear contrast to the normal homogeneous staining and sporadic mitosis seen in *Igf1r^{fl/fl}* (**Figure 22c**). Despite this presumptive higher proliferation, liver cellular density was unaffected (**Figure 22d**). Alterations in the lung were found in two different cell compartments: (1) the airway epithelium of terminal bronchioles and, (2) the alveolar parenchyma. When compared to controls, the distal bronchiolar epithelium in *Igf1r* conditional mutants was clearly flatter, showing frequent interruptions of its normal columnar organization, and reductions in: cell height, proportion of cells with apical region extruding into the bronchiolar lumen, and nuclear density (**Figure 22e**). All of these morphological alterations were less evident in the epithelium of proximal airways. However, the alveolar parenchyma in conditional mutant mice showed higher cellular density than controls, with frequent presence of cells in groups (**Figure 22f**). In contrast to *Igf1r^{fl/fl}* control mice, the seminiferous tubules of TMX-treated *UBC-CreERT2; Igf1r^{fl/fl}* testes showed reduced diameters and were severely depleted of germ cells (**Figure 22g**). A graphical representation of measurements of the seminiferous tubule diameters in both genotypes is shown in **Figure 22h**. The lack of germ cells in seminiferous tubules of mutant mice affected all different cell types, including spermatogonia, spermatocytes, and spermatids (**Figure 22g**, bottom panel). In contrast, the testicular peritubular capsule and Leydig cells were apparently normal (**Figures 21e and 22g**, bottom panels). Diminished spermatogenesis and lack of germ cell content in the seminiferous tubules would explain the reduced size of testes in TMX-treated *UBC-CreERT2; Igf1r^{fl/fl}* mice (**Table 2**).

4.1.5 Increased proliferation and normal apoptotic levels in liver and pulmonary alveolar parenchyma of *CreERT2*

In an attempt to explain the liver and lung alterations, cell proliferation and death rates were determined in mice with both genotypes. Proliferation analyses by Ki67 immuno-staining in sections of these tissues are shown in **Figure 23**. The proliferation rate in livers of TMX-treated *UBC-CreERT2; Igf1r^{fl/fl}* mice doubled that of *Igf1r^{fl/fl}* mice (**Figure 23a-b**), and even increased to almost three times higher when determined in hepatocytes (identified as cells with big rounded nuclei) ($2.42 \pm 0.42\%$ in *Igf1r^{fl/fl}* vs. $6.97 \pm 0.91\%$ in *CreERT2*; *** $p \leq 0.001$, Mann-Whitney U test). The lung epithelium in terminal bronchioles, although with higher mean values in the conditional mutants, did not show statistically significant difference in cell proliferation between genotypes (**Figure 23c-d**). However, the proliferation rate in the pulmonary alveolar parenchyma was again significantly higher in TMX-treated *UBC-CreERT2; Igf1r^{fl/fl}* mice than in controls (**Figure 23e-f**), which could explain the presence of cell cumuli in the pulmonary alveolar zone. To compare cell death levels between genotypes, apoptotic levels were determined using TUNEL (TdT-mediated dUTP nick labeling), however, differences between genotypes were not found to be significant in either the liver (0.54 ± 0.11 cells/105 μm^2 in *Igf1r^{fl/fl}* vs. 0.50 ± 0.22 cells/105 μm^2 in *CreERT2*) or the lung (4.7 ± 1.4 cells/cm² in *Igf1r^{fl/fl}* vs. 9.1 ± 2.1 cells/cm² in *CreERT2*). In any case, these apoptotic rates appear to be low, and it is difficult to assume that they may have physiological relevance.

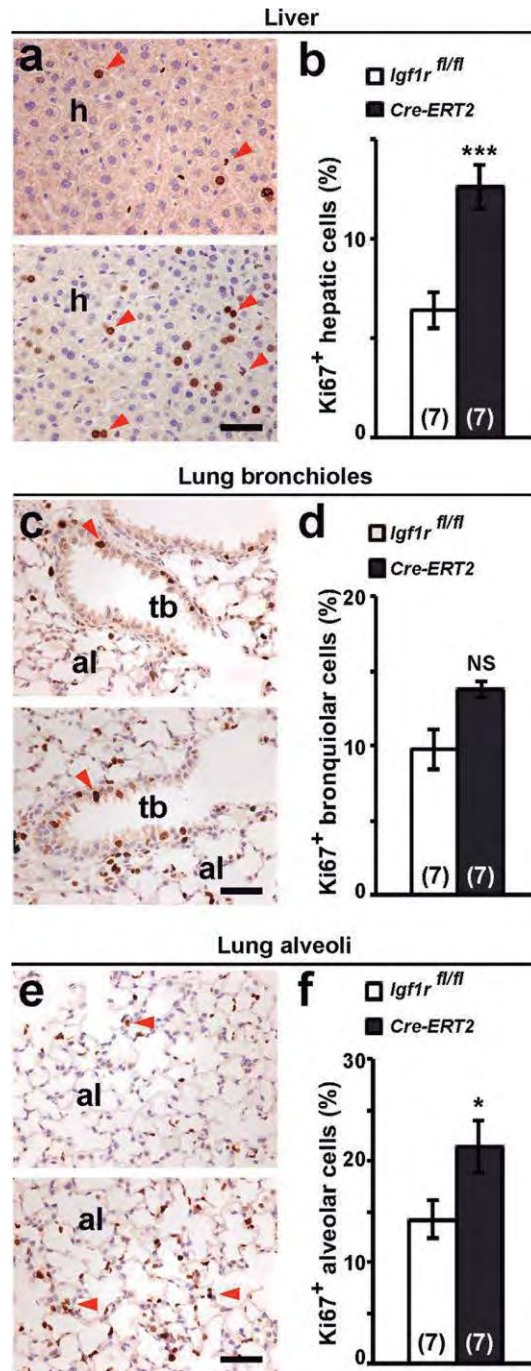


Figure 23. Increased proliferation levels in liver and lung after TMX-mediated *Igf1r* conditional deletion at D27. (**a**, **c**, **e**) Representative images of Ki67 immunostaining in liver (**a**), lung bronchioles (**c**) and lung alveolar parenchyma (**e**) at D27 after TMX treatment of *Igf1r^{fl/fl}* (upper panels) and *UBC-CreERT2; Igf1r^{fl/fl}* (lower panels). Note the increased presence of Ki67⁺ cells (brown arrowheads) in liver and alveolar parenchymas of *CreERT2* mice. h, Hepatic parenchyma, tb terminal bronchiole, al alveolar area. Scale bars 50 μ m. **b**, **d**, **f** Graphical representation of Ki67-based proliferation rates on specified tissues. In parentheses, number of mice evaluated. Values in graphs show mean \pm SEM. * $p < 0.05$; *** $p < 0.001$; NS, not significant.

4.2 IGF1R deficiency attenuates acute inflammatory response in a BLM-induced lung injury mouse model (Paper II)

4.2.1 Postnatal IGF1R deficiency in *CreERT2* mice causes a general inhibition of differentially expressed genes in the prepuberal lung

qRT-PCR and WB analyses on lung extracts of eight-week-old *CreERT2* mice verified efficient depletion of IGF1R expression at the RNA and protein levels (81% and 82%, respectively), when compared to their control littermates (*Igf1r^{fl/fl}*) (Figure 24a-b).

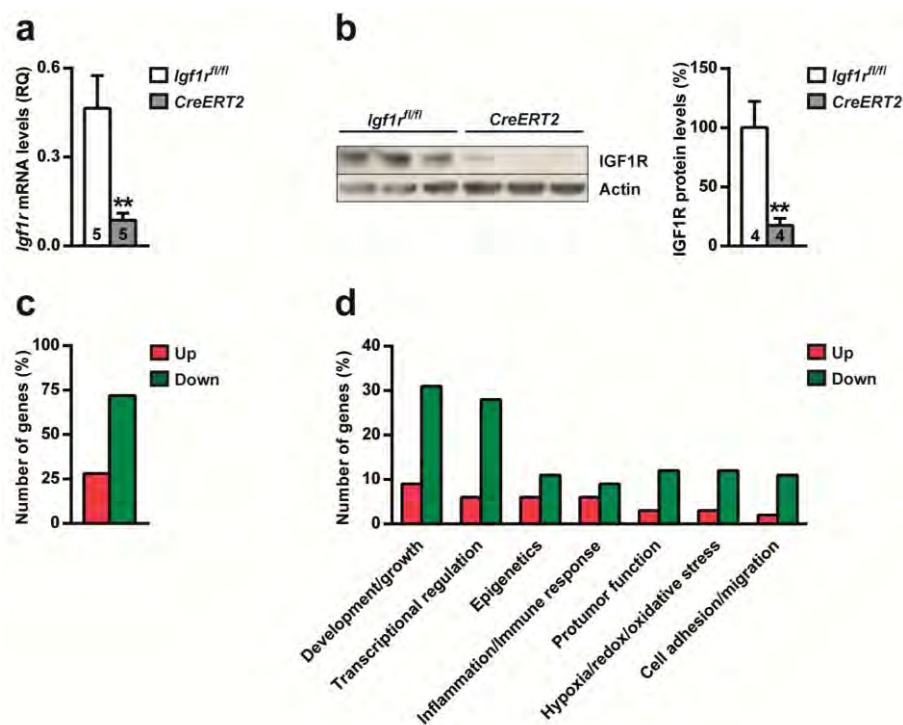


Figure 24. Decreased IGF1R expression levels and changes in the lung transcriptome of prepuberal IGF1R deficient mice. (a) *Igf1r* mRNA expression levels and (b) representative WB for IGF1R and graphical representation of densitometric measurements of band intensities (percentage) normalized to beta-Actin levels and quantified in eight-week-old *CreERT2* mice with respect to controls (*Igf1r^{fl/fl}*). (c) Number of differentially expressed genes (percentage) found with significant changes (FDR < 0.1) in the lungs of *CreERT2* mice (n = 3), and (d) representation of the percentage of *Igf1r* transcriptionally regulated genes involved in reported biological functions. Bars are color-coded in red and green for up- and down-regulated genes (respectively). Numbers within graphic bars indicate the number of mice analyzed and data are expressed as mean \pm SEM. **p < 0.01 (Mann-Whitney U test). Up, up-regulated; Down, down-regulated.

To determine the impact of *Igf1r* deficiency on global lung RNA expression, RNA-Seq was performed. Bioinformatics analyses were performed comparing *CreERT2* vs. *Igf1r^{fl/fl}* lung mRNA expression profiles (data submitted to Gene Expression Omnibus, accession number GSE88908). Establishing a False Discovery Rate (FDR) < 0.1, 65 differentially expressed genes were identified. 18 genes were up-regulated (28%) and 47 were down-regulated (72%) (Figure 24c and Table 3).

Table 3. RNAseq differential expression in the lung of *CreERT2* mice (FDR<0.2).

	Gene name	Description	Log2 fold change	Q-value/FDR
1	<i>Gpx8</i>	Glutathione peroxidase 8	33,33	5,08097E-11
2	<i>Igf1r</i>	Insulin-like growth factor 1 receptor	-2,35512	6,91951E-11
3	<i>Cyp11a1</i>	Cytochrome P450, family 1, subfamily a, polypeptide 1	2,22399	1,51895E-10
4	<i>Gnptg</i>	N-acetylglucosamine-1-phosphotransferase, gamma subunit	33,33	1,10271E-08
5	<i>Srrm2</i>	Serine/arginine repetitive matrix 2	-1,29438	2,90396E-06
6	<i>Nr1d2</i>	Nuclear receptor subfamily 1, group D, member 2	-1,43483	2,65234E-05
7	<i>Ppp1r2-ps4</i>	Protein phosphatase 1, regulatory (inhibitor) subunit 2, pseudogene 4	33,33	3,69653E-05
8	<i>Saa3</i>	Serum amyloid A 3	2,58211	7,26024E-05
9	<i>Epas1</i>	Endothelial PAS domain protein 1	-1,17128	8,78217E-05
10	<i>Spon2</i>	Spondin 2, extracellular matrix protein	1,76138	0,000320111
11	<i>Slco2a1</i>	Solute carrier organic anion transporter family, member 2a1	-1,08642	0,000596572
12	<i>Mll2</i>	Lysine (K)-specific methyltransferase 2D	-1,11086	0,000614606
13	<i>Npnt</i>	Nephronectin	-0,950843	0,000614606
14	<i>Hydin</i>	HYDIN, axonemal central pair apparatus protein	-1,51408	0,00123442
15	<i>Pcdh1</i>	Protocadherin 1	-0,92639	0,00123442
16	<i>Ly21</i>	Lysozyme 1	1,00162	0,00130818
17	<i>Top2a</i>	Topoisomerase (DNA) II alpha	1,19316	0,00146147
18	<i>Zbtb34</i>	Zinc finger and BTB domain containing 34	-33,33	0,00169479
19	<i>Cyyr1</i>	Cysteine and tyrosine-rich protein 1	-0,864652	0,00169479
20	<i>mt-Nd5</i>	NADH dehydrogenase 5, mitochondrial	-0,946779	0,00436231
21	<i>Ces1g</i>	Carboxylesterase 1G	2,10737	0,00454152
22	<i>Pcnx</i>	Pecanex homolog (Drosophila)	-0,989945	0,00483008
23	<i>Muc5b</i>	Mucin 5, subtype B, tracheobronchial	-1,04542	0,0066965
24	<i>Med13l</i>	Mediator complex subunit 13-like	-1,05975	0,0072912
25	<i>Lox</i>	Lysyl oxidase	-0,893177	0,00758989
26	<i>Tenc1</i>	Tensin 2	-0,95569	0,0130699
27	<i>Dnahc6</i>	Dynein, axonemal, heavy chain 6	-0,953513	0,0156303
28	<i>Hist1h1d</i>	Histone cluster 1, H1d	1,27832	0,0174382
29	<i>Atp2a3</i>	ATPase, Ca++ transporting, ubiquitous	-0,935091	0,0195047
30	<i>Zbtb16</i>	Zinc finger and BTB domain containing 16	-0,87579	0,0255043
31	<i>Svep1</i>	Sushi, von Willebrand factor type A, EGF and pentraxin domain containing 1	-0,82965	0,0288283
32	<i>Mki67</i>	Antigen identified by monoclonal antibody Ki 67	0,88978	0,0288283
33	<i>Snhg11</i>	Small nucleolar RNA host gene 11	-1,27045	0,0331612
34	<i>Hist1h2bb</i>	Histone cluster 1, H2bb	1,21471	0,0347587
35	<i>Zfp518b</i>	Zinc finger protein 518b	-33,33	0,0360491
36	<i>Zfx3</i>	Zinc finger homeobox 3	-0,987494	0,0371726
37	<i>Notch3</i>	Neurogenic locus homolog protein 3	-1,01305	0,0405676
38	<i>Foxo1</i>	Forkhead box O1	-1,02458	0,0411093
39	<i>Apol11b</i>	Apolipoprotein L 11b	-1,89341	0,0485738
40	<i>Syngap1</i>	Synaptic Ras GTPase activating protein 1 homolog (rat)	-33,33	0,0487062
41	<i>AC147987.1</i>	RIKEN cDNA 4933404012 gene	33,33	0,0492756
42	<i>C030017K20Rik</i>	RIKEN cDNA C030017K20 gene	-33,33	0,0507919
43	<i>Rab6b</i>	RAB6B, member RAS oncogene family	-1,17859	0,0507919
44	<i>Crebbp</i>	CREB binding protein	-0,854579	0,0508175
45	<i>Kif11</i>	Kinesin family member 11	1,18653	0,0508175
46	<i>Fancl</i>	Fanconi anemia, complementation group F	33,33	0,0536387
47	<i>Hr</i>	Hairless	-33,33	0,0546633
48	<i>Ptprb</i>	Protein tyrosine phosphatase, receptor type, B	-0,815991	0,0550762
49	<i>Gdgd3</i>	Glycerophosphodiester phosphodiesterase domain containing 3	-1,6275	0,0593667
50	<i>Marco</i>	Macrophage receptor with collagenous structure	1,43551	0,0632713
51	<i>Tet3</i>	Tet methylcytosine dioxygenase 3	-0,969638	0,065462
52	<i>mt-Cytb</i>	Cytochrome b, mitochondrial	-0,768723	0,0674572
53	<i>Luc7l2</i>	LUC7-like 2 (S. cerevisiae)	-0,472481	0,0674572
54	<i>Nav2</i>	Neuron navigator 2	-0,969168	0,0684272
55	<i>Ppp1r3c</i>	Protein phosphatase 1, regulatory (inhibitor) subunit 3C	1,13441	0,0712999
56	<i>Trim25</i>	Tripartite motif-containing 25	-1,04788	0,0733889
57	<i>Prrc2c</i>	Proline-rich coiled-coil 2C	-0,785804	0,0733889
58	<i>Mlxip</i>	MLX interacting protein	-0,877622	0,076686
59	<i>Polr2a</i>	Polymerase (RNA) II (DNA directed) polypeptide A	-0,816322	0,0776129
60	<i>Ep300</i>	E1A binding protein p300	-0,79195	0,0777767
61	<i>Abi3bp</i>	ABI gene family, member 3 (NESH) binding protein	-0,842908	0,0783232
62	<i>Tgfb3</i>	Transforming growth factor, beta receptor III	-0,794265	0,0902875
63	<i>Efnb2</i>	Ephrin B2	-0,983599	0,0926999
64	<i>Hnnpul2</i>	Heterogeneous nuclear ribonucleoprotein U-like 2	-0,81716	0,0936172
65	<i>Rps7</i>	Ribosomal protein S7	1,53422	0,093661
Genes with FDR between 0.10 and 0.20				
66	<i>Cd5l</i>	CD5 antigen-like	2,38007	0,11316
67	<i>Hist1h4m</i>	Histone cluster 1, H4m	33,33	0,114229
68	<i>Pdzd2</i>	PDZ domain containing 2	-0,725257	0,115581
69	<i>Btdb3</i>	BTB (POZ) domain containing 3	-0,70643	0,119155
70	<i>Sorbs3</i>	Sorbin and SH3 domain containing 3	-0,908928	0,120407
71	<i>Myo1d</i>	Myosin ID	-0,711134	0,120505
72	<i>Tubd1</i>	Tubulin, delta 1	33,33	0,124497
73	<i>Ska1</i>	Spindle and kinetochore associated complex subunit 1	33,33	0,124497
74	<i>Fam65a</i>	Family with sequence similarity 65, member A	-1,0518	0,124918
75	<i>Dnahc1</i>	Dynein, axonemal, heavy chain 1	-1,39517	0,127394
76	<i>mt-Nd6</i>	NADH dehydrogenase 6, mitochondrial	-0,805532	0,127994
77	<i>Pom121</i>	Nuclear pore membrane protein 121	33,33	0,127994
78	<i>Bmpr2</i>	Bone morphogenetic protein receptor, type II (serine/threonine kinase)	-0,708527	0,129371
79	<i>Hist1h1a</i>	Histone cluster 1, H1a	1,21029	0,129371
80	<i>Ptprg</i>	Protein tyrosine phosphatase, receptor type, G	-0,688689	0,129504
81	<i>Eif2c2</i>	Argonaute RISC catalytic subunit 2	-0,799781	0,134313
82	<i>Arhgap31</i>	Rho GTPase activating protein 31	-0,642048	0,134313
83	<i>Igf1bp3</i>	Insulin-like growth factor binding protein 3	0,800809	0,158183
84	<i>D730039F16Rik</i>	CutA divalent cation tolerance homolog-like	33,33	0,163078
85	<i>Pkd1</i>	Polycystic kidney disease 1 homolog	-0,696951	0,16421
86	<i>Baz2a</i>	Bromodomain adjacent to zinc finger domain, 2A	-0,812446	0,168588
87	<i>Atp5k</i>	ATP synthase, H+ transporting, mitochondrial F1F0 complex, subunit E	1,02612	0,169495
88	<i>Cd276</i>	CD276 antigen	33,33	0,172103
89	<i>Gm10277</i>	Predicted gene 10277	-33,33	0,174175
90	<i>Dock6</i>	Dedicator of cytokinesis 6	-0,848506	0,175012
91	<i>Parp4</i>	Poly (ADP-ribose) polymerase family, member 4	-0,838119	0,175012
92	<i>Plxna2</i>	Plexin A2	-0,703027	0,175012
93	<i>Sdj2l1</i>	Stromal cell-derived factor 2-like 1	1,20602	0,178254
94	<i>Nsun5</i>	NOL1/NOP2/Sun domain family, member 5	33,33	0,178254
95	<i>Crtc3</i>	CREB regulated transcription coactivator 3	-1,0953	0,182596
96	<i>Sh3pxd2a</i>	SH3 and PX domains 2A	-0,669411	0,182596
97	<i>Arid1a</i>	AT rich interactive domain 1A (SWI-like)	-0,819629	0,182803
98	<i>Crim1</i>	Cysteine rich transmembrane BMP regulator 1 (chordin like)	-0,714825	0,185107
99	<i>Smarca1</i>	SWI/SNF related, matrix associated, actin dependent regulator of chromatin, subfamily a, member 1	33,33	0,18851
100	<i>2900026A02Rik</i>	RIKEN cDNA 2900026A02 gene	-1,04303	0,191335
101	<i>Fmn12</i>	Formin-like 2	-0,82042	0,191335
102	<i>Shank2</i>	SH3/ankyrin domain gene 2	-1,65139	0,193573
103	<i>Pabpc1</i>	Poly(A) binding protein, cytoplasmic 1	-0,800107	0,193573
104	<i>mt-Nd4</i>	NADH dehydrogenase 4, mitochondrial	-0,676625	0,197356
105	<i>Brd4</i>	Bromodomain containing 4	-0,965817	0,198125
106	<i>Hspg2</i>	Perlecan (heparan sulfate proteoglycan 2)	-0,768995	0,198125
107	<i>Reck</i>	Reversion-inducing-cysteine-rich protein with kazal motifs	-0,854115	0,198715

The most significantly affected biological functions based on GO and Keyword annotations, as well as published reports, are shown in **Figure 24d**. Genes assigned to an extended list of these functions are displayed in **Table 4**.

Table 4. Biological functions and differentially expressed genes found with significant changes after RNAseq in the lung of *CreERT2* mice (FDR<0.1).

Biological functions	Up-regulated genes	Down-regulated genes
Development and growth	<i>Saa3, Mki67, Kif11, Fancf, Ppp1r3c, Rps7</i>	<i>Epas1, Npnt, Pcdh1, Lox, Tenc1, Zbtb16, Zfhx3, Notch3, Foxo1, Apol11b, Syngap1, Crebbp, Prprb, Luc7l2, Nav2, Prrc2c, Ep300, Abi3bp, Tgfbr3, Efnb2</i>
Transcriptional regulation	<i>Hist1h1d, Hist1h2bb, Ppp1r3c, Rps7</i>	<i>Srrm2, Nr1d2, Epas1, Zbtb34, Med13l, Zbtb16, Zfp518b, Zfhx3, Notch3, Foxo1, Crebbp, Hr, Tet3, Luc7l2, Mlxip, Polr2a, Ep300, Hnrnpul2</i>
Epigenetics	<i>Top2a, Hist1h1d, Hist1h2bb, Fancf</i>	<i>Mll2, Foxo1, Rab6b, Crebbp, Tet3, Polr2a, Ep300</i>
Inflammation and Immune response	<i>Saa3, Spon2, Lyz1, Marco</i>	<i>Nr1d2, Slco2a1, Muc5b, Foxo1, Trim25, Tgfbr3</i>
Protumor function	<i>Tp2a, Mki67</i>	<i>Epas1, Mll2, Atp2a3, Notch3, Trim25, Prrc2c, Abi3bp, Efnb2</i>
Hypoxia, redox function and Oxidative stress	<i>Gpx8, Cyp1a1</i>	<i>Nr1d2, Epas1, mt-Nd5, Foxo1, Hr, mt-Cytb, Ep300, Tgfbr3</i>
Cell adhesion and Migration	<i>Spon2</i>	<i>Npnt, Pcdh1, Tenc1, Svep1, Nav2, Tgfbr3, Efnb2</i>
Tumor suppression	-	<i>Zbtb16, Lox, Zfhx3, Notch3, Foxo1, Ep300, Tgfbr3</i>
Respiratory diseases	<i>Saa3, Marco</i>	<i>Epas1, Pcdh1, Muc5b, Notch3</i>
Vascular permeability and Hypertension	<i>Spon2</i>	<i>Epas1, Lox, Foxo1, Ptprb</i>
Insulin regulation and resistance	<i>Saa3</i>	<i>Epas1, Mll2, Atp2a3, Foxo1</i>
Metabolism	<i>Ces1g, Ppp1r3c</i>	<i>Nr1d2, Foxo1, Gdpd3</i>
Igf action regulation and signaling	-	<i>Muc5b, Lox, Foxo1, Crebbp, Efnb2</i>
Detoxification and damage resistance	<i>Cyp1a1, Spon2, Ces1g</i>	<i>Epas1, Notch3</i>
Cell transport	-	<i>Atp2a3, Apol11b, Rab6b</i>
Ciliary motility	<i>Kif11</i>	<i>Hydin, Dnahc6</i>
Other/Unknown	<i>Gnptg, Ppp1r2-ps4, Ac147987.1</i>	<i>Cypr1, Pcnx, Snhg11, C030017K20Rik, Syngap1</i>

Interestingly, the majority of genes in all categories were down-regulated. Most of them fall into three major categories: development/growth (*Mki67* and *Rps7*, up-regulated; *Notch3*, *Foxo1*, *Epas1* and *Tgfbr3*, down-regulated), transcriptional regulation and epigenetics (*Top2a*, *Hist1h1d* and *Hist1h2bb*, up-regulated; *Crebbp*, *Ep300*, *Polr2a*, *Zbtb34*, *Zbtb16*, *Zfp518b* and *Zfhx3*, down-regulated). Additional relevant biological functions of these genes include inflammation and immune response, followed by protumor

function, hypoxia/redox and oxidative stress, as well as cell adhesion and migration (**Table 4**). The top ten differentially expressed genes and their major biological functions are listed in **Table 5**.

Table 5. Top 10 differentially expressed genes in the lung of *CreERT2* mice, and their assigned main functions.

Accession No.	Gene name	Description	FDR	Main function
Upregulated				
NM_027127.2	<i>Gpx8</i>	Glutathione peroxidase 8	5.08 E-11	Antioxidative stress
NM_009992.4	<i>Cyp1a1</i>	Cytochrome P450, family 1, subfamily a, polypeptide 1	1.51 E-10	Antioxidative stress
NM_172529.3	<i>Gnptg</i>	N-acetylglucosamine-1-phosphotransferase, gamma subunit	1.10 E-08	Lysosome transport
AK015709	<i>Ppp1r2-ps4</i>	Protein phosphatase 1, regulatory (inhibitor) subunit 2, pseudogene 4	3.69 E-05	Unknown
NM_011315.3	<i>Saa3</i>	Serum amyloid A 3	7.26 E-05	Immune cell response
NM_133903.3	<i>Spon2</i>	Spondin 2, extracellular matrix protein	3.20 E-4	Immune cell response
Downregulated				
NM_010513.2	<i>Igf1r</i>	Insulin-like growth factor I receptor	6.91 E-11	Cell growth and survival
NM_175229.3	<i>Srrm2</i>	Serine/arginine repetitive matrix 2	2.90 E-06	Pre-mRNA splicing
NM_011584.4	<i>Nr1d2</i>	Nuclear receptor subfamily 1, group D, member 2	2.65 E-05	Transcriptional repression
NM_010137.3	<i>Epas1</i>	Endothelial PAS domain protein 1	8.78 E-05	Endothelial barrier function

As expected, *Igf1r* is the most down-regulated gene, followed by *Srrm2* (involved in pre-mRNA splicing), *Nr1d2* (transcriptional regulator) and *Epas1* (endothelial barrier integrity). The most up-regulated genes are *Gpx8* and *Cyp1a1*, both implicated in anti-oxidative stress, followed by *Gnptg* (lysosome transport), *Ppp1r2-ps4* (pseudogene) and *Saa3* and *Spon2*, both involved in the immune response.

4.2.2 IGF1R deficiency improves mouse survival and alters IGF system gene expression in early stages after BLM-mediated pulmonary injury

To further analyze how IGF1R affects lung homeostasis, *CreERT2* mice were treated with BLM to induce lung damage at six weeks of age (D0), and their survival was followed until D21 (**Figure 25a-b**). The percentage of survivors after BLM challenge was significantly higher in *CreERT2* mice (79%) than in *Igf1r^{fl/fl}* mice (33%), without gender differences. Interestingly, mortality predominantly affected mice within the first week of treatment, beginning at D3 (**Figure 25b**). qRT-PCR and WB analyses on lung extracts at D3 verified IGF1R reduced mRNA (88%) and protein (84%) levels in *CreERT2* mice (**Figure 25c-d**). In the search for possible compensatory effects on IGF system gene expression, the mRNA levels of *Igf1*, *Igfbp3*, *Igfbp5* and *Insr*, in addition to the IGF/Ins transcription factor-signaling mediator *Foxo1*, were determined by qRT-PCR. *Igf1* levels were found to be significantly diminished in *CreERT2* lungs but conversely, *Igfbp3*, *Igfbp5*, *Insr* and *Foxo1* levels were increased (**Figure 25e**).

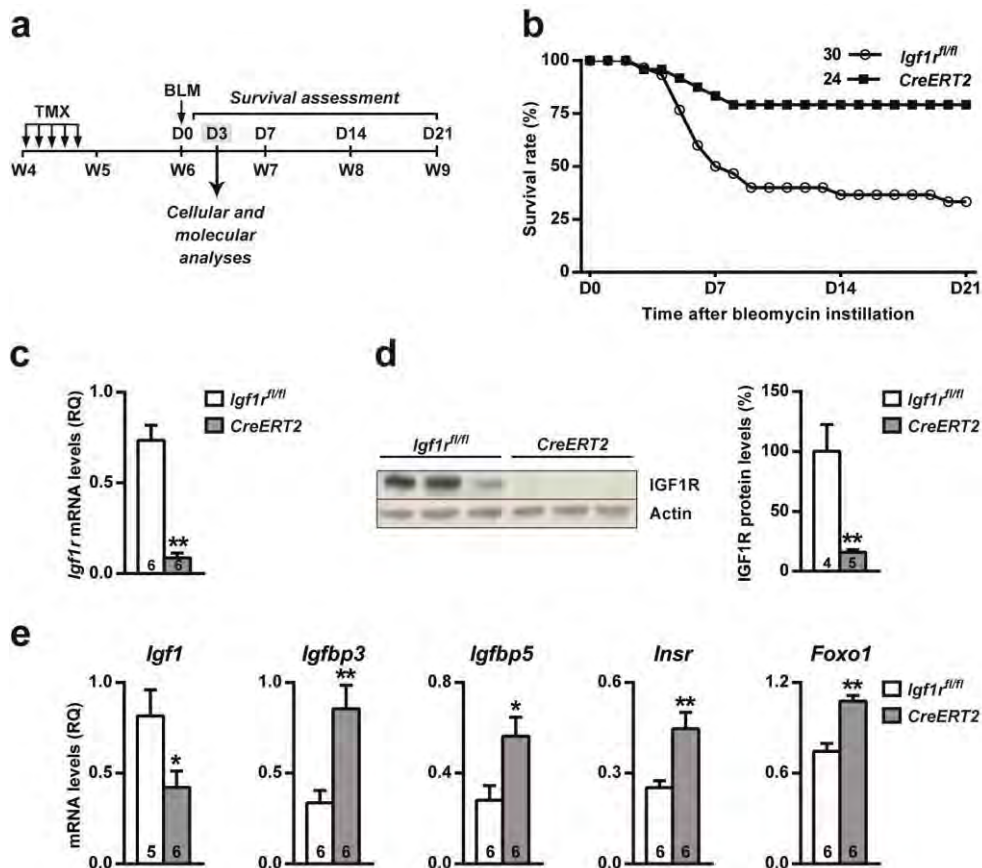


Figure 25. Establishment of the BLM-mediated acute lung injury model, and improved survival, reduced expression of IGF1R as well as changes in mRNA expression of IGF system genes in IGF1R-deficient mice. **(a)** Tamoxifen (TMX) was administered daily for five consecutive days to four-week-old *UBC-CreERT2*; *Igf1r^{fl/fl}* mice to induce a postnatal *Igf1r* gene conditional deletion using *Igf1r^{fl/fl}* mice as experimental controls. Six-week-old mice were intra-tracheally instilled with 2.5 μ l/g BLM (2 U/ml) or saline using a ketamine-xylazine anesthetic combination. Cellular and molecular analyses were assessed on day (D) 3, based on survival curves. **(b)** Survival rates after BLM challenge determined over a follow-up period of 21 days in *CreERT2* (n = 24) and *Igf1r^{fl/fl}* mice (n = 30). Data are expressed as the percentage of mice alive at each time point. **(c)** *Igf1r* mRNA expression levels, **(d)** representative Western blots for IGF1R and graphical representation of densitometric measurements of band intensities (percentage) normalized to beta-Actin levels, and **(e)** mRNA expression of IGF system related genes (*Igf1*, *Igfbp3*, *Igfbp5*, *Insr* and *Foxo1*) in lungs of *CreERT2* vs. *Igf1r^{fl/fl}* mice at D3 post-intratracheal instillation. Numbers within graphic bars indicate the number of mice analyzed and data are expressed as mean \pm SEM. * p <0.05; ** p <0.01 (Mann-Whitney U test). BLM, bleomycin.

4.2.3 IGF1R depletion protects against lung vascular fragility and permeability, and reduces inflammatory cell presence in BALF after BLM treatment

Since BLM causes an acute increase in total cells and protein concentration in BALF, BALFs from saline- (SAL) and BLM-treated mice from both genotypes were analyzed at D3 (**Figure 26a**). To evaluate lung vascular fragility and permeability, the presence of erythrocytes and the protein concentration in BALF were quantified. Interestingly, the increased erythrocyte presence (10-fold) found in BALF of *Igf1r^{fl/fl}* from BLM compared to SAL-treated mice, was not as pronounced (4-fold) in *CreERT2* mice. It is important to mention that erythrocyte counts from SAL-treated *CreERT2* mice were significantly reduced (3-fold) with respect to *Igf1r^{fl/fl}*, and were even more accentuated (6-fold) after BLM challenge (**Figure**

26b). Only *Igf1^{fl/fl}* BALF protein levels were found to be increased (2-fold) when comparing SAL- to BLM-treated mice, whereas in *CreERT2* mice, protein levels remained unchanged after BLM treatment (**Figure 26c**). In parallel, total and differential cell counts for neutrophils, macrophages and lymphocytes were severely attenuated in BALF from BLM-challenged *CreERT2* lungs with respect to their SAL-treated controls (**Figure 26d**).

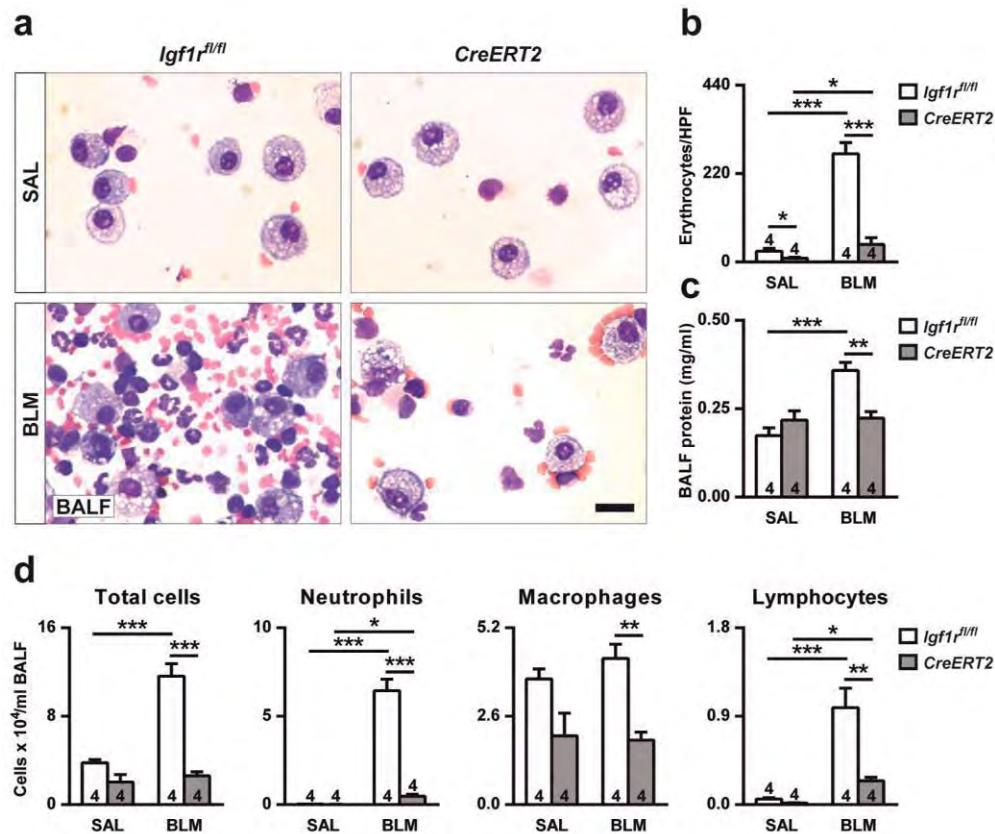


Figure 26. Reduced vascular fragility and lung permeability, and diminished leukocyte presence in BALF of IGF1R-deficient mice after BLM treatment. (a) Representative cytopsin images, (b) quantification of number of erythrocytes per HPF, (c) total protein concentration and, (d) total and differential cell counts performed on cytopsin preparations of BALF from saline- or BLM-treated *CreERT2* vs. *Igf1^{fl/fl}* mice at D3. Scale bar: 20 μ m. Numbers within graphic bars indicate the number of mice analyzed and data are expressed as mean \pm SEM. * $p < 0.05$; ** $p < 0.01$ *** $p < 0.001$ (Dunn Sidak multiple comparison test). SAL, saline; BLM, bleomycin; BALF, bronchoalveolar lavage fluid; HPF, high-power field.

Additionally, differential cell counts in BALF were also calculated as a proportion with respect to total absolute cell numbers, and expressed as percentages (**Table 6**). Although BLM-treated *Igf1^{fl/fl}* mice demonstrated a significant increment in BALF total cells (3-fold) compared to SAL-treated mice, *CreERT2* mice did not show such an increase. Differential cell counts for neutrophils, macrophages and lymphocytes in BLM-challenged *Igf1^{fl/fl}* mice exhibited the same marked increase. Furthermore, total and differential cell counts in BALF of IGF1R-deficient mice showed a severe attenuation with respect to *Igf1^{fl/fl}* (**Figure 26d**).

Table 6. Differential BALF cell counts represented as the percentage of each cell type to total cell counts in *Igf1r^{f/f}* and *CreERT2* mice.

Cell type	Condition	<i>Igf1r^{f/f}</i>	<i>CreERT2</i>
Neutrophils	SAL	0.833 ± 0.166	0.833 ± 0.396
	BLM	55.416 ± 1.535	17.250 ± 3.119 ***
Macrophages	SAL	97.583 ± 0.567	98.998 ± 0.192
	BLM	37.166 ± 2.558	73.250 ± 2.495 ***
Lymphocytes	SAL	1.583 ± 0.416	0.999 ± 0.360
	BLM	8.333 ± 0.990	9.500 ± 1.040

Data are expressed as mean ± SEM. *** p<0.001, when comparing *Igf1r^{f/f}* vs. *CreERT2* on each condition. SAL, saline; BLM, bleomycin.

4.2.4 IGF1R deficiency reduces proliferation and attenuates acute lung inflammation and bone marrow neutrophilopoiesis after BLM-challenge

Inflamed lung areas were measured at D3, and were found to be markedly reduced in BLM-treated *CreERT2* lungs (7-fold) (Figure 27a-b).

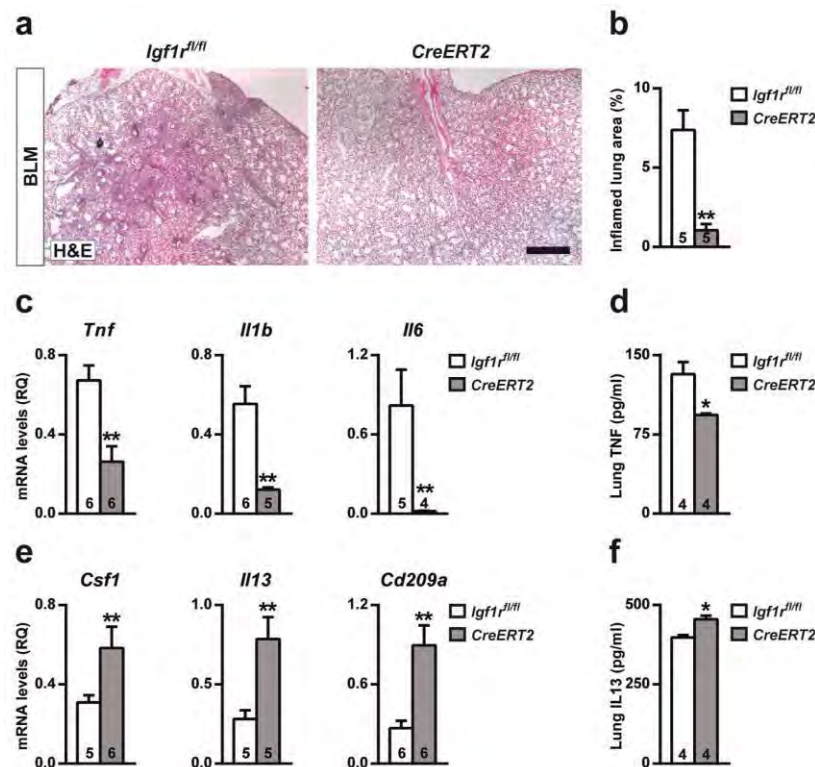


Figure 27. Decreased inflammation and increased resolution marker levels in IGF1R-deficient lungs following BLM treatment. (a) Representative images of H&E stained inflamed lung sections (scale bar: 0.5 mm), (b) quantification of inflamed lung area to total lung surface, (c,e) lung tissue mRNA expression of proinflammatory (*Tnf*, *Il1b* and *Il6*) and injury resolution phase (*Il13*, *Csf1* and *Cd209a*) markers, and (d,f) TNF and IL13 levels in lung homogenate from BLM-treated *CreERT2* mice at D3. Numbers within graphic bars indicate the number of mice analyzed and data are expressed as mean ± SEM. *p<0.05; **p<0.01 (Mann-Whitney U test). BLM, bleomycin.

To verify and further investigate the mechanism by which IGF1R deficiency blocks inflammatory cell recruitment to the lung, mRNA expression analysis of different inflammatory markers was performed. Pro-inflammatory cytokines *Tnf*, *Il1b* and *Il6* were found to be significantly down-regulated in *CreERT2* lungs (**Figure 27c**), and the reduction of TNF protein levels was confirmed by ELISA (**Figure 27d**). Conversely, mRNA expression levels of the injury resolution-phase markers *Csf1*, *Il13* and *Cd209a* were significantly increased (**Figure 27e**). Despite clearly increased *Il13* mRNA levels, protein levels were found to be only slightly increased (**Figure 27f**).

Cell proliferation evaluated in lung perivascular areas and in the alveolar parenchyma by Ki67 immuno-staining on D3 was found to be substantially reduced in *CreERT2* mice (3-fold in both cases) (**Figure 28a-b**).

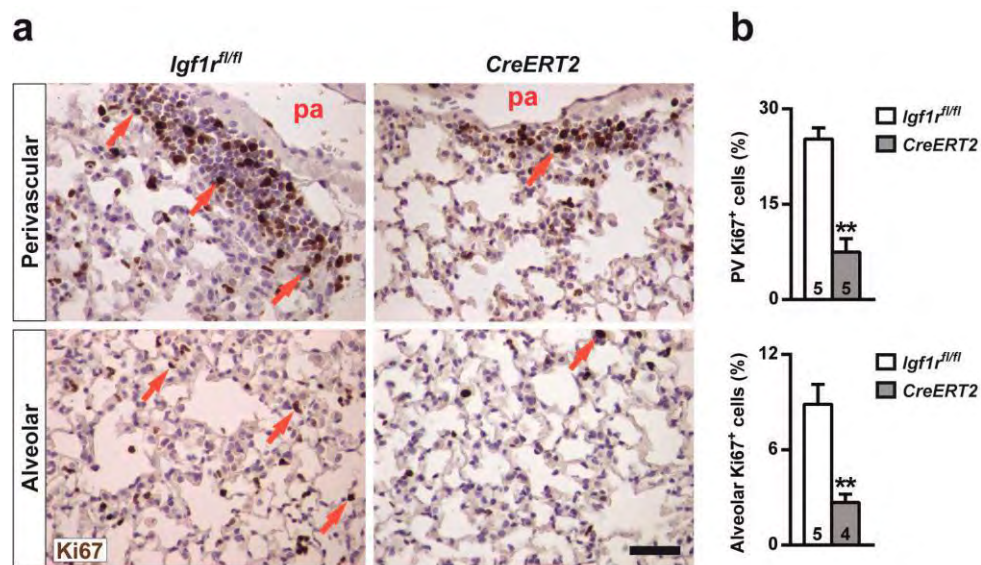


Figure 28. Diminished cell proliferation in IGF1R-deficient lungs after BLM challenge. (a) Representative images of Ki67 immuno-staining (in brown, orange arrows) under the pulmonary artery (top) and in the alveolar parenchyma (bottom), and (b) quantification of cell proliferation rates (Ki67⁺) in BLM treated *CreERT2* vs. *Igf1r^{fl/fl}* lungs at D3 (scale bar: 20 μ m). Numbers within graphic bars indicate the number of mice analyzed and data are expressed as mean \pm SEM. **p<0.01 (Mann-Whitney U test). PV, perivascular; pa, pulmonary artery.

As an indirect measure of inflammatory cell presence in the lung, mRNA levels of neutrophil chemotaxis (*Cxcl1*), neutrophil (*Ly6g*) and macrophage (*Marco* and *Adgre1*) markers were determined. *Cxcl1* levels were greatly reduced in IGF1R-deficient lungs, and *Ly6g*, *Marco* and *Adgre1* markers also showed a significant reduction (**Figure 29a**).

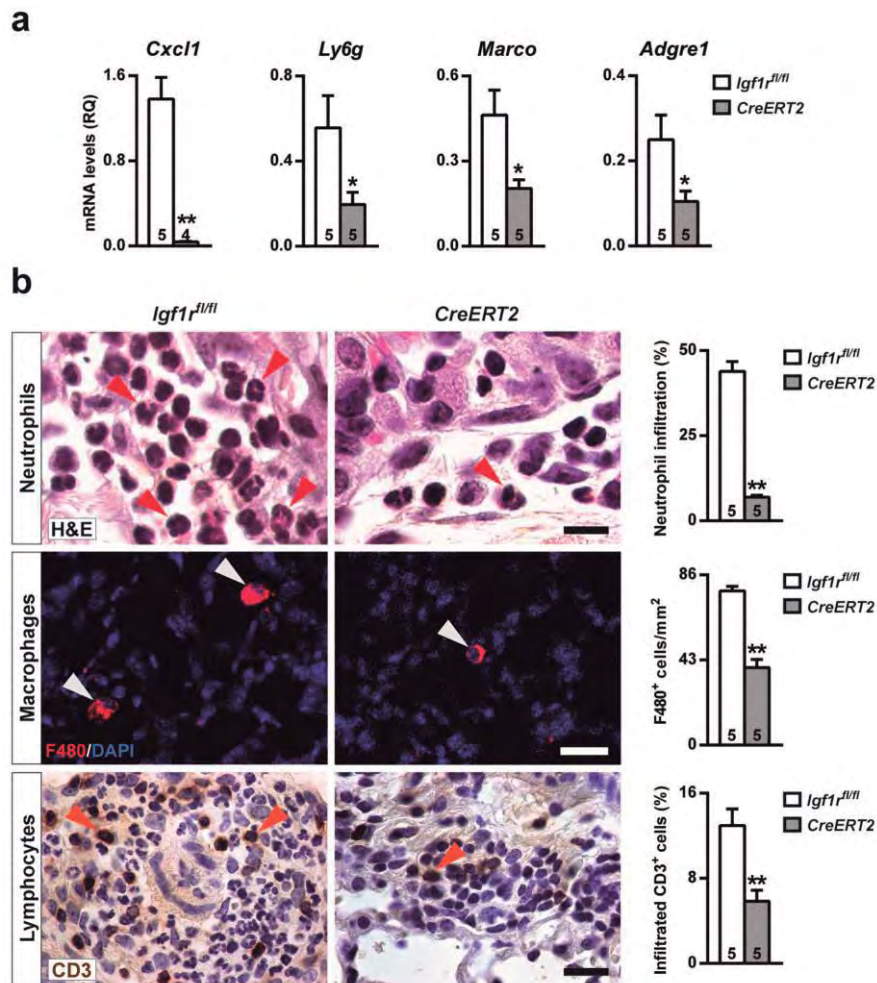


Figure 29. Reduced inflammatory cell infiltration in IGF1R-deficient lungs after BLM treatment. (a) Lung mRNA expression of neutrophil chemotaxis (*Cxcl1*), neutrophil (*Ly6g*) and macrophage (*Adgre1* and *Marco*) markers and (b) representative H&E, as well as F4/80 and CD3 immunostained sections, and quantification of neutrophils (red arrowheads, upper panels), alveolar macrophages (white arrowheads, middle panels) and lymphocytes (orange arrowheads, bottom panels) in BLM treated *CreERT2* vs. *Igf1r^{fl/fl}* lungs at D3. Scale bars: 10 μ m (upper panels) and 20 μ m (middle and bottom panels). Numbers within graphic bars indicate the number of mice analyzed and data are expressed as mean \pm SEM. * $p < 0.05$; ** $p < 0.01$ (Mann-Whitney U test).

Neutrophilic infiltration found in perivascular areas was 44% and 7% of total infiltrates for *Igf1r^{fl/fl}* and *CreERT2* BLM-challenged lungs, respectively (Figure 28b, upper panel). F4/80 immunostaining revealed a significant decrease for both alveolar macrophage numbers (50%), and volumes ($360.1 \pm 17.1 \mu\text{m}^3$ vs. $78.1 \pm 5.3 \mu\text{m}^3$; $p = 0.009$) (Figure 29b, middle panel). In view of the reduced presence of BALF lymphocytes in mutant mice, infiltration into the lung was also assessed by immunostaining for CD3. Accordingly, lymphocyte counts were also diminished (45%) in *CreERT2* lungs (Figure 29b, bottom panel).

To verify reduced neutrophil infiltration in IGF1R-deficient mice, total and neutrophil counts were performed in bone marrow cytopspins obtained from mice of both genotypes after BLM treatment. As

expected, total cells and neutrophils were found to be diminished in *CreERT2* mice with respect to *Igf1^{fl/fl}* BLM-challenged lungs (2- and 5-fold, respectively) (Figure 30a-b).

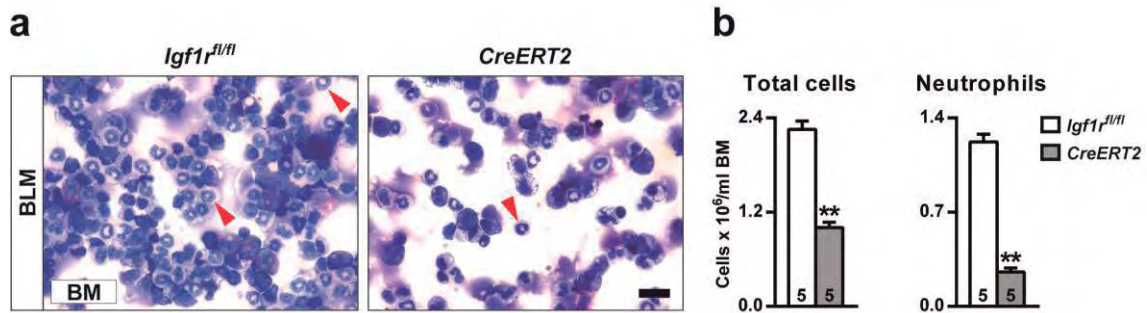


Figure 30. Reduced total and neutrophil counts in bone marrow from IGF1R-deficient mice. (a,b) Representative images, and total and neutrophil (red arrowheads) counts in bone marrow cytopsin preparations from BLM-treated *CreERT2* vs. *Igf1^{fl/fl}* mice at D3. Scale bar: 20 μ m. Numbers within graphic bars indicate the number of mice analyzed and data are expressed as mean \pm SEM. ** $p < 0.01$ (Mann-Whitney U test). BLM, bleomycin; BM, bone marrow.

4.2.5 IGF1R deficiency reduces alveolar damage and HIF1A expression in BLM-challenged lungs

To determine the effect of IGF1R depletion on alveolar damage after BLM challenge, alveolar epithelial cell type-specific markers were quantified by qRT-PCR on D3. Transcript levels of alveolar epithelial cell type 1 (*Aqp5*) and 2 (*Sftpc*) markers were found to be significantly increased in *CreERT2* BLM-challenged lungs. However, IGF1R-deficient lungs demonstrated significantly decreased levels of the hypoxia-inducible factor 1 subunit alpha (*Hif1a*) (Figure 31a).

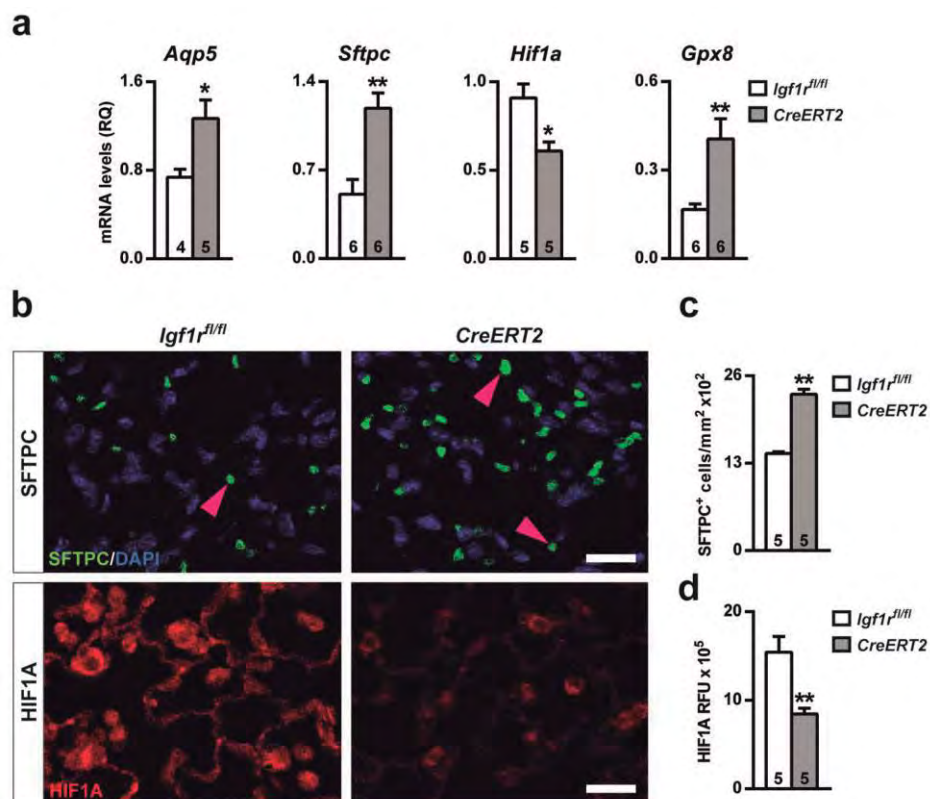


Figure 31. Reduced alveolar damage and HIF1A expression in BLM-challenged lungs of IGF1R-deficient mice. **(a)** Changes in mRNA expression of alveolar (*Aqp5* and *Sftpc*), response to hypoxia (*Hif1a*), and antioxidative stress (*Gpx8*) markers, **(b)** representative SFTPC (pink arrowheads) and HIF1A immunostained sections (upper and bottom panels, respectively), **(c)** number of SFTPC positive cells per unit area of lung tissue, and **(d)** quantification of HIF1A relative fluorescence intensity in lungs of *CreERT2* and *Igf1r^{fl/fl}* mice at D3 after BLM treatment. Scale bars: 20 μ m. Numbers within graphic bars indicate the number of mice analyzed and data are expressed as mean \pm SEM. * $p < 0.05$; ** $p < 0.01$ (Mann-Whitney U test). RFU, relative fluorescence units.

Since the RNA-seq indicated that the anti-oxidative stress marker *Gpx8* was the most up-regulated gene in *CreERT2* unchallenged lungs, its mRNA expression was assayed in BLM-treated lungs, and also found to be increased in IGF1R-deficient mice with respect to controls (**Figure 31a**). SFTPC and HIF1A expression determined by immunohistochemistry verified mRNA expression levels (**Figure 31b**). In accordance, the number of SFTPC⁺ cells was significantly increased (1.6-fold) (**Figure 31c**), and conversely, HIF1A relative fluorescence intensity was found to be diminished (1.8-fold) in IGF1R-deficient lungs (**Figure 31d**).

4.3 Attenuated airway hyperresponsiveness and mucus secretion in HDM-exposed IGF1R-deficient mice (Paper III)

4.3.1 Depletion of IGF1R in CreERT2 mutant mice and changes in expression of IGF system genes after the HDM challenge

To verify the IGF1R depletion and investigate the influence of allergic inflammation on the IGF system, qRT-PCR and WB analyses were performed on lung extracts of *CreERT2* mutant mice and their control littermates (*Igf1r^{fl/fl}*) after four weeks of repeated exposure to PBS or HDM (**Figure 17**). mRNA expression levels demonstrated an efficient depletion of *Igf1r* in *CreERT2* PBS-treated mice (90%) and without changes between HDM-treated groups. In addition, HDM treatment decreased *Igf1r* mRNA levels in *Igf1r^{fl/fl}* mice (81%) (**Figure 32a**). WB analysis corroborated these results, showing a significant reduction in IGF1R protein levels in *CreERT2* PBS-treated mice (87%), and no differences between HDM-treated groups (**Figure 32b**). *Igf1r* deficiency caused a significant increase in mRNA expression of *Igf1* and *Insr* expression levels in PBS-treated mice, but not for *Igfbp3* and *Igfbp5*. Even though HDM treatment significantly reduced the expression levels of *Insr*, *Igfbp3*, and *Igfbp5* in both genotypes without affecting *Igf1*, *Igf1r* depletion led to a significant increase in the expression of all IGF system genes measured (**Figure 32c**).

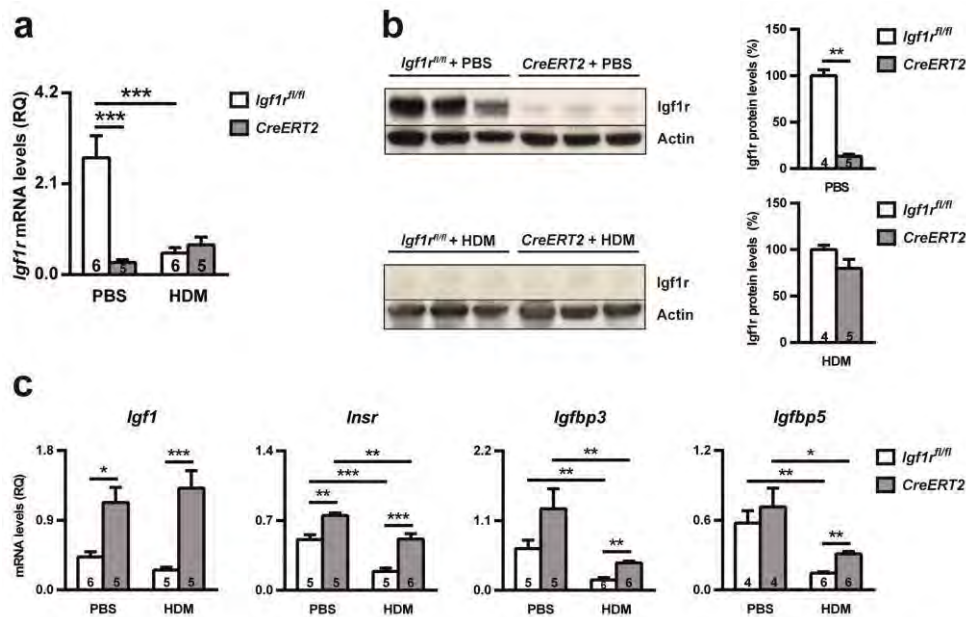


Figure 32. Efficient depletion of IGF1R and changes in expression of the IGF system genes in lungs of *CreERT2* mice after HDM-induced allergic airway inflammation. (a) *Igf1r* mRNA expression levels normalized to 18S expression; (b) representative WB for IGF1R and graphical representations of densitometric measurements of band intensities normalized to beta-actin levels; and (c) lung tissue mRNA expression of IGF system-related genes in PBS- and HDM-exposed *Igf1r^{fl/fl}* and *CreERT2* mice. Numbers within graphic bars indicate the number of mice analyzed, and data are expressed as mean \pm SEM. * $p < 0.05$; ** $p < 0.01$; *** $p < 0.001$ (Mann-Whitney U and Dunn-Sidak multiple comparison tests). HDM, house dust mite; PBS, phosphate buffered saline.

4.3.2 IGF1R deficiency improves lung function and counteracts allergic airway inflammation and airway remodeling in HDM-treated mice

To assess whether IGF1R deficiency has an effect on lung mechanics, airway responsiveness to inhaled methacholine was measured (**Figure 33**). Compared with PBS, HDM-challenged *Igf1r^{fl/fl}* mice displayed airway hyperresponsiveness (AHR) with an increased response for the proximal, Rn, and distal parameters, G and H. The AHR seen in both the proximal and distal parts of the lung was, however, not present in *CreERT2* HDM-treated mice, which showed similar functional responses as PBS-treated mice. These findings show that IGF1R deficiency improves mouse lung function at both central and peripheral levels after HDM-mediated asthma.

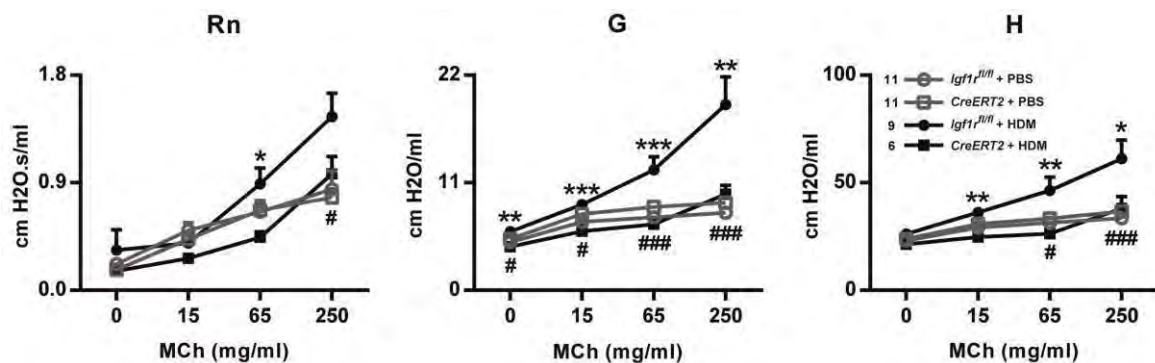


Figure 33. IGF1R deficiency decreases AHR after house dust mite challenge. Resistance of conducting airways (Rn), tissue damping (G), and tissue elastance (H) to MCh evaluated with the flexiVent system. Numbers in graphic legends indicate the number of mice analyzed, and data are expressed as mean \pm SEM. * *Igf1r^{fl/fl}* + HDM vs *CreERT2* + HDM; # *Igf1r^{fl/fl}* + HDM vs *Igf1r^{fl/fl}* + PBS. One symbol, $p < 0.05$; two symbols, $p < 0.01$; three symbols, $p < 0.001$ (Dunn-Sidak multiple comparison test). MCh, methacholine; HDM, house dust mite; PBS, phosphate buffered saline.

Although differences counting circulating macrophages, lymphocytes, and neutrophils were not found, HDM-treated *Igf1r^{fl/fl}* mice showed increased eosinophil numbers in blood (4-fold), when compared to PBS-treated. The *CreERT2* HDM-challenged mice did not show such an increase when compared to PBS-treated (**Figure 34a**). Allergen-treated *Igf1r^{fl/fl}* mice demonstrated a significant increase in total cells in BALF (8-fold) compared to PBS-treated control mice. HDM-challenged *CreERT2* mice also displayed an increase in total cell numbers (6-fold), although significantly lower than that observed in *Igf1r^{fl/fl}* mice (**Figure 34b**). Differential cell counts in BALF from *Igf1r^{fl/fl}* and *CreERT2* mice exhibited a marked increase in lymphocyte (49- and 25-fold, respectively) and neutrophil (45- and 40-fold, respectively) numbers in HDM-challenged mice, without significant differences between genotypes. The eosinophils were also increased after HDM in *Igf1r^{fl/fl}* mice (40-fold); however, this phenomenon was not observed in *CreERT2* mice, which roughly showed basal eosinophil counts (**Figure 34b**).

In HDM-exposed mice, the total IgE concentration in serum was highly increased in both genotypes after HDM exposure when compared to PBS-exposed mice (>90%) (**Figure 34c**). In addition, IL13 levels in lung homogenates were significantly higher in HDM-treated *Igf1r^{fl/fl}* mice compared to PBS-exposed mice (27%), whereas HDM-challenged *CreERT2* lungs displayed normal values (**Figure 34d**).

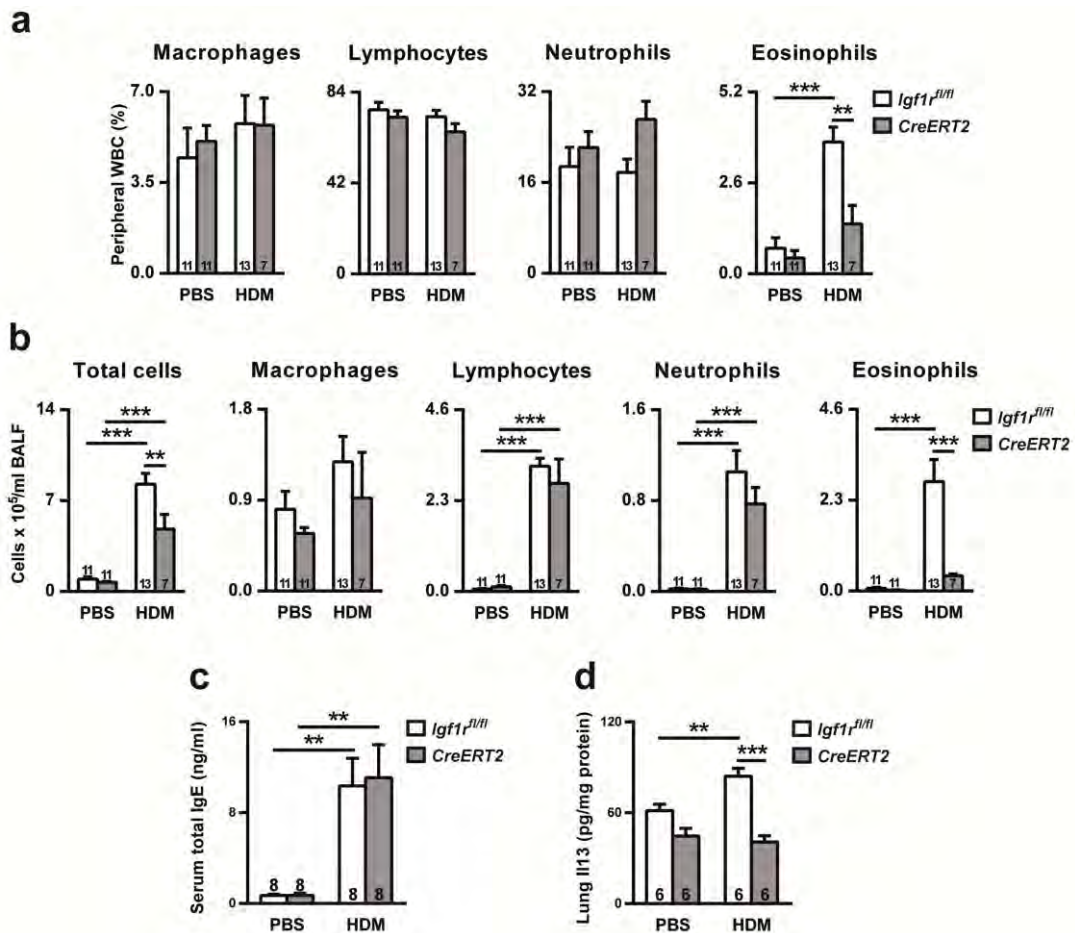


Figure 34. IGF1R depletion attenuates the increase in blood and BALF eosinophils, and IL13 levels in lung homogenates after exposure to house dust mite. (a) Peripheral white blood cell counts on blood smear preparations; (b) total and differential cell counts performed on cytospin preparations of BALF; and (c) serum total IgE and (d) IL13 levels in lung homogenate quantified by ELISA. Numbers within graphic bars indicate the number of mice analyzed, and data are expressed as mean \pm SEM. ** $p < 0.01$; *** $p < 0.001$ (Dunn-Sidak multiple comparison test). HDM, house dust mite; PBS, phosphate buffered saline.

In an attempt to determine how IGF1R deficiency protects against HDM-mediated allergic airway inflammation at the histopathological level, several asthma-related features were measured in airways: inflamed lung area, number of PAS⁺ cells, collagen staining, and smooth muscle thickness. Assessment of all of these features revealed increased values in HDM-challenged lungs of both genotypes compared to their PBS-treated controls. Measurements that were markedly increased in case of *Igf1r^{fl/fl}* mice displayed a milder increase in allergen-treated *CreERT2* lungs (Figure 35).

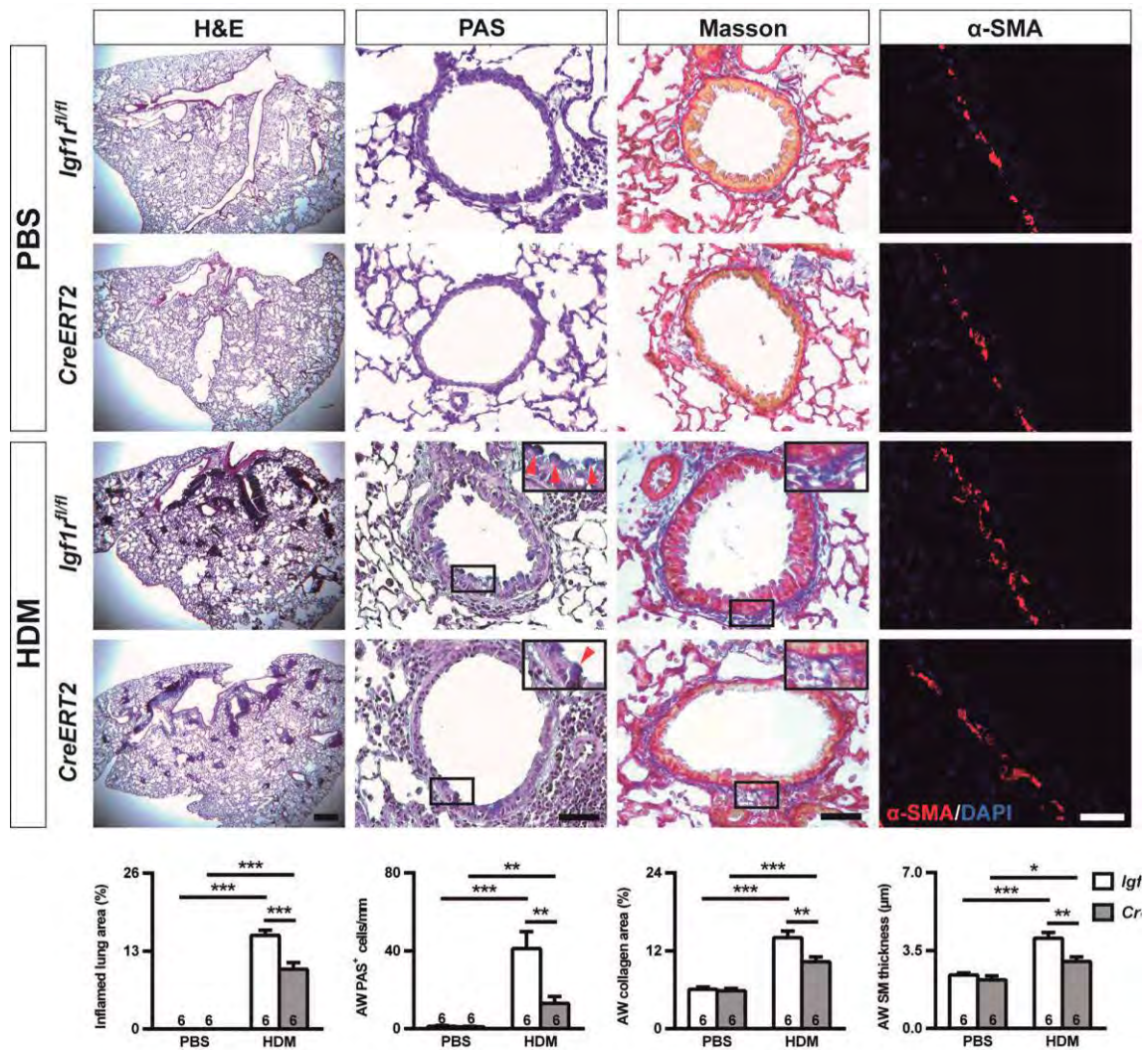


Figure 35. Reduced allergic airway inflammation, goblet cell hyperplasia, collagen content, and smooth muscle thickness in IGF1R-deficient mice after HDM exposure. Representative images of proximal airways showing inflamed lung areas (left) (scale bar: 0.5 mm); mucus-producing cells per epithelium length (red arrowheads in insets) (center left) and airway collagen content (center right) (scale bars: 50 μ m); and smooth muscle thickness (right) (scale bar: 20 μ m). Bottom graphs represent quantification of the abovementioned parameters. Numbers within graphic bars indicate the number of mice analyzed, and data are expressed as mean \pm SEM. * $p < 0.05$; ** $p < 0.01$; *** $p < 0.001$ (Dunn-Sidak multiple comparison test). H&E, hematoxylin and eosin; PAS, periodic acid-Schiff; α -SMA, alpha-smooth muscle actin; AW, airway; HDM, house dust mite; PBS, phosphate buffered saline; SM, smooth muscle.

4.3.3 IGF1R depletion attenuates airway hyperreactivity and enhances surfactant expression

Airway wall thickness was measured in the four experimental groups. Accordingly, *CreERT2* mice showed a significantly thinner airway after both treatments. However, whereas in *Igf1^{fl/fl}* mice, HDM challenge induced airway thickening (19%), HDM-exposed *CreERT2* lungs did not show such thickness (Figure 36a).

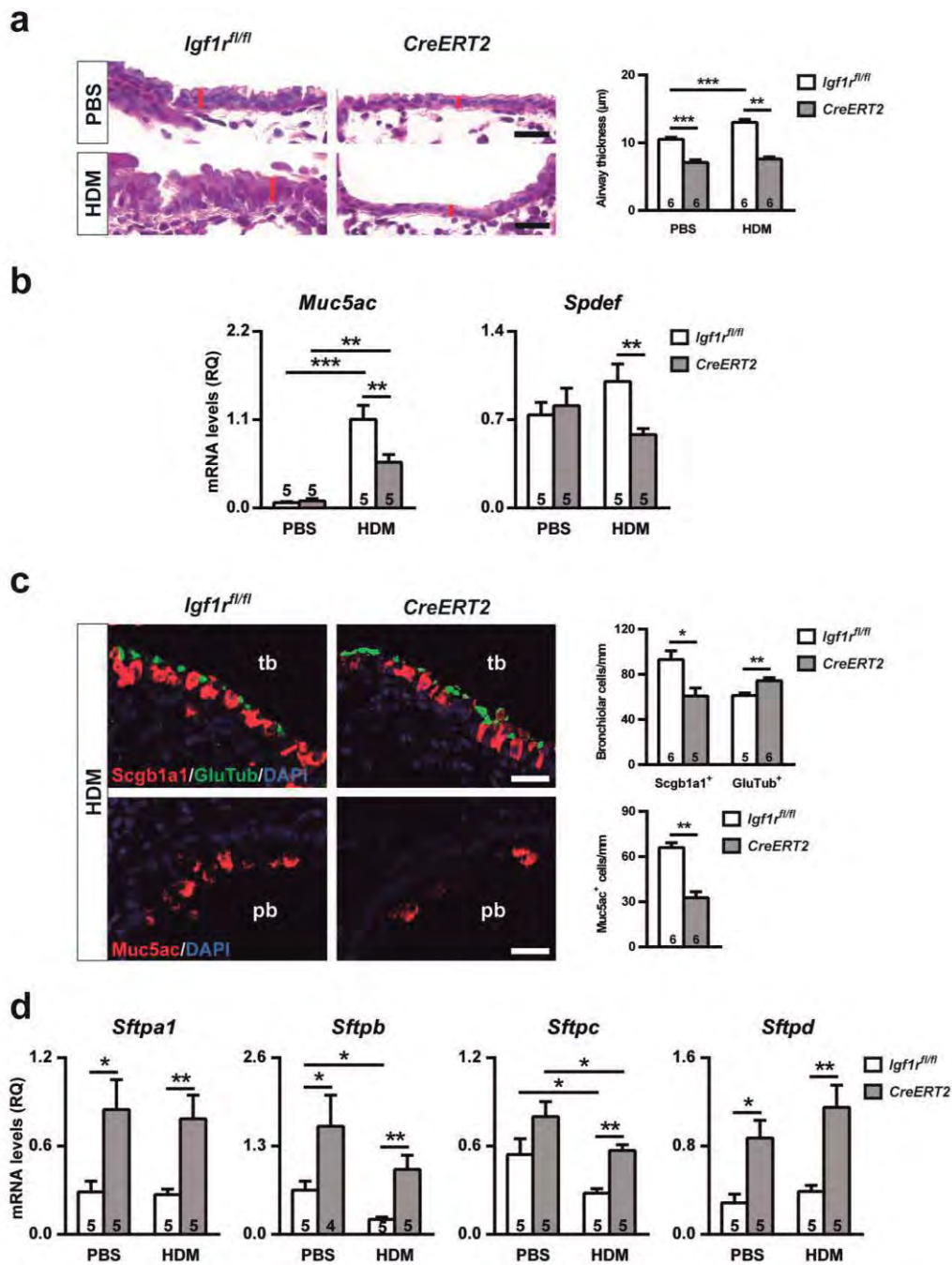


Figure 36. Attenuation of airway hyperreactivity and mucus secretion and increased expression of surfactant markers in HDM-exposed IGF1R-deficient mice. (a) Proximal airway wall thickness; (b) lung mRNA expression of the mucus secretion markers *Muc5ac* and *Spdef* normalized to 18S expression; (c) proportion of club (in red) and ciliated (in green) cells and quantification of MUC5AC (in red)-positive cells in terminal and proximal bronchioles, respectively; and (d) changes in mRNA expression of surfactant (*Sftp*) markers a1, b, c, and d in *CreERT2* mice. Scale bars: 20 μ m. Numbers within graphic bars indicate the number of mice analyzed, and data are expressed as mean \pm SEM. * p <0.05; ** p <0.01; *** p <0.001 (Mann-Whitney U test and Dunn-Sidak multiple comparison test). HDM, house dust mite; PBS, phosphate buffered saline; tb, terminal bronchioles; pb, proximal bronchioles; SCGB1A1, secretoglobin 1A1; GLUTUB, Glu-tubulin; MUC5AC, mucin 5ac.

To validate the increase in PAS⁺ cell numbers, mRNA levels of *Muc5ac* and the master regulator *Spdef* were measured. As expected, HDM-challenged *Igf1r^{fl/fl}* lungs showed significantly increased *Muc5ac* levels (16-fold) with respect to PBS-exposed controls. HDM-challenged *CreERT2* mice also demonstrated increased *Muc5ac* levels with respect to PBS-treated mice; however, this increase was significantly lower than that observed in *Igf1r^{fl/fl}* mice (7-fold) (**Figure 36b**, left). Correspondingly, mRNA levels of the master regulator *Spdef* were also reduced in HDM-challenged *CreERT2* mice (42%) (**Figure 36b**, right). Immunohistochemical analyses of the airway epithelium cellular composition in HDM-exposed lungs revealed a significant decrease in SCGB1A1⁺ club cells (35%) and a concomitant increase in GLUTUB⁺ cells in *CreERT2* mice (17%). Furthermore, the proportion in MUC5AC⁺ cells was also diminished in IGF1R-deficient mice (50%) (**Figure 36c**).

Finally, to elucidate how IGF1R depletion improves peripheral lung function, mRNA expression levels of the surfactant markers *Sftpa1*, *Sftpb*, *Sftpc*, and *Sftpd* (**Figure 36d**) were evaluated. IGF1R deficiency caused a generalized increase in all markers measured after both PBS and HDM treatments, although *Sftpc* changes were not significant in PBS-exposed mice. In addition, whereas *Sftpa1* and *Sftpd* levels showed similar changes in expression levels in PBS- and HDM-challenged mice, *Sftpc* levels were significantly reduced in HDM-challenged mice of both genotypes, and *Sftpb* was only found to be reduced in *Igf1r^{fl/fl}* animals.

4.4 Characterization of the acute inflammatory profile and resolution of airway inflammation after *Igf1r*-gene targeting in a murine model of HDM-induced asthma (Paper IV)

4.4.1 Characterization of the murine acute allergic profile

Inbred C57BL/6 mice were subjected to an acute HDM exposure to study the progressive changes in BALF and lung (Figure 37a).

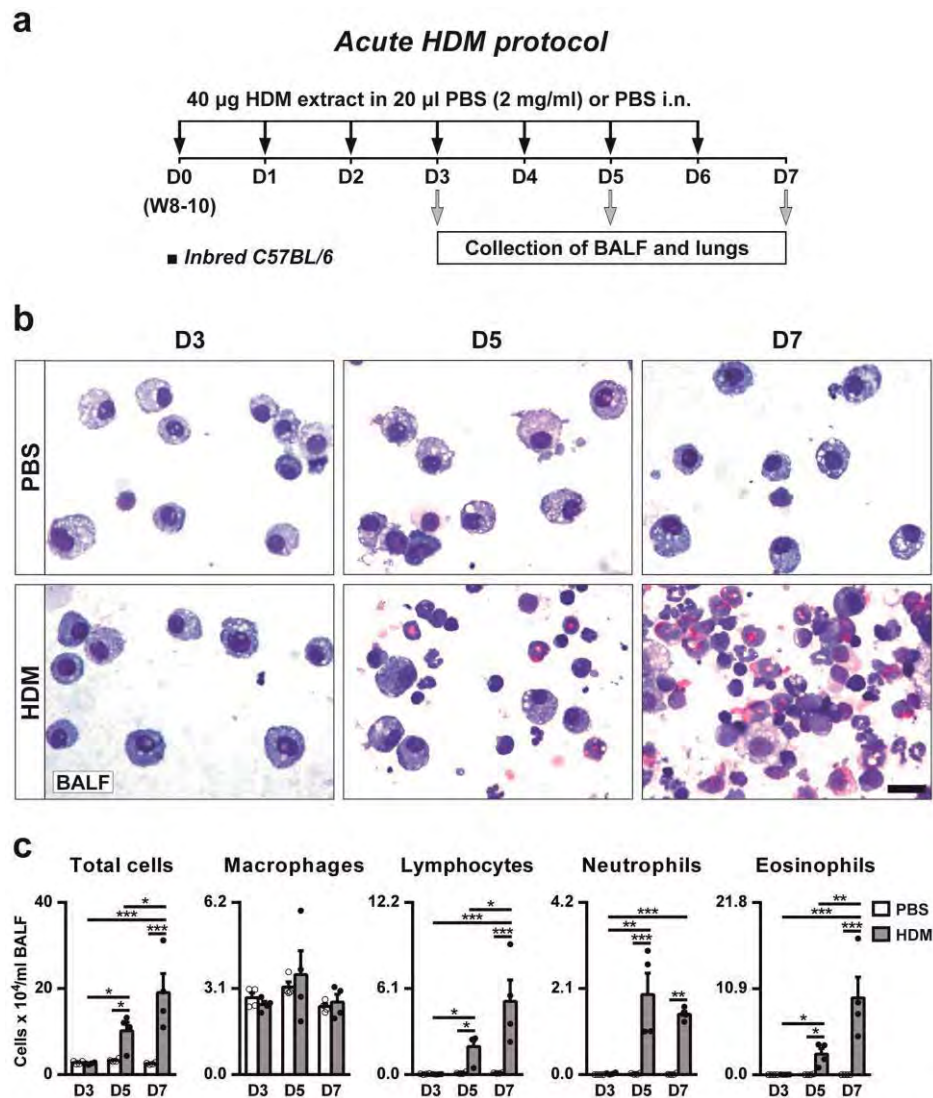


Figure 37. Protocol for acute HDM exposure and progressive accumulation of inflammatory cells in BALF of inbred C57BL/6 mice. **(a)** Eight- to ten-week-old (W8-10) inbred C57BL/6 female mice were intranasally challenged with daily consecutive doses of 40 µg of HDM extract in 20 µl of PBS (2 mg/ml) or equal volume of PBS. BALF and lungs were collected 24 h after the last exposure on days [D] 3, D5 or D7. **(b-c)** Representative images of BALF cytopsin preparations (scale bar: 20 µm) and total and differential cell counts in BALF from PBS- or HDM-treated inbred C57BL/6 mice at D3, D5 and D7. Data are expressed as mean ± SEM (n = 4 animals per group). *p<0.05; **p<0.01; ***p<0.001 (Dunn-Sidak multiple comparison test). HDM, house dust mite; PBS, phosphate buffered saline.

Total cell counts were significantly increased at day D5 and D7, reaching the highest numbers at D7 (**Figure 37b-c**). Differential cell counts in BALF showed a marked increase in lymphocyte, neutrophil and eosinophil numbers at D5 and D7, whilst macrophage counts remained unchanged. Lymphocyte and eosinophil numbers were higher at D7 without changes in neutrophil counts between D5 and D7 (**Figure 37b-c**).

Inflamed lung area, airway thickness, number of PAS⁺ cells and collagen staining were only significantly changed at D7, with the exception of the inflamed lung area parameter which was increased at D5, although to a lesser degree than at D7 (**Figure 38**).

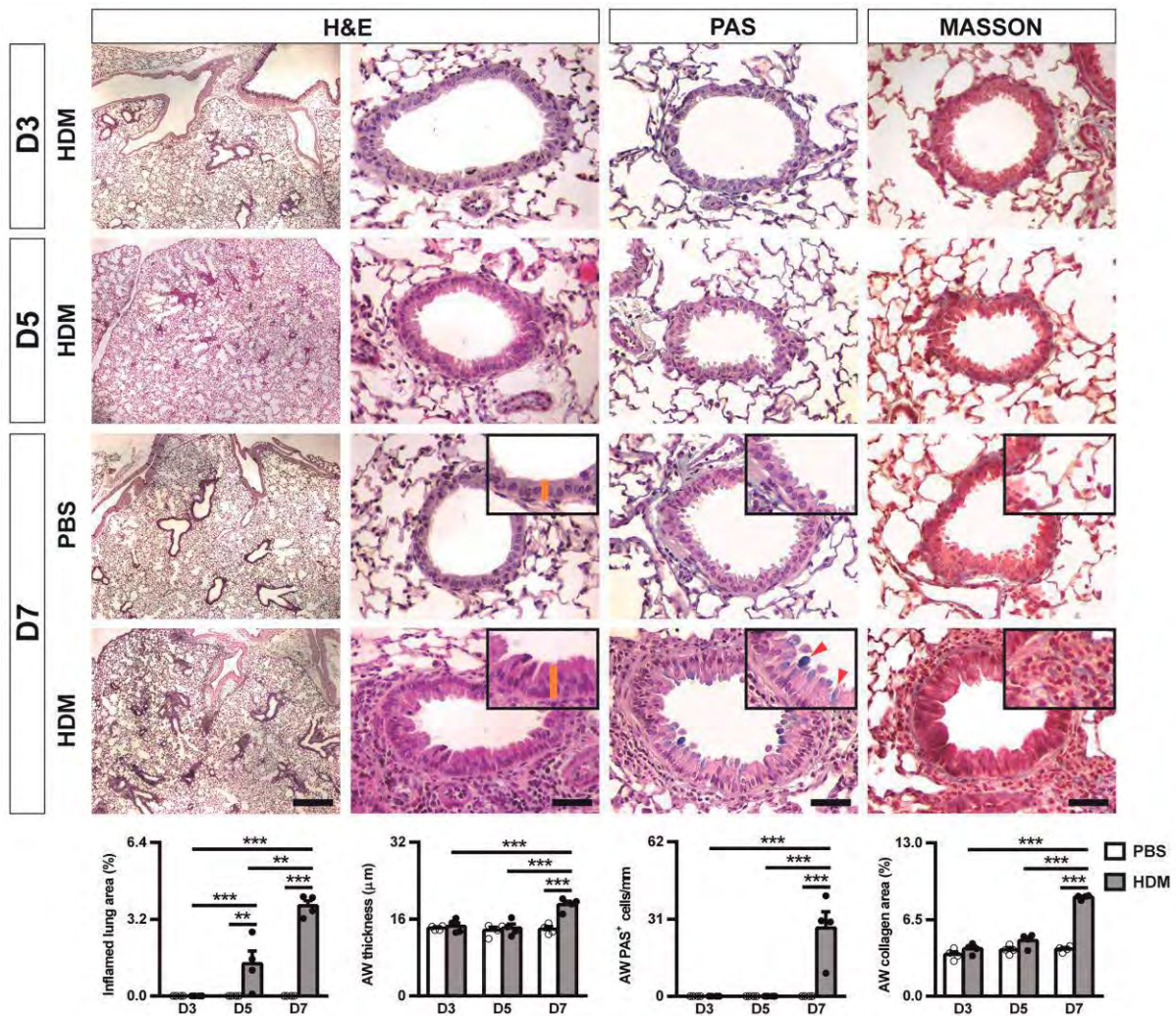


Figure 38. Progressive increase in airway inflammation and remodeling after acute HDM exposure in inbred C57BL/6 mice. Representative images of proximal airways showing inflamed lung areas (left) (scale bar: 0.5 mm), and airway thickness (orange bars in insets) (center left), mucus-producing cells per epithelium length (red arrowheads in insets) (center right) and collagen content (right) (scale bars: 50 µm) in PBS- or HDM-treated C57BL/6 mice at D3, D5 and D7. Bottom graphs represent quantification of the abovementioned parameters. Data are expressed as mean ± SEM (n = 4 animals per group). **p<0.01; ***p<0.001 (Dunn-Sidak multiple comparison test). H&E, Hematoxylin and eosin; PAS, Periodic Acid Schiff; AW, airway; HDM, house dust mite; PBS, phosphate buffered saline.

Lung mRNA expression analysis demonstrated a significant up-regulation of the allergic airway inflammation markers *Il33*, *Cd4*, *Il4*, *Il10*, *Il13*, *Ccl11*, *Ccl2*, *Cxcl1*, *Tnf* and *Il1b* in addition to the airway remodeling indicators *Acta2*, *Muc5ac* and *Col1a1*. *Tslp* and *Ccl5* expression was not found to be induced by HDM, and *Il25* expression was not able to be measured due to low to undetectable levels (**Figure 39a-b**). It should be noted that mRNA expression of *Il33*, *Cd4*, *Tnf*, *Il1b* and *Col1a1* markers was induced at D7 unlike all other markers which were already significantly increased at D5 but in general in a lesser extent than at D7. The increased *Ccl11* expression was validated by CCL11 protein levels (**Figure 39c**).

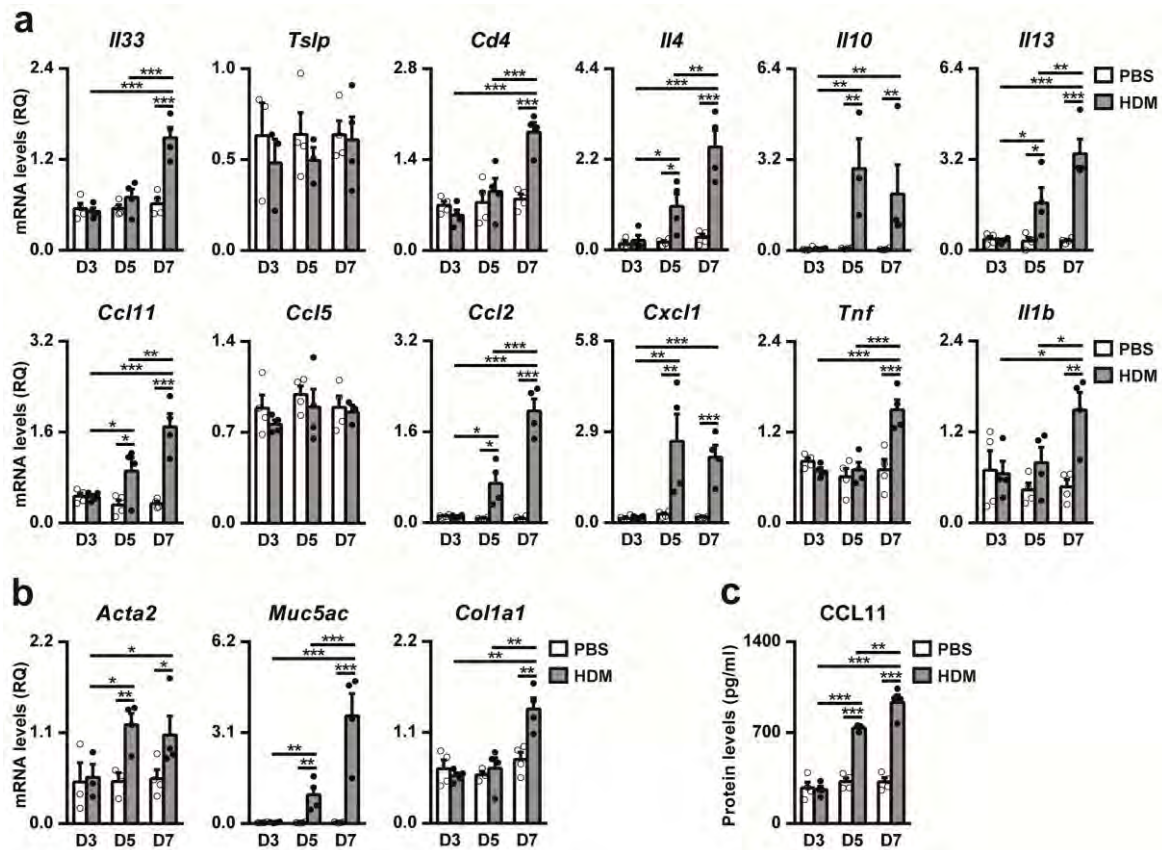


Figure 39. Expression of airway inflammation and remodeling markers after acute HDM treatment in inbred C57BL/6 mice. (a) Lung tissue mRNA expression levels of dendritic cell activators (*Il33* and *Tslp*), T-lymphocyte marker (*Cd4*), Th2 cytokines (*Il4*, *Il10* and *Il13*), eosinophil (*Ccl11* and *Ccl5*), macrophage (*Ccl2*) and neutrophil (*Cxcl1*) chemoattractants and Th1 cytokines (*Tnf* and *Il1b*); (b) bronchoconstriction (*Acta2*), goblet cell hyperplasia (*Muc5ac*) and collagen deposition (*Col1a1*) markers, and (c) CCL11 protein levels in lung homogenates in PBS- or HDM-treated inbred C57BL/6 mice at D3, D5 and D7. Data are expressed as mean \pm SEM (n = 3-4 animals per group). *p<0.05; **p<0.01; ***p<0.001 (Dunn-Sidak multiple comparison test). HDM, house dust mite; PBS, phosphate buffered saline.

4.4.2 Decreased HDM-induced neutrophilopoiesis and eosinophilopoiesis, and IL13, CCL11 and IgE serum levels after preventively-induced *Igf1r* deficiency

Together, the results presented in the previous section indicate that D7 is an appropriate time point to study the acute allergic phenotype after HDM challenge. Thus, *Igf1r* deficiency was preventively-induced to study the implication of *Igf1r* in acute asthma pathobiology (**Figure 40a**).

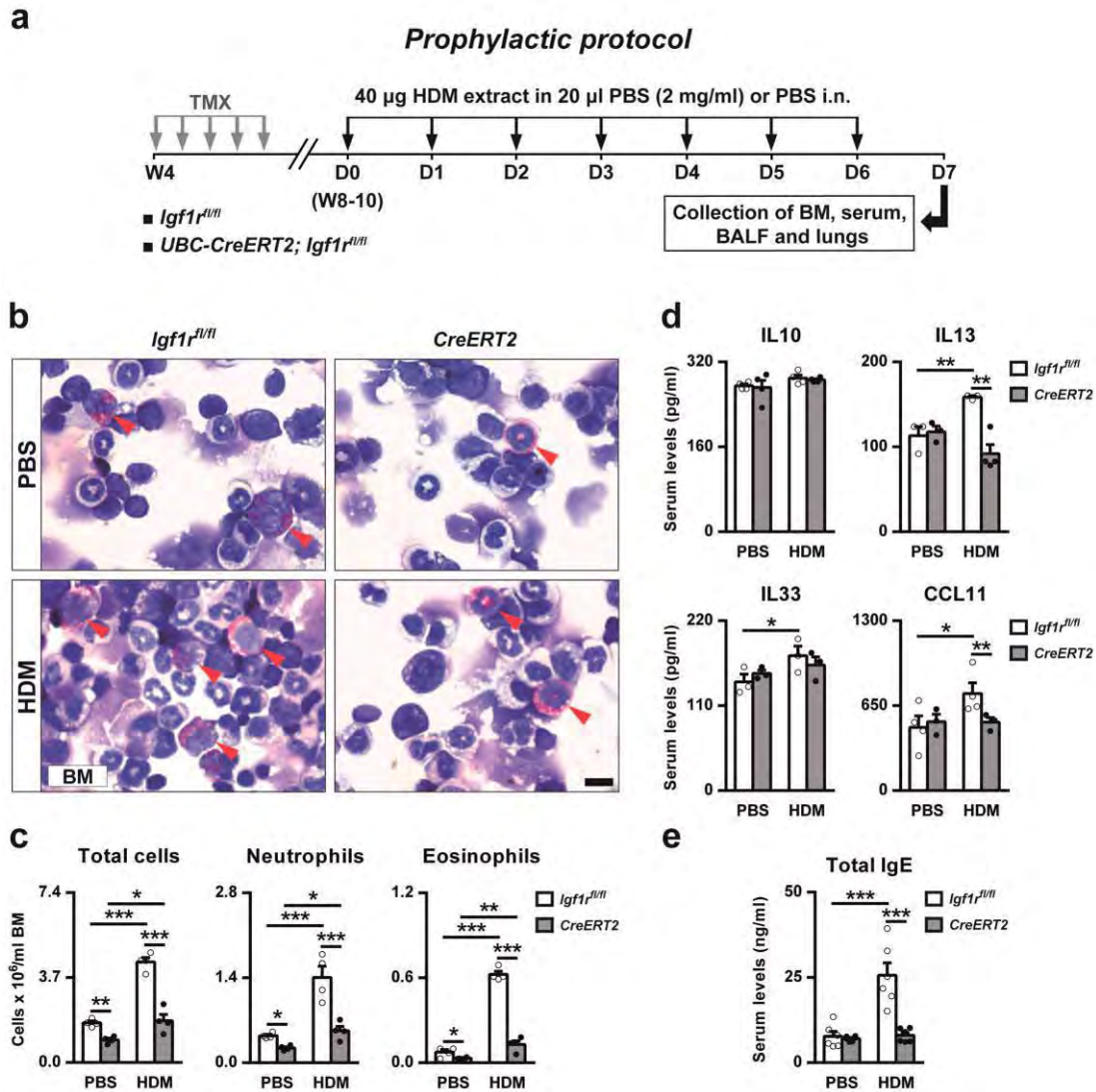


Figure 40. Protocol for prophylactic induction of *Igf1r* deficiency and HDM treatment, bone marrow cell counts and circulating levels of allergy-related markers. (a) *Igf1r^{fl/fl}* (controls) and *UBC-CreERT2; Igf1r^{fl/fl}* female mice were treated with tamoxifen (TMX) for five consecutive days at four weeks of age (W4) to induce a postnatal *Igf1r* gene deletion (López *et al.*, 2015). Then, eight- to 10-week-old (W8-10) *Igf1r^{fl/fl}* and *UBC-CreERT2; Igf1r^{fl/fl}* female mice were intranasally challenged with seven daily consecutive doses of 40 µg of HDM extract in 20 µl of PBS (2 mg/ml) or equal volume of PBS. Bone marrow, serum, BALF and lungs were harvested 24 h after last dose on D7. (b-c) Representative images and total, neutrophil and eosinophil (red arrowheads) counts in bone marrow (BM) cytopsin preparations (Scale bar: 10 µm; n = 4 animals per group) and (d-e) serum levels of IL10, IL13, IL33, CCL11 and IgE (n = 3-6 animals per group) in PBS- or HDM-exposed *Igf1r*-deficient vs. *Igf1r^{fl/fl}* mice. Data are expressed as mean ± SEM. *p<0.05; **p<0.01; ***p<0.001 (Dunn-Sidak multiple comparison test). HDM, house dust mite; PBS, phosphate buffered saline.

Total and differential cell counts in bone marrow cytopsin and measurement of serum levels of several cytokines and IgE were performed in *Igf1r*-deficient and *Igf1r^{fl/fl}* mice. Total, neutrophil and eosinophil counts in bone marrow were found to be diminished in HDM-treated *Igf1r*-depleted compared to *Igf1r^{fl/fl}* lungs. This phenomenon was also evident within PBS-treated groups. In spite of *Igf1r^{fl/fl}* mice showed increased neutrophil and eosinophil numbers after HDM treatment, *Igf1r*-deficient mice did not

show such an increase (**Figure 40b-c**). Serum IL33 levels showed only a slight increase in HDM-exposed *Igf1r^{fl/fl}* mice. In addition, IL13, CCL11 and IgE levels were significantly increased in *Igf1r^{fl/fl}* mice after HDM treatment, whereas *Igf1r*-depleted mice exhibited normal values (**Figure 40d-e**).

4.4.3 Preventively-induced *Igf1r* deficiency reduces inflammation and remodeling features

Following allergen challenge, *Igf1r^{fl/fl}* mice demonstrated a significant increase in total BALF cells. This effect was less pronounced in *Igf1r*-deficient mice. HDM-treated *Igf1r^{fl/fl}* and *Igf1r*-depleted mice showed a marked increase in macrophage, lymphocyte, neutrophil and eosinophil numbers in BALF. Notably, *Igf1r*-deficient mice demonstrated a modest decrease in lymphocyte and neutrophil counts along with a pronounced reduction in eosinophil numbers respect to *Igf1r^{fl/fl}* mice (**Figure 41a**).

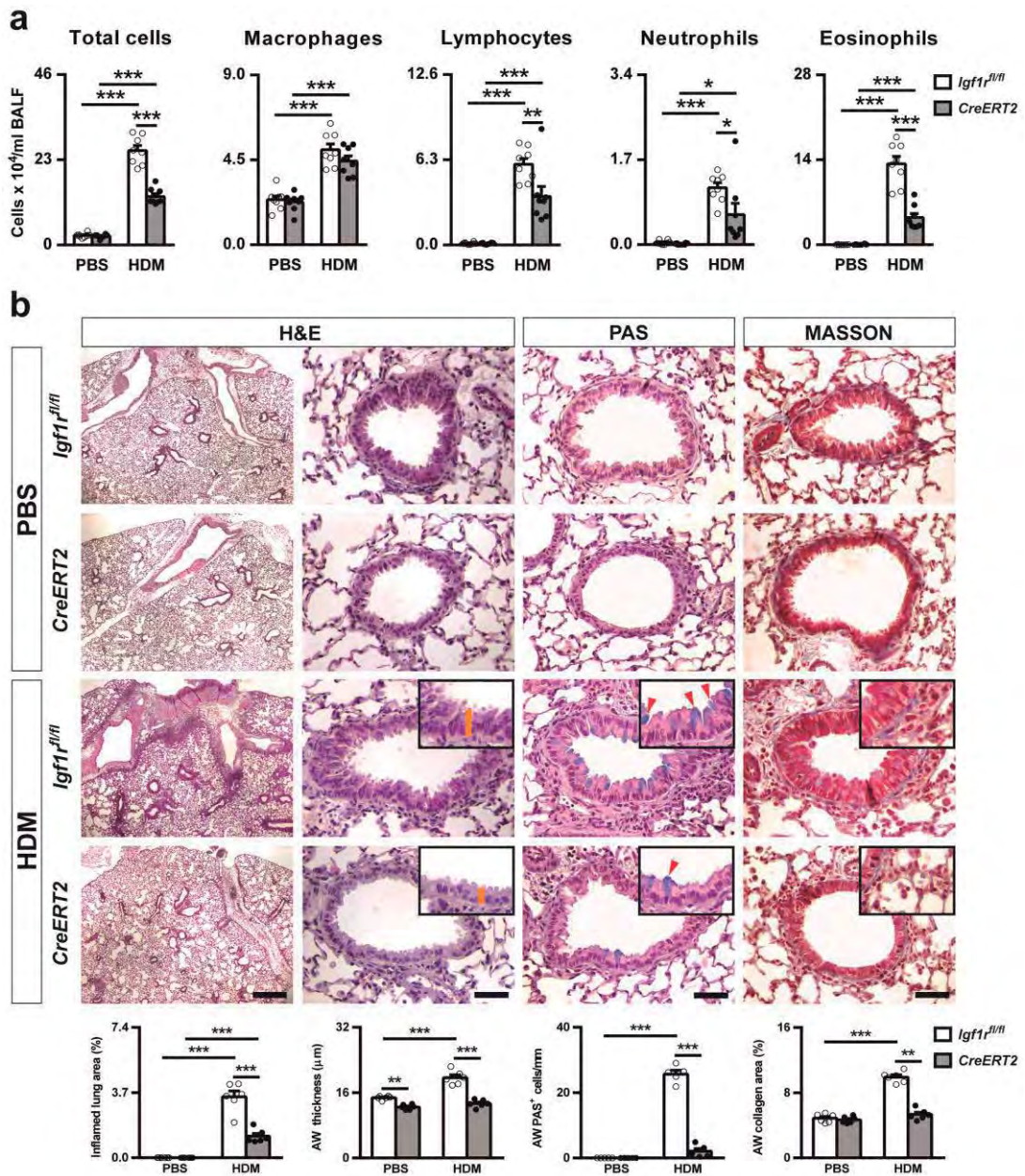


Figure 41. *Igf1r* deficiency decreases airway inflammation and remodeling after HDM exposure. (a) Total and differential cell counts performed on cytospin preparations of BALF (n = 8 animals per group) and (b) representative images of proximal airways showing inflamed lung areas (left) (scale bar: 0.5 mm); airway thickness (orange bars in insets) (center left), mucus-producing cells per epithelium length (red arrowheads in insets) (center right) and collagen content (right) (scale bars: 50 μ m; n = 5-6 animals per group) in PBS- or HDM-exposed *Igf1r*-deficient vs. *Igf1r^{fl/fl}* mice. Bottom graphs represent quantification of the abovementioned parameters. Data are expressed as mean \pm SEM *p<0.05; **p<0.01; ***p<0.001 (Dunn-Sidak multiple comparison test). H&E, Hematoxylin and eosin; PAS, Periodic Acid Schiff; AW, airway; HDM, house dust mite; PBS, phosphate buffered saline.

Inflamed lung area, number of PAS⁺ cells, collagen staining and airway thickness were notably decreased in lungs from HDM-treated *Igf1r*-deficient mice compared to lungs from *Igf1r^{fl/fl}* mice. Whereas HDM induced airway thickening in *Igf1r^{fl/fl}* mice, this phenomenon was not observed in *Igf1r*-depleted lungs (**Figure 41b**).

4.4.4 Preventively-induced *Igf1r* deficiency involves changes in expression of IGF system genes and reduces allergy-related marker levels

As a complement to the BALF and histopathology analyses, a molecular analysis of IGF system genes and allergic inflammation and remodeling markers was performed (**Figure 42**). mRNA expression profiles demonstrated an efficient depletion of *Igf1r* levels with *Igf1r*-deficient PBS- and HDM-treated mice showing a reduction of 84% and 67% respectively. HDM treatment increased *Igf1r* expression in *Igf1r^{fl/fl}* (17%) and *Igf1r*-depleted (2-fold) lungs. *Igf1* levels were significantly increased in *Igf1r*-deficient PBS- or HDM-treated mice. This effect was augmented in HDM-challenged animals. In addition, HDM treatment increased *Insr*, *Igfbp3* and *Igfbp5* levels in *Igf1r*-deficient lungs. *Igfbp3* expression was decreased in both genotypes (**Figure 42a**). mRNA levels of all allergic airway inflammation- and remodeling-related markers tested, with the exception of IL5, were strongly induced by HDM and reduced in *Igf1r*-deficient mice, except Cd4 levels (**Figure 42b-c**). The goblet cell hyperplasia marker *Spdef* was also evaluated and found to be significantly decreased in *Igf1r*-deficient HDM-exposed lungs (data not shown, 2-fold reduction). Protein levels of IL13, IL33, and CCL11 were consistent with the mRNA expression profiles. IL10 levels were only increased in HDM-treated *Igf1r^{fl/fl}* lungs (**Figure 42d**).

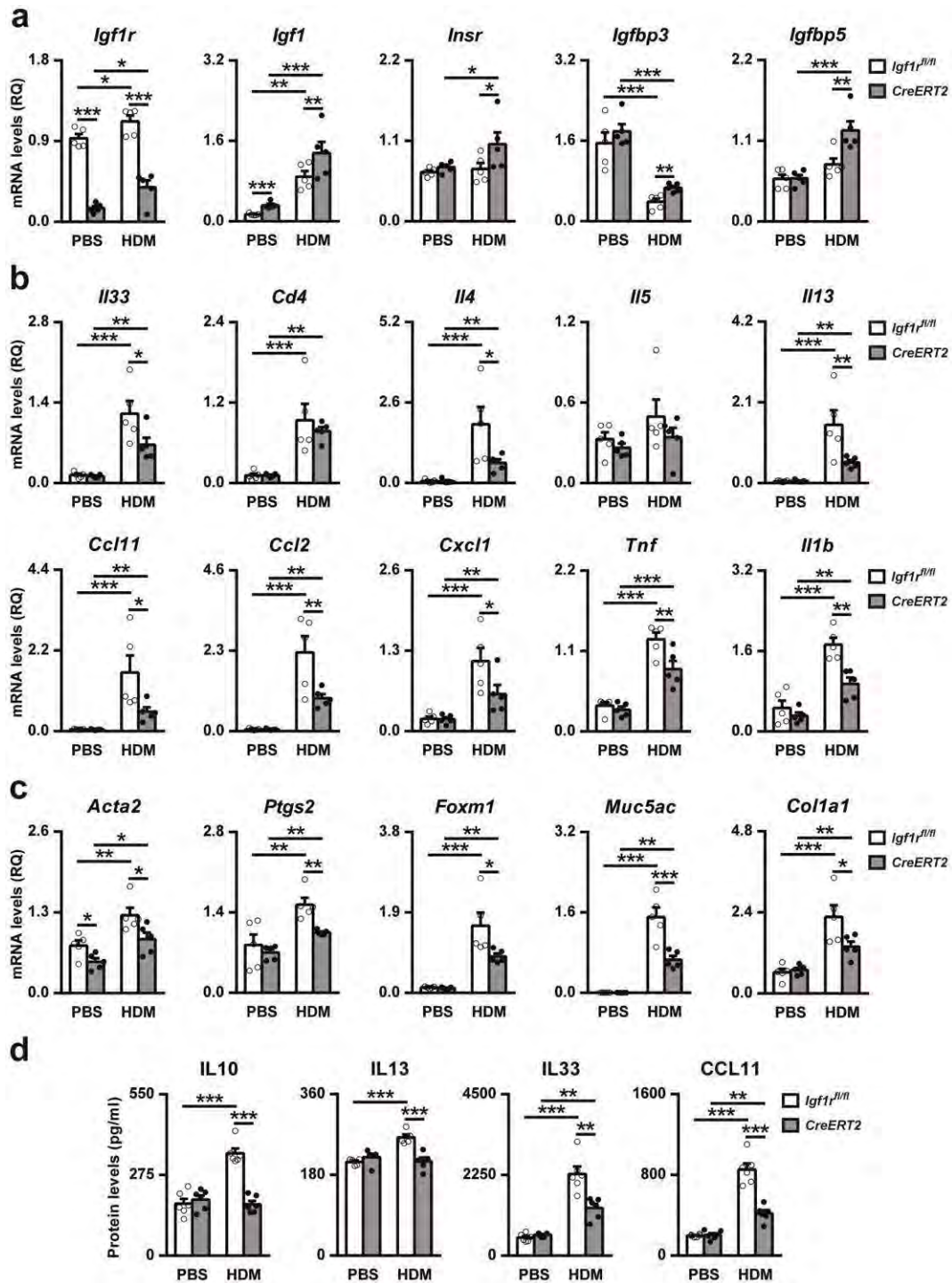


Figure 42. Expression of IGF genes and airway inflammation and remodeling markers in HDM-exposed *Igf1r*-deficient lungs. Lung tissue mRNA expression levels of (a) IGF-system genes (*Igf1r*, *Igf1*, *Insr*, *Igfbp3* and *Igfbp5*); (b) dendritic cell activator (*Il33*), T-lymphocyte marker (*Cd4*), Th2 cytokines (*Il4*, *Il5* and *Il13*), eosinophil (*Ccl11*), macrophage (*Ccl2*) and neutrophil (*Cxcl1*) chemoattractants and Th1 cytokines (*Tnf* and *Il1b*); (c) bronchoconstriction (*Acta2* and *Ptgs2*), goblet cell hyperplasia (*Foxm1* and *Muc5ac*) and collagen deposition (*Col1a1*) markers, and (d) IL10, IL13, IL33 and CCL11 protein levels in lung homogenates in PBS- and HDM-exposed *Igf1r*-deficient and *Igf1^{fl/fl}* mice. Data are expressed as mean \pm SEM (n = 5-6 animals per group). *p<0.05; **p<0.01; ***p<0.001 (Dunn-Sidak multiple comparison test). HDM, house dust mite; PBS, phosphate buffered saline.

4.4.5 Therapeutic *Igf1r*-gene targeting reduces circulating IL33, CCL11 and IgE levels, inflammation and remodeling features

Igf1r-deficiency was therapeutically induced in mice to evaluate the resolution of airway inflammation following HDM exposure (Figure 43a). Therapeutic *Igf1r*-gene targeting after TMX administration significantly decreased IL33 and CCL11 serum levels in *CreERT2* compared to non-TMX-treated mice, whereas IL10 and IL13 levels remained unchanged. *Igf1r* depletion significantly reduced IL13, IL33, CCL11 and IgE levels at D14 with respect to *Igf1r^{fl/fl}* TMX-treated animals. Interestingly, IL10 and IL13 serum levels increased from D7 to D14 in *Igf1r^{fl/fl}* mice (Figure 43b-c).

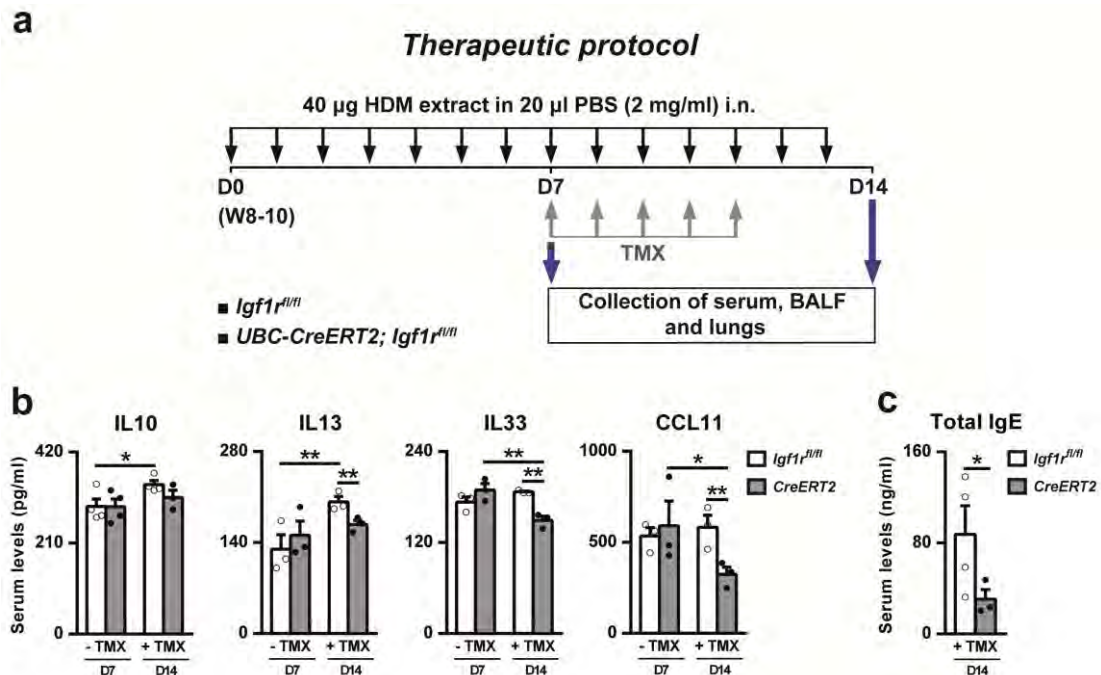


Figure 43. Protocol for therapeutic induction of *Igf1r* deficiency, HDM treatment and circulating levels of allergy-related markers. (a) Eight- to 10-week-old (W8-10) *Igf1r^{fl/fl}* and *UBC-CreERT2; Igf1r^{fl/fl}* female mice were intranasally challenged with seven (first set of animals non-treated with TMX and sacrificed at D7) or fourteen (second set of animals receiving five consecutive intraperitoneal TMX injections between D7 and D11 to induce *Igf1r* deletion in *UBC-CreERT2; Igf1r^{fl/fl}* mice to generate *CreERT2* mice) daily consecutive doses of 40 µg of HDM extract in 20 µl of PBS (2 mg/ml). Serum, BALF and lungs were collected 24 h after the last exposure. (b-c) Serum levels of IL10, IL13, IL33, CCL11 and IgE (n = 3-4 animals per group) in HDM-exposed *CreERT2* vs. *Igf1r^{fl/fl}* mice after the TMX treatment (D14) (+ TMX). Note that the *CreERT2* term used at D7 (- TMX) refers to *UBC-CreERT2; Igf1r^{fl/fl}* mice. Data are expressed as mean ± SEM. *p<0.05; **p<0.01 (Mann-Whitney U and Dunn-Sidak multiple comparison tests). HDM, house dust mite; PBS, phosphate buffered saline; TMX, tamoxifen.

Total cells in BALF were found to be increased in *Igf1r^{fl/fl}* at D14 and substantially reduced in *CreERT2* animals following TMX administration. This effect was attributed primarily to changes in neutrophil and eosinophil counts, since macrophage and lymphocyte numbers remained unchanged (Figure 44a).

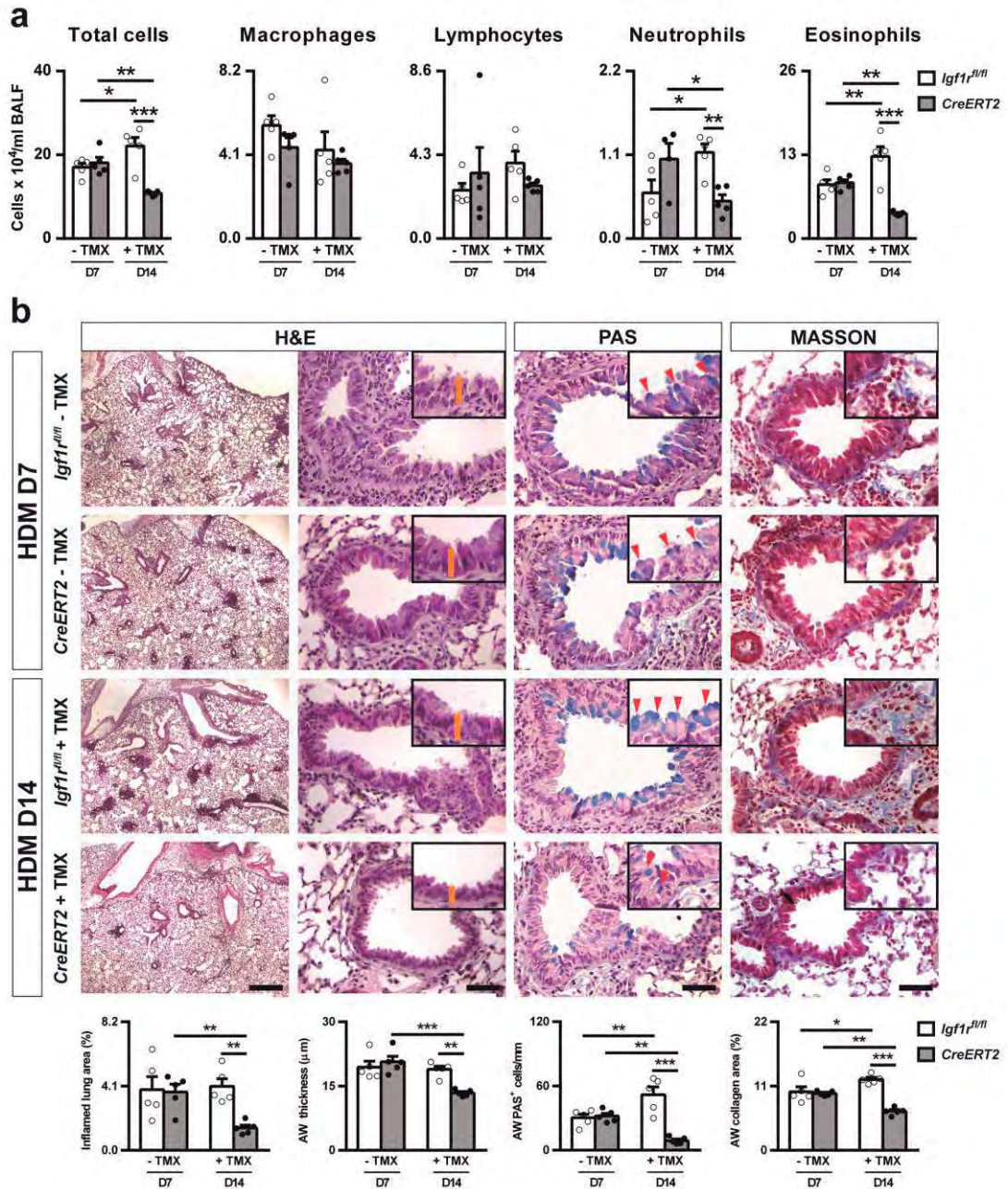


Figure 44. Therapeutic targeting of *Igf1r* reduces airway inflammation and remodeling features after HDM exposure. (a) Total and differential cell counts performed on cytospin preparations of BALF (n = 4-5 animals per group). (b) Representative images of proximal airways showing inflamed lung areas (left) (scale bar: 0.5 mm) and airway thickness (orange bars in insets) (center left), mucus-producing cells per epithelium length (red arrowheads in insets) (center right) and collagen content (right) (scale bars: 50 μm) in HDM-exposed *CreERT2* vs. *Igf1r^{fl/fl}* mice non-treated with TMX (D7) (- TMX) or after the TMX treatment (D14) (+ TMX). Note that the *CreERT2* term used at D7 (- TMX) refers to *UBC-CreERT2; Igf1r^{fl/fl}* mice. Bottom graphs represent quantification of the abovementioned parameters (n = 5 animals per group). Data are expressed as mean ± SEM. *p<0.05; **p<0.01; ***p<0.001 (Dunn-Sidak multiple comparison test). H&E, Hematoxylin and eosin; PAS, Periodic Acid Schiff; AW, airway; HDM, house dust mite; PBS, phosphate buffered saline; TMX, tamoxifen.

Inflamed lung area, airway thickness, PAS⁺ cell numbers and collagen staining were clearly counteracted in *CreERT2* lungs after TMX administration compared to *CreERT2* non-TMX- and *Igf1r^{f/f}* TMX-treated mice (**Figure 44b**).

4.4.6 Therapeutic targeting of *Igf1r* diminishes expression of allergic inflammation and remodeling-related markers, and circulating IL33 and CCL11 levels

Following TMX administration, *Igf1r* mRNA expression was found to be significantly reduced in *CreERT2* mice compared to *Igf1r^{f/f}* (85%) and *CreERT2* non-TMX-treated mice (88%) (**Figure 45a**).

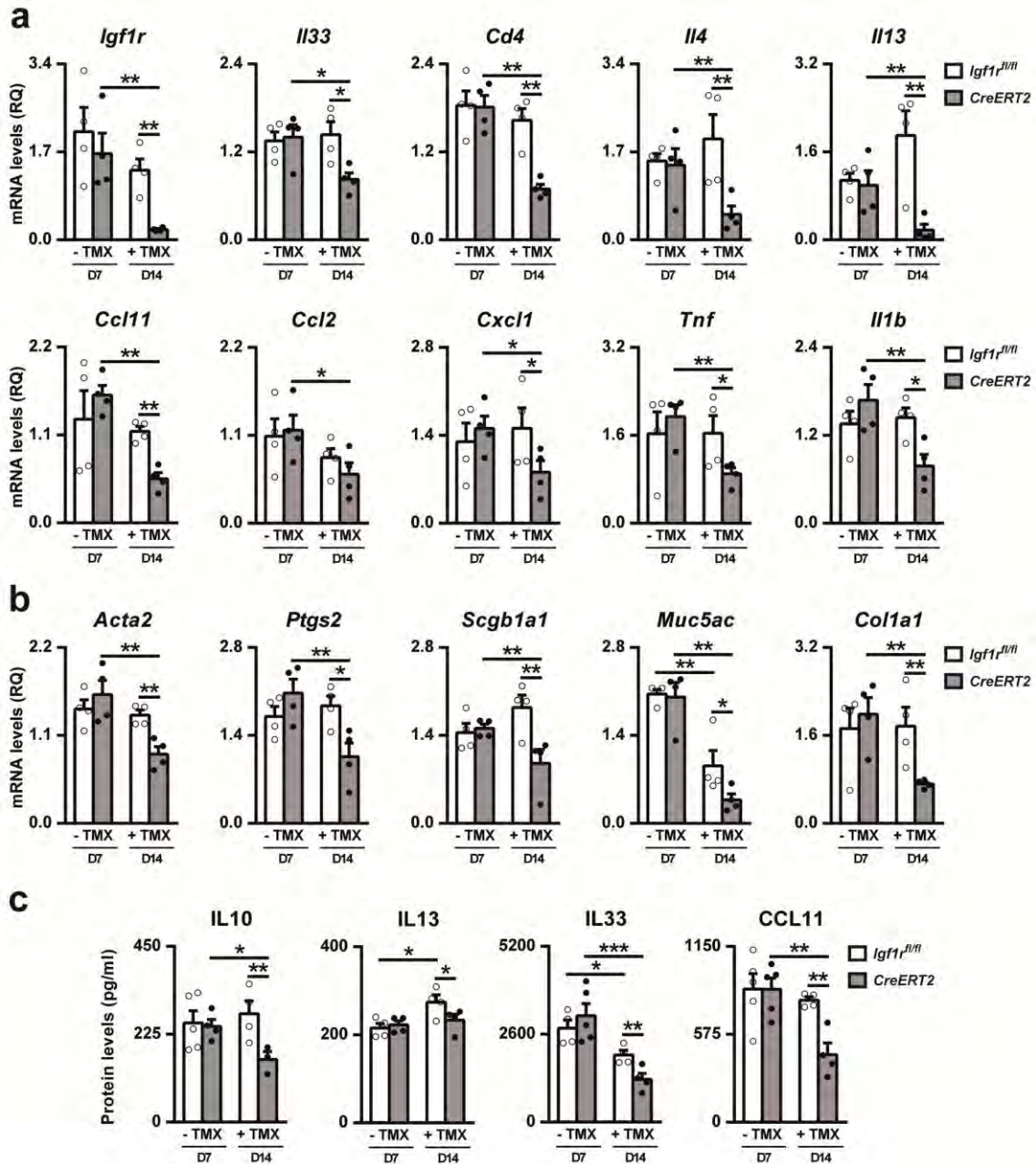


Figure 45. Therapeutic *Igf1r*-gene targeting diminishes expression of airway inflammation and remodeling-related markers after HDM exposure. Lung tissue mRNA expression levels of (a) Insulin-like growth factor 1 receptor (*Igf1r*), dendritic cell activator (*Il33*), T-lymphocyte marker (*Cd4*), Th2 cytokines (*Il4* and *Il13*), eosinophil (*Ccl11*), macrophage (*Ccl2*) and neutrophil (*Cxcl1*) chemoattractants and Th1 cytokines (*Tnf* and *Il1b*) and (b) bronchoconstriction (*Acta2* and *Ptgs2*), goblet cell hyperplasia (*Scgb1a1* and *Muc5ac*) and collagen deposition (*Col1a1*) markers, and (c) IL33, IL10, IL13 and CCL11 protein levels in lung homogenates (n = 3-5 animals per group). Quantifications were performed in HDM-exposed *CreERT2* vs. *Igf1^{fl/fl}* mice non-treated with TMX (D7) (- TMX) or after the TMX treatment (D14) (+ TMX). Note that the *CreERT2* term used at D7 (- TMX) refers to *UBC-CreERT2; Igf1^{fl/fl}* mice. Data are expressed as mean ± SEM. *p<0.05; **p<0.01; ***p<0.001 (Dunn-Sidak multiple comparison test). HDM, house dust mite; PBS, phosphate buffered saline; TMX, tamoxifen.

On the other hand, mRNA levels of the allergic airway inflammation- and remodeling-related markers demonstrated a significant reduction in *CreERT2* compared to *Igf1^{fl/fl}* and *CreERT2* non-TMX-treated mice following TMX treatment. *Ccl2* expression was only found reduced in *Igf1r*-deficient mice compared to *CreERT2* TMX-untreated animals (**Figure 45a-b**). Analysis of IL13, IL33 and CCL11 protein levels in lung homogenates supported mRNA data and IL10 levels were found to be significantly decreased in *CreERT2* mice after TMX administration (**Figure 45c**).

5 DISCUSSION

Firstly, *UBC-CreERT2; Igf1r^{Δ/Δ}* (*CreERT2*) mutant mice were generated to analyze the differential organ phenotypes after a postnatal generalized *Igf1r* conditional deletion. Notably, *UBC-CreERT2; Igf1r^{f/f}* mice efficiently delete *Igf1r* upon postnatal tamoxifen administration in multiple mouse organs. From this study it was concluded that *CreERT2* mice have advantages over conventional *Igf1r* knockout mice, such as avoiding the perinatal lethality and preventing possible cascades of compensatory responses occurring during early development, which can complicate interpretation of the phenotype, and that IGF1R function is highly dependent on cell, tissue and organ type.

Hereafter, it was studied the functional implication of IGF1R in acute lung inflammation using a BLM mouse model. First, the lung transcriptome was analyzed in unchallenged *CreERT2* mutants. In general terms, *CreERT2* mice showed decreased expression of genes related to transcriptional regulation and differentially expressed genes with potentially protective roles related to epigenetics, redox and oxidative stress. Noteworthy, since *CreERT2* mice showed resistance to BLM-mediated acute lung injury by counteracting lung inflammation and alveolar damage, IGF1R may then be considered as an important player in murine acute lung inflammation.

On the other hand, it was studied the implication of IGF1R on airway hyperreactivity and mucus secretion in a chronic HDM model of asthma. Thus, *CreERT2* mutant mice showed reduced allergic airway inflammation and remodeling, mucus production and AHR after chronic HDM exposure. Additionally, the study of allergy dynamics in inbred C57BL/6 after acute HDM-induced allergy, showed a progressive increase in allergic airway inflammation. Moreover, preventively-induced *Igf1r*-deficiency ameliorates typical asthmatic features following acute HDM treatment and the therapeutic targeting of *Igf1r* promotes the resolution of established allergic airway inflammation in *CreERT2* mice. In conclusion, these results demonstrate that IGF1R plays a key role in murine HDM-induced allergic airway inflammation.

5.1 Differential organ phenotypes after postnatal *Igf1r* gene conditional deletion induced by tamoxifen in *UBC-CreERT2; Igf1r^{f/f}* double transgenic mice (Paper I)

In an attempt to elude the sex effects caused by endogenous estrogens present in females, which could nonspecifically activate the *CreERT2* fusion protein prior to TMX administration, males were exclusively analyzed in this study. Preliminary observations made in *Igf1r* conditional mutant females preclude that they also are growth deficient, although to a lesser extent than males. Accordingly, female mice were reported to show lesser postnatal growth deficit than males in case of IGF1R deficiency (Holzenberger *et al.*, 2000; Holzenberger *et al.*, 2001).

As expected, *Igf1r* conditional mutants showed growth retardation that affected various tissues to different degrees. Thus, diverse IGF1R-deficient mice were described with growth deficit during both embryonic and postnatal development (Baker *et al.*, 1993; Holzenberger *et al.*, 2001), and total knockout mice for IGF genes demonstrated that lung, muscle, skeleton and skin are more dependent on IGFs than other organs during embryonic development (Fernandez-Moreno *et al.*, 2004; Liu *et al.*, 1993; Pichel *et al.*,

2003). Postnatally, IGF1/IGF1R signaling deficiency was described to differentially reduce adipose and cochlear growth (Camarero *et al.*, 2001; Holzenberger *et al.*, 2001; Kloting *et al.*, 2008). Increased organ to body weight ratios in spleen and heart found in *CreERT2* mutants coincide with data collected by Wang *et al.* (1999) when analyzing IGF1-deficient mice, and reduced testis size was also described in mice with an *Igf1r* conditional deletion in Sertoli cells (Pitetti *et al.*, 2013). Body parts that highly contribute to total mouse weight (e.g. muscle, skeleton, skin, and adipose tissue), and whose growth is heavily dependent on IGFs, were not measured in the mutants, but their growth deficit would possibly explain whole mice delayed growth. Surprisingly, changes in lung weight of *CreERT2* mutants were not found, even though both prenatal and postnatal growth of this organ was extensively described to be highly dependent on IGF signaling (Epaud *et al.*, 2012; Liu *et al.*, 1993; Moreno-Barriuso *et al.*, 2006; Pais *et al.*, 2013; Wang *et al.*, 1999). This discrepancy could be attributed either to differences in the mouse model or timing of tissue analyses in each study.

PCR assays of genomic DNA from TMX-treated *UBC-CreERT2; Igf1r^{fl/fl}* mice showed the *Igf1r* deletion in all tissues analyzed. However, the presence in all samples of faint bands corresponding in size with the floxed (*Igf1r^{fl}*) allele precluded a certain level of mosaicism. Furthermore, the low intensity of the floxed bands, compared with the heavy intensity shown by the deleted (*Igf1r^d*) bands, may not reflect the real proportion of cells with a total *Igf1r* knockout. Actually, generation of the deleted allele amplicon would be highly favored in the amplification reaction due to its shorter size (491 bp vs. 1300 bp of the *Igf1r^{fl}* allele), and because it only contains one loxP site (in contrast, the *Igf1r^{fl}* allele contains two). It has been proposed that loxP sites could interfere with PCR amplification caused by secondary structures formed within the DNA (Feil *et al.*, 2009; Ikeno *et al.*, 2012; Liu *et al.*, 1998). In addition, it is possible that a portion of cells may have suffered the deletion in only one of the *Igf1r^{fl}* alleles resulting in heterozygosis of the *Igf1r* locus.

The efficiency of TMX-mediated *Igf1r* deletion occurs with different degrees of mosaicism as revealed by different technical assays. It varies between mice, even in the same organ, as demonstrated by PCR analysis of genomic DNA; among organs, as reflected by qRT-PCR quantitation of *Igf1r* mRNA expression; and even in tissue areas or cell types within the same organ, as shown by immuno-staining for IGF1R. Although the ultimate reason for *Igf1r* differential recombination efficiency remains to be determined, it could be attributed to experimental variability, differential tissue access of TMX, varying levels of *UBC-CreERT2* transgene expression in adult tissues, or even to differential accessibility of Cre to loxP targets due to alternative chromatin conformations (Birling *et al.*, 2009; Kellendonk *et al.*, 1999).

Despite mosaicism, *Igf1r* mRNA expression was significantly reduced in all tissues analyzed, ranging from 81% in kidney to 47% in spleen. Accordingly, Ruzankina *et al.* (2007) described variable efficiency of *UBC-CreERT2* transgenic mice in deleting a floxed form of the *Atr* gene, although they claim recombination efficiencies higher than 70%. However, in their experimental set up, Cre only needed to excise one of the *Atr* floxed alleles, since the other one was already a null variant (Ruzankina *et al.*, 2007), while in *UBC-CreERT2; Igf1r^{fl/fl}* mice, two recombination events are needed to delete both of the *Igf1r^{fl}* alleles. Since the recombinase is only transiently active during the TMX induction period (Feil *et al.*, 2009), this requirement could reduce the efficiency in generating *Igf1r* knockout cells. Furthermore, the Cre

recombination yield obtained with a particular gene or tissue is not predictable. Indeed, the chromatin structure at the locus of interest, the state of DNA methylation and its transcriptional activity seem to affect Cre efficiency (Birling *et al.*, 2009; Vooijs *et al.*, 2001). The discrepancies found in certain organs in the reduction of IGF1R between mRNA (qRT-PCR) and protein (immuno-staining) levels could be due to aberrant molecules of mRNA generated by alternative splicing bypassing the deletion of exon 3 in the *Igf1r* gene. These mRNA forms can be detected by qRT-PCR, but not translated into IGF1R functional protein (Kloting *et al.*, 2008).

Decreased levels of IGF1R in *UBC-CreERT2; Igf1r^{fl/fl}* TMX-treated males resulted in diverse organ phenotypes, again corroborating differential organ susceptibility to IGF1R signaling. The testes were the most affected organ, showing a strong reduction in germ cell content and spermatogenesis progression, which would explain their growth deficit. Since similar phenotypes were previously described in mice with a conditional deletion of *Igf1r* in Sertoli cells, results from the present study help emphasize the essential role of this receptor in mediating cell signaling in the aforementioned testicular cells (Froment *et al.*, 2007; Pitetti *et al.*, 2013). Histological changes were also found in liver and alveolar lung parenchyma, perceived as abundant mitotic figures in the liver and increased cell density in alveolar areas, most probably a consequence of their increased proliferation rates. In addition, morphological changes in lung epithelial cells of the terminal bronchioles could be a result of alterations in differentiation of Clara cells, which are highly abundant in terminal airways and express prominent levels of IGF1R (Morrissey and Hogan 2010; Pais *et al.*, 2013). Accordingly, lack of IGF1 and IGF1R was reported to promote cell proliferation and to alter epithelial differentiation not only in the lung (Epaud *et al.*, 2012; Liu *et al.*, 1993; Moreno-Barriuso *et al.*, 2006; Pais *et al.*, 2013), but also in the prostate (Sutherland *et al.*, 2008). However, the increased cell proliferation rates found in the liver of IGF1R in *CreERT2* mutants contrast with impaired proliferation rates reported in mice deprived of *Igf1r* in hepatocytes (Desbois-Mouthon *et al.*, 2006), a discrepancy that might be attributed to a differential *Igf1r* conditional deletion in distinct hepatic cell types. Notwithstanding the prominent hepatic and alveolar parenchymal cell proliferation found in the *Igf1r* conditional mutants, without affecting total organ weight or liver cell density, apoptotic rates in these organs were in the basal range (White *et al.*, 2012; Zhu *et al.*, 2009). In accordance, hypoplastic prenatal lungs of IGF1-deficient mice have also been reported to be highly proliferative without changes in apoptosis (Pais *et al.*, 2013). In any case, understanding the kinetics of cell death in each model system is critical, and proper timing of the experimental design may be crucial to identify apoptosis (Elmore 2007). Finally, a group of organs, including kidney, spleen and cochlea, did not show evident histological alterations, which would support a less crucial IGF1R functional implication in these organs. However, it is well known that inner ear development is highly dependent on IGF signaling, mainly during postnatal cochlear maturation (Camarero *et al.*, 2001; Okano *et al.*, 2011). It would be of interest to analyze the cochlea of *CreERT2* mutants at later developmental stages to see if decreased levels of IGF1R predispose mice to hearing-loss with aging, as previously stated (Riquelme *et al.*, 2010).

From this study it can be concluded that *CreERT2* mutants are a useful model for studying a generalized functional deficit of IGF1R during postnatal development. They have advantages over conventional *Igf1r* knockout mice, such as avoiding the perinatal lethality and preventing possible

cascades of compensatory responses occurring during early development, which can complicate interpretation of the phenotype. In a sense, they could be considered an acute model of postnatal IGF1R deficit, contrasting with the total *Igf1r* knockout model that would better serve as a chronic model. In any case, conditional mutations are more informative if they can be induced at will at a chosen time during the life of the animal. Furthermore, a temporally controlled Cre/lox system would allow one to limit unwanted Cre activity and associated side effects, such as ectopic recombination due to transient Cre expression during development or potential toxic effects due to prolonged high levels of Cre activity (Feil 2007). Knowing that *CreERT2* mutants respond well to TMX treatment, alternative experimental set ups will be easy to plan by changing the timing of TMX administration, either at early or later postnatal stages, or even during embryogenesis (Feil *et al.*, 2009), and they could easily offer additional perspectives for the *in vivo* study of IGF1R signaling. Longitudinal studies on organs of these mice could serve to study IGF-signaling disorders associated with aging (e.g. in the inner ear (Riquelme *et al.*, 2010)) or in long-term progression diseases, like cancer or fibrosis.

5.2 IGF1R deficiency attenuates acute inflammatory response in a BLM-induced lung injury mouse model (Paper II)

Lung transcriptome analysis of *CreERT2* mice demonstrated a general inhibition of differentially expressed genes, as similarly reported in prenatal *Igf1*-deficient lungs (Pais *et al.*, 2013). H1 histones *Hist1h1d* and *Hist1h2bb*, as well as *Hist1h4m* and *Hist1h1a* (**Table 3**) were found to be up-regulated in *CreERT2* lungs. In this regard, it is widely known that H1 histones participate in chromatin condensation therefore repressing gene expression (Happel and Doenecke 2009; Harshman *et al.*, 2013). Additionally, the histone acetyltransferases *Crebbp* and *Ep300*, both transcriptional co-activators, were found down-regulated in IGF1R-deficient lungs. In an inflammatory context, CREBBP and EP300 were reported to activate NF- κ B-mediated pro-inflammatory gene expression in response to oxidative stress (Bayarsaihan *et al.*, 2011; Happel and Doenecke 2009; Rajendrasozhan *et al.*, 2009). Thus, increased H1 histone together with lower acetyltransferase expression would result in a more condensed chromatin state, less accessible to transcription factors. Furthermore, the lower expression observed for mitochondrial respiratory chain complexes I (*mt-Nd4*, *mt-Nd5* and *mt-Nd6*) and III (*mt-Cytb*) genes (**Table 3**) could result in decreased electron transport chain activity and consequently, in a reduction of reactive oxygen species production, since these complexes were reported to govern the response to hypoxia (Holzerova and Prokisch 2015; Schumacker *et al.*, 2014). In parallel, *Gpx8* and *Cyp1a1*, both involved in alleviating oxidative stress and inflammation (Lingappan *et al.*, 2014; Yamada *et al.*, 2012), were the two most up-regulated genes. Overall, these results indicate that IGF1R deficiency could potentially be associated with a higher capacity to endure oxidant-induced injury.

After BLM treatment *CreERT2* mice showed improved survival. Similar results were observed in acute lung injury mouse models with compromised IGF1R activity (Ahamed *et al.*, 2005; Choi *et al.*, 2009). Moreover, IGF1R-deficient lungs showed increased *Igfbp3*, *Igfbp5*, *Insr* and *Foxo1* levels after BLM challenge, possibly due to compensatory effects in response to IGF1R deficiency, as reported (Buck *et al.*,

2010; López *et al.*, 2016). Specifically, IGFBP3 and IGFBP5 have shown protective properties in the mouse lung (Alami *et al.*, 2008; Lee *et al.*, 2011; Vijayan *et al.*, 2013).

Remarkably, *CreERT2* mice showed decreased total proteins in BALF, an indicator of reduced vascular permeability. This finding together with diminished erythrocyte counts are in accordance with the lower vascular extravasation reported in hypomorphic IGF1R-deficient mice (Ahamed *et al.*, 2005). Furthermore, the decreased presence of different inflammatory cell types in *CreERT2* lungs was reflected in BALF cell counts, and supported by reduced proliferation in perivascular and alveolar areas. Diminished *Cxcl1* and *Ly6g* mRNA levels were verified by reduced neutrophilic infiltration into *CreERT2* lungs. Considering that normal neutrophil bone marrow counts in mice are around 36.9% (Yang *et al.*, 2013), BLM clearly induced bone marrow neutrophilopoiesis in *Igf1r^{fl/fl}* (54.25%) mice, unlike in IGF1R-deficient mice (25.44%). Similarly, pharmacological IGF1R blocking was recently reported to decrease the number of peripheral white blood cells (Moody *et al.*, 2014; Osorio *et al.*, 2016). Altogether, these results demonstrate that the lack of IGF1R efficiently counteracts the acute BLM-induced neutrophilia, a major inflammatory player in this model.

Concerning TNF and *Il1b*, *CreERT2* lungs showed decreased expression of these cytokines, the most relevant in the lung during the early phase of BLM response (Cavarra *et al.*, 2004; Grommes *et al.*, 2011). Accordingly, PREX1, an IGF1R signaling activator, has been shown to have a pro-inflammatory role after BLM treatment, and *Prex1*-deficient mice mirrored the pro-inflammatory profile shown by IGF1R-deficient mice at D3 (Liang *et al.*, 2016). In addition, activation of the IGF1R/PI3K/AKT/mTOR signaling pathway was reported to promote lung injury and repair (Hu *et al.*, 2016; Kral *et al.*, 2016), and IGF1R signaling promotes TNF-induced activation of NF- κ B, a major pathway involved in inflammation (Li *et al.*, 2015). Likewise, IGF1R plays an important role in initiation of the inflammatory process, as ablation of the macrophage IGF1/IGF1R signaling axis in mice inhibits the NLRP3 inflammasome, a protein complex triggered in the lung upon BLM-induced damage (Gasse *et al.*, 2009; Spadaro *et al.*, 2016). During inflammation, while M1 macrophages contribute to tissue injury after excessive production of pro-inflammatory mediators (e.g., TNF and IL1), M2 macrophages lead to resolution of inflammation and tissue repair upon anti-inflammatory cytokine activation (e.g., IL13 and CSF1) (Laskin *et al.*, 2011; Reales-Calderón *et al.*, 2014). In this regard, both diminished expression of *Tnf*, *Il1b* and *Il6* as well as elevated levels of *Csf1*, *Il13* and *Cd209a* found in *CreERT2* lungs would promote a pulmonary environment enriched in M2 macrophages. Noteworthy, IL13 was reported to protect against acute hyperoxic lung injury and *Cd209a* expression was found to be increased in the resolution-phase macrophages after peritonitis induction in mice (Corne *et al.*, 2000; Stables *et al.*, 2011). Altogether, these data support the idea that IGF1R deficiency would facilitate dampening of innate/adaptive immunity and resolution of inflammation.

Following BLM-induced lung injury, increased expression of the alveolar markers *Aqp5* and SFTPC was found in *CreERT2* lungs. Accordingly, AQP5 expression was reported to be decreased in BLM-challenged lungs (Gao *et al.*, 2013), and its reduced levels were shown to contribute to abnormal fluid fluxes during pulmonary inflammation in mice (Towne *et al.*, 2000). In addition, SFTPC-deficient mice had increased mouse mortality, neutrophilic inflammation, and alveolar damage following BLM treatment (Lawson *et al.*, 2005). In line with results from this study, *Sfptc* mRNA levels were also found to be

increased in *CreERT2* lungs after allergic airway inflammation (Piñeiro-Hermida *et al.*, 2017a). Thus, it appears that IGF1R deficiency confers a protective role against alveolar damage.

As a master transcriptional regulator of the adaptive response to hypoxia, HIF1A uses CREBBP and EP300 as transcriptional co-activators. Thus, decreased *Crebbp* and *Ep300* transcriptional levels in non-challenged *CreERT2* lungs could contribute to HIF1A reduced expression after BLM challenge. In accordance, alveolar type 2 cell-specific *Hif1a* knockout mice demonstrated milder pulmonary inflammation (Suresh *et al.*, 2014), supporting that HIF1A could play an important role in acute lung inflammation.

Although a significant reduction of IGF1R expression was observed in *CreERT2* lungs, TMX-mediated IGF1R deletion may occur with different degrees of mosaicism in different cell types. Thus, IGF1R generalized deletion cannot be used to deduce in which cells IGF1R signaling is crucial for promoting acute lung inflammation. Furthermore, the variability of intratracheal administration of BLM and the effect of the genetic background on phenotypic variations should also be considered as important constraints to this study.

5.3 Attenuated airway hyperresponsiveness and mucus secretion in HDM-exposed IGF1R-deficient mice (Paper III)

IGF1R-deficient mice are bred from a C57BL/6 genetic background, which usually do not display strong airway inflammation or AHR in response to allergen challenge (Safholm *et al.*, 2011; Swedin *et al.*, 2010). To overcome this constraint, a specific protocol using repetitive exposures to HDM during four weeks was used to induce AHR. HDM exposure decreased the IGF1R levels in *Igf1r^{fl/fl}* mice similarly to those observed in the *CreERT2* animals. Although the mechanism behind this unexpected reduction is unknown, it could be a long-term effect occurring after tissue remodeling has been established. In addition, an increased expression of other IGF system genes was also observed in *CreERT2* mutant lungs. The upregulation of *Igf1*, *Insr*, *Igfbp3*, and *Igfbp5* in PBS-exposed mice is possibly a compensatory effect in response to IGF1R deficiency, as previously reported in lungs from mice with compromised *Igf1r* signaling in the respiratory epithelium (López *et al.*, 2016). Accordingly, it has been previously reported that exogenous IGFBP3 and IGFBP5 administration blocks physiological consequences of asthma in OVA-challenged mice and enhances epithelial cell adhesion to maintain the epithelial-mesenchymal boundary (Kim *et al.*, 2012b; Lee *et al.*, 2011; Vijayan *et al.*, 2013). Thus, *Igfbp3* and *Igfbp5* could mediate protective properties against HDM-mediated allergic inflammation.

A marked increase in AHR was found in both the proximal and distal parts of *Igf1r^{fl/fl}* mice after HDM exposure, as has been reported in mice subjected to a similar allergenic challenge (Piyasada *et al.*, 2016; van der Velden *et al.*, 2014). The repeated exposure of mice to HDM also increased total cell number in BALF as well as airway remodeling parameters such as cell hyperplasia, collagen deposition, smooth muscle cells, and mucus production, all findings previously reported (Fattouh *et al.*, 2011). Furthermore, increases in airway thickness, serum total IgE, and lung IL13 levels similar to those observed herein have also been reported elsewhere (Piyasada *et al.*, 2016; Post *et al.*, 2014; Tomlinson *et al.*, 2010). All of these

features were reflected in *Igf1r^{f/f}* HDM-challenged lungs and support the effectiveness of HDM sensitization protocol.

Interestingly, the HDM-induced effects for several of measured parameters decreased in the *CreERT2* mice. In particular, AHR was not found in the IGF1R-deficient mice. AHR is considered to be dependent on several features, such as remodeling and mucus production (Busse 2010; Evans *et al.*, 2015). These features were all found decreased, albeit not totally normalized in the *CreERT2* IGF1R-deficient mice. On this basis, it was recently reported that IGF1R plays an important role in the initiation of the inflammatory process (Spadaro *et al.*, 2016) and that IGF1R signaling promotes activation of the NF- κ B pathway, a critical regulator of immune responses orchestrating HDM-induced airway inflammation, AHR, and fibrotic remodeling (Li *et al.*, 2015; Tully *et al.*, 2013). In a lung fibrosis model, it was reported that IGF1R blockade decreased α -SMA protein expression and collagen content in bleomycin-injured mice (Choi *et al.*, 2009; Hung *et al.*, 2013). Blockade of IL13 activity after chronic HDM sensitization has been shown to reduce eosinophilia in BALF, peribronchial collagen, and goblet cell hyperplasia, findings that are in accordance with unaltered IL13 levels by HDM exposure in *CreERT2* mutant lungs (Tomlinson *et al.*, 2010).

Whereas HDM caused a clear increase in eosinophils in blood and BALF of *Igf1r^{f/f}* mice, their levels remained close to basal in *CreERT2* IGF1R-deficient mice. It has been previously shown that IGF1R deregulation decreases the number of peripheral white blood cells, thus providing evidence implicating IGF1R in promoting bone marrow myeloid cell generation (Moody *et al.*, 2014; Osorio *et al.*, 2016). The reduced eosinophil counts observed in blood and BALF from *CreERT2* mutant mice led us to speculate that IGF1R could have an important role in proliferation and/or differentiation of myeloid progenitors and their recruitment to the lung, especially with respect to eosinophils. Further studies are needed to confirm this hypothesis.

The reduced proportion of club cells found in distal airways of *CreERT2* mutant lungs is in accordance with a recent study in which it was demonstrated that a lung epithelial-specific *Igf1r* deficiency in mice caused delayed differentiation of club cells in terminal bronchioles (López *et al.*, 2016). In response to allergen stimulation, club cells differentiate into goblet cells through transcriptional activation of the master regulator *Spdef*. Subsequently, the increase in MUC5AC expression through transcriptional activation of SPDEF in goblet cells contributes to both goblet cell hyperplasia and mucus hyperproduction (Chen *et al.*, 2009; Ren *et al.*, 2013). In this context, delayed club cell differentiation in *CreERT2* airways may result in decreased transdifferentiation into goblet cells, with a concomitant reduction in goblet cell hyperplasia and mucus production. In accordance with depleted *Spdef* and MUC5AC expression in *CreERT2* mice, *Spdef*-deficient mice showed an improved lung function as well as a reduced number of BALF eosinophils, and targeted silencing of SPDEF in airway epithelial cells *in vitro* reduces MUC5AC expression (Rajavelu *et al.*, 2015; Song *et al.*, 2015). Furthermore, *Muc5ac* deficiency in mice abolishes AHR and inflammation (Evans *et al.*, 2015; Koeppen *et al.*, 2013). As such, a reduction in mucus production may contribute to the improved lung function in *CreERT2* mutant mice observed in this study. It has also been demonstrated that IL13 stimulation of human airway epithelial cells induced MUC5AC expression (Gomperts *et al.*, 2007). Together, these findings support a role for IGF1R in lung

airway epithelium transdifferentiation to the mucosecretory cell fate during chronic allergic airway inflammation.

Pulmonary surfactant proteins are essential for lung function and homeostasis after birth (Whitsett *et al.*, 2010). While surfactant proteins B and C showed a critical role in the preservation of lung function, the immunomodulatory proteins A and D were reported to play an important role during allergic airway inflammation (Glasser *et al.*, 2013; Ikegami *et al.*, 2005; Ledford *et al.*, 2012; Ogawa *et al.*, 2014). In this study it was also observed that IGF1R deficiency causes a general increase in surfactant expression basally and after the HDM challenge. On this basis, it can be concluded that increased expression of surfactant markers improves lung function of *CreERT2* mice and also is important for maintenance of homeostasis in the lung.

Although little is known about the role of IGFs in patients with asthma, previous reports in humans support data found in mice. Thus, corticosteroid treatment in asthma can reduce the lamina reticular thickness by reduction of IGF1 expression with consequent inhibition of the airway infiltration by inflammatory cells and therefore help to prevent remodeling of the airways (Hoshino *et al.*, 1998). Moreover, IGFBP3 secreted by IGF1-stimulated airway epithelial cells during allergic inflammation was suggested to be involved in allergic airway remodeling (Veraldi *et al.*, 2009). Considering that there are no effective therapies available to prevent asthma, targeting IGF signaling can be an attractive therapeutic strategy. Actually, treatment to inhibit the IGF1 action in cancer has been performed but did not show a uniform benefit among patients (Belfiore *et al.*, 2009). Conversely, targeting IGF1R, which is currently being exhaustively evaluated in clinical trials for oncologic patients (Iams *et al.*, 2015), could be emphasized as an approach for the treatment of asthma.

5.4 Characterization of the acute inflammatory profile and resolution of airway inflammation after *Igf1r*-gene targeting in a murine model of HDM-induced asthma (Paper IV)

Noteworthy, very few studies have reported the acute effects after HDM exposure in mice. In this regard, total and eosinophil counts in BALF and IL13 expression in the lung were found significantly increased one week after repetitive intranasal HDM exposure in mice (Gregory *et al.*, 2009). Furthermore, total and differential BALF cell counts, peribronchial inflammation and goblet cell hyperplasia were notably increased after 10 consecutive days of intranasal HDM challenge in mice (Cates *et al.*, 2004). In the present study acute HDM exposure in inbred C57BL/6 mice demonstrated a progressive increase in inflammatory cells in BALF, airway remodeling and mRNA expression of allergic airway inflammation and remodeling markers up to D7. Consistent with increased *Il33* expression it was previously reported that IL33, but not TSLP or IL25, is central to HDM allergic sensitization (Chu *et al.*, 2013).

Preventive induction of *Igf1r* deficiency in PBS-treated mice led to similar *Igf1r*-depleted expression to that observed in unchallenged mice of similar age (Piñeiro-Hermida *et al.*, 2017a). In addition, *Igf1r* and *Igf1* levels increased after HDM exposure. Accordingly, IGF1R and IGF1 expression was found to be increased in BAL cells and bronchial biopsies of asthmatic patients (Esnault *et al.*, 2013; Hoshino *et al.*, 1998). The upregulation of *Igf1* in PBS-treated *Igf1r*-depleted mice or *Igf1* and *Insr* by HDM

was possibly due to compensatory effects in response to *Igf1r* deficiency (Piñeiro-Hermida *et al.*, 2017a). Regarding increased *Igfbp3* and *Igfbp5* levels in HDM-treated *Igf1r*-deficient mice, exogenous IGFBP3 and IGFBP5 administration blocks the physiological consequences of asthma and enhances epithelial cell adhesion to maintain the epithelial-mesenchymal boundary (Kim *et al.*, 2012b; Lee *et al.*, 2011; Vijayan *et al.*, 2013). From these data it can be concluded that both *Igf1r* and *Igf1* may be important mediators in the establishment of murine asthma, and that *Igfbp3* and *Igfbp5* could play protective roles against HDM-induced allergic inflammation.

Whereas acute HDM treatment caused a clear increase in eosinophil and neutrophil numbers in the bone marrow of *Igf1r^{fl/fl}* mice, their levels remained close to basal after preventively-induced *Igf1r* deficiency. In this regard, it was recently published a selective decrease in circulating eosinophils after chronic HDM exposure and reduced neutrophil numbers after acute-induced lung injury in the same mutant mouse line (Piñeiro-Hermida *et al.*, 2017a; Piñeiro-Hermida *et al.*, 2017b). Thus, IGF1R could have an important role in bone marrow myelopoiesis after HDM-induced allergy.

Following HDM challenge, decreased total and eosinophil counts in BALF and reduced asthmatic features after preventively-induced *Igf1r* deficiency are consistent with published data on IGF1R-deficient mice after chronic HDM exposure (Piñeiro-Hermida *et al.*, 2017a). Notably, neutrophil and eosinophil presence in BALF and asthma-related features were counteracted in a similar manner in HDM-treated mice following therapeutic targeting of *Igf1r*.

IGF1R plays an important role in initiation of the inflammatory process, since IGF1R deficient mice showed reduced *Il1b* and *Tnf* expression (Piñeiro-Hermida *et al.*, 2017b). This is consistent with the decreased expression of *Il1b* and *Tnf* either after preventive or therapeutic-induced *Igf1r* deficiency. In this regard, it was reported that both IL1B and TNF are required for allergen-specific Th2 cell activation and for the development of AHR in mice (Nakae *et al.*, 2003; Nakae *et al.*, 2007). Accordingly, IGF1R-deficient mice exhibited no AHR after chronic HDM exposure (Piñeiro-Hermida *et al.*, 2017a).

Lung inflammation in asthma is typically orchestrated by activation of innate immune cells followed by an exacerbated Th2-biased inflammation and synthesis of allergen-specific IgE antibody, which initiates the release of inflammatory mediators from immune cells (Busse and Lemanske 2001; Jacquet 2011). In this line, following HDM exposure, *Igf1r^{fl/fl}* mice demonstrated increased levels of serum total IgE that were counteracted upon both the preventive and therapeutic strategies. Accordingly, elevated levels of serum total IgE have been reported in HDM-challenged mice and in patients with allergic asthma [Piñeiro-Hermida *et al.*, 2017a; Schulman *et al.*, 2015].

Upon allergen exposure, IL33 is mainly released from the airway epithelium to participate in the induction of Th2 immunity and is important for the establishment and maintenance of allergic response (Makrinioti *et al.*, 2014). IL33 levels were significantly reduced in serum and lungs after therapeutic-induced *Igf1r* deficiency but only in lungs following preventive-induced deficiency. Accordingly, increased expression of IL33 in the airway epithelium and serum of asthmatic patients was correlated with disease severity (Prefontaine *et al.*, 2010; Raeiszadeh Jahromi *et al.*, 2014). Additional reports have shown that IL33 exacerbates murine allergic bronchoconstriction and that resolution of allergic airway inflammation and AHR is dependent upon disruption of IL33 signaling in mice (Kearley *et al.*, 2009; Sjöberg *et al.*, 2015).

Notably, lung epithelial-specific *Igf1r* deficiency in mice caused delayed differentiation of the airway epithelium, a major source of IL33 (Kouzaki *et al.*, 2011; López *et al.*, 2016). IGF1R-deficient lungs showed a reduced proportion of club cells in distal airways after chronic HDM exposure (Piñeiro-Hermida *et al.*, 2017a) and therefore this phenomenon could be manifested as a reduced IL33 release from the airway epithelium by HDM.

Attenuated increase in IL13 levels in serum and lungs was observed following preventive or therapeutic induction of *Igf1r* deficiency. Since IL13 levels are increased in serum of asthmatic patients, it is considered a biomarker of disease severity (Gaye *et al.*, 2015). Blockade of IL13 activity in mice after HDM sensitization reduces eosinophilia in BALF, peribronchial collagen, and goblet cell hyperplasia (Tomlinson *et al.*, 2010). These findings are in accordance with results presented in this study and in a recent publication in which IGF1R-deficient mice also showed unaltered IL13 levels after chronic HDM exposure (Piñeiro-Hermida *et al.*, 2017a).

Following HDM treatment IL10 levels were found to be decreased after both the preventive and therapeutic strategies. Even though IL10 is a regulatory cytokine with immunosuppressive and anti-inflammatory properties, its role in asthma remains unclear. IL10 is necessary for the expression of AHR after allergic sensitization in mice and its levels in serum were reported differently altered in asthmatic patients (Justice *et al.*, 2001; Raeiszadeh Jahromi *et al.*, 2014; Zhang *et al.*, 2013).

CCL11 is also a potential diagnostic marker for asthma since it is significantly increased in serum of asthmatic patients (Wu *et al.*, 2014). CCL11 levels in serum and lungs were found after both the preventive and therapeutic approaches. Notably, enhanced expression of CCL11 in the bronchial epithelium of asthmatic patients was found to be associated with the development of AHR (Ying *et al.*, 1997). After allergen exposure, the eosinophil chemoattractant CCL11 is released by the airway epithelium in response to cytokines such as IL4, IL13 and TNF (Conroy and Williams 2001). In the present study, reduced IL13, *Il4* and *Tnf* levels in HDM-treated mice after preventive- or therapeutic-induced *Igf1r* deficiency supported depleted CCL11 levels. Of note, club cell-derived CCL11 is crucial for the accumulation of eosinophils during allergic lung inflammation (Sonar *et al.*, 2012).

The reduced number in PAS⁺ cells was validated by decreased expression of the goblet cell hyperplasia markers *Foxm1*, *Spdef* and *Muc5ac* following preventive induction of *Igf1r* deficiency and by decreased expression of *Scgb1a1* and *Muc5ac* after the therapeutic approach. After allergen stimulation FOXM1 induces differentiation of club cells into goblet cells through transcriptional activation of SPDEF. Then, increased MUC5AC expression by SPDEF in goblet cells contributes to goblet cell hyperplasia and mucus hyperproduction (Ren *et al.*, 2013). In accordance, blockade of FOXM1 activity in mice after HDM exposure led to reduced goblet cell hyperplasia and decreased number of eosinophils in BALF (Sun *et al.*, 2017; Swedin *et al.*, 2010). Furthermore, both lung epithelial-specific *Igf1r* deficiency in mice and chronically HDM-challenged IGF1R-depleted mice showed delayed club cell differentiation which could result in decreased goblet cell hyperplasia and mucus production (López *et al.*, 2016; Piñeiro-Hermida *et al.*, 2017a).

Both *Acta2* (α -SMA) and *Ptgs2* (COX2) levels were found to be decreased following preventive and therapeutic approaches. Accordingly, airway smooth muscle thickness was substantially reduced in

IGF1R-deficient mice after chronic HDM exposure (Piñeiro-Hermida *et al.*, 2017a) and pharmacological COX2 inhibition after allergen challenge in mice reduced inflammatory cells in BALF (Swedin *et al.*, 2010). Moreover, decreased *Col1a1* expression following the preventive and therapeutic approaches supported the reduced collagen deposition around the airways.

The proposed mechanism for reduced susceptibility to allergic airway inflammation in IGF1R-deficient mice (**Figure 46**) is supported by results from the present study and additional reports. Following HDM exposure *Igf1r* deficiency counteracts collagen deposition, smooth muscle thickening and mucus secretion. The airway epithelium is known to be a major source of IL33 and its delayed differentiation by *Igf1r* deficiency could diminish IL33 levels after HDM treatment, reducing the induction of Th2 immunity and particularly IL13 expression. After HDM exposure, IL13 normally stimulates goblet cell differentiation in the airway epithelium which leads to goblet cell hyperplasia and mucus hyperproduction in addition to triggering the release of CCL11. Delayed differentiation of the airway epithelium caused by *Igf1r* deficiency together with diminished IL13 levels may inhibit differentiation of goblet cells and CCL11 production, reducing mucus secretion and eosinophil recruitment to the lung. Additionally, decreased eosinophilopoiesis in bone marrow of *Igf1r*-deficient mice can also substantially contribute to reduced eosinophil presence in the lung (Kearley *et al.*, 2009; López *et al.*, 2016; Nakae *et al.*, 2007; Piñeiro-Hermida *et al.*, 2017a; Sonar *et al.*, 2012; Ying *et al.*, 1997).

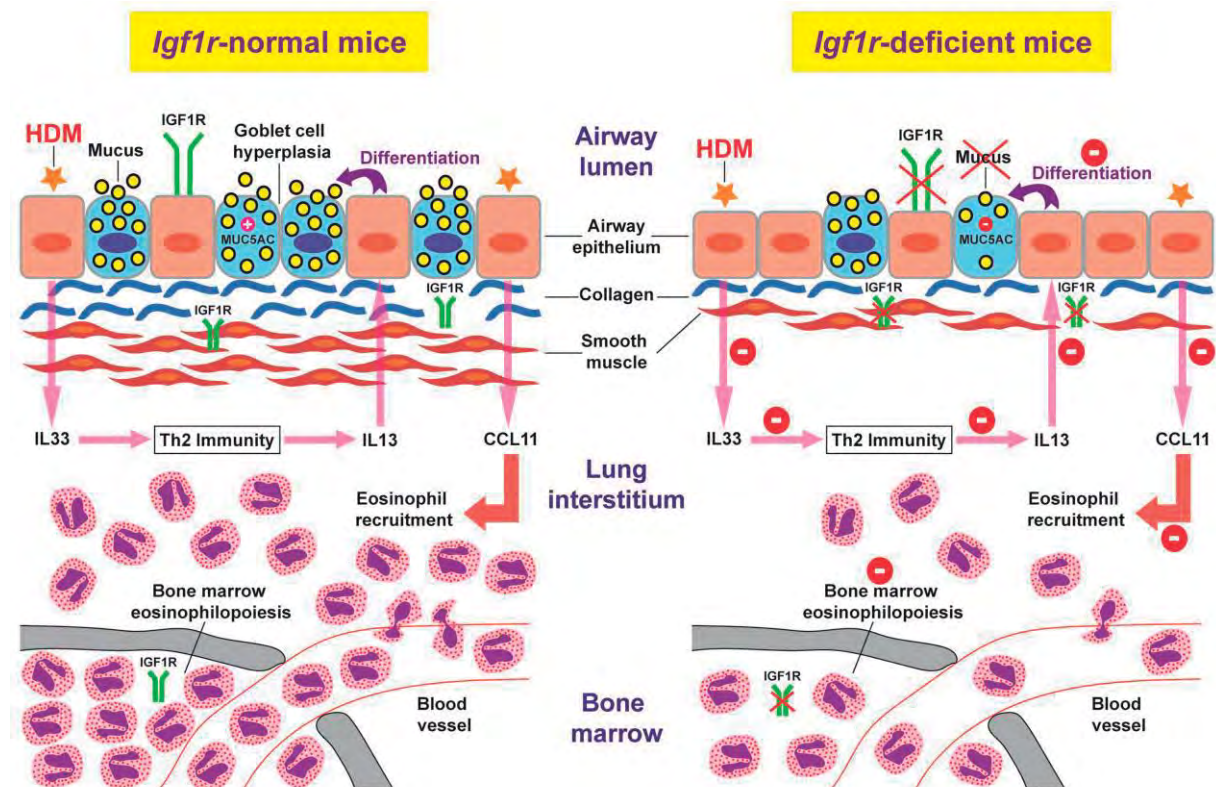


Figure 46. Proposed mechanism for reduced susceptibility to allergic airway inflammation.

Although the short-term therapeutically-induced and generalized *Igf1r* deficiency presented in this study efficiently resolves established allergic airway inflammation, TMX-mediated *Igf1r* deletion in mice may occur with different degrees of mosaicism in different cell types. Thus, *Igf1r* generalized deficiency cannot be used to deduce in which cells IGF1R signaling is crucial for promoting allergic airway inflammation. Furthermore, the variability of intranasal administration of HDM and the effect of the genetic background on phenotypic variations should also be considered as constraints to this study.

6 CONCLUSIONS

The main conclusions from this thesis are:

1. *The postnatal induction of IGF1R deficiency in mice allows avoiding the perinatal lethality and prevents possible cascades of compensatory responses occurring during early development, which can complicate interpretation of the phenotype. In addition, it was also demonstrated that IGF1R function is highly dependent on cell, tissue and organ type.*
2. *Since IGF1R deficient mice showed resistance to BLM-mediated acute lung injury by counteracting lung inflammation and alveolar damage, IGF1R can then be considered an important player in murine acute lung inflammation.*
3. *IGF1R is now considered to play a key role in HDM-driven allergic airway inflammation in mice, since IGF1R deficiency attenuates AHR, airway remodeling and mucus secretion after chronic HDM exposure and that therapeutic targeting of IGF1R resolves HDM-driven allergic airway inflammation.*
4. *IGF1R is suggested to be a potential candidate to develop novel clinical trials focused on the study of systemic IGF1R inhibitors that could be more efficient in counteracting the inflammatory response at different levels, since IGF1R deficiency attenuates bone marrow neutrophilopoiesis and eosinophilopoiesis after BLM treatment and HDM exposure, respectively.*
5. *These findings contribute toward a better understanding of the importance of IGF1R as a potential target for future therapeutic approaches in respiratory diseases with persistent damage and inflammation.*

7 REFERENCES

- Abbas A, Imrie H, Viswambharan H, Sukumar P, Rajwani A, Cubbon RM, *et al.* The insulin-like growth factor-1 receptor is a negative regulator of nitric oxide bioavailability and insulin sensitivity in the endothelium. *Diabetes* 2011; 60(8):2169-2178.
- Abuzzahab MJ, Schneider A, Goddard A, Grigorescu F, Lautier C, Keller E, *et al.* IGF-I receptor mutations resulting in intrauterine and postnatal growth retardation. *N Engl J Med* 2003; 349(23):2211-2222.
- Agulló-Ortuño MT, Díaz-García CV, Agudo-López A, Pérez C, Cortijo A, Paz-Ares L, *et al.* Relevance of insulin-like growth factor 1 receptor gene expression as a prognostic factor in non-small cell lung cancer. *J Cancer Res Clinical Oncol* 2015; 141(1):43-53.
- Ahamed K, Epaud R, Holzenberger M, Bonora M, Flejou JF, Puard J, *et al.* Deficiency in type 1 insulin-like growth factor receptor in mice protects against oxygen-induced lung injury. *Respir Res* 2005; 6:31-41.
- Ahasic AM, Zhao Y, Su L, Sheu CC, Thompson BT, Christiani DC. Adiponectin gene polymorphisms and acute respiratory distress syndrome susceptibility and mortality. *PLoS One* 2014; 9(2):e89170.
- Alami N, Page V, Yu Q, Jerome L, Paterson J, Shiry L, *et al.* Recombinant human insulin-like growth factor-binding protein 3 inhibits tumor growth and targets the Akt pathway in lung and colon cancer models. *Growth Horm IGF Res* 2008; 18(6):487-496.
- Annunziata M1, Granata R, Ghigo E. The IGF system. *Acta Diabetol* 2011; 48(1):1-9.
- Baker J, Liu JP, Robertson EJ, Efstratiadis A. Role of insulin-like growth factors in embryonic and postnatal growth. *Cell* 1993; 75(1):73-82.
- Bargagli E, Olivieri C, Bennett D, Prasse A, Muller-Quernheim J, Rottoli P. Oxidative stress in the pathogenesis of diffuse lung diseases: a review. *Respir Med* 2009; 103(9):1245-1256.
- Bayarsaihan, D. Epigenetic mechanisms in inflammation. *J Dent Res* 2011; 90(1):9-17
- Belfiore A, Frasca F, Pandini G, Sciacca L, Vigneri R. Insulin receptor isoforms and insulin receptor/insulin-like growth factor receptor hybrids in physiology and disease. *Endocr Rev* 2009; 30(6):586-623.
- Birling MC, Gofflot F, Warot X. Site-specific recombinases for manipulation of the mouse genome. *Methods Mol Biol* 2009; 561:245-263.
- Bonnette SG, Hadsell DL. Targeted disruption of the IGF-I receptor gene decreases cellular proliferation in mammary terminal end buds. *Endocrinology* 2001; 142(11):4937-4945.
- Buck E, Gokhale PC, Koujak S, Brown E, Eyzaguirre A, Tao N, *et al.* Compensatory insulin receptor (IR) activation on inhibition of insulin-like growth factor-1 receptor (IGF-1R): rationale for cotargeting IGF-1R and IR in cancer. *Mol Cancer Ther* 2010; 9(10):2652-2664.
- Buday T, Plevkova J. House dust mite allergy models-reliability for research of airway defensive mechanisms. *Open J Mol Integrative Physiol* 2014; 4(3):27-35.
- Busse WW, Lemanske RF Jr. Asthma. *N Engl J Med* 2001; 344(5):350-362.
- Busse WW. The relationship of airway hyperresponsiveness and airway inflammation: airway hyperresponsiveness in asthma: its measurement and clinical significance. *Chest* 2010; 138(2 Suppl):4S-10S.

Calderón MA, Linneberg A, Kleine-Tebbe J, De Blay F, Hernandez Fernandez de Rojas D, Virchow JC, *et al.* Respiratory allergy caused by house dust mites: what do we really know? *J Allergy Clin Immunol* 2015; 136(1):38-48.

Camarero G1, Avendano C, Fernandez-Moreno C, Villar A, Contreras J, de Pablo F, *et al.* Delayed inner ear maturation and neuronal loss in postnatal Igf-1-deficient mice. *J Neurosci* 2001; 21(19):7630-7641.

Cates EC, Fattouh R, Wattie J, Inman MD, Goncharova S, Coyle AJ, *et al.* Intranasal exposure of mice to house dust mite elicits allergic airway inflammation via a GM-CSF-mediated mechanism. *J Immunol* 2004; 173(10): 6384-6392.

Cavarra E, Carraro F, Fineschi S, Naldini A, Bartalesi B, Pucci A, *et al.* Early response to bleomycin is characterized by different cytokine and cytokine receptor profiles in lungs. *Am J Physiol Lung Cell Mol Physiol* 2004; 287(6):L1186-1192.

Chen J, Stubbe J. Bleomycins: towards better therapeutics. *Nat Rev Cancer* 2005; 5(2):102-112.

Chen G, Korfhagen TR, Xu Y, Kitzmiller J, Wert SE, Maeda Y, *et al.* SPDEF is required for mouse pulmonary goblet cell differentiation and regulates a network of genes associated with mucus production. *J Clin Invest* 2009; 119(10):2914-2924.

Cheresh P, Kim SJ, Tulasiram S, Kamp DW. Oxidative stress and pulmonary fibrosis. *Biochim Biophys Acta* 2013; 1832(7):1028-1040.

Choi JE, Lee SS, Sunde DA, Huizar I, Haugk KL, Thannickal VJ, *et al.* Insulin-like growth factor-I receptor blockade improves outcome in mouse model of lung injury. *Am J Respir Crit Care Med* 2009; 179(3):212-219.

Chow CW, Herrera Abreu MT, Suzuki T, Downey GP. Oxidative stress and acute lung injury. *Am J Respir Cell Mol Biol* 2003; 29(4):427-431.

Chu DK, Llop-Guevara A, Walker TD, Flader K, Goncharova S, Boudreau JE, *et al.* IL-33, but not thymic stromal lymphopoietin or IL-25, is central to mite and peanut allergic sensitization. *J Allergy Clin Immunol* 2013; 131(1): 187-200.

Conroy DM, Williams TJ. Eotaxin and the attraction of eosinophils to the asthmatic lung. *Respir Res* 2001; 2(3): 150-156.

Conway EM, Pikor LA, Kung SH, Hamilton MJ, Lam S, Lam WL, *et al.* Macrophages, inflammation, and lung cancer. *Am J Respir Crit Care Med* 2016; 193(2):116-130 (2016).

Corne J, Chupp G, Lee CG, Homer RJ, Zhu Z, Chen Q, *et al.* IL-13 stimulates vascular endothelial cell growth factor and protects against hyperoxic acute lung injury. *J Clin Invest* 2000; 106(6):783-791.

Corvaia N, Beck A, Caussanel V, Goetsch L. Insulin-like growth factor receptor type I as a target for cancer therapy. *Front Biosci (Schol Ed)* 2013; 5:439-450.

Crudden C, Girnita A, Girnita L. Targeting the IGF-1R: the tale of the tortoise and the hare. *Front Endocrinol (Lausanne)* 2015; 6:64.

Danielian PS, White R, Hoare SA, Fawell SE, Parker MG. Identification of residues in the estrogen receptor that confer differential sensitivity to estrogen and hydroxytamoxifen. *Mol Endocrinol* 1993; 7(2):232-240.

Della Latta V, Cecchetti A, Del Ry S, Morales MA. Bleomycin in the setting of lung fibrosis induction: from biological mechanisms to counteractions. *Pharmacol Res* 2015; 97:122-130.

Desbois-Mouthon C, Wendum D, Cadoret A, Rey C, Leneuve P, Blaise A, *et al.* Hepatocyte proliferation during liver regeneration is impaired in mice with liver-specific IGF-1R knockout. *FASEB J* 2006; 20(6):773-775.

Elmore S. Apoptosis: a review of programmed cell death. *Toxicol Pathol* 2007; 35(4):495-516.

Engberding N, San Martin A, Martin-Garrido A, Koga M, Pounkova L, Lyons E, *et al.* Insulin-like growth factor-1 receptor expression masks the antiinflammatory and glucose uptake capacity of insulin in vascular smooth muscle cells. *Arterioscler Thromb Vasc Biol* 2009; 29(3):408-415.

Epaud R, Aubey F, Xu J, Chaker Z, Clemessy M, Dautin A, *et al.* Knockout of insulin-like growth factor-1 receptor impairs distal lung morphogenesis. *PLoS One* 2012; 7(11):e48071.

Erle DJ, Sheppard D. The cell biology of asthma. *J Cell Biol* 2014; 205(5):621-631.

Esnault S, Kelly EA, Schwantes EA, Liu LY, DeLain LP, Hauer JA, *et al.* Identification of genes expressed by human airway eosinophils after an in vivo allergen challenge. *PLoS One* 2013; 8(7):e67560.

Evans CM, Raclawska DS, Ttofali F, Liptzin DR, Fletcher AA, Harper DN, *et al.* The polymeric mucin Muc5ac is required for allergic airway hyperreactivity. *Nat Commun* 2015; 6:6281.

Fahy JV. Type 2 inflammation in asthma-present in most, absent in many. *Nat Rev Immunol* 2015; 15(1):57-65.

Fattouh R, Al-Garawi A, Fattouh M, Arias K, Walker TD, Goncharova S, *et al.* Eosinophils are dispensable for allergic remodeling and immunity in a model of house dust mite-induced airway disease. *Am J Respir Crit Care Med* 2011; 183(2):179-188.

Feil R. Conditional somatic mutagenesis in the mouse using site-specific recombinases. *Handb Exp Pharmacol* 2007; 178:3-28.

Feil R, Wagner J, Metzger D, Chambon P. Regulation of Cre recombinase activity by mutated estrogen receptor ligand-binding domains. *Biochem Biophys Res Commun* 1997; 237(3):752-757.

Feil S, Valtcheva N, Feil R. Inducible Cre mice. *Methods Mol Biol* 2009; 530:343-363.

Fernandez-Moreno C, Pichel JG, Chesnokova V, De Pablo F. Increased leptin and white adipose tissue hypoplasia are sexually dimorphic in *Lif* null/*Igf-I* haploinsufficient mice. *FEBS Lett* 2004; 557(1-3):64-68.

Foskett AM, Bazhanov N, Ti X, Tiblow A, Bartosh TJ, Prockop DJ, *et al.* Phase-directed therapy: TSG-6 targeted to early inflammation improves bleomycin-injured lungs. *Am J Phys Lung Cell Mol Phys* 2014; 306(2):L120-131.

Froment P, Vigier M, Nègre D, Fontaine I, Beghelli J, Cosset FL, *et al.* Inactivation of the IGF-I receptor gene in primary Sertoli cells highlights the autocrine effects of IGF-I. *J Endocrinol* 2007; 194(3):557-568.

Gannage-Yared MH, Klammt J, Chouery E, Corbani S, Megarbane H, Abou Ghoch J, *et al.* Homozygous mutation of the IGF1 receptor gene in a patient with severe pre- and postnatal growth failure and congenital malformations. *Eur J Endocrinol* 2013; 168(1):K1-7.

Gao X, Wang G, Zhang W, Peng Q, Xue M, Jinhong H, *et al.* Expression of pulmonary aquaporin 1 is dramatically upregulated in mice with pulmonary fibrosis induced by bleomycin. *Arch Med Sci* 2013; 9(5):916-921.

Gasse P, Riteau N, Charron S, Girre S, Fick L, Pétrilli V, *et al.* Uric acid is a danger signal activating NALP3 inflammasome in lung injury inflammation and fibrosis. *Am J Respir Crit Care Med* 2009; 179(10):903-913.

Gaye B, Sikkema D, Lee TN. Development of an ultra-sensitive single molecule counting assay for the detection of interleukin-13 as a marker for asthmatic severity. *J Immunol Methods* 2015; 426: 82-5.

Girnit L, Worrall C, Takahashi S, Seregard S, Girnit A. Something old, something new and something borrowed: emerging paradigm of insulin-like growth factor type 1 receptor (IGF-1R) signaling regulation. *Cell Mol Life Sci* 2014; 71(13):2403-2427.

Glasser SW, Maxfield MD, Ruetschilling TL, Akinbi HT, Baatz JE, Kitzmiller JA, *et al.* Persistence of LPS-induced lung inflammation in surfactant protein-C-deficient mice. *Am J Respir Cell Mol Biol* 2013; 49(5):845-854.

Gregory LG, Causton B, Murdoch JR, Mathie SA, O'Donnell V, Thomas CP, *et al.* Inhaled house dust mite induces pulmonary T helper 2 cytokine production. *Clin Exp Allergy* 2009; 39(10):1597-610.

Gregory LG, Lloyd CM. Orchestrating house dust mite-associated allergy in the lung. *Trends Immunol* 2011; 32(9):402-411.

Gomperts BN, Kim LJ, Flaherty SA, Hackett BP. IL-13 regulates cilia loss and foxj1 expression in human airway epithelium. *Am J Respir Cell Mol Biol* 2007; 37(3):339-346.

Grommes J, Soehnlein O. Contribution of neutrophils to acute lung injury. *Mol Med* 2011; 17(3-4):293-307.

Hammad H, Lambrecht BN. Dendritic cells and epithelial cells: linking innate and adaptive immunity in asthma. *Nat Rev Immunol* 2008; 8(3):193-204.

Happel N, Doenecke D. Histone H1 and its isoforms: contribution to chromatin structure and function. *Gene* 2009; 431(1-2):1-12.

Harshman SW, Young NL, Parthun MR, Freitas MA. H1 histones: current perspectives and challenges. *Nucleic Acids Res* 2013; 41(21):9593-9609.

Hayashi S, McMahon AP. Efficient recombination in diverse tissues by a tamoxifen-inducible form of Cre: a tool for temporally regulated gene activation/inactivation in the mouse. *Dev Biol* 2002; 244(2):305-318.

Herriges M, Morrisey EE. Lung development: orchestrating the generation and regeneration of a complex organ. *Development* 2014; 141(3):502-513.

Hogan BL, Barkauskas CE, Chapman HA, Epstein JA, Jain R, Hsia CC, *et al.* Repair and regeneration of the respiratory system: complexity, plasticity, and mechanisms of lung stem cell function. *Cell Stem Cell* 2014; 15(2):123-138.

Holzerova E, Prokisch H. Mitochondria: much ado about nothing? How dangerous is reactive oxygen species production? *Int J Biochem Cell Biol* 2015; 63:16-20.

Holzenberger M, Leneuve P, Hamard G, Ducos B, Perin L, Binoux M, *et al.* A targeted partial invalidation of the insulin-like growth factor I receptor gene in mice causes a postnatal growth deficit. *Endocrinology* 2000; 141(7):2557-2566.

Holzenberger M, Hamard G, Zaoui R, Leneuve P, Ducos B, Beccavin C, *et al.* Experimental IGF-I receptor deficiency generates a sexually dimorphic pattern of organ-specific growth deficits in mice, affecting fat tissue in particular. *Endocrinology* 2001; 142(10):4469-4478.

Hoshino M, Nakamura Y, Sim JJ, Yamashiro Y, Uchida K, Hosaka K, *et al.* Inhaled corticosteroid reduced lamina reticularis of the basement membrane by modulation of insulin-like growth factor (IGF)-I expression in bronchial asthma. *Clin Exp Allergy* 1998; 28(5):568-577.

Hsu E, Feghali-Bostwick CA. Insulin-like growth factor-II is increased in systemic sclerosis-associated pulmonary fibrosis and contributes to the fibrotic process via Jun N-terminal kinase- and phosphatidylinositol-3 kinase-dependent pathways. *Am J Pathol* 2008; 172(6):1580-1590.

Hu Y, Lou J, Mao YY, Lai TW, Liu LY, Zhu C, *et al.* Activation of MTOR in pulmonary epithelium promotes LPS-induced acute lung injury. *Autophagy* 2016; 12(12):2286-2299.

Hung CF, Rohani MG, Lee SS, Chen P, Schnapp LM. Role of IGF-1 pathway in lung fibroblast activation. *Respir Res* 2013; 14:102.

Iams WT, Lovly CM. Molecular pathways: clinical applications and future direction of insulin-like growth factor-1 receptor pathway blockade. *Clin Cancer Res* 2015; 21(19):4270-4277.

Ikegami M, Whitsett JA, Martis PC, Weaver TE. Reversibility of lung inflammation caused by SP-B deficiency. *Am J Physiol Lung Cell Mol Physiol* 2005; 289(6):L962-L970.

Ikeno M, Suzuki N, Kamiya M, Takahashi Y, Kudoh J, Okazaki T. LINE1 family member is negative regulator of HLA-G expression. *Nucl Acids Res* 2012; 40(21):10742-10752.

Johnson ER, Matthay MA. Acute lung injury: epidemiology, pathogenesis, and treatment. *J Aerosol Med Pulm Drug Deliv* 2010; 23(4):243-252.

Jacquet A. The role of innate immunity activation in house dust mite allergy. *Trends Mol Med* 2011; 17(10):604-611.

Justice JP, Shibata Y, Sur S, Mustafa J, Fan M, Van Scott MR. IL-10 gene knockout attenuates allergen-induced airway hyperresponsiveness in C57BL/6 mice. *Am J Physiol Lung Cell Mol Physiol* 2001; 280(2): L363-368.

Kellendonk C, Tronche F, Casanova E, Anlag K, Opherck C, Schütz G. Inducible site-specific recombination in the brain. *J Mol Biol* 1999; 285(1):175-182.

Kasper D, Fauci A, Hauser S, Longo D, Jameson JL, Loscalzo J. Harrison's Principles of Internal Medicine, 19th Edition. *McGraw-Hill Education* 2015.

Kearley J, Buckland KF, Mathie SA, Lloyd CM. Resolution of allergic inflammation and airway hyperreactivity is dependent upon disruption of the T1/ST2-IL-33 pathway. *Am J Respir Crit Care Med* 2009; 179(9):772-781.

Kim TH, Chow YH, Gill SE, Schnapp LM. Effect of insulin-like growth factor blockade on hyperoxia-induced lung injury. *Am J Respir Cell Mol Biol* 2012a; 47(3):372-378.

Kim SR, Lee KS, Lee KB, Lee YC. Recombinant IGFBP-3 inhibits allergic lung inflammation, VEGF production, and vascular leak in a mouse model of asthma. *Allergy* 2012b; 67(7):869-877.

Klötting N, Koch L, Wunderlich T, Kern M, Ruschke K, Krone W, *et al.* Autocrine IGF-1 action in adipocytes controls systemic IGF-1 concentrations and growth. *Diabetes* 2008; 57(8):2074-2082.

Koeppen M, McNamee EN, Brodsky KS, Aherne CM, Faigle M, Downey GP, *et al.* Detrimental role of the airway mucin Muc5ac during ventilator-induced lung injury. *Mucosal Immunol* 2013; 6(4):762-775.

Kotton DN, Morrissey EE. Lung regeneration: mechanisms, applications and emerging stem cell populations. *Nat Med* 2014; 20(8):822-832.

Kouzaki H, Iijima K, Kobayashi T, O'Grady SM, Kita H. The danger signal, extracellular ATP, is a sensor for an airborne allergen and triggers IL-33 release and innate Th2-type responses. *J Immunol* 2011; 186(7): 4375-4387.

Kral JB, Kuttke M, Schrottmaier WC, Birnecker B, Warszawska J, Wernig C, *et al.* Sustained PI3K Activation exacerbates BLM-induced Lung Fibrosis via activation of pro-inflammatory and pro-fibrotic pathways. *Sci Rep* 2016; 6:23034.

Lambrecht BN, Hammad H. The airway epithelium in asthma. *Nat Med* 2012; 18(5):684-692.

Lambrecht BN, Hammad H. The immunology of asthma. *Nat Immunol* 2015; 16(1):45-56.

Laskin DL, Sunil VR, Gardner CR, Laskin JD. Macrophages and tissue injury: agents of defense or destruction? *Ann Rev Pharm Toxicol* 2011; 51:267-288.

Lawson WE, Polosukhin VV, Stathopoulos GT, Zoia O, Han W, Lane KB, *et al.* Increased and prolonged pulmonary fibrosis in surfactant protein C-deficient mice following intratracheal bleomycin. *Am J Pathol* 2005; 167(5):1267-1277.

Ledford JG, Mukherjee S, Kislan MM, Nugent JL, Hollingsworth JW, Wright JR. Surfactant protein-A suppresses eosinophil-mediated killing of *Mycoplasma pneumoniae* in allergic lungs. *PLoS One* 2012; 7(2):e32436.

Lee YC, Jogie-Brahim S, Lee DY, Han J, Harada A, Murphy LJ, *et al.* Insulin-like growth factor-binding protein-3 (IGFBP-3) blocks the effects of asthma by negatively regulating NF- κ B signaling through IGFBP-3R-mediated activation of caspases. *J Biol Chem* 2011; 286(20):17898-17909.

Lemanske RF Jr, Busse WW. Asthma: clinical expression and molecular mechanisms. *J Allergy Clin Immunol* 2010; 125(2 Suppl 2):S95-102.

LeRoith D, Roberts CT Jr. The insulin-like growth factor system and cancer. *Cancer Lett* 2003; 195(2):127-137.

Li S, Pinard M, Wang Y, Yang L, Lin R, Hiscott J, *et al.* Crosstalk between the TNF and IGF pathways enhances NF- κ B activation and signaling in cancer cells. *Growth Horm IGF Res* 2015; 25(5):253-261.

Liang Q, Cheng N, Zhang G, Liang Y, Qian F, Wu D, *et al.* Identification of P-Rex1 as an anti-inflammatory and anti-fibrogenic target for pulmonary fibrosis. *Sci Rep* 2016; 6:25785.

Lingappan K, Jiang W, Wang L, Wang G, Couroucli XI, Shivanna B, *et al.* Mice deficient in the gene for cytochrome P450 (CYP)1A1 are more susceptible than wild-type to hyperoxic lung injury: evidence for protective role of CYP1A1 against oxidative stress. *Toxicol Sci* 2014; 141(1):68-77.

Liu JP, Baker J, Perkins AS, Robertson EJ, Efstratiadis A. Mice carrying null mutations of the genes encoding insulin-like growth factor I (Igf-1) and type 1 IGF receptor (Igf1r). *Cell* 1993; 75(1):59-72.

Liu Q, Li MZ, Leibham D, Cortez D, Elledge SJ. The univector plasmid-fusion system, a method for rapid construction of recombinant DNA without restriction enzymes. *Curr Biol* 1998; 8(24):1300-1309.

López IP, Rodríguez-de la Rosa L, Pais RS, Piñeiro-Hermida S, Torrens R, Contreras J, *et al.* Differential organ phenotypes after postnatal *Igf1r* gene conditional deletion induced by tamoxifen in *UBC-CreERT2; Igf1r^{fl/fl}* double transgenic mice. *Transgenic Res* 2015; 24(2):279-294.

López IP, Piñeiro-Hermida S, Pais RS, Torrens R, Hoeflich A, Pichel JG. Involvement of *Igf1r* in bronchiolar epithelial regeneration: role during repair kinetics after selective club cell ablation. *PLoS One* 2016; 11(11):e0166388.

Lukacs NW. Role of chemokines in the pathogenesis of asthma. *Nat Rev Immunol* 2001; 1(2):108-116.

Makrinioti H, Toussaint M, Jackson DJ, Walton RP, Johnston SL. Role of interleukin 33 in respiratory allergy and asthma. *Lancet Respir Med* 2014; 2(3):226-237.

Martin, M. Cutadapt removes adapter sequences from high-throughput sequencing reads. *EMBnet J* 2011; 17(1):10-12.

Masoli M, Fabian D, Holt S, Beasley R; Global Initiative for Asthma (GINA) Program. The global burden of asthma: executive summary of the GINA Dissemination Committee report. *Allergy* 2004; 59(5):469-478.

Mattioni T, Louvion JF, Picard D. Regulation of protein activities by fusion to steroid binding domains. *Methods Cell Biol* 1994; 43(Pt A):335-352.

Matute-Bello G, Frevert CW, Martin TR. Animal models of acute lung injury. *Am J Physiol Lung Cell Mol Physiol* 2008; 295(3):L379-399.

Melgert BN, Postma DS, Kuipers I, Geerlings M, Luinge MA, van der Strate BW, *et al.* Female mice are more susceptible to the development of allergic airway inflammation than male mice. *Clin Exp Allergy* 2005; 35(11):1496-1503.

Metzger D, Chambon P. Site- and time-specific gene targeting in the mouse. *Methods* 2001; 24(1):71-80.

Mittal M, Siddiqui MR, Tran K, Reddy SP, Malik AB. Reactive oxygen species in inflammation and tissue injury. *Antioxid Redox Signal* 2014; 20(7):1126-1167.

Moeller A, Ask K, Warburton D, Gauldie J, Kolb M. The bleomycin animal model: a useful tool to investigate treatment options for idiopathic pulmonary fibrosis? *Int J Biochem Cell Biol* 2008 40(3):362-382.

Moldoveanu B, Otmishi P, Jani P, Walker J, Sarmiento X, Guardiola J, *et al.* Inflammatory mechanisms in the lung. *J Inflamm Res* 2009; 2:1-11.

Moody G, Beltran PJ, Mitchell P, Cajulis E, Chung YA, Hwang D, *et al.* IGF1R blockade with ganitumab results in systemic effects on the GH-IGF axis in mice. *J Endocrinol* 2014; 221(1):145-155.

Moore BB, Hogaboam CM. Murine models of pulmonary fibrosis. *Am J Physiol Lung Cell Mol Physiol.* 2008; 294(2):L152-160.

Moreno-Barriuso N, Lopez-Malpartida AV, de Pablo F, Pichel JG. Alterations in alveolar epithelium differentiation and vasculogenesis in lungs of LIF/IGF-I double deficient embryos. *Dev Dyn* 2006; 235(8):2040-2050.

Morrissey EE, Hogan BL. Preparing for the first breath: genetic and cellular mechanisms in lung development. *Dev Cell* 2010; 18(1):8-23.

Mouratis MA, Aidinis V. Modeling pulmonary fibrosis with bleomycin. *Curr Opin Pulm Med* 2011; 17(5):355-61.

Nakae S, Komiyama Y, Yokoyama H, Nambu A, Umeda M, Iwase M, *et al.* IL-1 is required for allergen-specific Th2 cell activation and the development of airway hypersensitivity response. *Int Immunol* 2003; 15(4):483-490.

Nakae S, Lunderius C, Ho LH, Schafer B, Tsai M, Galli SJ. TNF can contribute to multiple features of ovalbumin-induced allergic inflammation of the airways in mice. *J Allergy Clin Immunol* 2007; 119(3): 680-686.

Nef S, Verma-Kurvari S, Merenmies J, Vassalli J-D, Efstratiadis A, Accili D, *et al.* Testis determination requires insulin receptor family function in mice. *Nature* 2003; 426(6964):291-295

Ogawa H, Ledford JG, Mukherjee S, Aono Y, Nishioka Y, Lee J, *et al.* Surfactant protein D attenuates sub-epithelial fibrosis in allergic airways disease through TGF-beta. *Respir Res* 2014; 15:143.

Okano T, Xuan S, Kelley MW. Insulin-like growth factor signaling regulates the timing of sensory cell differentiation in the mouse cochlea. *J Neurosci* 2011; 31(49):18104-18118.

Osorio FG, Soria-Valles C, Santiago-Fernández O, Bernal T, Mittelbrunn M, Colado E, *et al.* Loss of the proteostasis factor AIRAPL causes myeloid transformation by deregulating IGF-1 signaling. *Nat Med* 2016; 22(1):91-96.

Pais RS, Moreno-Barriuso N, Hernández-Porras I, López IP, De Las Rivas J, Pichel JG. Transcriptome analysis in prenatal IGF1-deficient mice identifies molecular pathways and target genes involved in distal lung differentiation. *PLoS One* 2013; 8(12):e83028.

Pala L, Giannini S, Rosi E, Cresci B, Scano G, Mohan S *et al.* Direct measurement of IGF-I and IGFBP-3 in bronchoalveolar lavage fluid from idiopathic pulmonary fibrosis. *J Endocrinol Invest* 2001; 24(11):856-864.

Pichel JG, Fernandez-Moreno C, Vicario-Abejon C, Testillano PS, Patterson PH, de Pablo F. Developmental cooperation of leukemia inhibitory factor and insulin-like growth factor I in mice is tissue-specific and essential for lung maturation involving the transcription factors Sp3 and TTF-1. *Mech Dev* 2003; 120(3):349-361

Piñeiro-Hermida S, Gregory JA, Lopez IP, Torrens R, Ruiz-Martinez C, Adner M, *et al.* Attenuated airway hyperresponsiveness and mucus secretion in HDM-exposed IGF1R-deficient mice. *Allergy* (2017a); 72(9):1317-1326.

Piñeiro-Hermida S, López IP, Alfaro-Arnedo E, Torrens R, Iñiguez M, Alvarez-Erviti L, *et al.* IGF1R deficiency attenuates acute inflammatory response in a bleomycin-induced lung injury mouse model. *Sci Rep* (2017b); 7(1):4290.

Pitetti JL, Calvel P, Zimmermann C, Conne B, Papaioannou MD, Aubry F, *et al.* An essential role for insulin and IGF1 receptors in regulating sertoli cell proliferation, testis size, and FSH action in mice. *Mol Endocrinol* 2013; 27(5):814-827.

Piyadasa H, Altieri A, Basu S, Schwartz J, Halayko AJ, Mookherjee N. Biosignature for airway inflammation in a house dust mite-challenged murine model of allergic asthma. *Biol Open* 2016; 5(2):112-121.

Pollak MN, Schernhammer ES, Hankinson SE. Insulin-like growth factors and neoplasia. *Nat Rev Cancer* 2004; 4(7):505-518.

Pollak M. Insulin and insulin-like growth factor signaling in neoplasia. *Nat Rev Cancer* 2008; 8(12):915-928.

Possa SS, Leick EA, Prado CM, Martins MA, Tibério IF. Eosinophilic inflammation in allergic asthma. *Front Pharmacol* 2013; 4:46.

Post S, Heijink IH, Petersen AH, de Bruin HG, van Oosterhout AJ, Nawijn MC. Protease-activated receptor-2 activation contributes to house dust mite-induced IgE responses in mice. *PLoS One* 2014; 9(3):e91206.

Postma DS, Rabe KF. The Asthma-COPD overlap syndrome. *N Engl J Med* 2015; 373(13):1241-1249.

Prefontaine D, Nadigel J, Chouiali F, Audusseau S, Semlali A, Chakir J, *et al.* Increased IL-33 expression by epithelial cells in bronchial asthma. *J Allergy Clin Immunol* 2010; 125(3):752-754.

Raeiszadeh Jahromi S, Mahesh PA, Jayaraj BS, Madhunapantula SR, Holla AD, Vishweswaraiah S, *et al.* Serum levels of IL-10, IL-17F and IL-33 in patients with asthma: a case-control study. *J Asthma* 2014; 51(10):1004-1013.

Raile K, Klammt J, Schneider A, Keller A, Laue S, Smith R, *et al.* Clinical and functional characteristics of the human Arg59Ter insulin-like growth factor I receptor (IGF1R) mutation: implications for a gene dosage effect of the human IGF1R. *J Clin Endocrinol Metab* 2006; 91(6):2264-2271.

Rajavelu P, Chen G, Xu Y, Kitzmiller JA, Korfhagen TR, Whitsett JA. Airway epithelial SPDEF integrates goblet cell differentiation and pulmonary Th2 inflammation. *J Clin Invest* 2015; 125(5):2021-2031.

Rajendrasozhan S, Yao H, Rahman I. Current perspectives on role of chromatin modifications and deacetylases in lung inflammation in COPD. *COPD* 2009; 6(4):291-297.

Rawlins EL, Hogan BL. Epithelial stem cells of the lung: privileged few or opportunities for many? *Development* 2006; 133(13):2455-65.

Reales-Calderón JA, Aguilera-Montilla N, Corbí ÁL, Molero G, Gil C. Proteomic characterization of human proinflammatory M1 and anti-inflammatory M2 macrophages and their response to *Candida albicans*. *Proteomics* 2014; 14(12):1503-1518.

Reinert T, Serodio da Rocha Baldotto C, Pereira Nunes FA, Alves de Souza Scheliga, A. Bleomycin-induced lung injury. *Journal of Cancer Research* 2013; 2013:480608.

Ren X, Shah TA, Ustiyani V, Zhang Y, Shinn J, Chen G, *et al.* FOXM1 promotes allergen-induced goblet cell metaplasia and pulmonary inflammation. *Mol Cell Biol* 2013; 33(2):371-386.

Riquelme R, Cediell R, Contreras J, la Rosa Lourdes RD, Murillo-Cuesta S, Hernandez-Sanchez C, *et al.* A comparative study of age-related hearing loss in wild type and insulin-like growth factor I deficient mice. *Front Neuroanat* 2010; 4:27-39.

Roback EW, Barakat AJ, Dev VG, Mbikay M, Chretien M, Butler MG. An infant with deletion of the distal long arm of chromosome 15 (q26.1-qter) and loss of insulin-like growth factor 1 receptor gene. *Am J Med Genet* 1991; 38(1):74-79.

Rock JR, Randell SH, Hogan BL. Airway basal stem cells: a perspective on their roles in epithelial homeostasis and remodeling. *Dis Model Mech* 2010; 3(9-10):545-556.

Rock JR, Hogan BL. Epithelial progenitor cells in lung development, maintenance, repair, and disease. *Annu Rev Cell Dev Biol* 2011; 27:493-512.

Rodrigues SF, Granger DN. Blood cells and endothelial barrier function. *Tissue Barriers* 2015; 3(1-2):e978720.

Rom WN1, Pääkkö P. Activated alveolar macrophages express the insulin-like growth factor-I receptor. *Am J Respir Cell Mol Biol* 1991; 4(5):432-9.

Ruan W, Ying K. Abnormal expression of IGF-binding proteins, an initiating event in idiopathic pulmonary fibrosis? *Pathol Res Pract* 2010; 206(8):537-543.

Ruzankina Y, Pinzon-Guzman C, Asare A, Ong T, Pontano L, Cotsarelis G, *et al.* Deletion of the developmentally essential gene ATR in adult mice leads to age-related phenotypes and stem cell loss. *Cell Stem Cell* 2007; 1(1):113-126.

Säfholm J, Lövdahl C, Swedin L, Boels PJ, Dahlén SE, Arner A, *et al.* Inflammation-induced airway smooth muscle responsiveness is strain dependent in mice. *Pulm Pharmacol Ther* 2011; 24(4):361-366.

Schulman ES, Pohlig C. Rationale for specific allergen testing of patients with asthma in the clinical pulmonary office setting. *Chest* 2015; 147(1):251-258.

Schumacker PT, Gillespie MN, Nakahira K, Choi AM, Crouser ED, Piantadosi CA, *et al.* Mitochondria in lung biology and pathology: more than just a powerhouse. *Am J Physiol Lung Cell Mol Physiol* 2014; 306(11):L962-974.

Scolnick JA, Cui K, Duggan CD, Xuan S, Yuan X-B, Efstratiadis A, *et al.* Role of IGF signaling in olfactory sensory map formation and axon guidance. *Neuron* 2008; 57(6):847-857.

Sjöberg LC, Gregory JA, Dahlén SE, Nilsson GP, Adner M. Interleukin-33 exacerbates allergic bronchoconstriction in the mice via activation of mast cells. *Allergy* 2015; 70(5):514-521.

Smith TJ. Insulin-like growth factor-I regulation of immune function: a potential therapeutic target in autoimmune diseases? *Pharmacol Rev* 2010; 62(2):199-236.

Sonar SS, Ehmke M, Marsh LM, Dietze J, Dudda JC, Conrad ML, *et al.* Clara cells drive eosinophil accumulation in allergic asthma. *Eur Respir J* 2012; 39(2):429-438.

Song J, Meyer K, Kistemaker LE, Gosens R, Hiemstra PS, Rots M, *et al.* Targeted silencing of master transcription factor SPDEF to reduce mucus production in airway diseases by epigenetic editing. *Eur Respir J* 2015; 46:OA486.

Spadaro O, Goldberg EL, Camell CD, Youm YH, Kopchick JJ, Nguyen KY, *et al.* Growth hormone receptor deficiency protects against age-related NLRP3 inflammasome activation and immune senescence. *Cell Rep* 2016; 14(7):1571-1580.

Stables MJ, Shah S, Camon EB, Lovering RC, Newson J, Bystrom J, *et al.* Transcriptomic analyses of murine resolution-phase macrophages. *Blood* 2011; 118(26):e192-208.

Sullivan JP, Minna JD, Shay JW. Evidence for self-renewing lung cancer stem cells and their implications in tumor initiation, progression, and targeted therapy. *Cancer Metastasis Rev* 2010; 29(1):61-72.

Sun L, Ren X, Wang IC, Pradhan A, Zhang Y, Flood HM, *et al.* The FOXM1 inhibitor RCM-1 suppresses goblet cell metaplasia and prevents IL-13 and STAT6 signaling in allergen-exposed mice. *Sci Signal* 2017; 10(475):eaai8583.

Suresh MV, Ramakrishnan SK, Thomas B, Machado-Aranda D, Bi Y, Talarico N, *et al.* Activation of hypoxia-inducible factor-1 α in type 2 alveolar epithelial cell is a major driver of acute inflammation following lung contusion. *Crit Care Med* 2014; 42(10):e642-653.

Sutherland BW, Knoblaugh SE, Kaplan-Lefko PJ, Wang F, Holzenberger M, Greenberg NM. Conditional deletion of insulin-like growth factor-I receptor in prostate epithelium. *Cancer Res* 2008; 68(9):3495-3504.

Swedin L, Ellis R, Kemi C, Ryrfeldt A, Inman M, Dahlen SE, *et al.* Comparison of aerosol and intranasal challenge in a mouse model of allergic airway inflammation and hyperresponsiveness. *Int Arch Allergy Immunol* 2010; 153(3):249-258.

Takasaka N, Araya J, Hara H, Ito S, Kobayashi K, Kurita Y, *et al.* Autophagy induction by SIRT6 through attenuation of insulin-like growth factor signaling is involved in the regulation of human bronchial epithelial cell senescence. *J Immunol* 2014; 192(3):958-968.

The Global Asthma Report 2014. Auckland, New Zealand: Global Asthma Network, 2014.

Todd NW, Luzina IG, Atamas SP. Molecular and cellular mechanisms of pulmonary fibrosis. *Fibrogenesis Tissue Repair* 2012; 5(1):11.

Tomlinson KL, Davies GC, Sutton DJ, Palframan RT. Neutralisation of interleukin-13 in mice prevents airway pathology caused by chronic exposure to house dust mite. *PLoS One* 2010; 5(10):e13136.

Towne JE, Harrod KS, Krane CM, Menon AG. Decreased expression of aquaporin (AQP)1 and AQP5 in mouse lung after acute viral infection. *Am J Respir Cell Mol Biol* 2000; 22(1):34-44.

Trapnell C, Roberts A, Goff L, Pertea G, Kim D, Kelley DR, *et al.* Differential gene and transcript expression analysis of RNA-seq experiments with TopHat and Cufflinks. *Nat Protoc* 2012; 7(3):562-578.

Tully JE, Hoffman SM, Lahue KG, Nolin JD, Anathy V, Lundblad LK, *et al.* Epithelial NF- κ B orchestrates house dust mite-induced airway inflammation, hyperresponsiveness, and fibrotic remodeling. *J Immunol* 2013; 191(12):5811-5821.

Uhlen M, Fagerberg L, Hallstrom BM, Lindskog C, Oksvold P, Mardinoglu A, *et al.* Proteomics. Tissue based map of the human proteome. *Science* 2015; 347(6220):1260419.

van der Velden JL, Hoffman SM, Alcorn JF, Tully JE, Chapman DG, Lahue KG, *et al.* Absence of c-Jun NH2-terminal kinase 1 protects against house dust mite-induced pulmonary remodeling but not airway hyperresponsiveness and inflammation. *Am J Physiol Lung Cell Mol Physiol* 2014; 306(9):L866-875.

Varela-Nieto I, Murillo-Cuesta S, Rodriguez-de la Rosa L, Lassatetta L, Contreras J. IGF-I deficiency and hearing loss: molecular clues and clinical implications. *Pediatr Endocrinol Rev* 2013; 10(4):460-472.

Veraldi KL, Gibson BT, Yasuoka H, Myerburg MM, Kelly EA, Balzar S, *et al.* Role of insulin-like growth factor binding protein-3 in allergic airway remodeling. *Am J Respir Crit Care Med* 2009; 180(7):611-617.

Vijayan A, Guha D, Ameer F, Kaziri I, Mooney CC, Bennett L, *et al.* IGFBP-5 enhances epithelial cell adhesion and protects epithelial cells from TGF β 1-induced mesenchymal invasion. *Int J Biochem Cell Biol* 2013; 45(12):2774-2785.

Volckaert T, De Langhe S. Lung epithelial stem cells and their niches: Fgf10 takes center stage. *Fibrogenesis Tissue Repair* 2014; 7:8.

Vooijs M, Jonkers J, Berns A. A highly efficient ligand regulated Cre recombinase mouse line shows that LoxP recombination is position dependent. *EMBO Rep* 2001; 2(4):292-297.

Walenkamp MJ, Karperien M, Pereira AM, Hilhorst-Hofstee Y, van Doorn J, Chen JW, *et al.* Homozygous and heterozygous expression of a novel insulin-like growth factor-I mutation. *J Clin Endocrinol Metab* 2005; 90(5):2855-2864.

Walenkamp MJ, de Muinck Keizer-Schrama SM, de Mos M, Kalf ME, van Duyvenvoorde HA, Boot AM, *et al.* Successful long-term growth hormone therapy in a girl with haploinsufficiency of the insulin-like growth factor-I receptor due to a terminal 15q26.2-qter deletion detected by multiplex ligation probe amplification. *J Clin Endocrinol Metab* 2008; 93(6):2421-2425.

Walkin L, Herrick SE, Summers A, Brenchley PE, Hoff CM, Korstanje R *et al.* The role of mouse strain differences in the susceptibility to fibrosis: a systematic review. *Fibrogenesis Tissue Repair* 2013; 6(1):18.

Wang J, Zhou J, Powell-Braxton L, Bondy C. Effects of Igf1 gene deletion on postnatal growth patterns. *Endocrinology* 1999; 140(7):3391-3394.

Werner H, Bruchim I. The insulin-like growth factor-I receptor as an oncogene. *Arch Physiol Biochem* 2009; 115(2):58-71.

- White LE, Santora RJ, Cui Y, Moore FA, Hassoun HT. TNFR1-dependent pulmonary apoptosis during ischemic acute kidney injury. *Am J Physiol Lung Cell Mol Physiol* 2012; 303(5):L449-459.
- Whitsett JA, Wert SE, Weaver TE. Alveolar surfactant homeostasis and the pathogenesis of pulmonary disease. *Annu Rev Med* 2010; 61:105-119.
- Whitsett JA, Alenghat T. Respiratory epithelial cells orchestrate pulmonary innate immunity. *Nat Immunol* 2015; 16(1):27-35.
- Withers DJ, Burks DJ, Towery HH, Altamuro SL, Flint CL, White MF. Irs-2 coordinates Igf-1 receptor-mediated beta-cell development and peripheral insulin signalling. *Nat Genet* 1999; 23(1):32-40.
- Wu D, Zhou J, Bi H, Li L, Gao W, Huang M, *et al.* CCL11 as a potential diagnostic marker for asthma? *J Asthma* 2014; 51(8):847-854.
- Wynn TA. Integrating mechanisms of pulmonary fibrosis. *J Exp Med* 2011; 208(7):1339-1350.
- Yamada Y, Limmon GV, Zheng D, Li N, Li L, Yin L, *et al.* Major shifts in the spatio-temporal distribution of lung antioxidant enzymes during influenza pneumonia. *PLoS One* 2012; 7(2):e31494.
- Yamashita N, Tashimo H, Ishida H, Matsuo Y, Arai H, Nagase H, *et al.* Role of insulin-like growth factor-I in allergen-induced airway inflammation and remodeling. *Cell Immunol* 2005; 235(2): 85-91.
- Yang M, Büsche G, Ganser A, Li Z. Morphology and quantitative composition of hematopoietic cells in murine bone marrow and spleen of healthy subjects. *Ann Hematol* 2013; 92(5):587-594.
- Ye J, Wen L, Liu DL, Lai GX. ATF3 and extracellular matrix-related genes associated with the process of chronic obstructive pulmonary. *Lung* 2014; 192(6):881-888.
- Ying S, Robinson DS, Meng Q, Rottman J, Kennedy R, Ringler DJ, *et al.* Enhanced expression of eotaxin and CCR3 mRNA and protein in atopic asthma. Association with airway hyperresponsiveness and predominant co-localization of eotaxin mRNA to bronchial epithelial and endothelial cells. *Eur J Immunol* 1997; 27(12):3507-16.
- Zhang YL, Luan B, Wang XF, Qiao JY, Song L, Lei RR, *et al.* Peripheral blood MDSCs, IL-10 and IL-12 in children with asthma and their importance in asthma development. *PLoS One* 2013; 8(5):e63775.
- Zhu M, Ji G, Jin G, Yuan Z. Different responsiveness to a high-fat/cholesterol diet in two inbred mice and underlying genetic factors: a whole genome microarray analysis. *Nutr Metab* 2009; 6:43.

8 APPENDICES

Differential organ phenotypes after postnatal *Igf1r* gene conditional deletion induced by tamoxifen in *UBC-CreERT2*; *Igf1r^{fl/fl}* double transgenic mice

Icíar Paula López · Lourdes Rodriguez-de la Rosa ·
Rosete Sofia Pais · Sergio Piñeiro-Hermida · Raquel Torrens ·
Julio Contreras · Isabel Varela-Nieto · José García Pichel

Received: 31 July 2014 / Accepted: 9 September 2014 / Published online: 20 September 2014
© Springer International Publishing Switzerland 2014

Abstract Insulin-like growth factor type 1 receptor (IGF1R) is a ubiquitously expressed tyrosine kinase that regulates cell proliferation, differentiation and survival. It controls body growth and organ homeostasis, but with specific functions depending on developmental time and cell type. Human deficiency in IGF1R is involved in growth failure, microcephaly, mental retardation and deafness, and its overactivation is implicated in oncogenesis. *Igf1r*-deficient mice die at birth due to growth retardation and respiratory failure. Although multiple

Igf1r tissue-specific mutant lines have been analyzed postnatally, using *Igf1r*-floxed (*Igf1r^{fl/fl}*) mice mated with diverse cell-type recombinase Cre-expressing transgenics, no mouse models for the study of generalized *Igf1r* deficiency in adults have been reported. To this end we generated *UBC-CreERT2*; *Igf1r^{fl/fl}* transgenic mice with an inducible deletion of *Igf1r* activated by tamoxifen. Tamoxifen administration to 4 week-old prepuberal male mice delayed their growth, producing a distinct impact on organ size 4 weeks later. Whereas testes were smaller, spleen and heart showed an increased organ to body weight ratio. Mosaic *Igf1r* genomic deletions caused a significant reduction in *Igf1r* mRNA in all organs analyzed, resulting in diverse phenotypes. While kidneys, spleen and cochlea had unaltered gross morphology, testes revealed halted spermatogenesis, and liver and alveolar lung parenchyma showed increased cell proliferation rates without affecting apoptosis. We demonstrate that *UBC-CreERT2* transgenic mice efficiently delete *Igf1r* upon postnatal tamoxifen treatment in multiple mouse organs, and corroborate that IGF1R function is highly dependent on cell, tissue and organ type.

I. P. López · R. S. Pais · S. Piñeiro-Hermida ·
R. Torrens · J. G. Pichel (✉)
Centro de Investigación Biomédica de la Rioja (CIBIR),
Fundación Rioja Salud, 26006 Logroño, Spain
e-mail: jgpichel@riojasalud.es

L. Rodriguez-de la Rosa · J. Contreras · I. Varela-Nieto
Grupo de Neurobiología de la Audición, Instituto de
Investigaciones Biomédicas Alberto Sols, Consejo
Superior de Investigaciones Científicas-Universidad
Autónoma de Madrid, 28029 Madrid, Spain

L. Rodriguez-de la Rosa · J. Contreras · I. Varela-Nieto
Centro de Investigación Biomédica en Red de
Enfermedades Raras (CIBERER), Instituto de Salud
Carlos III, Madrid, Spain

L. Rodriguez-de la Rosa · I. Varela-Nieto
Instituto de Investigación Hospital Universitario La Paz
(IdiPAZ), Madrid, Spain

J. Contreras
Facultad de Veterinaria, Universidad Complutense,
Madrid, Spain

Keywords IGF1R · Transgenic mouse · Cre/lox
system · *UBC-CreERT2* mice · Cochlea · Lung

Introduction

Insulin-like growth factor type 1 receptor (IGF1R) is a transmembrane tyrosine kinase receptor activated by




SCIENTIFIC REPORTS



OPEN

IGF1R deficiency attenuates acute inflammatory response in a bleomycin-induced lung injury mouse model

Sergio Piñeiro-Hermida¹, Iciar P. López¹, Elvira Alfaro-Arnedo¹, Raquel Torrens¹, María Iñiguez², Lydia Alvarez-Erviti³, Carlos Ruiz-Martínez⁴ & José G. Pichel¹ 

IGF1R (Insulin-like Growth Factor 1 Receptor) is a tyrosine kinase with pleiotropic cellular functions. IGF activity maintains human lung homeostasis and is implicated in pulmonary diseases such as cancer, ARDS, COPD, asthma and fibrosis. Here we report that lung transcriptome analysis in mice with a postnatally-induced *Igf1r* gene deletion showed differentially expressed genes with potentially protective roles related to epigenetics, redox and oxidative stress. After bleomycin-induced lung injury, IGF1R-deficient mice demonstrated improved survival within a week. Three days post injury, IGF1R-deficient lungs displayed changes in expression of IGF system-related genes and reduced vascular fragility and permeability. Mutant lungs presented reduced inflamed area, down-regulation of pro-inflammatory markers and up-regulation of resolution indicators. Decreased inflammatory cell presence in BALF was reflected in diminished lung infiltration mainly affecting neutrophils, also corroborated by reduced neutrophil numbers in bone marrow, as well as reduced lymphocyte and alveolar macrophage counts. Additionally, increased SFTPC expression together with hindered HIF1A expression and augmented levels of *Gpx8* indicate that IGF1R deficiency protects against alveolar damage. These findings identify IGF1R as an important player in murine acute lung inflammation, suggesting that targeting IGF1R may counteract the inflammatory component of many lung diseases.

Inflammation is a relevant component of many lung diseases including ARDS, COPD, asthma, cancer, fibrosis and pneumonia^{1–5}. Early inflammatory stages of lung injury have been experimentally studied using the bleomycin (BLM) mouse model because of its low complexity and high reproducibility. BLM treatment mediates the generation of reactive oxygen species and subsequent DNA damage in the lung^{6–8}. In mice, BLM induces alveolar damage and pulmonary inflammation with an initial elevation of cytokines such as IL1B, TNF and IL6, which lead to acute lung injury within a week^{6–8}. These pro-inflammatory mediators, released by alveolar macrophages, up-regulate the expression of cell adhesion molecules and stimulate the endothelium to produce chemokines, which in turn promote migration of neutrophils into alveolar spaces. Activation of both neutrophils and macrophages further induces the release of additional pro-inflammatory mediators and reactive oxygen species, resulting in apoptosis or necrosis of alveolar type 1 cells, and consequently increased permeability of the alveolar-capillary barrier, lung edema and inactivation of surfactant production^{5,9,10}.

The insulin-like growth factor 1 receptor (IGF1R) is a ubiquitously expressed membrane-bound tyrosine kinase that mediates the positive effects of its ligands, IGF1 and IGF2, to control a number of essential biological outcomes. IGF activity and availability are modulated by six high-affinity IGF binding proteins (IGFBPs). IGF1R signaling primarily results in activation of the MAP Kinase and PI3 Kinase/Akt downstream pathways that modulate multiple cellular functions at the endocrine, paracrine and autocrine levels such as growth, proliferation, differentiation, survival, adhesion and migration^{11,12}. IGF activity was extensively reported in maintaining

¹Lung Cancer and Respiratory Diseases Unit, Centro de Investigación Biomédica de La Rioja (CIBIR), Fundación Rioja Salud, Logroño, Spain. ²Genomics Core Facility, Centro de Investigación Biomédica de La Rioja (CIBIR), Fundación Rioja Salud, Logroño, Spain. ³Molecular Neurobiology Unit, Centro de Investigación Biomédica de la Rioja (CIBIR), Fundación Rioja Salud, Logroño, Spain. ⁴Pneumology Service, Hospital San Pedro, Logroño, Spain. Correspondence and requests for materials should be addressed to J.G.P. (email: jgpichel@riojasalud.es)

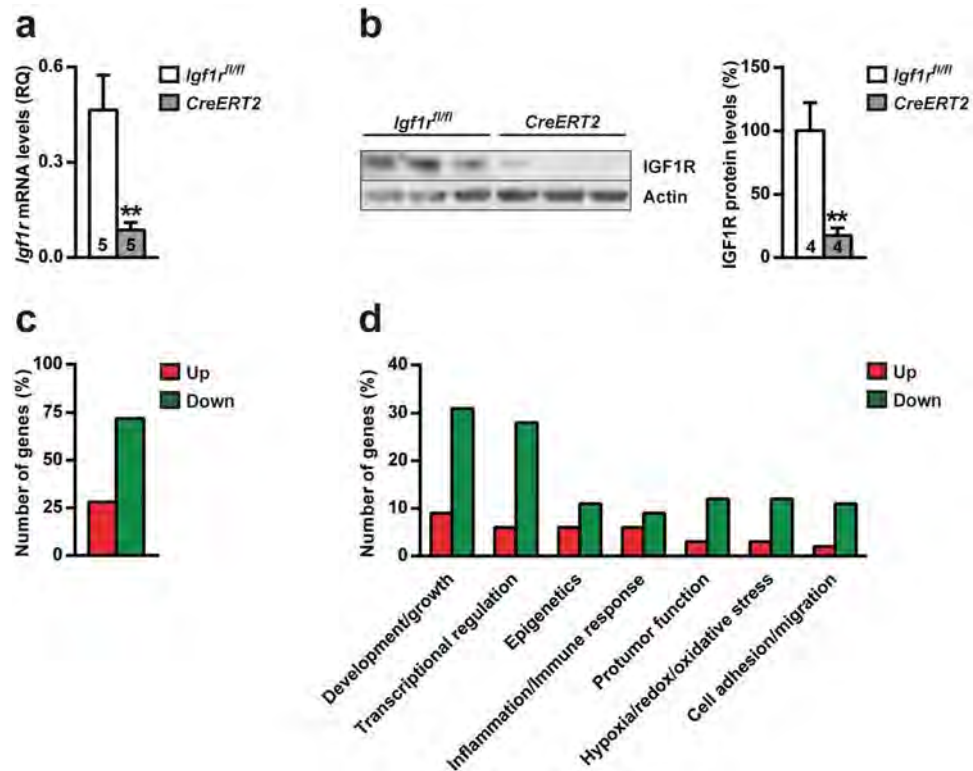


Figure 1. Decreased IGF1R expression levels and changes in the lung transcriptome of prepubertal IGF1R-deficient mice. (a) *Igf1r* mRNA expression levels and (b) representative Western blots for IGF1R and graphical representation of densitometric measurements of band intensities (percentage) normalized to beta-Actin levels and quantified in eight-week-old *UBC-CreERT2*; *Igf1r^{fl/fl}* (*CreERT2*) mice with respect to controls (*Igf1r^{fl/fl}*). (c) Number of differentially expressed genes (percentage) found with significant changes (FDR < 0.1) in the lungs of *UBC-CreERT2*; *Igf1r^{fl/fl}* (*CreERT2*) mice (n = 3), and (d) representation of the percentage of *Igf1r*-transcriptionally regulated genes involved in reported biological functions. Bars are color-coded in red and green for up- and down-regulated genes (respectively). Numbers within graphic bars indicate the number of mice analyzed and data are expressed as mean \pm SEM. $^{***}p < 0.01$ (Mann-Whitney U test). Up, up-regulated; Down, down-regulated.

human lung homeostasis, as it is involved in relevant respiratory diseases including cancer, COPD, fibrosis and ARDS^{13–16}.

IGF1R is highly relevant in the murine lung, displaying the highest activation levels of any organ upon challenge with IGF1¹⁷. Additionally, epithelial-specific *Igf1r* deficient mice showed disturbed airway epithelial differentiation after naphthalene-induced club cell injury¹⁸, and mice with compromised IGF1R signalling displayed oxidative stress resistance^{19,20}. Moreover, ablation of the macrophage IGF1-IGF1R axis inhibits the NLRP3 inflammasome, a protein complex that is activated in response to BLM-induced acute lung injury, which indicates that IGF1R plays an important role in initiation of the inflammatory process^{21,22}. On this basis, we aimed to study the implications of IGF1R on the inflammatory process that occurs during BLM-induced acute lung injury. For this purpose we used the recently characterized *Igf1r* conditional mutant mice *UBC-CreERT2*; *Igf1r^{fl/fl}* (*CreERT2*)²³. In this study, lung transcriptome analysis of *CreERT2* mice showed differential expression of genes that could serve a protective role in the lung, and it was also demonstrated that IGF1R deficiency confers resistance to BLM-mediated acute lung injury by counteracting the pulmonary inflammatory response. These results contribute toward a better understanding of the importance of IGF1R as a potential target for future therapeutic approaches in lung diseases with an inflammatory component.

Results

Postnatal IGF1R deficiency in *CreERT2* mice causes a general inhibition of differentially expressed genes in the prepubertal lung. To study the effect of IGF1R deficiency in the postnatal mouse lung, *CreERT2* mice were treated with tamoxifen at four weeks of age to induce *Igf1r* gene deletion²³. Quantitative real-time PCR (qRT-PCR) and Western blot analyses on lung extracts of eight-week-old *CreERT2* tamoxifen-treated mice verified efficient depletion of IGF1R expression at the RNA and protein levels (81% and 82%, respectively), when compared to their control littermates (*Igf1r^{fl/fl}*) (Fig. 1a,b). To determine the impact of *Igf1r* deficiency on global lung RNA gene expression, RNA-Seq was performed. After bioinformatics analyses comparing *CreERT2* vs. *Igf1r^{fl/fl}* lung mRNA expression profiles, significant changes in gene expression were found (data submitted to Gene Expression Omnibus, accession number GSE88908). Establishing a False Discovery Rate (FDR) < 0.1, 65 differentially expressed genes were identified. 18 genes were up-regulated (28%)

Accession No.	Gene name	Description	FDR	Main function
Up-regulated				
NM_027127.2	<i>Gpx8</i>	Glutathione peroxidase 8	5.08 E-11	Antioxidative stress
NM_009992.4	<i>Cyp1a1</i>	Cytochrome P450, family 1, subfamily a, polypeptide 1	1.51 E-10	Antioxidative stress
NM_172529.3	<i>Gnptg</i>	N-acetylglucosamine-1-phosphotransferase, gamma subunit	1.10 E-08	Lysosome transport
AK015709	<i>Ppp1r2-ps4</i>	Protein phosphatase 1, regulatory (inhibitor) subunit 2, pseudogene 4	3.69 E-05	Unknown
NM_011315.3	<i>Saa3</i>	Serum amyloid A 3	7.26 E-05	Immune cell response
NM_133903.3	<i>Spon2</i>	Spondin 2, extracellular matrix protein	3.20 E-4	Immune cell response
Down-regulated				
NM_010513.2	<i>Igf1r</i>	Insulin-like growth factor I receptor	6.91 E-11	Cell growth and survival
NM_175229.3	<i>Srrm2</i>	Serine/arginine repetitive matrix 2	2.90 E-06	Pre-mRNA splicing
NM_011584.4	<i>Nr1d2</i>	Nuclear receptor subfamily 1, group D, member 2	2.65 E-05	Transcriptional regulation
NM_010137.3	<i>Epas1</i>	Endothelial PAS domain protein 1	8.78 E-05	Endothelial barrier integrity

Table 1. Top 10 differentially expressed genes in the lung of *UBC-CreERT2*; *Igf1^{fl/fl}* mutant mice, and their assigned main functions.

and 47 were down-regulated (72%) (Fig. 1c and Supplementary Table S1). The most significantly affected biological functions based on GO and Keyword annotations, as well as published reports, are shown in Fig. 1d, and genes assigned to an extended list of these functions are displayed in Supplementary Table S2. Interestingly, the majority of genes in all categories were down-regulated. Most of them fall into three major categories: development/growth (*Mki67* and *Rps7*, up-regulated; *Notch3*, *Foxo1*, *Epas1* and *Tgfbr3*, down-regulated), transcriptional regulation and epigenetics (*Top2a*, *Hist1h1d* and *Hist1h2bb*, up-regulated; *Crebbp*, *Ep300*, *Polr2a*, *Zbtb34*, *Zbtb16*, *Zfp518b* and *Zfhx3*, down-regulated). Additional relevant biological functions of these genes include inflammation and immune response, followed by protumor function, hypoxia/redox and oxidative stress, as well as cell adhesion and migration (Supplementary Table S2). The top ten differentially expressed genes and their major biological functions are listed in Table 1. As expected, *Igf1r* is the most down-regulated gene, followed by *Srrm2* (involved in pre-mRNA splicing), *Nr1d2* (transcriptional regulator) and *Epas1* (endothelial barrier integrity). The most up-regulated genes are *Gpx8* and *Cyp1a1*, both implicated in anti-oxidative stress, followed by *Gnptg* (lysosome transport), *Ppp1r2-ps4* (pseudogene) and *Saa3* and *Spon2*, both involved in the immune response.

IGF1R deficiency improves mouse survival and alters IGF system gene expression in early stages after BLM-mediated pulmonary injury.

To further analyze how IGF1R affects lung homeostasis, *CreERT2* mice were treated with BLM to induce lung damage at six weeks of age (D0), and their survival was followed until D21 (Fig. 2a,b). The percentage of survivors after BLM challenge was significantly higher in *CreERT2* mice (79%) than in *Igf1^{fl/fl}* mice (33%), without gender differences. Interestingly, mortality predominantly affected mice within the first week of treatment, beginning at D3 (Fig. 2b). qRT-PCR and Western blot analyses on lung extracts at D3 verified IGF1R reduced mRNA (88%) and protein (84%) levels in *CreERT2* mice (Fig. 2c,d). In our search for possible compensatory effects on IGF system gene expression, we determined the mRNA levels of *Igf1*, *Igfbp3*, *Igfbp5* and *Insr*, in addition to the IGF/Ins transcription factor-signaling mediator *Foxo1*, by qRT-PCR. *Igf1* levels were found to be significantly diminished in *CreERT2* lungs but conversely, *Igfbp3*, *Igfbp5*, *Insr* and *Foxo1* levels were increased (Fig. 2e).

IGF1R depletion protects against lung vascular fragility and permeability, and reduces inflammatory cell presence in BALF after BLM treatment.

Since BLM causes an acute increase in total cells and protein concentration in bronchioalveolar lavage fluid (BALF)⁶, BALFs from saline- (SAL) and BLM-treated mice from both genotypes were analyzed at D3 (Fig. 3a). To evaluate lung vascular fragility and permeability, the presence of erythrocytes and the protein concentration in BALF were quantified. Interestingly, the increased erythrocyte presence (10-fold) found in BALF of *Igf1^{fl/fl}* from BLM compared to SAL-treated mice, was not as pronounced (4-fold) in *CreERT2* mice. It is important to mention that erythrocyte counts from SAL-treated *CreERT2* mice were significantly reduced (3-fold) with respect to *Igf1^{fl/fl}*, and were even more accentuated (6-fold) after BLM challenge (Fig. 3b). Only *Igf1^{fl/fl}* BALF protein levels were found to be increased (2-fold) when comparing SAL- to BLM-treated mice, whereas in *CreERT2* mice, protein levels remained unchanged after BLM treatment (Fig. 3c). In parallel, total and differential cell counts for neutrophils, macrophages and lymphocytes were severely attenuated in BALF from BLM-challenged *CreERT2* lungs with respect to their SAL-treated controls (Fig. 3d). Additionally, differential cell counts were also calculated as a proportion with respect to total absolute cell numbers, and expressed as percentages (Supplementary Table S3). Although BLM-treated *Igf1^{fl/fl}* mice demonstrated a significant increment in BALF total cells (3-fold) compared to SAL-treated mice, *CreERT2* mice did not show such an increase. Differential cell counts for neutrophils, macrophages and lymphocytes in BLM-challenged *Igf1^{fl/fl}* mice exhibited the same marked increase. Furthermore, total and differential cell counts in BALF of IGF1R-deficient mice showed a severe attenuation with respect to *Igf1^{fl/fl}* (Fig. 3d).

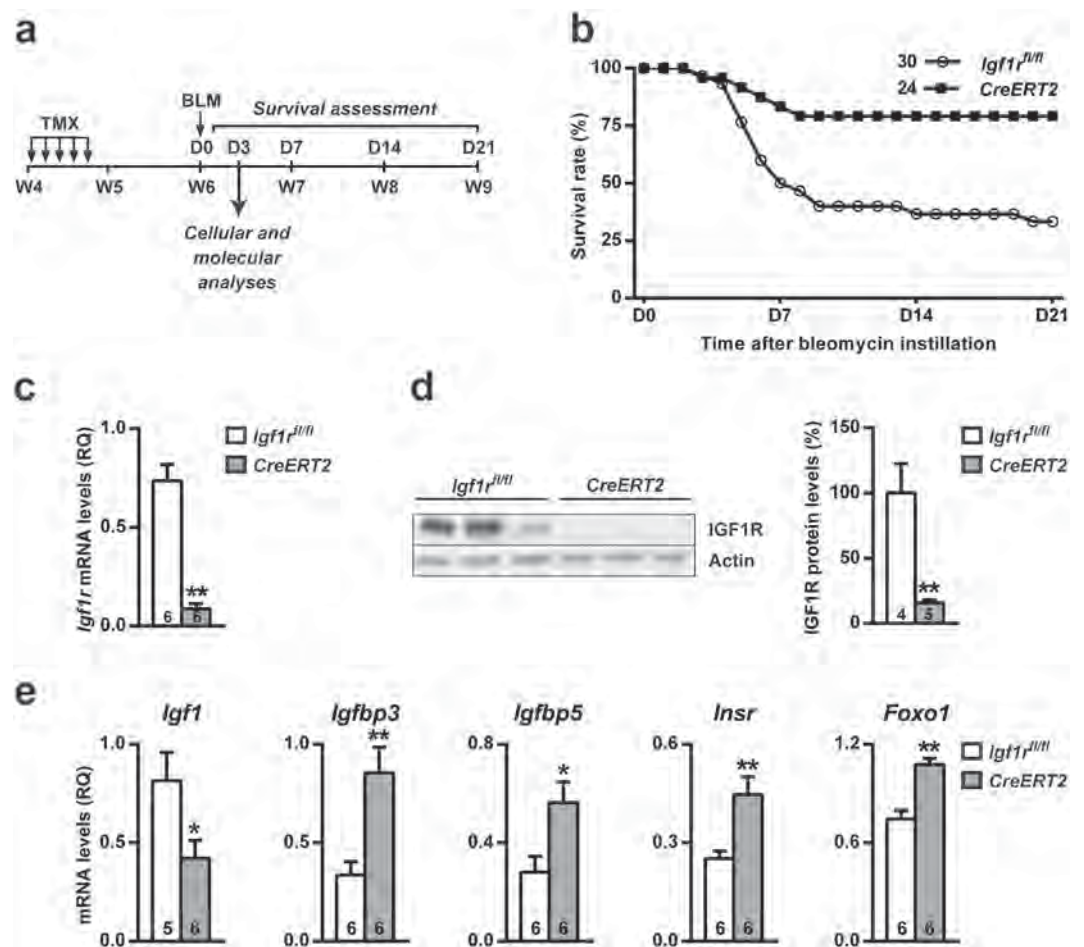


Figure 2. Establishment of the BLM-mediated acute lung injury model, and improved survival, reduced expression of IGF1R as well as changes in mRNA expression of IGF system genes in IGF1R-deficient mice. (a) Tamoxifen (TMX) was administered daily for five consecutive days to four-week-old *UBC-CreERT2; Igf1r^{fl/fl}* (*CreERT2*) mice to induce a postnatal *Igf1r* gene conditional deletion as previously described using *Igf1r^{fl/fl}* mice as experimental controls²³. Six-week-old mice were intra-tracheally instilled with 2.5 μ l/g BLM (2 U/ml) or saline using a ketamine-xylazine anesthetic combination. Cellular and molecular analyses were assessed on day (D) 3, based on survival curves. (b) Survival rates after BLM challenge determined over a follow-up period of 21 days in *UBC-CreERT2; Igf1r^{fl/fl}* (*CreERT2*) (n = 24) and *Igf1r^{fl/fl}* mice (n = 30). Data are expressed as the percentage of mice alive at each time point. (c) *Igf1r* mRNA expression levels, (d) representative Western blots for IGF1R and graphical representation of densitometric measurements of band intensities (percentage) normalized to beta-Actin levels, and (e) mRNA expression of IGF system related genes (*Igf1*, *Igfbp3*, *Igfbp5*, *Insr* and *Foxo1*) in lungs of *UBC-CreERT2; Igf1r^{fl/fl}* (*CreERT2*) vs. *Igf1r^{fl/fl}* mice at D3 post-intratracheal instillation. Numbers within graphic bars indicate the number of mice analyzed and data are expressed as mean \pm SEM. * $p < 0.05$; ** $p < 0.01$ (Mann-Whitney U test). BLM, bleomycin.

IGF1R deficiency reduces proliferation and attenuates acute lung inflammation and bone marrow neutrophilopoiesis after BLM-challenge. Inflamed lung areas were measured at D3, and were found to be markedly reduced in BLM-treated *Cre-ERT2* lungs (7-fold) (Fig. 4a,b). To verify and further investigate the mechanism by which IGF1R deficiency blocks inflammatory cell recruitment to the lung, mRNA expression analysis of different inflammatory markers was performed. Pro-inflammatory cytokines *Tnf*, *Il1b* and *Il6* were found to be significantly down-regulated in *CreERT2* lungs (Fig. 4c), and the reduction of TNF protein levels was confirmed by ELISA (Fig. 4d). Conversely, mRNA expression levels of the injury resolution-phase markers *Csf1*, *Il13* and *Cd209a* were significantly increased (Fig. 4e). Despite clearly increased *Il13* mRNA levels, protein levels were found to be only slightly increased (Fig. 4f). Cell proliferation evaluated in lung perivascular areas and in the alveolar parenchyma by Ki67 immuno-staining on D3 was found to be substantially reduced in *CreERT2* mice (3-fold in both cases) (Fig. 5a,b). As an indirect measure of inflammatory cell presence in the lung, mRNA levels of neutrophil chemotaxis (*Cxcl1*), neutrophil (*Ly6g*) and macrophage (*Marco* and *Adgre1*) markers were determined. *Cxcl1* levels were greatly reduced in IGF1R-deficient lungs, and *Ly6g*, *Marco* and *Adgre1* markers also showed a significant reduction (Fig. 6a). Neutrophilic infiltration found in perivascular areas was 44% and 7% of total infiltrates for *Igf1r^{fl/fl}* and *CreERT2* BLM-challenged lungs, respectively (Fig. 6b, upper panel). F4/80 immunostaining revealed a significant decrease for both alveolar macrophage numbers (50%), and volumes ($360.1 \pm 17.1 \mu\text{m}^3$ vs. $78.1 \pm 5.3 \mu\text{m}^3$; $p = 0.009$)

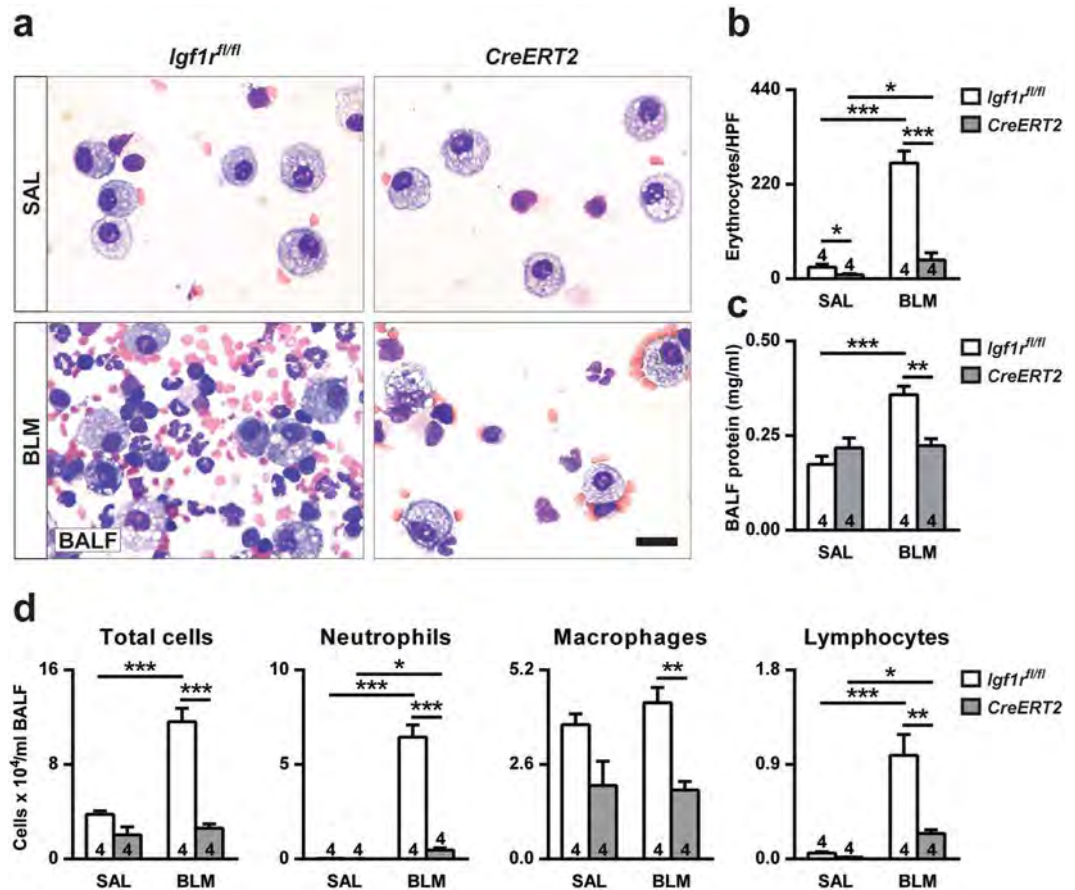


Figure 3. Reduced vascular fragility and lung permeability, and diminished leukocyte presence in BALF of IGF1R-deficient mice after BLM treatment. (a) Representative cytopsin images, (b) quantification of number of erythrocytes per HPF, (c) total protein concentration and, (d) total and differential cell counts performed on cytopsin preparations of BALF from saline- or BLM-treated *UBC-CreERT2; Igf1r^{fl/fl}* (*CreERT2*) vs. *Igf1r^{fl/fl}* mice at D3. Scale bar: 20 μ m. Numbers within graphic bars indicate the number of mice analyzed and data are expressed as mean \pm SEM. * $p < 0.05$; ** $p < 0.01$ *** $p < 0.001$ (Dunn Sidak multiple comparison test). SAL, saline; BLM, bleomycin; BALF, bronchoalveolar lavage fluid; HPF, high-power field.

(Fig. 6b, middle panel). In view of the reduced presence of BALF lymphocytes in mutant mice, infiltration into the lung was also assessed by immunostaining for CD3. Accordingly, lymphocyte counts were also diminished (45%) in *CreERT2* lungs (Fig. 6b, bottom panel). To verify reduced neutrophil infiltration in IGF1R-deficient mice, total and neutrophil counts were performed in bone marrow cytopsin obtained from mice of both genotypes after BLM treatment. As expected, total cells and neutrophils were found to be diminished in *CreERT2* mice with respect to *Igf1r^{fl/fl}* BLM-challenged lungs (2- and 5-fold, respectively) (Fig. 7a,b).

IGF1R deficiency reduces alveolar damage and HIF1A expression in BLM-challenged lungs.

To determine the effect of IGF1R depletion on alveolar damage after BLM challenge, alveolar epithelial cell type-specific markers were quantified by qRT-PCR on D3. Transcript levels of alveolar epithelial cell type 1 (*Aqp5*) and 2 (*Sftpc*) markers were found to be significantly increased in *CreERT2* BLM-challenged lungs. However, IGF1R-deficient lungs demonstrated significantly decreased levels of the hypoxia-inducible factor 1 subunit alpha (*Hif1a*) (Fig. 8a). Since the RNA-seq indicated that the anti-oxidative stress marker *Gpx8* was the most up-regulated gene in *CreERT2* unchallenged lungs, its mRNA expression was assayed in BLM-treated lungs, and also found to be increased in IGF1R-deficient mice with respect to controls (Fig. 8a). SFTPC and HIF1A expression determined by immunohistochemistry verified mRNA expression levels (Fig. 8b). In accordance, the number of SFTPC⁺ cells was significantly increased (1.6-fold) (Fig. 8c), and conversely, HIF1A relative fluorescence intensity was found to be diminished (1.8-fold) in IGF1R-deficient lungs (Fig. 8d).

Discussion

This is the first report of the functional implication of IGF1R in acute lung inflammation using a BLM mouse model. First, we analyzed the lung transcriptome in recently reported IGF1R-deficient mice (*CreERT2*)²³ identifying differentially expressed genes with potentially protective roles. After BLM challenge, *CreERT2* mice showed resistance to BLM-mediated acute lung injury by counteracting lung inflammation and alveolar damage.

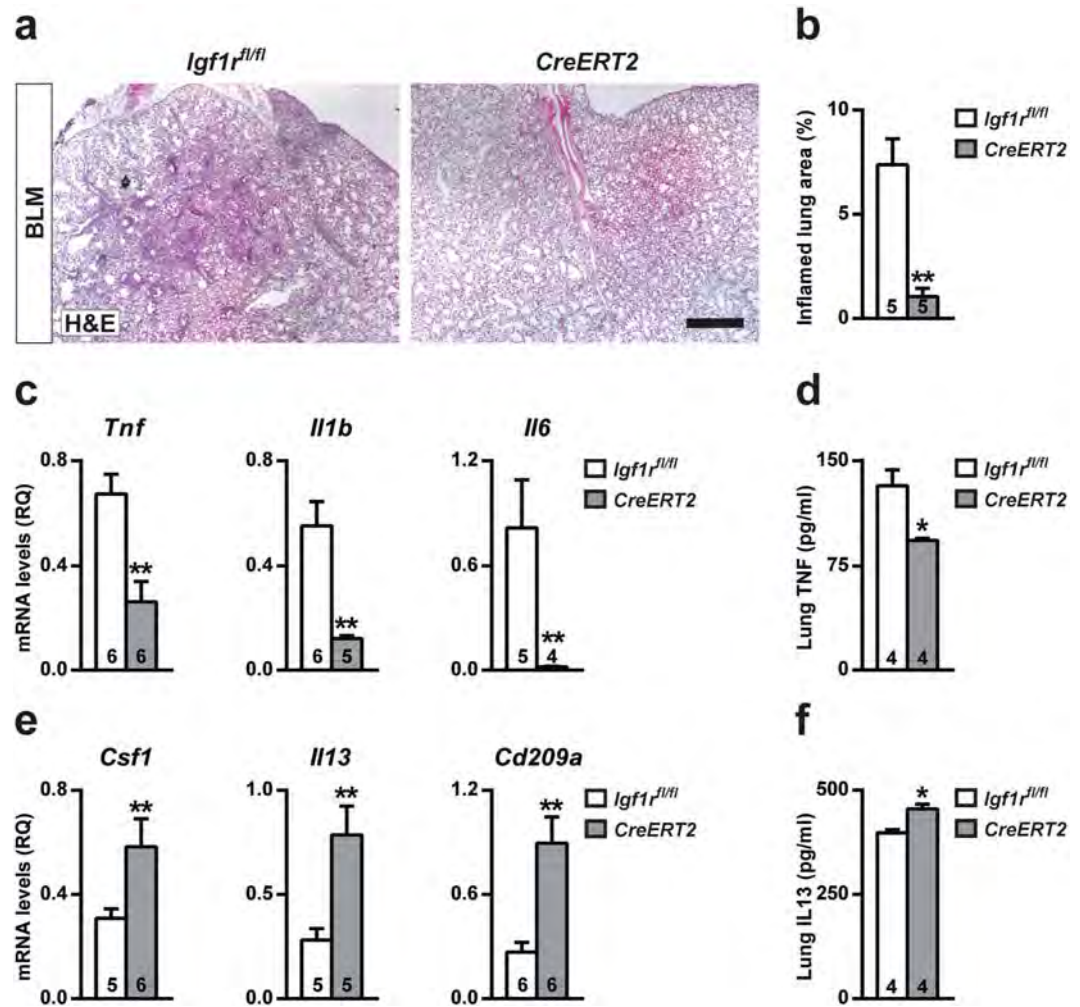


Figure 4. Decreased inflammation and increased resolution marker levels in IGF1R-deficient lungs following BLM treatment. (a) Representative images of H&E stained inflamed lung sections (scale bar: 0.5 mm), (b) quantification of inflamed lung area to total lung surface, (c,e) lung tissue mRNA expression of pro-inflammatory (*Tnf*, *Il1b* and *Il6*) and injury resolution phase (*Il13*, *Csf1* and *Cd209a*) markers, and (d,f) TNF and IL13 levels in lung homogenate from BLM-treated *UBC-CreERT2; Igf1r^{fl/fl}* (*CreERT2*) mice at D3. Numbers within graphic bars indicate the number of mice analyzed and data are expressed as mean ± SEM. * $p < 0.05$; ** $p < 0.01$ (Mann-Whitney U test). BLM, bleomycin.

Lung transcriptome analysis of *CreERT2* mice demonstrated a general inhibition of differentially expressed genes, as similarly reported in prenatal *Igf1*-deficient lungs²⁴. H1 histones *Hist1h1d* and *Hist1h2bb*, as well as *Hist1h4m* and *Hist1h1a* (Supplementary Table S1) were found to be up-regulated in *CreERT2* lungs. In this regard, it is widely known that H1 histones participate in chromatin condensation therefore repressing gene expression^{25,26}. Additionally, the histone acetyltransferases *Crebbp* and *Ep300*, both transcriptional co-activators, were found down-regulated in IGF1R-deficient lungs. In an inflammatory context, CREBBP and EP300 were reported to activate NF- κ B-mediated pro-inflammatory gene expression in response to oxidative stress^{26–28}. Thus, increased H1 histone together with lower acetyltransferase expression would result in a more condensed chromatin state, less accessible to transcription factors. Furthermore, the lower expression observed for mitochondrial respiratory chain complexes I (*mt-Nd4*, *mt-Nd5* and *mt-Nd6*) and III (*mt-Cytb*) genes (Supplementary Table S1) could result in decreased electron transport chain activity and consequently, in a reduction of reactive oxygen species production, since these complexes were reported to govern the response to hypoxia^{29,30}. In parallel, *Gpx8* and *Cyp1a1*, both involved in alleviating oxidative stress and inflammation^{31,32}, were the two most up-regulated genes. Overall, these results indicate that IGF1R deficiency could potentially be associated with a higher capacity to endure oxidant-induced injury.

After BLM treatment *CreERT2* mice showed improved survival. Similar results were observed in acute lung injury mouse models with compromised IGF1R activity^{20,33}. Moreover, IGF1R-deficient lungs showed increased *Igfbp3*, *Igfbp5*, *Insr* and *Foxo1* levels after BLM challenge, possibly due to compensatory effects in response to IGF1R deficiency, as reported^{18,34}. Specifically, IGFBP3 and IGFBP5 have shown protective properties in the mouse lung^{35–37}.

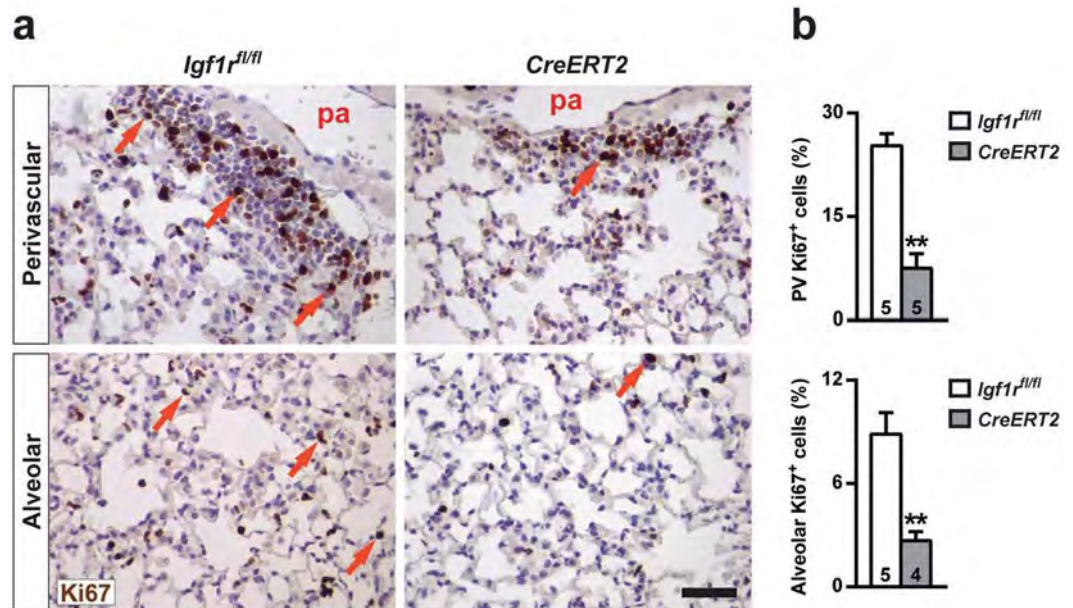


Figure 5. Diminished cell proliferation in IGF1R-deficient lungs after BLM challenge. (a) Representative images of Ki67 immuno-staining (in brown, orange arrows) under the pulmonary artery (top) and in the alveolar parenchyma (bottom), and (b) quantification of cell proliferation rates (Ki67⁺) in BLM treated *UBC-CreERT2; Igf1r^{fl/fl}* (*CreERT2*) vs. *Igf1r^{fl/fl}* lungs at D3 (scale bar: 20 μ m). Numbers within graphic bars indicate the number of mice analyzed and data are expressed as mean \pm SEM. ** $p < 0.01$ (Mann-Whitney U test). PV, perivascular; pa, pulmonary artery.

Remarkably, *CreERT2* mice showed decreased total proteins in BALF, an indicator of reduced vascular permeability. This finding together with diminished erythrocyte counts are in accordance with the lower vascular extravasation reported in hypomorphic IGF1R-deficient mice²⁰. Furthermore, the decreased presence of different inflammatory cell types in *CreERT2* lungs was reflected in BALF cell counts, and supported by reduced proliferation in perivascular and alveolar areas. Diminished *Cxcl1* and *Ly6g* mRNA levels were verified by reduced neutrophilic infiltration into *CreERT2* lungs. Considering that normal neutrophil bone marrow counts in mice are around 36.9%³⁸, BLM clearly induced bone marrow neutrophilopoiesis in *Igf1r^{fl/fl}* (54.25%) mice, unlike in IGF1R-deficient mice (25.44%). Similarly, pharmacological IGF1R blocking was recently reported to decrease the number of peripheral white blood cells^{17,39}. Altogether, these results demonstrate that the lack of IGF1R efficiently counteracts the acute BLM-induced neutrophilia, a major inflammatory player in this model.

Concerning TNF and *Il1b*, *CreERT2* lungs showed decreased expression of these cytokines, the most relevant in the lung during the early phase of BLM response^{10,40}. Accordingly, PREX1, an IGF1R signalling activator, has been shown to have a pro-inflammatory role after BLM treatment, and *Prex1*-deficient mice mirrored the pro-inflammatory profile shown by our IGF1R-deficient mice at D3⁴¹. In addition, activation of the IGF1R/PI3K/AKT/mTOR signalling pathway was reported to promote lung injury and repair^{42,43}, and IGF1R signaling promotes TNF-induced activation of NF- κ B, a major pathway involved in inflammation⁴⁴. Likewise, IGF1R plays an important role in initiation of the inflammatory process, as ablation of the macrophage IGF1/IGF1R signaling axis in mice inhibits the NLRP3 inflammasome, a protein complex triggered in the lung upon BLM-induced damage^{21,22}. During inflammation, while M1 macrophages contribute to tissue injury after excessive production of pro-inflammatory mediators (e.g., TNF and IL1B), M2 macrophages lead to resolution of inflammation and tissue repair upon anti-inflammatory cytokine activation (e.g., IL13 and CSF1)^{9,45}. In this regard, both diminished expression of *Tnf*, *Il1b* and *Il6* as well as elevated levels of *Csf1*, *Il13* and *Cd209a* found in *CreERT2* lungs would promote a pulmonary environment enriched in M2 macrophages. Noteworthy, IL13 was reported to protect against acute hyperoxic lung injury and *Cd209a* expression was found to be increased in the resolution-phase macrophages after peritonitis induction in mice^{46,47}. Altogether, these data support the idea that IGF1R deficiency would facilitate dampening of innate/adaptive immunity and resolution of inflammation.

Following BLM-induced lung injury we found increased expression of the alveolar markers *Aqp5* and SFTPC in *CreERT2* lungs. Accordingly, AQP5 expression was reported to be decreased in BLM-challenged lungs⁴⁸, and its reduced levels were shown to contribute to abnormal fluid fluxes during pulmonary inflammation in mice⁴⁹. In addition, SFTPC-deficient mice had increased mouse mortality, neutrophilic inflammation, and alveolar damage following BLM treatment⁵⁰. In line with our results, *Sftpc* mRNA levels were also found to be increased in *CreERT2* lungs after allergic airway inflammation⁵¹. Thus, it appears that IGF1R deficiency confers a protective role against alveolar damage.

As a master transcriptional regulator of the adaptive response to hypoxia, HIF1A uses CREBBP and EP300 as transcriptional co-activators. Thus, decreased *Crebbp* and *Ep300* transcriptional levels in non-challenged *CreERT2* lungs could contribute to HIF1A reduced expression after BLM challenge. In accordance, alveolar type

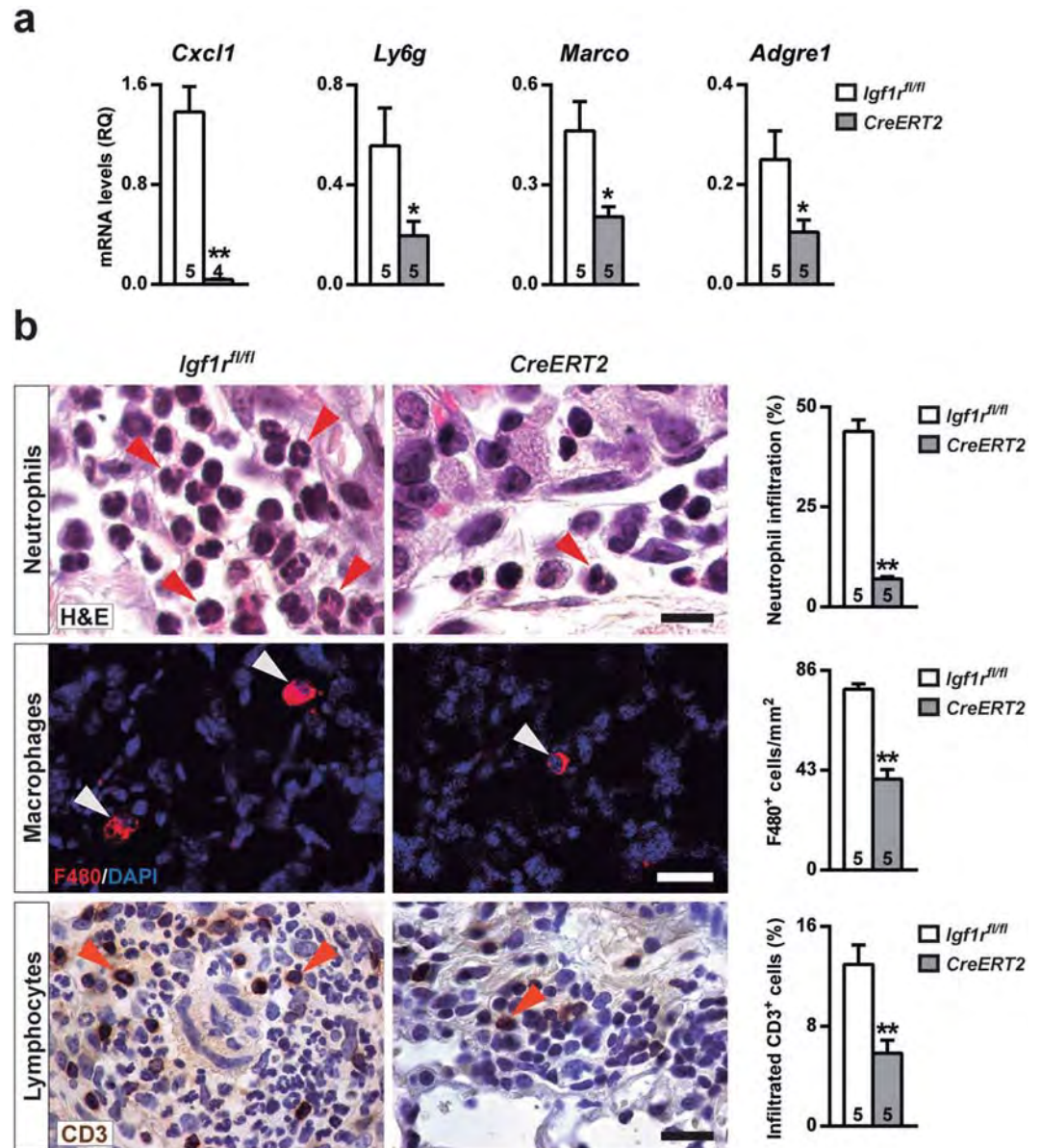


Figure 6. Reduced inflammatory cell infiltration in IGF1R-deficient lungs after BLM treatment. (a) Lung mRNA expression of neutrophil chemotaxis (*Cxcl1*), neutrophil (*Ly6g*) and macrophage (*Adgre1* and *Marco*) markers and (b) representative H&E, as well as F4/80 and CD3 immunostained sections, and quantification of neutrophils (red arrowheads, upper panels), alveolar macrophages (white arrowheads, middle panels) and lymphocytes (orange arrowheads, bottom panels) in BLM treated *UBC-CreERT2; Igf1r^{fl/fl}* (*CreERT2*) vs. *Igf1r^{fl/fl}* lungs at D3. Scale bars: 10 μ m (upper panels) and 20 μ m (middle and bottom panels). Numbers within graphic bars indicate the number of mice analyzed and data are expressed as mean \pm SEM. * p < 0.05; ** p < 0.01 (Mann-Whitney U test).

2 cell-specific *Hif1a* knockout mice demonstrated milder pulmonary inflammation⁵², supporting that HIF1A could play an important role in acute lung inflammation.

Although we demonstrate a significant reduction of IGF1R expression in *CreERT2* lungs, TMX-mediated IGF1R deletion may occur with different degrees of mosaicism in different cell types. Thus, IGF1R generalized deletion cannot be used to deduce in which cells IGF1R signaling is crucial for promoting acute lung inflammation. Furthermore, the variability of intratracheal administration of BLM and the effect of the genetic background on phenotypic variations should also be considered as constraints to this report.

In summary, we have shown that IGF1R deficiency in mice plays a key role in decreasing transcriptional activity, and confers protection against alveolar damage and pulmonary inflammation. Notably, our findings may contribute to understanding the importance of IGF1R as a potential target for future therapeutic approaches in respiratory diseases with persistent damage and inflammation.

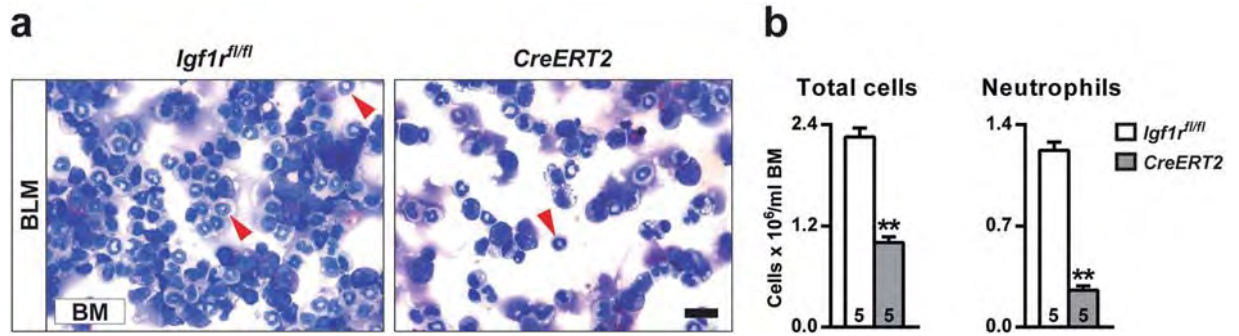


Figure 7. Reduced total and neutrophil counts in bone marrow from IGF1R-deficient mice. (a,b) Representative images, and total and neutrophil (red arrowheads) counts in bone marrow cytospin preparations from BLM-treated *UBC-CreERT2; Igf1r^{fl/fl} (CreERT2)* vs. *Igf1r^{fl/fl}* mice at D3. Scale bar: 20 μ m. Numbers within graphic bars indicate the number of mice analyzed and data are expressed as mean \pm SEM. ** $p < 0.01$ (Mann-Whitney U test). BLM, bleomycin; BM, bone marrow.

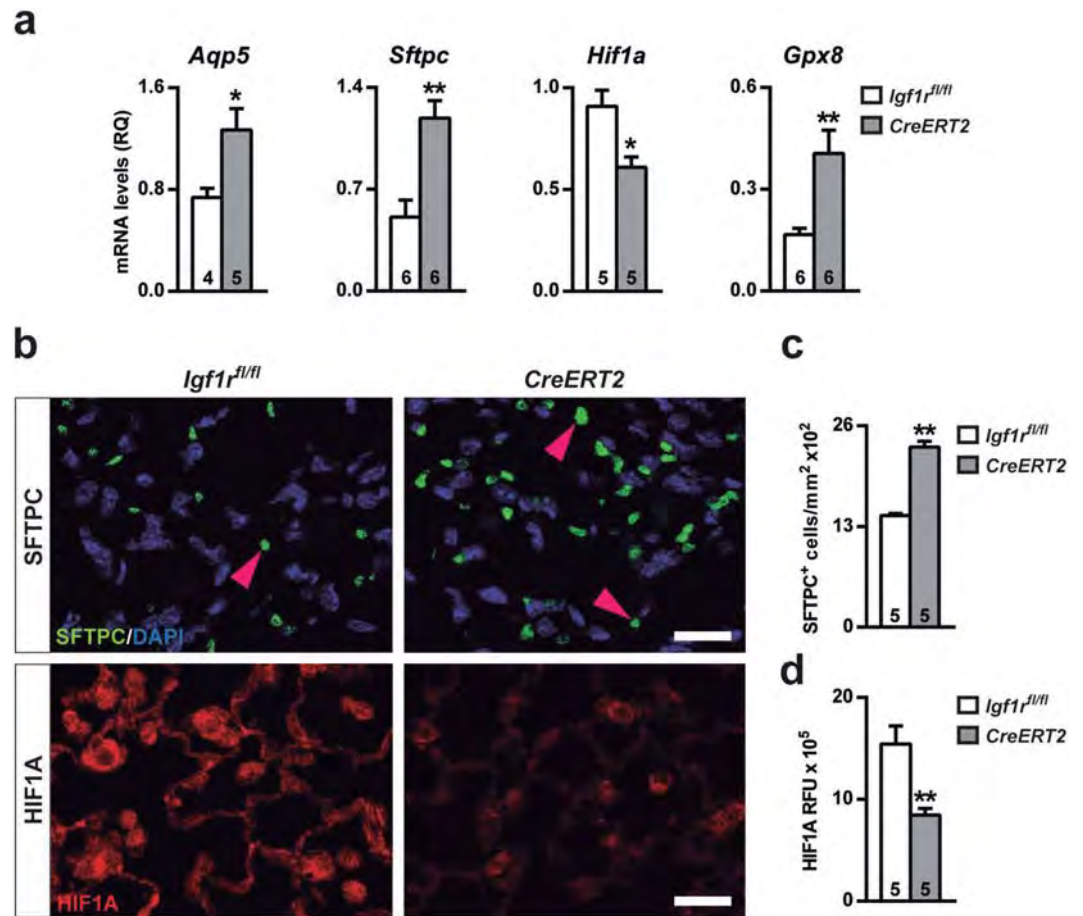


Figure 8. Reduced alveolar damage and HIF1A expression in BLM-challenged lungs of IGF1R-deficient mice. (a) Changes in mRNA expression of alveolar (*Aqp5* and *Sftpc*), response to hypoxia (*Hif1a*), and antioxidative stress (*Gpx8*) markers, (b) representative SFTPC (pink arrowheads) and HIF1A immunostained sections (upper and bottom panels, respectively), (c) number of SFTPC positive cells per unit area of lung tissue, and (d) quantification of HIF1A relative fluorescence intensity in lungs of *UBC-CreERT2; Igf1r^{fl/fl} (CreERT2)* and *Igf1r^{fl/fl}* mice at D3 after BLM treatment. Scale bars: 20 μ m. Numbers within graphic bars indicate the number of mice analyzed and data are expressed as mean \pm SEM. * $p < 0.05$; ** $p < 0.01$ (Mann-Whitney U test). RFU, relative fluorescence units.

Methods

Ethics Statement. All experiments and animal procedures were carried out following the guidelines laid down by the European Communities Council Directive of 24 November 1986 (86/609/EEC) and were revised and approved by the CIBIR Bioethics Committee (refs 03/12 and 13/12). All animals were bred and maintained under specific pathogen-free (SPF) conditions in laminar flow caging at the CIBIR animal facility.

Generation of *Igf1r*-deficient mice, establishment of the BLM-induced acute lung injury murine model and survival rate. *Ubc-Cre-ERT2; Igf1r^{fl/fl}* double transgenic mice were in a C57BL/6 enriched (at least six generation backcrosses to C57BL/6 strain) mixed genetic background. For experimental purposes, *Ubc-Cre-ERT2; Igf1r^{fl/fl}* double transgenic mice were crossed with *Igf1r^{fl/fl}* mice to directly generate descendants in equal proportions in the same litter, and *Igf1r^{fl/fl}* and *Ubc-Cre-ERT2; Igf1r^{fl/fl}* littermates were respectively used as experimental controls and mutants. Tamoxifen (TMX) was administered daily for five consecutive days to four-week-old mice of both genotypes to induce a postnatal *Igf1r* gene conditional deletion in *Ubc-Cre-ERT2; Igf1r^{fl/fl}* mice, as previously described²³. Two-month-old and six-week-old tamoxifen-treated *Ubc-Cre-ERT2; Igf1r^{fl/fl}* (*CreERT2*) and *Igf1r^{fl/fl}* mice were used for RNAseq analysis, and BLM treatment to induce lung injury, respectively. Six-week-old mice (equal sex proportions) of both genotypes were intra-tracheally instilled with either a single dose of 2.5 µl/g body weight of BLM sulfate (5 U/kg) (EMD Millipore, Billerica, MA) in saline (2 U/ml) or saline (SAL) at D0, under a ketamine-xylazine anesthetic combination in saline (100:10 mg/kg respectively; 10 µl/g). Animals were monitored for 21 days to determine survival rates of both *Ubc-Cre-ERT2; Igf1r^{fl/fl}* and *Igf1r^{fl/fl}* mice after BLM challenge. Those animals that reached the human endpoint, as specified by the CIBIR Bioethics Committee protocol ref. 13/12, were also considered to be dead animals at each time point. The human endpoint criteria were applied when there was severe involvement of one of the specific (body weight, respiratory pattern and bleeding), or moderate involvement of two or more of the general (appearance, natural behavior) or specific parameters occurred, according to our expert veterinary evaluation. For acute lung injury studies, animals were sacrificed and tissues were collected at D3 (Fig. 2a).

Tissue and BALF collection. Before tissue collection, animals were euthanized by intraperitoneal injection of 10 µl/g of a ketamine-xylazine anesthetic combination in saline (300:30 mg/kg respectively). Three different sets of mice were used for BALF, mRNA/Western blot/histology and ELISA, respectively. A first set was used to obtain BALF; lungs from saline or BLM-treated mice were lavaged twice with 0.8 ml cold PBS. From the second set, left lungs were inflated with formalin fixative, post-fixed by immersion in formalin for 8–10 h, embedded in paraffin and cut into 3 µm sections for histopathological evaluation or immunohistochemistry; and right lobes were separated and snap frozen in liquid nitrogen for qRT-PCR and Western blot. Left lungs from a third set of animals were harvested for ELISA analysis.

Quantification of BALF. Total cell number was counted and expressed as cells/ml BALF and differential cell counts were performed on May-Grünwald/Giemsa (Sigma-Aldrich, St. Louis, MO) stained cytopins from 4 animals per condition, blind counting a minimum of 300 cells per slide. Cells were determined to be macrophages, lymphocytes and neutrophils using standard morphology criteria. The average number of red blood cells per high-power field was obtained by evaluating 5 different fields on BALF cytopsin preparations. Total protein concentration in BALF supernatants was determined using the Pierce BCA Protein Assay Kit (Thermo Fisher Scientific, Waltham, MA).

Histopathological analyses and immunostaining. Quantification of inflammation was determined in H&E stained sections and expressed as the percentage of inflamed lung area to total section surface. Five BLM-treated left lungs per genotype were used. Inflamed lung areas were defined as darker H&E stained foci, where inflammatory cells accumulate massively, and delimited manually using the Fiji open-source image processing software package v1.48r (<https://fiji.sc>).

Immunohistological detection of proliferating cells was performed as described²³. Ki67 positive cells were counted using 5 or 10 fields per section per animal in perivascular and alveolar areas, respectively. The Ki67-labeling index was calculated as the number of Ki67 positive cells compared to the total cell number. Other histological and immunohistochemical quantifications were performed using 5 BLM-treated animals per genotype evaluating 5 different fields per lung. Determination of neutrophil and lymphocyte infiltration grades were assessed in lung perivascular areas on H&E and CD3 (ab5690 1:200, Abcam, Cambridge, UK) stained lung sections, and expressed as the number of neutrophils or lymphocytes to total cell infiltrates. Quantification of macrophages and alveolar type 2 cells was assessed in alveolar areas immunostained with anti-F4/80 (Clone MCA497GA 1:100, Bio-Rad, Langford, UK), and anti-SFTPC (AB3786, EMD Millipore, Billerica, MA) antibodies respectively, and expressed per unit area. Macrophage diameters were measured and volumes were extrapolated using the sphere volume formula. HIF1A expression was determined using the HIF1A antibody (ab2185 1:100, Abcam, Cambridge, UK) and expressed as relative fluorescence units (RFU) as previously described¹⁸. HIF1A relative fluorescence was evaluated using the Fiji software package.

Femoral bone marrow isolation. Bone marrow (BM) isolation was performed using 5 BLM-treated animals per genotype (1 femur per animal). After dissection, the femoral heads were incised and femurs were positioned in bottom perforated 0.5 ml tubes placed inside 1.5 ml tubes. After centrifugation at 10000 × g for 15 seconds, BM was suspended in 500 µl PBS and centrifuged at 300 × g for 5 min at 4 °C. Following aspiration of the supernatant, BM pellets were resuspended in 500 µl of ACK lysing buffer (Thermo Fisher Scientific, Waltham, MA) and after 10 minutes of incubation, 1 ml of PBS was added. Total cell numbers were counted and expressed as

cells/ml BM and neutrophil counts were performed on May-Grünwald/Giemsa (Sigma-Aldrich, St. Louis, MO) stained cytopins and 5 different fields per slide were blind counted.

RNA isolation, reverse transcription and qRT-PCR. Inferior lung lobes taken from eight-week-old mice or on D3 post-bleomycin were homogenized in TRIzol Reagent (Invitrogen, Carlsbad, CA) and total RNA was isolated using an RNeasy Mini Kit (Qiagen, Hilden, Germany). RNA from D3 post-bleomycin-treated mice was reverse transcribed to cDNA using SuperScript II First-Strand Synthesis System (Invitrogen, Carlsbad, CA) as per the manufacturer's specifications. cDNA samples were amplified by qRT-PCR in triplicate on a 7300 Real Time PCR instrument (Applied Biosystems, Foster City, CA), for each primer pair assayed (Supplementary Table S4). Results were normalized using the 18S rRNA gene as the endogenous control.

Lung transcriptome analysis. RNAseq analysis was performed on eight-week-old tamoxifen-treated *UBC-CreERT2; Igf1^{fl/fl}* and *Igf1^{fl/fl}* lungs (n = 3 per genotype). Approximately, 1 µg of total RNA from each sample was submitted to the CIBIR Genomics Core Facility for sequencing. Briefly, after verifying RNA quality in an Experion Bioanalyzer (BioRad), TruSeq total RNA libraries were generated according to the manufacturer's instructions (Illumina Inc). The libraries were sequenced in a Genome Analyzer IIx (Illumina Inc) to generate 150 single-end reads. *Mus musculus* GRCm38.71 (FASTA) from the Ensemble database was used as the reference genome. After removing adapter sequences with the Cutadapt software⁵³, mapping to the reference genome was performed with TopHat2 (version 2.5)⁵⁴. Gene expression quantification, normalization, and statistical analyses were performed with SeqSolve (Integromics). Expression data were normalized by calculating the fragments per kilobase of exon per million fragments mapped (FPKM) reads for each gene. *Igf1r*-transcriptionally regulated genes involved in biological processes were classified according to GO and Keyword annotations. Additionally, a PubMed search, and the Genecards and OMIM tools were used to help assign biological functions.

Western blot analysis. Superior lung lobes were solubilized in a 10 mM Tris/HCl (pH 7.4) buffer containing 0.1% sodium dodecyl sulfate, a protease inhibitor mixture, and DNase (Promega, Fitchburg, WI). Samples were separated in NuPAGE Novex 4–12% Bis-Tris Gel (Invitrogen, Carlsbad, CA) and transferred to a polyvinylidene difluoride membrane (EMD Millipore). Membranes were incubated with primary antibodies for IGF1R (#3027 Cell Signalling Inc., Danvers, MA) and beta-Actin (ab6276 Abcam, Cambridge, UK) at 1:1000 and 1:30000 dilutions respectively, and then incubated with horseradish peroxidase-conjugated anti-rabbit or anti-mouse antibodies (DAKO, Agilent technologies, Santa Clara, CA) for IGF1R and beta-Actin respectively, at a 3:10 dilution. Signals were detected using ECL Western Blot Substrate (Thermo Fisher Scientific, Waltham, MA) and Hyperfilm ECL (GE Healthcare, Little Chalfont, UK). Films were scanned and signals in the linear range were quantified using Image J and normalized to beta-Actin levels.

ELISAS. TNF and IL13 levels were determined in homogenized tissue lysates using left lungs with the help of mouse TNF-alpha Quantikine and IL-13 Duoset ELISA Kits (R&D Systems, Minneapolis, MN), according to the manufacturer's guidelines.

Statistics. Statistical analyses were performed using SPSS Statistics Software v21 for Windows. Differences between genotypes were evaluated for significance using the non-parametric Mann-Whitney U test or the Dunn Sidak test for multiple comparisons. Results are shown as mean values ± standard error of the mean (SEM). For all analyses, a *p* value < 0.05 was considered statistically significant.

References

- Moldoveanu, B. *et al.* Inflammatory mechanisms in the lung. *J Inflamm Res* **2**, 1–11 (2009).
- Postma, D. S. & Rabe, K. F. The Asthma-COPD overlap syndrome. *N Engl J Med* **373**, 1241–1249 (2015).
- Conway, E. M. *et al.* Macrophages, inflammation, and lung cancer. *Am J Respir Crit Care Med* **193**, 116–130 (2016).
- Wynn, T. A. Integrating mechanisms of pulmonary fibrosis. *J Exp Med* **208**, 1339–1350 (2011).
- Johnson, E. R. & Matthay, M. A. Acute lung injury: epidemiology, pathogenesis, and treatment. *J Aerosol Med Pulm Drug Deliv* **23**, 243–252 (2010).
- Foskett, A. M. *et al.* Phase-directed therapy: TSG-6 targeted to early inflammation improves bleomycin-injured lungs. *Am J Physiol Lung Cell Mol Phys* **306**, L120–L131 (2014).
- Della Latta, V., Cecchetti, A., Del Ry, S. & Morales, M. A. Bleomycin in the setting of lung fibrosis induction: From biological mechanisms to counteractions. *Pharmacol Res* **97**, 122–130 (2015).
- Moeller, A., Ask, K., Warburton, D., Gaudie, J. & Kolb, M. The bleomycin animal model: a useful tool to investigate treatment options for idiopathic pulmonary fibrosis? *Int J Biochem Cell Biol* **40**, 362–382 (2008).
- Laskin, D. L., Sunil, V. R., Gardner, C. R. & Laskin, J. D. Macrophages and tissue injury: agents of defense or destruction? *Ann Rev Pharm Toxicol* **51**, 267–288 (2011).
- Grommes, J. & Soehnlein, O. Contribution of neutrophils to acute lung injury. *Mol Med* **17**, 293–307 (2011).
- Girmita, L., Worrall, C., Takahashi, S., Seregard, S. & Girmita, A. Something old, something new and something borrowed: emerging paradigm of insulin-like growth factor type 1 receptor (IGF-1R) signaling regulation. *Cell Mol Life Sci* **71**, 2403–2427 (2014).
- Annunziata, M., Granata, R. & Ghigo, E. The IGF system. *Acta Diabetol* **48**, 1–9 (2011).
- Ahasic, A. M. *et al.* Adiponectin gene polymorphisms and acute respiratory distress syndrome susceptibility and mortality. *PLoS One* **9**, e89170 (2014).
- Pala, L. *et al.* Direct measurement of IGF-1 and IGFBP-3 in bronchoalveolar lavage fluid from idiopathic pulmonary fibrosis. *J Endocrinol Invest* **24**, 856–864 (2001).
- Takasaka, N. *et al.* Autophagy induction by SIRT6 through attenuation of insulin-like growth factor signaling is involved in the regulation of human bronchial epithelial cell senescence. *J Immunol* **192**, 958–968 (2014).
- Agullo-Ortuño, M. T. *et al.* Relevance of insulin-like growth factor 1 receptor gene expression as a prognostic factor in non-small-cell lung cancer. *J Cancer Res Clinical Oncol* **141**, 43–53 (2015).
- Moody, G. *et al.* IGF1R blockade with ganitumab results in systemic effects on the GH-IGF axis in mice. *J Endocrinol* **221**, 145–155 (2014).

18. López, I. P. *et al.* Involvement of Igf1r in bronchiolar epithelial regeneration: Role during repair kinetics after selective club cell ablation. *PLoS One* **11**, e166388 (2016).
19. Kim, T. H., Chow, Y. H., Gill, S. E. & Schnapp, L. M. Effect of insulin-like growth factor blockade on hyperoxia-induced lung injury. *Am J Respir Cell Mol Biol* **47**, 372–378 (2012).
20. Ahamed, K. *et al.* Deficiency in type 1 insulin-like growth factor receptor in mice protects against oxygen-induced lung injury. *Respir Res* **6**, 31–41 (2005).
21. Spadaro, O. *et al.* Growth hormone receptor deficiency protects against age-related NLRP3 inflammasome activation and immune senescence. *Cell Rep* **14**, 1571–1580 (2016).
22. Gasse, P. *et al.* Uric acid is a danger signal activating NALP3 inflammasome in lung injury inflammation and fibrosis. *Am J Respir Crit Care Med* **179**, 903–913 (2009).
23. Lopez, I. P. *et al.* Differential organ phenotypes after postnatal Igf1r gene conditional deletion induced by tamoxifen in UBC-CreERT2; Igf1r fl/fl double transgenic mice. *Transgenic Res* **24**, 279–294 (2015).
24. Pais, R. S. *et al.* Transcriptome analysis in prenatal IGF1-deficient mice identifies molecular pathways and target genes involved in distal lung differentiation. *PLoS One* **8**, e83028 (2013).
25. Harshman, S. W., Young, N. L., Parthun, M. R. & Freitas, M. A. H1 histones: current perspectives and challenges. *Nucleic Acids Res* **41**, 9593–9609 (2013).
26. Happel, N. & Doenecke, D. Histone H1 and its isoforms: contribution to chromatin structure and function. *Gene* **431**, 1–12 (2009).
27. Bayarsaihan, D. Epigenetic mechanisms in inflammation. *J Dent Res* **90**, 9–17 (2011).
28. Rajendrasozhan, S., Yao, H. & Rahman, I. Current perspectives on role of chromatin modifications and deacetylases in lung inflammation in COPD. *Copd* **6**, 291–297 (2009).
29. Holzerova, E. & Prokisch, H. Mitochondria: Much ado about nothing? How dangerous is reactive oxygen species production? *Int J Biochem Cell Biol* **63**, 16–20 (2015).
30. Schumacker, P. T. *et al.* Mitochondria in lung biology and pathology: more than just a powerhouse. *Am J Physiol Lung Cell Mol Physiol* **306**, L962–974 (2014).
31. Yamada, Y. *et al.* Major shifts in the spatio-temporal distribution of lung antioxidant enzymes during influenza pneumonia. *PLoS One* **7**, e31494 (2012).
32. Lingappan, K. *et al.* Mice deficient in the gene for cytochrome P450 (CYP)1A1 are more susceptible than wild-type to hyperoxic lung injury: evidence for protective role of CYP1A1 against oxidative stress. *Toxicol Sci* **141**, 68–77 (2014).
33. Choi, J. E. *et al.* Insulin-like growth factor-I receptor blockade improves outcome in mouse model of lung injury. *Am J Respir Crit Care Med* **179**, 212–219 (2009).
34. Buck, E. *et al.* Compensatory insulin receptor (IR) activation on inhibition of insulin-like growth factor-1 receptor (IGF-1R): rationale for cotargeting IGF-1R and IR in cancer. *Mol Cancer Ther* **9**, 2652–2664 (2010).
35. Vijayan, A. *et al.* IGFBP-5 enhances epithelial cell adhesion and protects epithelial cells from TGFbeta1-induced mesenchymal invasion. *Int J Biochem Cell Biol* **45**, 2774–2785 (2013).
36. Lee, Y. C. *et al.* Insulin-like growth factor-binding protein-3 (IGFBP-3) blocks the effects of asthma by negatively regulating NF-kappaB signaling through IGFBP-3R-mediated activation of caspases. *J Biol Chem* **286**, 17898–17909 (2011).
37. Alami, N. *et al.* Recombinant human insulin-like growth factor-binding protein 3 inhibits tumor growth and targets the Akt pathway in lung and colon cancer models. *Growth Horm IGF Res* **18**, 487–496 (2008).
38. Yang, M., Busche, G., Ganser, A. & Li, Z. Morphology and quantitative composition of hematopoietic cells in murine bone marrow and spleen of healthy subjects. *Ann Hematol* **92**, 587–594 (2013).
39. Osorio, F. G. *et al.* Loss of the proteostasis factor AIRAPL causes myeloid transformation by deregulating IGF-1 signaling. *Nat Med* **22**, 91–96 (2016).
40. Cavarra, E. *et al.* Early response to bleomycin is characterized by different cytokine and cytokine receptor profiles in lungs. *Am J Physiol Lung Cell Mol Physiol* **287**, L1186–1192 (2004).
41. Liang, Q. *et al.* Identification of P-Rex1 as an anti-inflammatory and anti-fibrogenic target for pulmonary fibrosis. *Sci Rep* **6**, 25785 (2016).
42. Hu, Y. *et al.* Activation of MTOR in pulmonary epithelium promotes LPS-induced acute lung injury. *Autophagy* **12**, 2286–2299 (2016).
43. Kral, J. B. *et al.* Sustained PI3K Activation exacerbates BLM-induced Lung Fibrosis via activation of pro-inflammatory and pro-fibrotic pathways. *Sci Rep* **6**, 23034 (2016).
44. Li, S. *et al.* Crosstalk between the TNF and IGF pathways enhances NF-kappaB activation and signaling in cancer cells. *Growth Horm IGF Res* **25**, 253–261 (2015).
45. Reales-Calderon, J. A., Aguilera-Montilla, N., Corbi, A. L., Molero, G. & Gil, C. Proteomic characterization of human proinflammatory M1 and anti-inflammatory M2 macrophages and their response to *Candida albicans*. *Proteomics* **14**, 1503–1518 (2014).
46. Corne, J. *et al.* IL-13 stimulates vascular endothelial cell growth factor and protects against hyperoxic acute lung injury. *J Clin Invest* **106**, 783–791 (2000).
47. Stables, M. J. *et al.* Transcriptomic analyses of murine resolution-phase macrophages. *Blood* **118**, e192–208 (2011).
48. Gao, X. *et al.* Expression of pulmonary aquaporin 1 is dramatically upregulated in mice with pulmonary fibrosis induced by bleomycin. *Arch Med Sci* **9**, 916–921 (2013).
49. Towne, J. E., Harrod, K. S., Krane, C. M. & Menon, A. G. Decreased expression of aquaporin (AQP)1 and AQP5 in mouse lung after acute viral infection. *Am J Respir Cell Mol Biol* **22**, 34–44 (2000).
50. Lawson, W. E. *et al.* Increased and prolonged pulmonary fibrosis in surfactant protein C-deficient mice following intratracheal bleomycin. *Am J Pathol* **167**, 1267–1277 (2005).
51. Pineiro-Hermida, S. *et al.* Attenuated airway hyperresponsiveness and mucus secretion in HDM-exposed Igf1r-deficient mice. *Allergy*, doi:10.1111/all.13142 (2017).
52. Suresh, M. V. *et al.* Activation of hypoxia-inducible factor-1alpha in type 2 alveolar epithelial cell is a major driver of acute inflammation following lung contusion. *Crit Care Med* **42**, e642–653 (2014).
53. Martin, M. Cutadapt removes adapter sequences from high-throughput sequencing reads. *EMBnet J.* **17**, 10–12 (2011).
54. Trapnell, C. *et al.* Differential gene and transcript expression analysis of RNA-seq experiments with TopHat and Cufflinks. *Nat Protoc* **7**, 562–578 (2012).

Acknowledgements

We are grateful to Drs J. Brüning (University of Cologne, Germany) and E. Brown (U Penn School of Medicine, PA) for providing *Igf1r^{fl/fl}* and *UBC-CreERT2* mouse lines, respectively. The authors thank Dr. C. Esmahan for the English language revision. S.P.-H. also thanks the Sistema Riojano de Innovación (Gobierno de La Rioja, Spain) for a PhD grant. S.P.-H., I.P.L. and J.G.P. are part of the European Cooperation in Science and Technology COST Action BM1201, Developmental Origins of Chronic Lung Disease. This work was supported by grants from the

Fundación Rioja Salud (Gobierno de La Rioja, Spain) to J.G.P. and co-funded by the ERDF (European Regional Development Fund) and the ESF (European Social Fund).

Author Contributions

S.P.-H., I.P.L. and J.G.P. proposed and conceived the project and designed the experiments. S.P.-H., I.P.L., E.A.-A., R.T. and J.G.P. performed the experiments. S.P.-H., I.P.L., E.A.-A., M.I., C.R.-M., L.A.-E. and J.G.P. analyzed the data and interpreted the experiments. M.I. and L.A.-E. contributed with reagents, materials and analytical tools. S.P.-H. and J.G.P. drafted and wrote the manuscript. All authors read, revised and approved the manuscript prior to submission.

Additional Information

Supplementary information accompanies this paper at doi:10.1038/s41598-017-04561-4

Competing Interests: The authors declare that they have no competing interests.

Publisher's note: Springer Nature remains neutral with regard to jurisdictional claims in published maps and institutional affiliations.



Open Access This article is licensed under a Creative Commons Attribution 4.0 International License, which permits use, sharing, adaptation, distribution and reproduction in any medium or format, as long as you give appropriate credit to the original author(s) and the source, provide a link to the Creative Commons license, and indicate if changes were made. The images or other third party material in this article are included in the article's Creative Commons license, unless indicated otherwise in a credit line to the material. If material is not included in the article's Creative Commons license and your intended use is not permitted by statutory regulation or exceeds the permitted use, you will need to obtain permission directly from the copyright holder. To view a copy of this license, visit <http://creativecommons.org/licenses/by/4.0/>.

© The Author(s) 2017

Supplementary Information for

***Igflr* deficiency attenuates acute inflammatory response in a bleomycin-induced lung injury mouse model**

Sergio Piñeiro-Hermida¹, Icíar P. López¹, Elvira Alfaro-Arnedo¹, Raquel Torrens¹, María Iñiguez², Lydia Alvarez-Erviti³, Carlos Ruíz-Martínez⁴, and José G. Pichel^{1,*}

¹ Lung Cancer and Respiratory Diseases Unit, ² Genomics Core Facility and ³ Molecular Neurobiology Unit; Centro de Investigación Biomédica de la Rioja (CIBIR), Fundación Rioja Salud. ⁴ Pneumology Service, Hospital San Pedro. Logroño, Spain.

Files included:

Supplementary Table S1. Differential gene expression determined by RNAseq in the lung of *UBC-CreERT2; Igflr^{fl/fl}* mutant mice (FDR < 0.2).

Supplementary Table S2. Biological functions and differentially expressed genes found with significant changes after RNAseq in the lung of *UBC-CreERT2; Igflr^{fl/fl}* mutant mice (FDR < 0.1).

Supplementary Table S3. Differential BALF cell counts represented as the percentage of each cell type to total cell counts in *Igflr^{fl/fl}* and *UBC-CreERT2; Igflr^{fl/fl}* mice.

Supplementary Table S4. Primer sets used for qRT-PCR .

Supplementary Table S1. Differential gene expression determined by RNAseq in the lung of *UBC-CreERT2; Igf1^{fl/fl}* mutant mice (FDR < 0.2)

Position	Gene name	Description	Log2 fold change	Q-value/FDR
1	Gpx8	Glutathione peroxidase 8	33.33	5.08097E-11
2	Igf1r	Insulin-like growth factor 1 receptor	-2.35512	6.91951E-11
3	Cyp11a1	Cytochrome P450, family 1, subfamily a, polypeptide 1	2.22399	1.51895E-10
4	Gnptg	N-acetylglucosamine-1-phosphotransferase, gamma subunit	33.33	1.10271E-08
5	Srrm2	Serine/arginine repetitive matrix 2	-1.29438	2.90396E-06
6	Nr1d2	Nuclear receptor subfamily 1, group D, member 2	-1.43483	2.65234E-05
7	Ppp1r2-ps4	Protein phosphatase 1, regulatory (inhibitor) subunit 2, pseudogene 4	33.33	3.69653E-05
8	Saa3	Serum amyloid A 3	2.58211	7.26024E-05
9	Epas1	Endothelial PAS domain protein 1	-1.17128	8.78217E-05
10	Spon2	Spondin 2, extracellular matrix protein	1.76138	0.000320111
11	Sloc2a1	Solute carrier organic anion transporter family, member 2a1	-1.08642	0.000596572
12	Mll2	Lysine (K)-specific methyltransferase 2D	-1.11086	0.000614606
13	Npnt	Nephronectin	-0.950843	0.000614606
14	Hydin	HYDIN, axonemal central pair apparatus protein	-1.51408	0.00123442
15	Pcdh1	Protocadherin 1	-0.92639	0.00123442
16	Lyz1	Lysozyme 1	1.00162	0.00130818
17	Top2a	Topoisomerase (DNA) II alpha	1.19316	0.00146147
18	Zbtb34	Zinc finger and BTB domain containing 34	-33.33	0.00169479
19	Cyyr1	Cysteine and tyrosine-rich protein 1	-0.864652	0.00169479
20	mt-Nd5	NADH dehydrogenase 5, mitochondrial	-0.946779	0.00436231
21	Ces1g	Carboxylesterase 1G	2.10737	0.00454152
22	Pcnx	Pecanex homolog (Drosophila)	-0.989945	0.00483008
23	Muc5b	Mucin 5, subtype B, tracheobronchial	-1.04542	0.0066965
24	Med13l	Mediator complex subunit 13-like	-1.05975	0.0072912
25	Lox	Lysyl oxidase	-0.893177	0.00758989
26	Tenc1	Tensin 2	-0.95569	0.0130699
27	Dnahc6	Dynein, axonemal, heavy chain 6	-0.953513	0.0156303
28	Hist1h1d	Histone cluster 1, H1d	1.27832	0.0174382
29	Atp2a3	ATPase, Ca++ transporting, ubiquitous	-0.935091	0.0195047
30	Zbtb16	Zinc finger and BTB domain containing 16	-0.87579	0.0255043
31	Svep1	Sushi, von Willebrand factor type A, EGF and pentraxin domain containing 1	-0.82965	0.0288283
32	Mki67	Antigen identified by monoclonal antibody Ki 67	0.88978	0.0288283
33	Snhg11	Small nucleolar RNA host gene 11	-1.27045	0.0331612
34	Hist1h2bb	Histone cluster 1, H2bb	1.21471	0.0347587
35	Zfp518b	Zinc finger protein 518b	-33.33	0.0360491
36	Zfx3	Zinc finger homeobox 3	-0.987494	0.0371726
37	Notch3	Neurogenic locus homolog protein 3	-1.01305	0.0405676
38	Foxo1	Forkhead box O1	-1.02458	0.0411093
39	Apol11b	Apolipoprotein L 11b	-1.89341	0.0485738
40	Syngap1	Synaptic Ras GTPase activating protein 1 homolog (rat)	-33.33	0.0487062
41	AC147987.1	RIKEN cDNA 4933404O12 gene	33.33	0.0492756
42	C030017K20Rik	RIKEN cDNA C030017K20 gene	-33.33	0.0507919
43	Rab6b	RAB6B, member RAS oncogene family	-1.17859	0.0507919
44	Crebbp	CREB binding protein	-0.854579	0.0508175
45	Kif11	Kinesin family member 11	1.18653	0.0508175
46	Fancl	Fanconi anemia, complementation group F	33.33	0.0536387
47	Hr	Hairless	-33.33	0.0546633
48	Ptpnb	Protein tyrosine phosphatase, receptor type, B	-0.815991	0.0550762
49	Gdpd3	Glycerophosphodiester phosphodiesterase domain containing 3	-1.6275	0.0593667
50	Marco	Macrophage receptor with collagenous structure	1.43551	0.0632713
51	Tet3	Tet methylcytosine dioxygenase 3	-0.969638	0.065462
52	mt-Cytb	Cytochrome b, mitochondrial	-0.768723	0.0674572
53	Luc7l2	LUC7-like 2 (S. cerevisiae)	-0.472481	0.0674572
54	Nav2	Neuron navigator 2	-0.969168	0.0684272
55	Ppp1r3c	Protein phosphatase 1, regulatory (inhibitor) subunit 3C	1.13441	0.0712999
56	Trim25	Tripartite motif-containing 25	-1.04788	0.0733889
57	Prrc2c	Proline-rich coiled-coil 2C	-0.785804	0.0733889
58	Mlxip	MLX interacting protein	-0.877622	0.076686
59	Polr2a	Polymerase (RNA) II (DNA directed) polypeptide A	-0.816322	0.0776129
60	Ep300	E1A binding protein p300	-0.79195	0.0777767
61	Abi3bp	ABI gene family, member 3 (NESH) binding protein	-0.842908	0.0783232
62	Tgfb3	Transforming growth factor, beta receptor III	-0.794265	0.0902875
63	Efnb2	Ephrin B2	-0.983599	0.0926999
64	Hnrnpul2	Heterogeneous nuclear ribonucleoprotein U-like 2	-0.81716	0.0936172
65	Rps7	Ribosomal protein S7	1.53422	0.093661
Genes with FDR between 0.10 and 0.20				
66	Cd5l	CD5 antigen-like	2.38007	0.11316
67	Hist1h4m	Histone cluster 1, H4m	33.33	0.114229
68	Pdzd2	PDZ domain containing 2	-0.725257	0.115581
69	Btbd3	BTB (POZ) domain containing 3	-0.70643	0.119155
70	Sorbs3	Sorbin and SH3 domain containing 3	-0.908928	0.120407
71	Myo1d	Myosin ID	-0.711134	0.120505
72	Tubd1	Tubulin, delta 1	33.33	0.124497
73	Ska1	Spindle and kinetochore associated complex subunit 1	33.33	0.124497
74	Fam65a	Family with sequence similarity 65, member A	-1.0518	0.124918
75	Dnahc1	Dynein, axonemal, heavy chain 1	-1.39517	0.127394
76	mt-Nd6	NADH dehydrogenase 6, mitochondrial	-0.805532	0.127994
77	Pom121	Nuclear pore membrane protein 121	33.33	0.127994
78	Bmpr2	Bone morphogenetic protein receptor, type II (serine/threonine kinase)	-0.708527	0.129371
79	Hist1h1a	Histone cluster 1, H1a	1.21029	0.129371
80	Ptpng	Protein tyrosine phosphatase, receptor type, G	-0.688689	0.129504
81	Eif2c2	Argonaute RISC catalytic subunit 2	-0.799781	0.134313
82	Arhgap31	Rho GTPase activating protein 31	-0.642048	0.134313
83	Igfbp3	Insulin-like growth factor binding protein 3	0.800809	0.158183
84	D730039F16Rik	CutA divalent cation tolerance homolog-like	33.33	0.163078
85	Pkd1	Polycystic kidney disease 1 homolog	-0.696951	0.16421
86	Baz2a	Bromodomain adjacent to zinc finger domain, 2A	-0.812446	0.168588
87	Atp5k	ATP synthase, H+ transporting, mitochondrial F1FO complex, subunit E	1.02612	0.169495
88	Cd276	CD276 antigen	33.33	0.172103
89	Gm10277	Predicted gene 10277	-33.33	0.174175
90	Dock6	Dedicator of cytokinesis 6	-0.848506	0.175012
91	Parp4	Poly (ADP-ribose) polymerase family, member 4	-0.838119	0.175012
92	Plxn2	Plexin A2	-0.703027	0.175012
93	Sdf2l1	Stromal cell-derived factor 2-like 1	1.20602	0.178254
94	Nsun5	NOL1/NOP2/Sun domain family, member 5	33.33	0.178254
95	Crtc3	CREB regulated transcription coactivator 3	-1.0953	0.182596
96	Sh3pxd2a	SH3 and PX domains 2A	-0.669411	0.182596
97	Arid1a	AT rich interactive domain 1A (SWI-like)	-0.819629	0.182803
98	Crim1	Cysteine rich transmembrane BMP regulator 1 (chordin like)	-0.714825	0.185107
99	Smarca1	SWI/SNF related, matrix associated, actin dependent regulator of chromatin, subfamily a, member 1	33.33	0.18851
100	2900026A02Rik	RIKEN cDNA 2900026A02 gene	-1.04303	0.191335
101	Fmnl2	Formin-like 2	-0.82042	0.191335
102	Shank2	SH3/ankyrin domain gene 2	-1.65139	0.193573
103	Pabpc1	Poly(A) binding protein, cytoplasmic 1	-0.800107	0.193573
104	mt-Nd4	NADH dehydrogenase 4, mitochondrial	-0.676625	0.197356
105	Brd4	Bromodomain containing 4	-0.965817	0.198125
106	Hspg2	Perlecan (heparan sulfate proteoglycan 2)	-0.768995	0.198125
107	Reck	Reversion-inducing-cysteine-rich protein with kazal motifs	-0.854115	0.198715

Supplementary Table S2. Biological functions and differentially expressed genes found with significant changes after RNAseq in the lung of *UBC-CreERT2; Igf1r^{fl/fl}* mutant mice (FDR < 0.1).

Biological functions	Up-regulated genes	Down-regulated genes
<i>Development and growth</i>	<i>Saa3, Mki67, Kif11, Fancf, Ppp1r3c, Rps7</i>	<i>Epas1, Npnt, Pcdh1, Lox, Tenc1, Zbtb16, Zfhx3, Notch3, Foxo1, Apol11b, Syngap1, Crebbp, Prprb, Luc7l2, Nav2, Prrc2c, Ep300, Abi3bp, Tgfr3, Efnb2</i>
<i>Transcriptional regulation</i>	<i>Hist1h1d, Hist1h2bb, Ppp1r3c, Rps7</i>	<i>Srrm2, Nr1d2, Epas1, Zbtb34, Med13l, Zbtb16, Zfp518b, Zfhx3, Notch3, Foxo1, Crebbp, Hr, Tet3, Luc7l2, Mxip, Polr2a, Ep300, Hnrnpul2</i>
<i>Epigenetics</i>	<i>Top2a, Hist1h1d, Hist1h2bb, Fancf</i>	<i>Mll2, Foxo1, Rab6b, Crebbp, Tet3, Polr2a, Ep300</i>
<i>Inflammation and Immune response</i>	<i>Saa3, Spon2, Lyz1, Marco</i>	<i>Nr1d2, Slco2a1, Muc5b, Foxo1, Trim25, Tgfr3</i>
<i>Protumoral activity</i>	<i>Tp2a, Mki67</i>	<i>Epas1, Mll2, Atp2a3, Notch3, Trim25, Prrc2c, Abi3bp, Efnb2</i>
<i>Hypoxia, redox and oxidative stress</i>	<i>Gpx8, Cyp1a1</i>	<i>Nr1d2, Epas1, mt-Nd5, Foxo1, Hr, mt-Cytb, Ep300, Tgfr3</i>
<i>Cell adhesion and migration</i>	<i>Spon2</i>	<i>Npnt, Pcdh1, Tenc1, Svep1, Nav2, Tgfr3, Efnb2</i>
<i>Tumor suppression</i>	-	<i>Zbtb16, Lox, Zfhx3, Notch3, Foxo1, Ep300, Tgfr3</i>
<i>Respiratory diseases</i>	<i>Saa3, Marco</i>	<i>Epas1, Pcdh1, Muc5b, Notch3</i>
<i>Vascular permeability and Hypertension</i>	<i>Spon2</i>	<i>Epas1, Lox, Foxo1, Ptprb</i>
<i>Insulin regulation and resistance</i>	<i>Saa3</i>	<i>Epas1, Mll2, Atp2a3, Foxo1</i>
<i>Metabolism</i>	<i>Ces1g, Ppp1r3c</i>	<i>Nr1d2, Foxo1, Gdgd3</i>
<i>Regulated by Igf action and signalling</i>	-	<i>Muc5b, Lox, Foxo1, Crebbp, Efnb2</i>
<i>Detoxification and damage resistance</i>	<i>Cyp1a1, Spon2, Ces1g</i>	<i>Epas1, Notch3</i>
<i>Cell transport</i>	-	<i>Atp2a3, Apol11b, Rab6b</i>
<i>Ciliary motility</i>	<i>Kif11</i>	<i>Hydin, Dnahe6</i>
<i>Other/Unknown</i>	<i>Gnptg, Ppp1r2-ps4, Ac147987.1</i>	<i>Cyyr1, Pcnx, Snhg11, C030017K20Rik, Syngap1</i>

Supplementary Table S3. Differential BALF cell counts represented as the percentage of each cell type to total cell counts in *Igf1r^{fl/fl}* and *UBC-CreERT2; Igf1r^{fl/fl}* mice.

Cell type	Condition	<i>Igf1r^{fl/fl}</i>	<i>CreERT2</i>
<i>Neutrophils</i>	SAL	0.833 ± 0.166	0.833 ± 0.396
	BLM	55.416 ± 1.535	17.250 ± 3.119 ***
<i>Macrophages</i>	SAL	97.583 ± 0.567	98.998 ± 0.192
	BLM	37.166 ± 2.558	73.250 ± 2.495 ***
<i>Lymphocytes</i>	SAL	1.583 ± 0.416	0.999 ± 0.360
	BLM	8.333 ± 0.990	9.500 ± 1.040


Data are expressed as mean ± SEM. *** p < 0.001, when comparing *Igf1r^{fl/fl}* vs. *UBC-CreERT2; Igf1r^{fl/fl}* on each condition. SAL, saline; BLM, bleomycin.

Supplementary Table S4. Primer sets used for qRT-PCR.

Gene	Accession No.	Forward primer (5'-3')	Reverse primer (5'-3')
<i>Adgre1</i>	NM_010130.4	ATACCCTCCAGCACATCCAG	CTCCCATCCTCCACATCAGT
<i>Aqp5</i>	NM_009701	GGTGGTCATGAATCGGTTTCAGC	GTCCTCCTCTGGCTCATATGTG
<i>Cd209a</i>	NM_133238.5	GAGATGACGGCTGGAATGAC	AGATGGTGGAGGGAGTTGG
<i>Csf1</i>	NM_007778.4	CGAGTCAACAGAGCAACCAA	TGCTTCCTGGGTCAAAAATC
<i>Cxcl1</i>	NM_008176.3	ATCCAGAGCTTGAAGGTGTTG	GTCTGTCTTCTTTCTCCGTTACTT
<i>Foxo1</i>	NM_019739.3	TTCTCTCGTCCCAACATCT	TGCTGTCCTGAAGTGTCTGC
<i>Gpx8</i>	NM_027127.2	ACATTCCCCATCTTCCACAA	ATTCCACCTTGGCTCCTTCT
<i>Hif1a</i>	NM_010431.2	TTGGAACGGTGGAAAAACTG	ACTTGGAGGGCTTGAGAAT
<i>Igf1</i>	NM_010512	CAGAAGCGATGGGAAAAT	GTGAAGGTGAGCAAGCAGAG
<i>Igf1r</i>	NM_010513	ATGGCTTCGTTATCCACGAC	AATGGCGGATCTTCACGTAG
<i>Igfbp3</i>	NM_008343.2	GCCCTCTGCCTTCTTGATTT	TCACTCGGTTATGGGTTTCC
<i>Igfbp5</i>	NM_010518.2	GATGAGACAGGAATCCGAACAAG	AATCCT TTGCGGTCACAGTTG
<i>Il1b</i>	NM_008361.3	GCAACTGTTCTGAACTCAACT	ATCTTTTGGGGTCCGTCAACT
<i>Il6</i>	NM_031168.1	ACGGCCTTCCCTACTTCACA	CATTCCACGATTTCCCAGA
<i>Il13</i>	NM_008355.3	GCCTCCCGATACCAAAAT	CTTCTCCTCAACCTCCTC
<i>Insr</i>	NM_010568.2	TCCTGAAGGAGCTGGAGGAGT	CTTTCGGGATGGCCTGG
<i>Ly6g</i>	NM_001310438.1	CCTGGTTTCAGTCTTCTGC	CACACACTACCCCAACTCA
<i>Marco</i>	NM_010766.2	TCCCTGTGATGGAGACCTTC	GTGAGCAGGATCAGGTGGAT
<i>Rn18s</i>	NR_003278.3	ATGCTCTTAGCTGAGTGTCCTCG	ATTCCTAGCTGCGGTATCCAGG
<i>Sftpc</i>	NM_011359	GAAGATGGCTCCAGAGAGCATC	GGACTCGGAACCAGTATCATGC
<i>Tnf</i>	NM_013693.3	GCCTCTTCTCATTCTGCTTG	CTGATGAGAGGGAGGCCATT



Attenuated airway hyperresponsiveness and mucus secretion in HDM-exposed Igf1r-deficient mice

S. Piñero-Hermida¹ | J. A. Gregory² | I. P. López¹ | R. Torrens¹ | C. Ruíz-Martínez³ | M. Adner² | J. G. Pichel¹ 

¹Lung Cancer and Respiratory Diseases Unit, Centro de Investigación Biomédica de la Rioja (CIBIR), Fundación Rioja Salud, Logroño, Spain

²Unit of Experimental Asthma and Allergy Research, Karolinska Institutet, Institute of Environmental Medicine (IMM), Stockholm, Sweden

³Pneumology Service, Hospital San Pedro, Logroño, Spain

Correspondence

José G. Pichel, Lung Cancer and Respiratory Diseases Unit, Oncology Area CIBIR (Centro de Investigación Biomédica de la Rioja), Fundación Rioja Salud, Logroño, Spain. Email: jgpichel@riojasalud.es

Funding information

Fundación Rioja Salud; ERDF (European Regional Development Fund) and the ESF (European Social Fund); Swedish Heart-Lung Foundation, Grant/Award Number: 20150525, 20130636; Konsul Th C Berghs research foundation; Karolinska Institutet; Centre for Allergy Research at Karolinska Institutet

Edited by: Hans-Uwe Simon

Abstract

Background: Asthma is a common chronic lung disease characterized by airflow obstruction, airway hyperresponsiveness (AHR), and airway inflammation. IGFs have been reported to play a role in asthma, but little is known about how the insulin-like growth factor 1 receptor (IGF1R) affects asthma pathobiology.

Methods: Female Igf1r-deficient and control mice were intranasally challenged with house dust mite (HDM) extract or PBS five days per week for four weeks. Lung function measurements, and bronchoalveolar lavage fluid (BALF), serum, and lungs were collected on day 28 for further cellular, histological, and molecular analysis.

Results: Following HDM exposure, the control mice responded with a marked AHR and airway inflammation. The Igf1r-deficient mice exhibited an increased expression of the IGF system and surfactant genes, which were decreased in a similar manner for control and Igf1r-deficient mice after HDM exposure. On the other hand, the Igf1r-deficient mice exhibited no AHR, and a selective decrease in blood and BALF eosinophils, lung Il13 levels, collagen, and smooth muscle, as well as a significant depletion of goblet cell metaplasia and mucus secretion markers after HDM exposure. The Igf1r-deficient mice displayed a distinctly thinner epithelial layer than control mice, but this was not altered by HDM.

Conclusions: Herein, we demonstrate by the first time that the Igf1r plays an important role in murine asthma, mediating both AHR and mucus secretion after HDM exposure. Thus, our study identifies IGF1R as a potential therapeutic target, not only for asthma but also for hypersecretory airway diseases.

KEYWORDS

airway hyperresponsiveness, allergy, asthma, house dust mite, Igf1r

1 | INTRODUCTION

Asthma is a chronic inflammatory disease of conducting airways characterized by airflow obstruction, bronchial hyperresponsiveness, and airway inflammation. It is widely considered that the airway epithelium is an essential controller of inflammatory, immune, and

regenerative responses in asthma. In response to allergen stimulation, the airway epithelium secretes fluids, antimicrobial proteins, and mucins which together with club cells represent a major part of the immunomodulatory barrier of the airway epithelium and orchestrate pulmonary innate immunity.^{1,2} Geographical variations notwithstanding, the majority of allergic asthmatic individuals are sensitive to house dust mite (HDM). HDM exhibits a complex mixture of molecules including proteases, allergen epitopes, and activators of

MA and JGP share senior authorship.

the innate immune system serving as adjuvants to disrupt intercellular tight junctions leading to cytokine, chemokine, and growth factor production and cellular influx, as well as airway remodeling and mucus hypersecretion.^{3–5}

The insulin-like growth factor 1 receptor (IGF1R) is a ubiquitously expressed membrane-bound tyrosine kinase receptor and a central member of the IGF system. This network comprises two major ligands (IGF1 and IGF2), different receptors and regulatory proteins, including IGF-binding proteins (IGFBPs), acting together to control multiple cellular functions such as growth, proliferation, differentiation, survival, adhesion, and migration.^{6,7} It has been reported that IGF1 is an important mediator of airway inflammation and remodeling in asthma and that IGFBP3 blocks the specific physiology of these pathological consequences.^{8–10} As the mechanisms of the IGF system in asthma are not defined, we aimed to study the implication of *Igf1r* in asthma. For this purpose, we subjected the *Igf1r* conditional mutant mice *UBC-CreERT2; Igf1r^{fl/fl} (CreERT2)*¹¹ to repeated HDM exposure. We demonstrate that *Igf1r* plays an important role in asthma, with implications in allergic inflammation, airway remodeling, mucus production, and AHR. As such, IGF1R may now be considered as a potential therapeutic target for asthma and other hypersecretory airway diseases.

2 | MATERIALS AND METHODS

2.1 | Ethical statement

All experiments and animal procedures conducted in Spain were carried out in accordance with the guidelines of the European Communities Council Directive (86/609/EEC) and were revised and approved by the CIBIR Bioethics Committee (ref. 03/12). All animal handling, including the experimentation conducted in Sweden, was carried out in accordance with ethical permit N152/15 approved by the Regional Committee of Animal Experimentation Ethics (Stockholm, Sweden).

2.2 | *Igf1r*-deficient mice and HDM sensitization protocol

UBC-CreERT2; Igf1r^{fl/fl} (CreERT2) mice were used to induce a postnatal *Igf1r* conditional gene deletion using *Igf1r^{fl/fl}* mice as experimental

controls, as previously described.¹¹ This transgenic line was in a C57BL/6-enriched (at least six generation backcrosses to C57BL/6 strain) mixed genetic background. Eight- to 10-week-old female mice were challenged by intranasal administration with 40 μ g of HDM extract (Greer Laboratories Inc, Lenoir, NC, USA) in 20 μ L of PBS (2 mg/mL) or equal volume of PBS under light isoflurane anesthesia, five days a week for four weeks (Figure 1). Females were used due to their reported higher susceptibility to allergic airway inflammation.¹² In addition, female mice present a less aggressive behavior, reducing casualties during transport between institutions and long experimental protocols implying intensive animal handling. All animals were bred and maintained under specific pathogen-free conditions at CIBIR and Karolinska Institutet animal facilities.

2.3 | *In vivo* measurement of pulmonary mechanics

Of 24 h after the final HDM exposure (day 28), mice were deeply anesthetized with a combination of Hypnorm (2.5 μ L/g) and midazolam (12.5 μ g/g), and lung function following exposure to increasing concentrations of aerosolized methacholine was evaluated using the flexiVent system (Scireq, Montreal, QC, Canada). Newtonian resistance (*Rn*), tissue damping (*G*), and tissue elastance (*H*) were determined by assuming a constant-phase model.

2.4 | Tissue collection and preparation

Bronchoalveolar lavage was performed immediately after pulmonary mechanics measurements. Lungs were lavaged twice with 0.8 mL cold PBS. Blood was collected by cardiac puncture, and serum was obtained by centrifugation and stored at -20°C until further usage. Following lung dissection, the left lung was removed and fixed in 4% formaldehyde and subsequently embedded in paraffin for histopathology and immunohistochemistry. Right lobes were separated and snap-frozen in liquid nitrogen for quantitative real-time PCR (qRT-PCR), Western blot (WB), and ELISA analyses.

2.5 | Quantification of BALF

Total cell number was counted and expressed as cells/mL BALF, and differential cell counts were performed on May-Grünwald/Giemsa (Sigma-Aldrich, St. Louis, MO, USA)-stained cytopspins, counting a

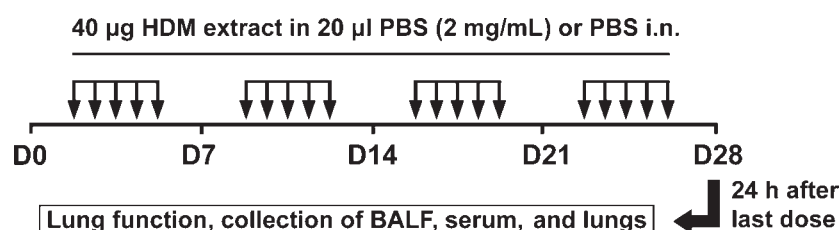


FIGURE 1 Protocol for intranasal exposure to house dust mite. Eight- to 10-week-old female *UBC-CreERT2; Igf1r^{fl/fl} (CreERT2)* mice and their controls (*Igf1r^{fl/fl}*)¹¹ were challenged by intranasal administration of 40 μ g of house dust mite (HDM) extract in 20 μ L of phosphate buffer saline (PBS) (2 mg/mL) or equal volume of PBS under inhaled isoflurane anesthesia, five days a week during four weeks. Lung function assessment and BALF, serum, and lungs were collected 24 h after the last exposure on day (D) 28

minimum of 300 cells per slide in a blinded fashion. Cells were distinguished into macrophages, lymphocytes, neutrophils, and eosinophils by standard morphology.

2.6 | Histopathological analysis and immunostaining

Paraffin-embedded tissues were cut into 3- μ m sections for histopathological evaluation or immunohistochemistry. Hematoxylin and eosin (H&E) staining was performed for quantification of inflamed lung areas and airway thickness. Periodic acid-Schiff (PAS) and Masson's trichrome staining protocols served to assess airway epithelial goblet cell abundance and collagen deposition, respectively. Immunostaining was performed using the following antibodies: α -SMA (Clone 1A4 1:100, Sigma-Aldrich, St. Louis, MO, USA), Scgb1a1 (Clone T18 1:400, Santa Cruz Biotech. Inc., Dallas, TX, USA), GluTub (Clone TU-20 1:300, EMD Millipore, Billerica, MA, USA), and Muc5ac (Clone 45M1 1:50, Thermo Fisher Scientific, Waltham, MA, USA). Histological quantifications were performed using six animals per condition evaluating four airways per animal. Quantification of PAS-, Scgb1a1-, GluTub-, and Muc5ac-positive cells was expressed as the number of positive cells per epithelium length (mm), and both the smooth muscle and airway thickness were assessed by means of three different measurements per airway. Fiji open-source image processing software package (<http://fiji.sc>) was used to quantify the percentage of collagen area as well as for epithelium length measurements.

2.7 | RNA isolation, reverse transcription, and qRT-PCR

Inferior lung lobes were homogenized in TRIzol (Invitrogen, Carlsbad, CA, USA), and total RNA was isolated using an RNeasy Mini Kit (Qiagen, Hilden, Germany) and reverse-transcribed to cDNA using SuperScript II First-Strand Synthesis System (Invitrogen) as per the manufacturer's specifications. cDNA samples were then amplified by qRT-PCR in triplicate reactions for each primer pair assayed (Table S1) on a 7300 Real-Time PCR Instrument (Applied Biosystems, Foster City, CA, USA), using SYBR Premix Ex Taq (Takara Bio Inc., Kusatsu, Japan). Results were normalized using 18S rRNA gene as endogenous control.

2.8 | ELISAS

Serum total IgE levels were assessed with an IgE mouse ELISA kit (Abcam, Cambridge, UK), and IL13 levels were determined in homogenized tissue lysates using the middle lung lobes with a mouse IL-13 Duoset ELISA Kit (R&D Systems, Minneapolis, MN, USA), according to the manufacturer's guidelines.

2.9 | Western blot analysis

Superior lung lobes were solubilized in a 10 mM Tris/HCl (pH 7.4) buffer containing 0.1% sodium dodecyl sulfate, a protease inhibitor

mixture, and DNase (Promega, Fitchburg, WI, USA). Samples were separated on NuPAGE Novex 4-12% Bis-Tris Gel (Invitrogen) and transferred to a polyvinylidene difluoride membrane (EMD Millipore). Membranes were incubated with primary antibodies for Igf1r (#3027 Cell Signaling Inc., Danvers, MA, USA) and beta-actin (ab6276 Abcam, Cambridge, UK) at 1:1000 and 1:30000 dilutions, respectively, and then incubated with horseradish peroxidase-conjugated anti-rabbit or anti-mouse antibodies (DAKO, Agilent technologies, Santa Clara, CA, USA) for Igf1r and beta-actin, respectively, at a 3:10 dilution. Signal was detected using ECL Western Blot Substrate (Thermo Fisher Scientific) and Hyperfilm ECL (GE Healthcare, Little Chalfont, UK). Films were scanned, and signals in the linear range were quantified using Fiji and normalized to beta-actin levels.

2.10 | Statistics

Statistical analyses were performed using SPSS Statistics Software v21 for Windows (IBM, Armonk, NY, USA). Differences between experimental groups were evaluated for significance using Mann-Whitney *U* and Dunn-Sidak multiple comparison tests. Results are shown as mean values \pm standard error of the mean (SEM). For all analysis, a *P* value $<.05$ was considered statistically significant.

3 | RESULTS

3.1 | Depletion of Igf1r in *CreERT2* mutant mice and changes in expression of IGF system genes after the HDM challenge

To verify the Igf1r depletion and investigate the influence of allergic inflammation on the IGF system, qRT-PCR and WB analyses were performed on lung extracts of *CreERT2* mutant mice and their control littermates (*Igf1^{fl/fl}*)¹¹ after four weeks of repeated exposure to PBS or HDM (Figure 1). mRNA expression levels demonstrated an efficient depletion of Igf1r in *CreERT2* PBS-treated mice (90%) and without changes between HDM-treated groups. In addition, HDM treatment decreased Igf1r mRNA levels in *Igf1^{fl/fl}* mice (81%) (Figure 2A). WB analysis corroborated these results, showing a significant reduction in Igf1r protein levels in *CreERT2* PBS-treated mice (87%), and no differences between HDM-treated groups (Figure 2B). Igf1r deficiency caused a significant increase in mRNA expression of *Igf1* and *Insr* expression levels in PBS-treated mice, but not for *Igf-bp3* and *Igf-bp5*. Even though HDM treatment significantly reduced the expression levels of *Insr*, *Igf-bp3*, and *Igf-bp5* in both genotypes without affecting *Igf1*, Igf1r depletion led to a significant increase in the expression of all IGF system genes measured (Figure 2C).

3.2 | Igf1r deficiency improves lung function and counteracts allergic airway inflammation and airway remodeling in HDM-treated mice

To assess whether Igf1r deficiency has an effect on lung mechanics, we measured airway responsiveness to inhaled methacholine

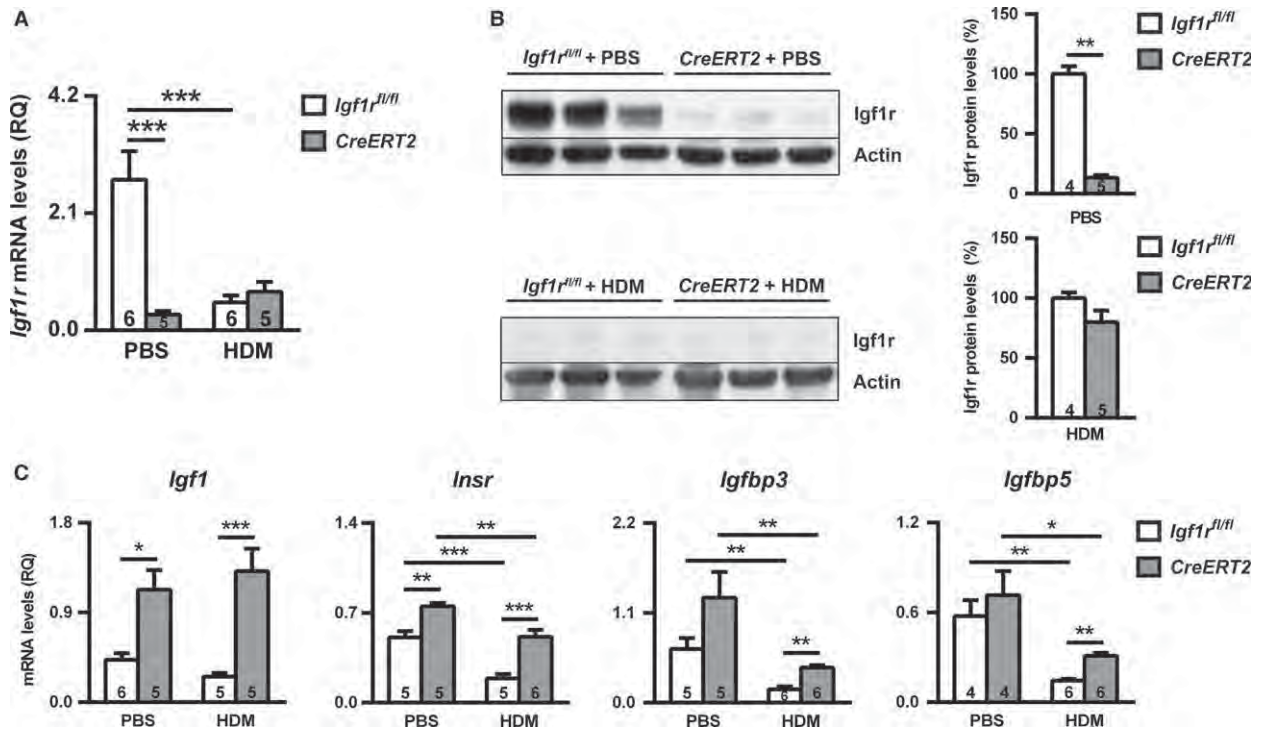


FIGURE 2 Efficient depletion of Igf1r and changes in expression of the IGF system genes in lungs of *CreERT2* mice after HDM-induced allergic airway inflammation. (A) *Igf1r* mRNA expression levels normalized to 18S expression; (B) representative Western blots for Igf1r and graphical representations of densitometric measurements of band intensities normalized to beta-actin levels; and (C) lung tissue mRNA expression of IGF system-related genes in PBS- and HDM-exposed *Igf1r^{fl/fl}* and *CreERT2* mice. Numbers within graphic bars indicate the number of mice analyzed, and data are expressed as mean ± SEM. **P*<.05; ***P*<.01; ****P*<.001 (Mann-Whitney *U* and Dunn-Sidak multiple comparison tests). HDM, house dust mite; PBS, phosphate buffered saline

(Figure 3). Compared with PBS, HDM-challenged *Igf1r^{fl/fl}* mice displayed AHR with an increased response for the proximal, *Rn*, and distal parameters, *G* and *H*. The AHR seen in both the proximal and distal parts of the lung was, however, not present in *CreERT2* HDM-treated mice, which showed similar functional responses as PBS-treated mice. These findings show that *Igf1r* deficiency improves mouse lung function at both central and peripheral levels after HDM-mediated asthma.

Although we did not find differences counting circulating macrophages, lymphocytes, and neutrophils, HDM-treated *Igf1r^{fl/fl}* mice showed increased eosinophil numbers in blood (4-fold), when compared to PBS-treated. The *CreERT2* HDM-challenged mice did not show such an increase when compared to PBS-treated (Figure 4A). Allergen-treated *Igf1r^{fl/fl}* mice demonstrated a significant increase in total cells in BALF (8-fold) compared to PBS-treated control mice. HDM-challenged *CreERT2* mice also displayed an increase in total

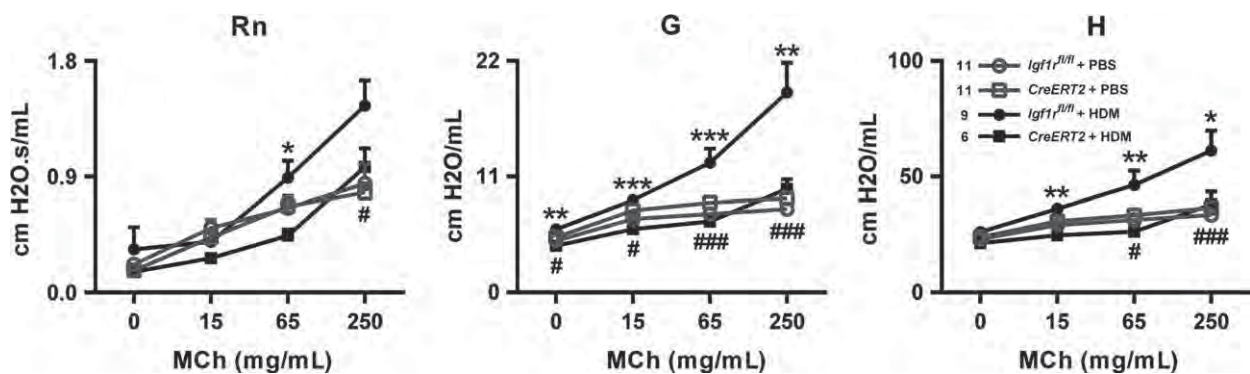


FIGURE 3 *Igf1r* deficiency decreases AHR after house dust mite challenge. Resistance of conducting airways (*Rn*), tissue damping (*G*), and tissue elastance (*H*) to MCh evaluated with the flexiVent system. Numbers in graphic legends indicate the number of mice analyzed, and data are expressed as mean ± SEM. * *Igf1r^{fl/fl}* + HDM vs *CreERT2* + HDM; # *Igf1r^{fl/fl}* + HDM vs *Igf1r^{fl/fl}* + PBS. One symbol, *P*<.05; two symbols, *P*<.01; three symbols, *P*<.001 (Dunn-Sidak multiple comparison test). MCh, methacholine; HDM, house dust mite; PBS, phosphate buffered saline

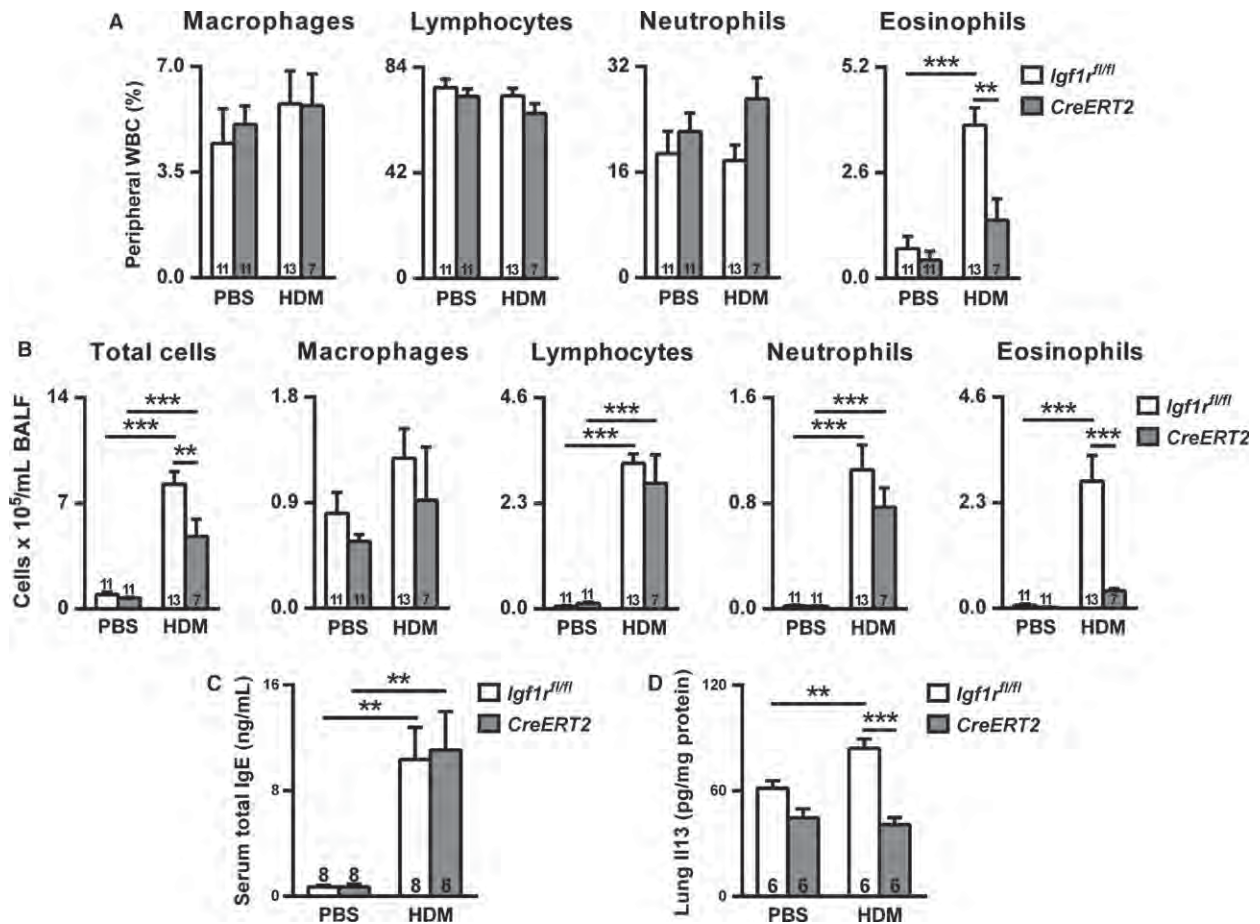


FIGURE 4 *Igf1r* depletion attenuates the increase in blood and BALF eosinophils, and Il13 levels in lung homogenate after exposure to house dust mite. (A) Peripheral white blood cell counts on blood smear preparations; (B) total and differential cell counts performed on cytospin preparations of BALF; and (C) serum total IgE and (D) Il13 levels in lung homogenate quantified by ELISA. Numbers within graphic bars indicate the number of mice analyzed, and data are expressed as mean \pm SEM. ** $P < .01$; *** $P < .001$ (Dunn-Sidak multiple comparison test). HDM, house dust mite; PBS, phosphate buffered saline

cell numbers (6-fold), although significantly lower than that observed in *Igf1r^{fl/fl}* mice (Figure 4B). Differential cell counts in BALF from *Igf1r^{fl/fl}* and *CreERT2* mice exhibited a marked increase in lymphocyte (49- and 25-fold, respectively) and neutrophil (45- and 40-fold, respectively) numbers in HDM-challenged mice, without significant differences between genotypes. The eosinophils were also increased after HDM in *Igf1r^{fl/fl}* mice (40-fold); however, this phenomenon was not observed in *CreERT2* mice, which roughly showed basal eosinophil counts (Figure 4B).

We found that in HDM-exposed mice, the total IgE concentration in serum was highly increased in both genotypes after HDM exposure when compared to PBS-exposed mice (>90%) (Figure 4C). In addition, we found that the level of Il13 in lung homogenates was significantly higher in HDM-treated *Igf1r^{fl/fl}* mice compared to PBS-exposed mice (27%), whereas HDM-challenged *CreERT2* lungs displayed normal values (Figure 4D).

In an attempt to determine how *Igf1r* deficiency protects against HDM-mediated allergic airway inflammation at the histopathological level, we measured several asthma-related features in airways: inflamed lung area, number of PAS⁺ cells, collagen staining, and

smooth muscle thickness. Assessment of all of these features revealed increased values in HDM-challenged lungs of both genotypes compared to their PBS-treated controls. Measurements that were markedly increased in case of *Igf1r^{fl/fl}* mice displayed a milder increase in allergen-treated *CreERT2* lungs (Figure 5).

3.3 | *Igf1r* depletion attenuates airway hyperreactivity and enhances surfactant expression

As we have previously reported that *Igf1r* deletion alters airway epithelium morphology and cellular composition,^{11,13} we next measured airway wall thickness in the four experimental groups. Accordingly, *CreERT2* mice showed a significantly thinner airway after both treatments. However, whereas in *Igf1r^{fl/fl}* mice, HDM challenge induced airway thickening (19%), HDM-exposed *CreERT2* mutant lungs did not show such thickness (Figure 6A). To validate the increase in PAS⁺ cell numbers we observed, mRNA levels of *Muc5ac* and the master regulator *Spdef* were measured. As expected, HDM-challenged *Igf1r^{fl/fl}* lungs showed significantly increased *Muc5ac* levels (16-fold) with respect to PBS-exposed controls. HDM-

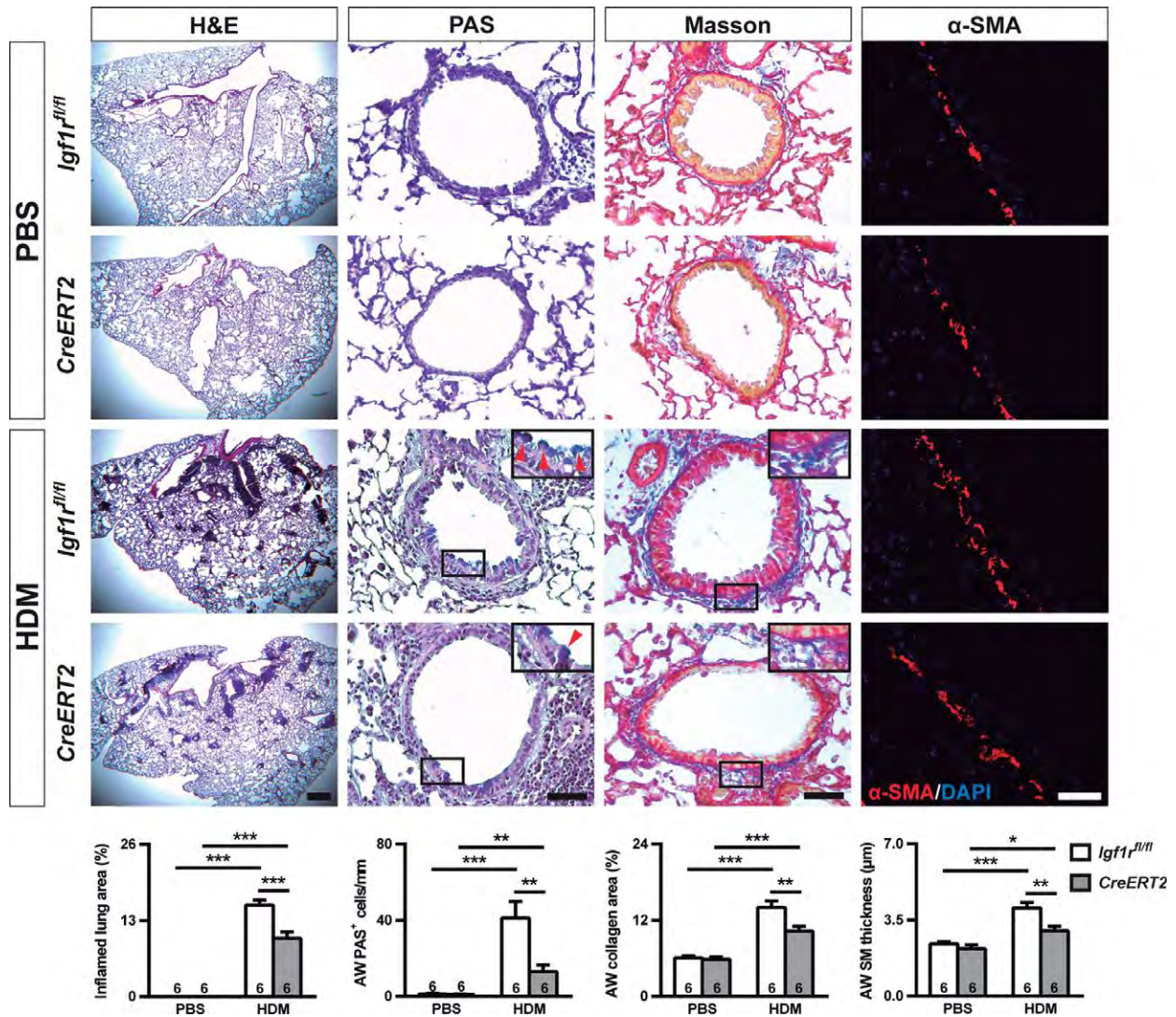


FIGURE 5 Reduced allergic airway inflammation, goblet cell hyperplasia, collagen content, and smooth muscle thickness in *Igf1r*-deficient mice after HDM exposure. Representative images of proximal airways showing inflamed lung areas (left) (scale bar: 0.5 mm); mucus-producing cells per epithelium length (red arrowheads in insets) (center left) and airway collagen content (center right) (scale bars: 50 μm); and smooth muscle thickness (right) (scale bar: 20 μm). Bottom graphs represent quantification of the abovementioned parameters. Numbers within graphic bars indicate the number of mice analyzed, and data are expressed as mean ± SEM. **P*<.05; ***P*<.01; ****P*<.001 (Dunn-Sidak multiple comparison test). H&E, hematoxylin and eosin; PAS, periodic acid-Schiff; α-SMA, alpha-smooth muscle actin; AW, airway; HDM, house dust mite; PBS, phosphate buffered saline; SM, smooth muscle

challenged *CreERT2* mice also demonstrated increased *Muc5ac* levels with respect to PBS-treated mice; however, this increase was significantly lower than that observed in *Igf1r^{fl/fl}* mice (7-fold) (Figure 6B, left). Correspondingly, mRNA levels of the master regulator *Spdef* were also reduced in HDM-challenged *CreERT2* mice (42%) (Figure 6B, right). Immunohistochemical analyses of the airway epithelium cellular composition in HDM-exposed lungs revealed a significant decrease in *Scg1a1⁺* club cells (35%) and a concomitant increase in *GluTub⁺* cells in *CreERT2* mice (17%). Furthermore, the proportion in *Muc5ac⁺* cells was also diminished in *Igf1r*-deficient mice (50%) (Figure 6C).

Finally, to elucidate how *Igf1r* depletion improves peripheral lung function, we evaluated mRNA expression levels of the surfactant markers *Sftpa1*, *Sftpb*, *Sftpc*, and *Sftpd* (Figure 6D). *Igf1r* deficiency

caused a generalized increase in all markers measured after both PBS and HDM treatments, although *Sftpc* changes were not significant in PBS-exposed mice. In addition, whereas *Sftpa1* and *Sftpd* levels showed similar changes in expression levels in PBS- and HDM-challenged mice, *Sftpc* levels were significantly reduced in HDM-challenged mice of both genotypes, and *Sftpb* was only found to be reduced in *Igf1r^{fl/fl}* animals.

4 | DISCUSSION

The present study shows that the marked AHR and airway inflammation induced by HDM in control mice were absent or attenuated in the *Igf1r*-deficient mice. This is the first study to report that

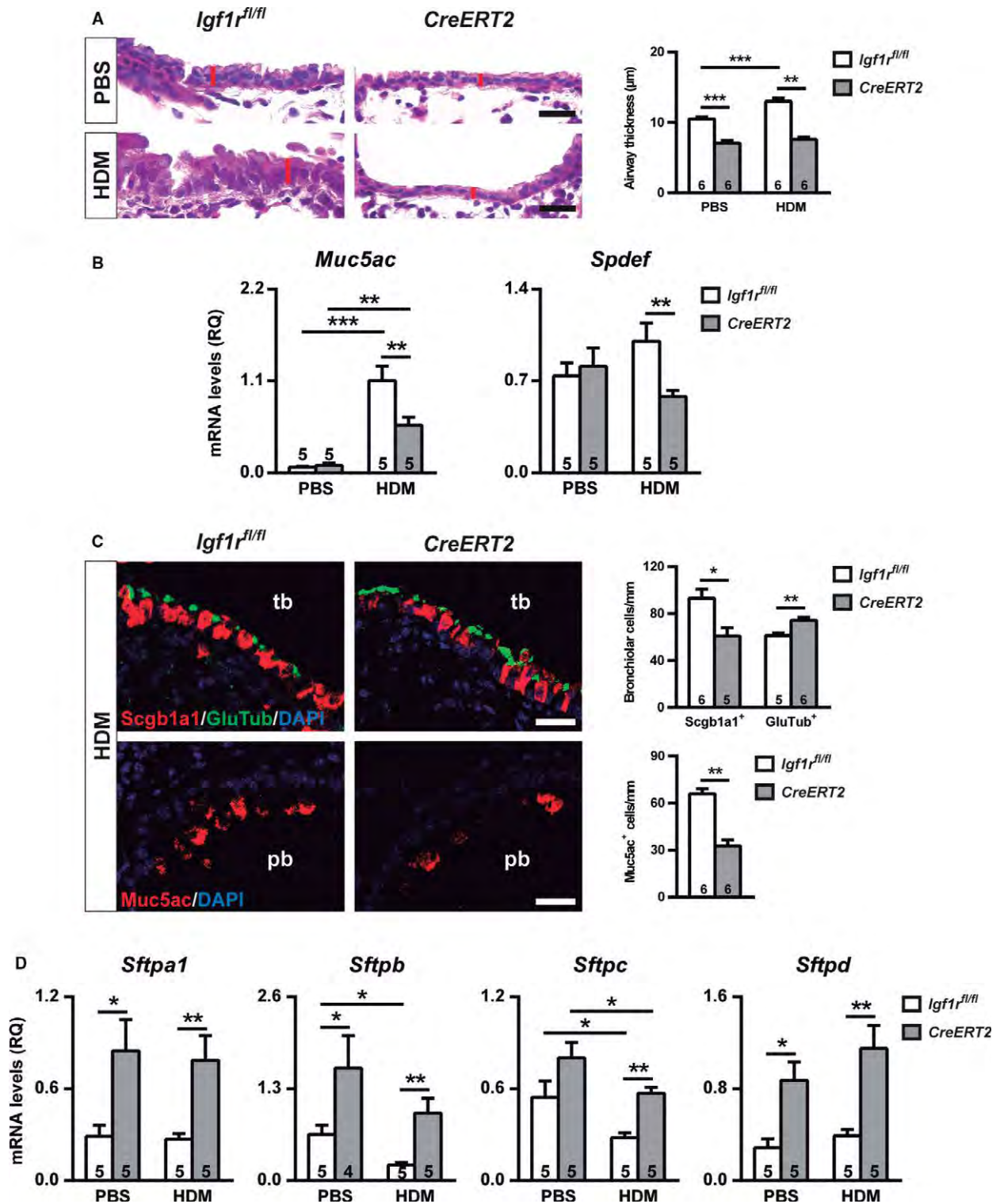


FIGURE 6 Attenuation of airway hyperreactivity and mucus secretion and increased expression of surfactant markers in HDM-exposed *Igf1r*-deficient mice. (A) Proximal airway wall thickness; (B) lung mRNA expression of the mucus secretion markers *Muc5ac* and *Spdef* normalized to 18S expression; (C) proportion of club (in red) and ciliated (in green) cells and quantification of *Muc5ac* (in red)-positive cells in terminal and proximal bronchioles, respectively; and (D) changes in mRNA expression of surfactant (*Sftp*) markers *a1*, *b*, *c*, and *d* in *CreERT2* mice. Scale bars: 20 μm . Numbers within graphic bars indicate the number of mice analyzed, and data are expressed as mean \pm SEM. * $P < .05$; ** $P < .01$; *** $P < .001$ (Mann-Whitney U test and Dunn-Sidak multiple comparison test). HDM, house dust mite; PBS, phosphate buffered saline; tb, terminal bronchioles; pb, proximal bronchioles; Scgb1a1, secretoglobulin 1A1; GluTub, Glu tubulin; Muc5ac, mucin 5ac

Igf1r can be important for both AHR and airway inflammation in asthma.

Igf1r-deficient mice are bred from a C57BL/6 genetic background, which usually do not display strong airway inflammation or AHR in response to allergen challenge.^{14,15} To overcome this constraint, a specific protocol using repetitive exposures to HDM during four weeks was used to induce AHR. HDM exposure decreased the Igf1r levels in *Igf1r^{fl/fl}* mice similarly to those observed in the *CreERT2* animals. Although the mechanism behind this unexpected reduction is unknown, it could be a long-term effect occurring after tissue remodeling has been established. We also observed an increased expression of additional IGF system genes in *CreERT2* mutant lungs. The upregulation of *Igf1*, *Insr*, *Igfbp3*, and *Igfbp5* in PBS-exposed mice is possibly a compensatory effect in response to Igf1r deficiency, as we have previously reported in lungs from mice with compromised Igf1r signaling in the respiratory epithelium.¹³ Accordingly, it has been previously reported that exogenous *Igfbp3* and *Igfbp5* administration blocks physiological consequences of asthma in OVA-challenged mice and enhances epithelial cell adhesion to maintain the epithelial-mesenchymal boundary.^{8,9,16} Thus, *Igfbp3* and *Igfbp5* could mediate protective properties against HDM-mediated allergic inflammation.

A marked increase in AHR was found in both the proximal and distal parts of *Igf1r^{fl/fl}* mice after HDM exposure, as has been reported in mice subjected to a similar allergenic challenge.^{17,18} The repeated exposure of mice to HDM also increased total cell number in BALF as well as airway remodeling parameters such as cell hyperplasia, collagen deposition, smooth muscle cells, and mucus production, all findings previously reported.⁵ Furthermore, increases in airway thickness, serum total IgE, and lung Il13 levels similar to those observed herein have also been reported elsewhere.^{17,19,20} All of these features were reflected in *Igf1r^{fl/fl}* HDM-challenged lungs and support the effectiveness of our HDM sensitization protocol.

Interestingly, the HDM-induced effects for several of our measured parameters were decreased in the *CreERT2* mice. In particular, AHR was not found in the Igf1r-deficient mice. AHR is considered to be dependent on several features, such as remodeling and mucus production.^{21,22} These features were all found decreased, albeit not totally normalized in the *CreERT2* Igf1r-deficient mice. On this basis, it was recently reported that Igf1r plays an important role in the initiation of the inflammatory process²³ and that Igf1r signaling promotes activation of the NF- κ B pathway, a critical regulator of immune responses orchestrating HDM-induced airway inflammation, AHR, and fibrotic remodeling.^{24,25} In a lung fibrosis model, it was reported that Igf1r blockade decreased α -SMA protein expression and collagen content in bleomycin-injured mice.^{26,27} Blockade of Il13 activity after chronic HDM sensitization has been shown to reduce eosinophilia in BALF, peribronchial collagen, and goblet cell hyperplasia, findings that are in accordance with our observation that Il13 levels were not altered by HDM exposure in lungs from *CreERT2* mutant mice.²⁰

Whereas HDM caused a clear increase in eosinophils in blood and BALF of *Igf1r^{fl/fl}* mice, their levels remained close to basal in

CreERT2 Igf1r-deficient mice. It has been previously shown that Igf1r deregulation decreases the number of peripheral white blood cells, thus providing evidence implicating Igf1r in promoting bone marrow myeloid cell generation.^{28,29} The reduced eosinophil counts observed in blood and BALF from *CreERT2* mutant mice led us to speculate that Igf1r could have an important role in proliferation and/or differentiation of myeloid progenitors and their recruitment to the lung, especially with respect to eosinophils. Further studies are needed to confirm this hypothesis.

The reduced proportion of club cells found in distal airways of *CreERT2* mutant lungs is in accordance with recent data published by our group where a lung epithelial-specific Igf1r deficiency in mice caused delayed differentiation of club cells in terminal bronchioles.¹³ In response to allergen stimulation, club cells differentiate into goblet cells through transcriptional activation of the master regulator *Spdef*. Subsequently, the increase in *Muc5ac* expression through transcriptional activation of *Spdef* in goblet cells contributes to both goblet cell hyperplasia and mucus hyperproduction.^{30,31} In this context, delayed club cell differentiation in *CreERT2* airways may result in decreased transdifferentiation into goblet cells, with a concomitant reduction in goblet cell hyperplasia and mucus production. In accordance with depleted *Spdef* and *Muc5ac* expression in *CreERT2* mice, *Spdef*-deficient mice showed an improved lung function as well as a reduced number of BALF eosinophils, and targeted silencing of SPDEF in airway epithelial cells in vitro reduces MUC5AC expression.^{32,33} Furthermore, *Muc5ac* deficiency in mice abolishes AHR and inflammation.^{22,34} As such, a reduction in mucus production may contribute to the improved lung function in *CreERT2* mutant mice observed in our study. It has also been demonstrated that Il13 stimulation of human airway epithelial cells induced MUC5AC expression.³⁵ Together, these findings support a role for Igf1r in lung airway epithelium transdifferentiation to the mucosecretory cell fate during chronic allergic airway inflammation.

Pulmonary surfactant proteins are essential for lung function and homeostasis after birth.³⁶ While surfactant proteins B and C showed a critical role in the preservation of lung function, the immunomodulatory proteins A and D were reported to play an important role during allergic airway inflammation.³⁷⁻⁴⁰ Here, we show that Igf1r deficiency causes a general increase in surfactant expression basally and after the HDM challenge. On this basis, we conclude that increased expression of surfactant markers improves lung function of *CreERT2* mice and also is important for maintenance of homeostasis in the lung.

Although little is known about the role of IGFs in patients with asthma, previous reports in humans support data found in mice. Thus, corticosteroid treatment in asthma can reduce the lamina reticular thickness by reduction of IGF1 expression with consequent inhibition of the airway infiltration by inflammatory cells and therefore help to prevent remodeling of the airways.⁴¹ Moreover, IGFBP3 secreted by IGF1-stimulated airway epithelial cells during allergic inflammation was suggested to be involved in allergic airway remodeling.⁴² Considering that there are no effective therapies available to prevent asthma, targeting IGF signaling can be an attractive

therapeutic strategy. Actually, treatment to inhibit the IGF1 action in cancer has been performed but did not show a uniform benefit among patients.⁴³ Conversely, targeting IGF1R, which is currently being exhaustively evaluated in clinical trials for oncologic patients,⁴⁴ could be emphasized as an approach for the treatment of asthma.

In conclusion, our results demonstrate that Igf1r plays a key role in murine asthma with important implications regarding allergic inflammation, airway remodeling, mucus production, and ultimately in AHR. Based on this putative prophylactic effect of Igf1r deficiency in counteracting asthma, it will be interesting to develop a therapeutic model to test whether targeting Igf1r signaling resolves established allergic airway inflammation. At present, there are no effective therapies to treat mucus hyperproduction associated with goblet cell hyperplasia. Thus, our study identifies IGF1R as a potential target for therapeutic development, not only for the treatment of asthma but also for hypersecretory airway diseases.

ACKNOWLEDGMENTS

We are grateful to Drs. J. Brüning (University of Cologne, Germany) and E. Brown (UPENN School of Medicine, PA) for providing *Igf1r^{fl/fl}* and *UBC-CreERT2* mouse lines, respectively. We also thank Lydia A. Ertivi (CIBIR, Spain) for helping with Western blots. S.P.-H. thanks the Sistema Riojano de Innovación (Gobierno de La Rioja, Spain) for a PhD grant. S.P.-H., J.A.G., I.P.L., M. A., and J.G.P. are part of the European Cooperation in Science and Technology COST Action BM1201, Developmental Origins of Chronic Lung Disease. This work was supported by grants from Fundación Rioja Salud (Gobierno de La Rioja, Spain) and cofunded by the ERDF (European Regional Development Fund) and the ESF (European Social Fund) to J.G.P., and the Swedish Heart-Lung Foundation (20150525, 20130636), the Konsul Th C Berghs research foundation, the Karolinska Institutet, and the Centre for Allergy Research at Karolinska Institutet to M.A.

CONFLICT OF INTEREST

The authors declare no conflict of interest.

AUTHOR CONTRIBUTION

S.P.-H., J.A.G., M.A., and J.G.P. proposed and conceived the project and designed the experiments. S.P.-H., J.A.G., I.P.L., R.T., M.A., and J.G.P. performed the experiments. S.P.-H., J.A.G., I.P.L., C.R.-M., M.A., and J.G.P. analyzed the data, interpreted the experiments, and contributed reagents, materials, and analytical tools. S.P.-H. and J.G.P. drafted and wrote the manuscript. All authors read, revised, and approved the manuscript before submission.

REFERENCES

- Lambrecht BN, Hammad H. The airway epithelium in asthma. *Nat Med*. 2012;18:684-692.
- Whitsett JA, Alenghat T. Respiratory epithelial cells orchestrate pulmonary innate immunity. *Nat Immunol*. 2015;16:27-35.
- Buday T, Plevkova J. House dust mite allergy models—reliability for research of airway defensive mechanisms. *Open J Mol Integrative Physiol*. 2014;4:27-35.
- Gregory LG, Lloyd CM. Orchestrating house dust mite-associated allergy in the lung. *Trends Immunol*. 2011;32:402-411.
- Fattouh R, Al-Garawi A, Fattouh M, et al. Eosinophils are dispensable for allergic remodeling and immunity in a model of house dust mite-induced airway disease. *Am J Respir Crit Care Med*. 2011;183:179-188.
- Girnita L, Worrall C, Takahashi S, Seregard S, Girnita A. Something old, something new and something borrowed: emerging paradigm of insulin-like growth factor type 1 receptor (IGF-1R) signaling regulation. *Cell Mol Life Sci*. 2014;71:2403-2427.
- Annunziata M, Granata R, Ghigo E. The IGF system. *Acta Diabetol*. 2011;48:1-9.
- Kim SR, Lee KS, Lee KB, Lee YC. Recombinant IGFBP-3 inhibits allergic lung inflammation, VEGF production, and vascular leak in a mouse model of asthma. *Allergy*. 2012;67:869-877.
- Lee YC, Jogie-Brahim S, Lee DY, et al. Insulin-like growth factor-binding protein-3 (IGFBP-3) blocks the effects of asthma by negatively regulating NF-kappaB signaling through IGFBP-3R-mediated activation of caspases. *J Biol Chem*. 2011;286:17898-17909.
- Yamashita N, Tashimo H, Ishida H, et al. Role of insulin-like growth factor-I in allergen-induced airway inflammation and remodeling. *Cell Immunol*. 2005;235:85-91.
- Lopez IP, Rodriguez-de la Rosa L, Pais RS, et al. Differential organ phenotypes after postnatal Igf1r gene conditional deletion induced by tamoxifen in UBC-CreERT2; Igf1r fl/fl double transgenic mice. *Transgenic Res*. 2015;24:279-294.
- Melgert BN, Postma DS, Kuipers I, et al. Female mice are more susceptible to the development of allergic airway inflammation than male mice. *Clin Exp Allergy*. 2005;35:1496-1503.
- López IP, Piñeiro-Hermida S, Pais RS, Torrens R, Hoefflich A, Pichel JG. Involvement of Igf1r in bronchiolar epithelial regeneration: role during repair kinetics after selective club cell ablation. *PLoS One*. 2016;11:e0166388.
- Saffholm J, Lovdahl C, Swedin L, et al. Inflammation-induced airway smooth muscle responsiveness is strain dependent in mice. *Pulm Pharmacol Ther*. 2011;24:361-366.
- Swedin L, Ellis R, Kemi C, et al. Comparison of aerosol and intranasal challenge in a mouse model of allergic airway inflammation and hyperresponsiveness. *Int Arch Allergy Immunol*. 2010;153:249-258.
- Vijayan A, Guha D, Ameer F, et al. IGFBP-5 enhances epithelial cell adhesion and protects epithelial cells from TGFbeta1-induced mesenchymal invasion. *Int J Biochem Cell Biol*. 2013;45:2774-2785.
- Piyadasa H, Altieri A, Basu S, Schwartz J, Halayko AJ, Mookherjee N. Biosignature for airway inflammation in a house dust mite-challenged murine model of allergic asthma. *Biol Open*. 2016;5:112-121.
- van der Velden JL, Hoffman SM, Alcorn JF, et al. Absence of c-Jun NH2-terminal kinase 1 protects against house dust mite-induced pulmonary remodeling but not airway hyperresponsiveness and inflammation. *Am J Physiol Lung Cell Mol Physiol*. 2014;306:L866-L875.
- Post S, Heijink IH, Petersen AH, de Bruin HG, van Oosterhout AJ, Nawijn MC. Protease-activated receptor-2 activation contributes to house dust mite-induced IgE responses in mice. *PLoS One*. 2014;9:e91206.
- Tomlinson KL, Davies GC, Sutton DJ, Palframan RT. Neutralisation of interleukin-13 in mice prevents airway pathology caused by chronic exposure to house dust mite. *PLoS One*. 2010;5:e13136.
- Busse WW. The relationship of airway hyperresponsiveness and airway inflammation: airway hyperresponsiveness in asthma: its measurement and clinical significance. *Chest*. 2010;138(2 Suppl):4S-10S.
- Evans CM, Raclawska DS, Ttofali F, et al. The polymeric mucin Muc5ac is required for allergic airway hyperreactivity. *Nat Commun*. 2015;6:6281.

23. Spadaro O, Goldberg EL, Camell CD, et al. growth hormone receptor deficiency protects against age-related NLRP3 inflammasome activation and immune senescence. *Cell Rep*. 2016;14:1571-1580.
24. Li S, Pinar M, Wang Y, et al. Crosstalk between the TNF and IGF pathways enhances NF-kappaB activation and signaling in cancer cells. *Growth Horm IGF Res*. 2015;25:253-261.
25. Tully JE, Hoffman SM, Lahue KG, et al. Epithelial NF-κB orchestrates house dust mite-induced airway inflammation, hyperresponsiveness, and fibrotic remodeling. *J Immunol*. 2013;191:5811-5821.
26. Hung CF, Rohani MG, Lee SS, Chen P, Schnapp LM. Role of IGF-1 pathway in lung fibroblast activation. *Respir Res*. 2013;14:102.
27. Choi JE, Lee SS, Sunde DA, et al. Insulin-like growth factor-I receptor blockade improves outcome in mouse model of lung injury. *Am J Respir Crit Care Med*. 2009;179:212-219.
28. Osorio FG, Soria-Valles C, Santiago-Fernandez O, et al. Loss of the proteostasis factor AIRAPL causes myeloid transformation by deregulating IGF-1 signaling. *Nat Med*. 2016;22:91-96.
29. Moody G, Beltran PJ, Mitchell P, et al. IGF1R blockade with ganitumab results in systemic effects on the GH-IGF axis in mice. *J Endocrinol*. 2014;221:145-155.
30. Chen G, Korfhagen TR, Xu Y, et al. SPDEF is required for mouse pulmonary goblet cell differentiation and regulates a network of genes associated with mucus production. *J Clin Invest*. 2009;119:2914-2924.
31. Ren X, Shah TA, Ustiyani V, et al. FOXM1 promotes allergen-induced goblet cell metaplasia and pulmonary inflammation. *Mol Cell Biol*. 2013;33:371-386.
32. Song J, Meyer K, Kistemaker LE, et al. Targeted silencing of master transcription factor SPDEF to reduce mucus production in airway diseases by epigenetic editing. *Eur Respir J*. 2015;46(Suppl 59):OA486.
33. Rajavelu P, Chen G, Xu Y, Kitzmiller JA, Korfhagen TR, Whitsett JA. Airway epithelial SPDEF integrates goblet cell differentiation and pulmonary Th2 inflammation. *J Clin Invest*. 2015;125:2021-2031.
34. Koeppen M, McNamee EN, Brodsky KS, et al. Detrimental role of the airway mucin Muc5ac during ventilator-induced lung injury. *Mucosal Immunol*. 2013;6:762-775.
35. Gomperts BN, Kim LJ, Flaherty SA, Hackett BP. IL-13 regulates cilia loss and foxj1 expression in human airway epithelium. *Am J Respir Cell Mol Biol*. 2007;37:339-346.
36. Whitsett JA, Wert SE, Weaver TE. Alveolar surfactant homeostasis and the pathogenesis of pulmonary disease. *Annu Rev Med*. 2010;61:105-119.
37. Glasser SW, Maxfield MD, Ruetschilling TL, et al. Persistence of LPS-induced lung inflammation in surfactant protein-C-deficient mice. *Am J Respir Cell Mol Biol*. 2013;49:845-854.
38. Ikegami M, Whitsett JA, Martis PC, Weaver TE. Reversibility of lung inflammation caused by SP-B deficiency. *Am J Physiol Lung Cell Mol Physiol*. 2005;289:L962-L970.
39. Ogawa H, Ledford JG, Mukherjee S, et al. Surfactant protein D attenuates sub-epithelial fibrosis in allergic airways disease through TGF-beta. *Respir Res*. 2014;15:143.
40. Ledford JG, Mukherjee S, Kiskan MM, Nugent JL, Hollingsworth JW, Wright JR. Surfactant protein-A suppresses eosinophil-mediated killing of *Mycoplasma pneumoniae* in allergic lungs. *PLoS One*. 2012;7:e32436.
41. Hoshino M, Nakamura Y, Sim JJ, et al. Inhaled corticosteroid reduced lamina reticularis of the basement membrane by modulation of insulin-like growth factor (IGF)-I expression in bronchial asthma. *Clin Exp Allergy*. 1998;28:568-577.
42. Veraldi KL, Gibson BT, Yasuoka H, et al. Role of insulin-like growth factor binding protein-3 in allergic airway remodeling. *Am J Respir Crit Care Med*. 2009;180:611-617.
43. Belfiore A, Frasca F, Pandini G, Sciacca L, Vigneri R. Insulin receptor isoforms and insulin receptor/insulin-like growth factor receptor hybrids in physiology and disease. *Endocr Rev*. 2009;30:586-623.
44. Iams WT, Lovly CM. Molecular pathways: clinical applications and future direction of insulin-like growth factor-1 receptor pathway blockade. *Clin Cancer Res*. 2015;21:4270-4277.

SUPPORTING INFORMATION

Additional Supporting Information may be found online in the supporting information tab for this article.

How to cite this article: Piñeiro-Hermida S, Gregory JA, López IP, et al. Attenuated airway hyperresponsiveness and mucus secretion in HDM-exposed *Igf1r*-deficient mice. *Allergy*. 2017;00:1–10. <https://doi.org/10.1111/all.13142>

Supplementary Table S1. Primer sets used for qRT-PCR.

Gene	Accession No.	Forward primer (5'-3')	Reverse primer (5'-3')
<i>Igflr</i>	NM_010513	ATGGCTTCGTTATCCACGAC	AATGGCGGATCTTCACGTAG
<i>Igfbp3</i>	NM_008343.2	GCCCTCTGCCTTCTTGATTT	TCACTCGGTTATGGGTTTCC
<i>Igfbp5</i>	NM_010518.2	GATGAGACAGGAATCCGAACAAG	AATCCT TTGCGGTCACAGTTG
<i>Insr</i>	NM_010568.2	TCCTGAAGGAGCTGGAGGAGT	CTTTCGGGATGGCCTGG
<i>Muc5ac</i>	NM_010844.1	CACACACAACCACTCAACCA	TCTCTCTCCGCTCCTCTCAA
<i>Rn18s</i>	NR_003278.3	ATGCTCTTAGCTGAGTGTCCTCG	ATTCCTAGCTGCGGTATCCAGG
<i>Sftpa1</i>	NM_023134.4	CCATCGCAAGCATTACAAAG	CACAGAAGCCCCATCCAG
<i>Sftpb</i>	NM_147779.2	CTGCTGCTTCCTACCCTCTG	ATCCTCACACTCTTGGCACA
<i>Sftpc</i>	NM_011359	GAAGATGGCTCCAGAGAGCAT C	GGACTCGGAACCAGTATCATGC
<i>Sftpd</i>	NM_009160.2	TGAGAATGCTGCCATACAGC	GAATAGACCAGGGGCTCTCC
<i>Spdef</i>	NM_013891.4	GGCCAGCCATGAACTATGAT	GGTAGACAAGGCGCTGAGAG

Characterization of the acute inflammatory profile and resolution of airway inflammation after *Igfl1*-gene targeting in a murine model of HDM-induced asthma

Sergio Piñeiro-Hermida¹, Elvira Alfaro-Arnedo¹, Joshua A. Gregory^{2#}, Raquel Torrens¹, Carlos Ruíz-Martínez³, Mikael Adner², Icíar P. López¹ and José G. Pichel^{1*}

¹Lung Cancer and Respiratory Diseases Unit, Centro de Investigación Biomédica de la Rioja (CIBIR), Fundación Rioja Salud, Logroño, Spain.

²Unit of Experimental Asthma and Allergy Research, Karolinska Institutet, Institute of Environmental Medicine (IMM), Stockholm, Sweden.

³Pneumology Service, Hospital San Pedro, Logroño, Spain.

[#]Current affiliation: Adlego Biomedical AB, Uppsala, Sweden.

*José G. Pichel, corresponding author.

Correspondence to

José G. Pichel, Lung Cancer and Respiratory Diseases Unit, CIBIR (Centro de Investigación Biomédica de la Rioja), Fundación Rioja Salud, Logroño, Spain.

e-mail: jgpichel@riojasalud.es

Short title: Acute inflammatory profile and resolution of inflammation after *Igfl1*-gene targeting in a HDM model of asthma

Abstract

Asthma is a chronic inflammatory disease characterized by bronchial hyperresponsiveness, mucus overproduction and airway remodeling. Notably, we have recently demonstrated that insulin-like growth factor 1 receptor (IGF1R) deficiency in mice attenuates airway hyperresponsiveness and mucus secretion after chronic house dust mite (HDM) exposure. On this basis, inbred C57BL/6 and *Igf1r*-deficient mice were given HDM extract to study the acute inflammatory profile and implication of *Igf1r* in acute asthma pathobiology. Additionally, *Igf1r*-deficiency was therapeutically induced in mice to evaluate the resolution of HDM-induced inflammation. Acute HDM exposure in inbred C57BL/6 mice led to a progressive increase in inflammation, airway remodeling and associated molecular indicators. Preventively-induced *Igf1r*-deficiency showed reduced neutrophil and eosinophil numbers in BALF and bone marrow, a significant reduction of airway remodeling and decreased levels of related markers. In addition, therapeutic targeting of *Igf1r* promoted the resolution of HDM-induced-inflammation. Our results demonstrate for the first time that *Igf1r* is important in acute asthma pathobiology and resolution of HDM-induced inflammation. Thus, IGF1R is suggested to be a promising candidate for future therapeutic approaches for the treatment and prevention of asthma.

Introduction

Asthma is a chronic inflammatory disease characterized by airway hyperresponsiveness (AHR), mucus overproduction and airway wall remodeling [1]. House dust mite (HDM)-derived allergens and specifically those arising from the species *Dermatophagoides pteronyssinus* are the most important source of mite-related allergens in asthmatic patients [2]. In response to allergen stimulation the airway epithelium secretes fluids, antimicrobial proteins, and mucins, which together with club cells represent a major component of the immunomodulatory barrier of the airway epithelium [3].

The insulin-like growth factor 1 receptor (IGF1R) is a ubiquitously expressed tyrosine kinase and a central member of the IGF axis. The IGF axis is comprised of two major ligands (IGF1 and IGF2), different receptors and regulatory proteins such as IGF-binding proteins (IGFBPs), acting together to control a number of essential cellular functions including proliferation, differentiation, survival, adhesion and migration [4]. Although little is known about the role of IGFs in human asthma, IGF1 and IGFBP3 were suggested to be involved in allergic airway inflammation and remodeling [5,6]. Additionally, IGF1R was found to be upregulated in BAL cells of asthmatic patients [7]. In mice, IGF1 was reported to be a relevant mediator of allergic airway inflammation and remodeling, and that IGFBP3 blocks the specific physiological consequences of this pathology [8-10]. Notably, we have recently reported that IGF1R plays an important role in initiation of the inflammatory response in mice, and the importance of IGF1R in the pathogenesis of murine asthma, mediating both AHR and mucus secretion after chronic HDM exposure [11,12]. Thus, we aimed to further investigate the involvement of IGF1R in allergic airway inflammation. For this purpose, *Igf1r* deficiency was preventively or therapeutically induced in mice to evaluate the

implication of *Igf1r* in acute asthma pathobiology and resolution of airway inflammation following HDM exposure. The main finding of this study is that therapeutic targeted deletion of *Igf1r* resolves HDM-induced inflammation in mice. We assert that IGF1R is suggested to be a promising candidate for future therapeutic approaches for the treatment and prevention of asthma.

Materials and Methods

Ethics approval

All experiments and animal procedures conducted were carried out in accordance with the guidelines of the European Communities Council Directive (86/609/EEC) and were revised and approved by the CIBIR Bioethics Committee (refs. JGP02_1 and JGP02_2).

HDM sensitization protocols and preventive and therapeutic targeting of *Igf1r*

Eight- to 10-week-old (W8-10) female mice were intranasally challenged with consecutive doses of 40 µg of HDM extract (Greer Laboratories Inc, Lenoir, NC, USA) in 20 µl of PBS (2 mg/ml) or equal volume of PBS under light isoflurane anesthesia. Females were used due to their reported higher susceptibility to allergic airway inflammation [13]. Three different protocols of HDM sensitization were used: i) inbred C57Bl/6 mice were given seven doses of HDM extract or PBS and BALF and lungs were collected 24 h after the last exposure on days (D) 3, D5 or D7 (acute HDM protocol) (Fig 1A); ii) *Igf1r^{fl/fl}* (controls) and *UBC-CreERT2; Igf1r^{fl/fl}* mice were treated with tamoxifen (TMX) for five consecutive days at four weeks of age to induce a postnatal *Igf1r* gene deletion in *UBC-CreERT2; Igf1r^{fl/fl}* mice [14]. After TMX treatment, *UBC-CreERT2; Igf1r^{A/A}* (*CreERT2*) and *Igf1r^{fl/fl}* mice were administered with seven doses of HDM extract or PBS and bone marrow, serum, BALF and lungs were harvested 24 h after last dose on D7 (prophylactic protocol) (Fig 4A); and iii) *Igf1r^{fl/fl}* and *UBC-CreERT2; Igf1r^{fl/fl}* mice were challenged with seven (first set of animals non-

treated with TMX and sacrificed at D7) or fourteen doses of HDM extract or PBS (second set of animals receiving five consecutive intraperitoneal TMX injections between D7 and D11 to induce *Igf1r* deletion in *UBC-CreERT2; Igf1r^{fl/fl}* mice, to generate *CreERT2* mice), followed by serum, BALF and lung tissue collection 24 h after the last exposure (therapeutic protocol) (Fig 7A). *UBC-CreERT2; Igf1r^{fl/fl}* double transgenic mice were in a C57BL/6-enriched (at least six generation backcrosses to C57BL/6 strain) mixed genetic background. All animals were bred and maintained under specific pathogen-free conditions at CIBIR animal facilities.

Tissue collection and preparation

Twenty-four hours after the final HDM exposure, animals were euthanized by intraperitoneal injection of 10 µl/g of a ketamine-xylazine anesthetic combination in saline (300:30 mg/kg respectively). Immediately, lungs were lavaged twice with 0.8 ml cold PBS to obtain the bronchoalveolar lavage fluid (BALF). Blood was collected by cardiac puncture, and serum was obtained and stored at -80°C until further use. Following lung dissection, the left lung was fixed in 4% formaldehyde and embedded in paraffin for histopathology. Right lobes were separated and snap-frozen in liquid nitrogen for quantitative real-time PCR (qRT-PCR) and ELISA analyses. Additionally, femoral bone marrow was isolated as previously described [11]. Three different sets of mice were used respectively for BALF, histology/molecular analyses and bone marrow cell counts.

Quantification of BALF and bone marrow

Total cell number was counted and expressed as cells/ml BALF or bone marrow, and differential cell counts were performed on May-Grünwald/Giemsa (Sigma-Aldrich, St. Louis, MO, USA)-stained cytopins, counting a minimum of 300 cells per slide or five

fields per slide in BALF and bone marrow cytospins, respectively. Determination of differential cell counts was performed using standard morphology criteria.

Histopathological analysis

Paraffin embedded left lungs were cut into 3 μm sections, evaluating a minimum of four airways per animal. Hematoxylin and eosin (H&E) staining was performed for quantification of inflamed lung areas and airway thickness. Quantification of inflammation was conducted as previously described [11]. Airway thickness was assessed by means of three different measurements per airway. Periodic acid-Schiff (PAS) and Masson's trichrome staining protocols served to visualize the degree of goblet cell hyperplasia and collagen deposition. Fiji open-source image processing software package v1.48r (<http://fiji.sc>) was used to quantify the area of inflammation, airway thickness, collagen content and epithelium length measurements.

RNA isolation, qRT-PCR and ELISAS

RNA isolation and qRT-PCR was performed using inferior lung lobes, as previously described [12]. A full list of primer sets used is provided in S1 Table. Cytokines were analyzed in serum and tissue homogenate supernatants from middle lung lobes using mouse IL13 DuoSet and IL10, IL33 and CCL11 Quantikine ELISA Kits (R&D systems, Minneapolis, MN, USA).

Statistical analyses

Statistical analyses were carried out using SPSS Statistics Software v21 for windows (IBM, Armonk, NY, USA). Differences between experimental groups were evaluated for significance using the non-parametric Mann-Whitney U test or the Dunn-Sidak test for multiple comparisons. Results are shown as mean values \pm standard error of the mean (SEM). For all analyses, a p value < 0.05 was considered statistically significant.

Results

Characterization of the murine acute allergic profile

Inbred C57BL/6 mice were subjected to an acute HDM exposure to study the progressive changes in BALF and lung (Fig 1A). Total cell counts were significantly increased at day D5 and D7, reaching the highest numbers at D7 (Fig 1B-C). Differential cell counts in BALF showed a marked increase in lymphocyte, neutrophil and eosinophil numbers at D5 and D7, whilst macrophage counts remained unchanged. Lymphocyte and eosinophil numbers were higher at D7 without changes in neutrophil counts between D5 and D7 (Fig 1B-C).

Inflamed lung area, airway thickness, number of PAS⁺ cells and collagen staining were only significantly changed at D7, with the exception of the inflamed lung area parameter which was increased at D5, although to a lesser degree than at D7 (Fig 2).

Lung mRNA expression analysis demonstrated a significant up-regulation of the allergic airway inflammation markers *Il33*, *Cd4*, *Il4*, *Il10*, *Il13*, *Ccl11*, *Ccl2*, *Cxcl1*, *Tnf* and *Il1b* in addition to the airway remodeling indicators *Acta2*, *Muc5ac* and *Colla1*. *Tslp* and *Ccl5* expression was not found to be induced by HDM, and *Il25* expression was not able to be measured due to low to undetectable levels (Fig 3A-B). It should be noted that mRNA expression of *Il33*, *Cd4*, *Tnf*, *Il1b* and *Colla1* markers was induced at D7 unlike all other markers which were already significantly increased at D5 but in general in a lesser extent than at D7. The increased *Ccl11* expression was validated by CCL11 protein levels (Fig 3C).

Decreased HDM-induced neutrophilopoiesis and eosinophilopoiesis, and IL13, CCL11 and IgE serum levels after preventively-induced *Igf1r* deficiency

Together, the results presented in the previous section indicate that D7 is an appropriate time point to study the acute allergic phenotype after HDM challenge. Thus, *Igf1r*

deficiency was preventively-induced to study the implication of *Igf1r* in acute asthma pathobiology (Fig 4A).

Total and differential cell counts in bone marrow cytopins and measurement of serum levels of several cytokines and IgE were performed in *Igf1r*-deficient and *Igf1r^{fl/fl}* mice. Total, neutrophil and eosinophil counts in bone marrow were found to be diminished in HDM-treated *Igf1r*-depleted compared to *Igf1r^{fl/fl}* lungs. This phenomenon was also evident within PBS-treated groups. In spite of *Igf1r^{fl/fl}* mice showed increased neutrophil and eosinophil numbers after HDM treatment, *Igf1r*-deficient mice did not show such an increase (Fig 4B-C). Serum IL33 levels showed only a slight increase in HDM-exposed *Igf1r^{fl/fl}* mice. In addition, IL13, CCL11 and IgE levels were significantly increased in *Igf1r^{fl/fl}* mice after HDM treatment, whereas *Igf1r*-depleted mice exhibited normal values (Fig 4D-E).

Preventively-induced *Igf1r* deficiency reduces inflammation and remodeling features

Following allergen challenge, *Igf1r^{fl/fl}* mice demonstrated a significant increase in total BALF cells. This effect was less pronounced in *Igf1r*-deficient mice. HDM-treated *Igf1r^{fl/fl}* and *Igf1r*-depleted mice showed a marked increase in macrophage, lymphocyte, neutrophil and eosinophil numbers in BALF. Notably, *Igf1r*-deficient mice demonstrated a modest decrease in lymphocyte and neutrophil counts along with a pronounced reduction in eosinophil numbers respect to *Igf1r^{fl/fl}* mice (Fig 5A).

Inflamed lung area, number of PAS⁺ cells, collagen staining and airway thickness were notably decreased in lungs from HDM-treated *Igf1r*-deficient mice compared to lungs from *Igf1r^{fl/fl}* mice. Whereas HDM induced airway thickening in *Igf1r^{fl/fl}* mice, this phenomenon was not observed in *Igf1r*-depleted lungs (Fig 5B).

Preventively-induced *Igf1r* deficiency involves changes in expression of IGF system genes and reduces allergy-related marker levels

As a complement to the BALF and histopathology analyses, a molecular analysis of IGF system genes and allergic inflammation and remodeling markers was performed. mRNA expression profiles demonstrated an efficient depletion of *Igf1r* levels with *Igf1r*-deficient PBS- and HDM-treated mice showing a reduction of 84% and 67% respectively. HDM treatment increased *Igf1r* expression in *Igf1r^{fl/fl}* (17%) and *Igf1r*-depleted (2-fold) lungs. *Igf1* levels were significantly increased in *Igf1r*-deficient PBS- or HDM-treated mice. This effect was augmented in HDM-challenged animals. In addition, HDM treatment increased *Insr*, *Igfbp3* and *Igfbp5* levels in *Igf1r*-deficient lungs. *Igfbp3* expression was decreased in both genotypes (Fig 6A). mRNA levels of all allergic airway inflammation- and remodeling-related markers tested, with the exception of IL5, were strongly induced by HDM and reduced in *Igf1r*-deficient mice, except Cd4 levels (Fig 6B-C). The goblet cell hyperplasia marker *Spdef* was also evaluated and found to be significantly decreased in *Igf1r*-deficient HDM-exposed lungs (data not shown, 2-fold reduction). Protein levels of IL13, IL33, and CCL11 were consistent with the mRNA expression profiles. IL10 levels were only increased in HDM-treated *Igf1r^{fl/fl}* lungs (Fig 6D).

Therapeutic *Igf1r*-gene targeting reduces circulating IL33, CCL11 and IgE levels, inflammation and remodeling features

Igf1r-deficiency was therapeutically induced in mice to evaluate the resolution of airway inflammation following HDM exposure (Fig 7A). Therapeutic *Igf1r*-gene targeting after TMX administration significantly decreased IL33 and CCL11 serum levels in *CreERT2* compared to non-TMX-treated mice, whereas IL10 and IL13 levels remained unchanged. *Igf1r* depletion significantly reduced IL13, IL33, CCL11 and IgE

levels at D14 with respect to *Igf1r^{fl/fl}* TMX-treated animals. Interestingly, IL10 and IL13 serum levels increased from D7 to D14 in *Igf1r^{fl/fl}* mice (Fig 7B-C).

Total cells in BALF were found to be increased in *Igf1r^{fl/fl}* at D14 and substantially reduced in *CreERT2* animals following TMX administration. This effect was attributed primarily to changes in neutrophil and eosinophil counts, since macrophage and lymphocyte numbers remained unchanged (Fig 8A).

Inflamed lung area, airway thickness, PAS⁺ cell numbers and collagen staining were clearly counteracted in *CreERT2* lungs after TMX administration compared to *CreERT2* non-TMX- and *Igf1r^{fl/fl}* TMX-treated mice (Fig 8B).

Therapeutic *Igf1r*-gene targeting diminishes expression of allergic inflammation and remodeling-related markers

Following TMX administration, *Igf1r* mRNA expression was found to be significantly reduced in *CreERT2* mice compared to *Igf1r^{fl/fl}* (85%) and *CreERT2* non-TMX-treated mice (88%). mRNA levels of the allergic airway inflammation- and remodeling-related markers demonstrated a significant reduction in *CreERT2* compared to *Igf1r^{fl/fl}* and *CreERT2* non-TMX-treated mice following TMX treatment. *Ccl2* expression was only found reduced in *Igf1r*-deficient mice compared to *CreERT2* TMX-untreated animals (Fig 9A-B). Analysis of IL13, IL33 and CCL11 protein levels in lung homogenates supported mRNA data and IL10 levels were found to be significantly decreased in *CreERT2* mice after TMX administration (Fig 9C).

Discussion

Here we report the progressive changes after acute HDM-induced inflammation in mice. We also demonstrate that preventively-induced *Igf1r*-deficiency ameliorates typical asthmatic features and that therapeutic targeting of *Igf1r* promotes the resolution of HDM-induced inflammation in mice.

Noteworthy, very few studies have reported the acute effects after HDM exposure in mice. In this regard, total and eosinophil counts in BALF and IL13 expression in the lung were found significantly increased one week after repetitive intranasal HDM exposure in mice [15]. Furthermore, total and differential BALF cell counts, peribronchial inflammation and goblet cell hyperplasia were notably increased after 10 consecutive days of intranasal HDM challenge in mice [16]. In the present study HDM exposure in inbred C57BL/6 mice demonstrated a progressive increase in inflammatory cells in BALF, airway remodeling and mRNA expression of allergic airway inflammation and remodeling markers up to D7. Consistent with our results on increased *Il33* expression, it was previously reported that IL33, but not TSLP or IL25, is central to HDM allergic sensitization [17].

Preventive induction of *Igf1r* deficiency in PBS-treated mice led to similar *Igf1r*-depleted expression to that observed in unchallenged mice of similar age [11]. In addition, *Igf1r* and *Igf1* levels increased after HDM exposure. Accordingly, IGF1R and IGF1 expression was found to be increased in BAL cells and bronchial biopsies of asthmatic patients [5,7]. The upregulation of *Igf1* in PBS-treated *Igf1r*-depleted mice or *Igf1* and *Insr* by HDM was possibly due to compensatory effects in response to *Igf1r* deficiency [12]. Regarding increased *Igfbp3* and *Igfbp5* levels in HDM-treated *Igf1r*-deficient mice, exogenous IGFBP3 and IGFBP5 administration blocks the physiological consequences of asthma and enhances epithelial cell adhesion to maintain the epithelial-

mesenchymal boundary [9,10,18]. From these data we can conclude that both *Igf1r* and *Igf1* may be important mediators in the establishment of murine asthma, and that *Igf1r* and *Igf1* could play protective roles against HDM-induced allergic inflammation.

Whereas acute HDM treatment caused a clear increase in eosinophil and neutrophil numbers in the bone marrow of *Igf1r^{fl/fl}* mice, their levels remained close to basal after preventively-induced *Igf1r*-deficiency. Recent data published by our group showed a selective decrease in circulating eosinophils after chronic HDM exposure and reduced neutrophil numbers after acute-induced lung injury in the same mutant mouse line [11,12]. Thus, IGF1R could have an important role in bone marrow myelopoiesis after HDM-induced allergy.

Following HDM challenge, decreased total and eosinophil counts in BALF and reduced asthmatic features after preventively-induced *Igf1r* deficiency are consistent with published data on IGF1R-deficient mice after chronic HDM exposure [12]. Notably, neutrophil and eosinophil presence in BALF and asthma-related features were counteracted in a similar manner in HDM-treated mice following therapeutic targeting of *Igf1r*.

We demonstrated that IGF1R plays an important role in initiation of the inflammatory process, since IGF1R deficient mice showed reduced *Il1b* and *Tnf* expression [11]. This is consistent with the decreased expression of *Il1b* and *Tnf* either after preventive or therapeutic-induced *Igf1r* deficiency. In this regard, it was reported that both IL1B and TNF are required for allergen-specific Th2 cell activation and for the development of AHR in mice [19,20]. Accordingly, we have reported that IGF1R-deficient mice exhibited no AHR after chronic HDM exposure [12].

Lung inflammation in asthma is typically orchestrated by activation of innate immune cells followed by an exacerbated Th2-biased inflammation and synthesis of allergen-

specific IgE antibody, which initiates the release of inflammatory mediators from immune cells [21,22]. In this line, following HDM exposure, *Igf1r^{fl/fl}* mice demonstrated increased levels of serum total IgE that were counteracted upon both the preventive and therapeutic strategies. Accordingly, elevated levels of serum total IgE have been reported in HDM-challenged mice and in patients with allergic asthma [12,23].

Upon allergen exposure, IL33 is mainly released from the airway epithelium to participate in the induction of Th2 immunity and is important for the establishment and maintenance of allergic response [24]. IL33 levels were significantly reduced in serum and lungs after therapeutic-induced *Igf1r* deficiency but only in lungs following preventive-induced deficiency. Accordingly, increased expression of IL33 in the airway epithelium and serum of asthmatic patients was correlated with disease severity [25,26]. Additional reports have shown that IL33 exacerbates murine allergic bronchoconstriction and that resolution of allergic airway inflammation and AHR is dependent upon disruption of IL33 signaling in mice [27,28]. Notably, lung epithelial-specific *Igf1r* deficiency in mice caused delayed differentiation of the airway epithelium, a major source of IL33 [29,30]. IGF1R-deficient lungs showed a reduced proportion of club cells in distal airways after chronic HDM exposure [12] and therefore this phenomenon could be manifested as a reduced IL33 release from the airway epithelium by HDM.

Here we report attenuated increase in IL13 levels in serum and lungs following preventive or therapeutic induction of *Igf1r* deficiency. Since IL13 levels are increased in serum of asthmatic patients, it is considered a biomarker of disease severity [31]. Blockade of IL13 activity in mice after HDM sensitization reduces eosinophilia in BALF, peribronchial collagen, and goblet cell hyperplasia [32]. These findings are in accordance with results presented in this study and in a recent publication from our

group in which IGF1R-deficient mice also showed unaltered IL13 levels after chronic HDM exposure [12].

Following HDM treatment IL10 levels were found to be decreased after both the preventive and therapeutic strategies. Even though IL10 is a regulatory cytokine with immunosuppressive and anti-inflammatory properties, its role in asthma remains unclear. IL10 is necessary for the expression of AHR after allergic sensitization in mice and its levels in serum were reported differently altered in asthmatic patients [26,33,34]. CCL11 is also a potential diagnostic marker for asthma since it is significantly increased in serum of asthmatic patients [35]. We found reduced CCL11 levels in serum and lungs after both the preventive and therapeutic approaches. Notably, enhanced expression of CCL11 in the bronchial epithelium of asthmatic patients was found to be associated with the development of AHR [36]. After allergen exposure, the eosinophil chemoattractant CCL11 is released by the airway epithelium in response to cytokines such as IL4, IL13 and TNF [37]. In the present study, reduced IL13, *Il4* and *Tnf* levels in HDM-treated mice after preventive- or therapeutic-induced *Igflr* deficiency supported depleted CCL11 levels. Of note, club cell-derived CCL11 is crucial for the accumulation of eosinophils during allergic lung inflammation [38].

The reduced number in PAS⁺ cells was validated by decreased expression of the goblet cell hyperplasia markers *Foxm1*, *Spdef* and *Muc5ac* following preventive induction of *Igflr* deficiency and by decreased expression of *Scgb1a1* and *Muc5ac* after the therapeutic approach. After allergen stimulation FOXM1 induces differentiation of club cells into goblet cells through transcriptional activation of SPDEF. Then, increased MUC5AC expression by SPDEF in goblet cells contributes to goblet cell hyperplasia and mucus hyperproduction [39]. In accordance, blockade of FOXM1 activity in mice after HDM exposure led to reduced goblet cell hyperplasia and decreased number of

eosinophils in BALF [39,40]. Furthermore, we recently demonstrated that lung epithelial-specific *Igflr* deficiency in mice and chronically HDM-challenged IGF1R-depleted mice showed delayed club cell differentiation which could result in decreased goblet cell hyperplasia and mucus production [12,29].

Both *Acta2* (α -SMA) and *Ptgs2* (COX2) levels were found to be decreased following preventive and therapeutic approaches. Accordingly, airway smooth muscle thickness was substantially reduced in IGF1R-deficient mice after chronic HDM exposure [12] and pharmacological COX2 inhibition after allergen challenge in mice reduced inflammatory cells in BALF [41]. Moreover, decreased *Colla1* expression following the preventive and therapeutic approaches supported the reduced collagen deposition around the airways. The proposed mechanism regarding the reduced susceptibility to allergic airway inflammation in *Igflr*-deficient mice upon HDM-challenge is summarized in Fig 10.

Although the short-term therapeutically-induced and generalized *Igflr* deficiency presented in this report efficiently resolves established allergic airway inflammation, TMX-mediated *Igflr* deletion in mice may occur with different degrees of mosaicism in different cell types. Thus, *Igflr* generalized deficiency cannot be used to deduce in which cells IGF1R signaling is crucial for promoting allergic airway inflammation. Furthermore, the variability of intranasal administration of HDM and the effect of the genetic background on phenotypic variations should also be considered as constraints to this report.

Here we demonstrate that therapeutic targeted deletion of *Igflr* resolves allergic airway inflammation in response to HDM. These results reinforce our previous findings on the role of IGF1R in allergy, placing it as a potential candidate to develop novel clinical

trials focused on the study of systemic IGF1R inhibitors that could be more efficient in counteracting the asthmatic response at different levels.

Supporting information

S1 Table. Primer sets used for qRT-PCR.

Funding

This work was supported by grants from the Fundación Rioja Salud (Gobierno de La Rioja, Spain), ERDF (European Regional Development Fund) and the ESF (European Social Fund) to JGP; and the Swedish Heart-Lung Foundation (20150525, 20130636), the Konsul Th C Berghs research foundation, the Karolinska Institutet, and the Centre for Allergy Research at Karolinska Institutet to MA. JAG was working at the “Unit of Experimental Asthma and Allergy Research, Karolinska Institutet, Institute of Environmental medicine (IMM), Stockholm, Sweden” at the time the study was performed and “Adlego Biomedical AB” (current affiliation) had no interest or involvement or contributed any funding in any way with the study.

Acknowledgements

We are grateful to Drs. J. Brüning (Max-Planck Institute, Cologne, Germany) and E. Brown (UPENN School of Medicine, PA) for providing *Igf1r^{fl/fl}* and *UBC-CreERT2* mouse lines, respectively. S.P.-H. thanks the Sistema Riojano de Innovación (Gobierno de La Rioja, Spain) for a PhD grant.

Author contributions

Conceptualization: SPH JGP

Data curation: SPH

Formal analysis: SPH

Funding acquisition: JGP MA

Investigation: SPH EAA RT

Methodology: SPH EAA RT

Project administration: JGP

Resources: JGP MA

Supervision: JGP

Validation: SPH, JGP

Visualization: SPH

Writing – original draft: SPH JGP

Writing – review & editing: SPH EAA JAG CRM MA IPL JGP

References

1. Fahy JV. Type 2 inflammation in asthma-present in most, absent in many. *Nat Rev Immunol.* 2015;15: 57-65.
2. Calderon MA, Linneberg A, Kleine-Tebbe J, De Blay F, Hernandez Fernandez de Rojas D, Virchow JC, et al. Respiratory allergy caused by house dust mites: What do we really know? *J Allergy Clin Immunol.* 2015;136: 38-48.
3. Whitsett JA, Alenghat T. Respiratory epithelial cells orchestrate pulmonary innate immunity. *Nat Immunol.* 2015;16: 27-35.
4. Girnita L, Worrall C, Takahashi S, Seregard S, Girnita A. Something old, something new and something borrowed: emerging paradigm of insulin-like growth factor type 1 receptor (IGF-1R) signaling regulation. *Cell Mol Life Sci.* 2014;71: 2403-27.
5. Hoshino M, Nakamura Y, Sim JJ, Yamashiro Y, Uchida K, Hosaka K, et al. Inhaled corticosteroid reduced lamina reticularis of the basement membrane by modulation of insulin-like growth factor (IGF)-I expression in bronchial asthma. *Clin Exp Allergy.* 1998;28: 568-77.
6. Veraldi KL, Gibson BT, Yasuoka H, Myerburg MM, Kelly EA, Balzar S, et al. Role of insulin-like growth factor binding protein-3 in allergic airway remodeling. *Am J Respir Crit Care Med.* 2009;180: 611-17.
7. Esnault S, Kelly EA, Schwantes EA, Liu LY, DeLain LP, Hauer JA, et al. Identification of genes expressed by human airway eosinophils after an in vivo allergen challenge. *PLoS One.* 2013;8: e67560.
8. Yamashita N, Tashimo H, Ishida H, Matsuo Y, Arai H, Nagase H, et al. Role of insulin-like growth factor-I in allergen-induced airway inflammation and remodeling. *Cell Immunol.* 2005;235: 85-91.
9. Lee YC, Jogie-Brahim S, Lee DY, Han J, Harada A, Murphy LJ, et al. Insulin-like growth factor-binding protein-3 (IGFBP-3) blocks the effects of asthma by negatively regulating NF-kappaB signaling through IGFBP-3R-mediated activation of caspases. *J Biol Chem.* 2011;286: 17898-909.
10. Kim SR, Lee KS, Lee KB, Lee YC (2012) Recombinant IGFBP-3 inhibits allergic lung inflammation, VEGF production, and vascular leak in a mouse model of asthma. *Allergy.* 2012;67: 869-77.
11. Piñeiro-Hermida S, Lopez IP, Alfaro-Arnedo E, Torrens R, Iñiguez M, Alvarez-Erviti L, et al. IGF1R deficiency attenuates acute inflammatory response in a bleomycin-induced lung injury mouse model. *Sci Rep.* 2017;7: 4290.
12. Piñeiro-Hermida S, Gregory JA, Lopez IP, Torrens R, Ruiz-Martinez C, Adner M, et al. Attenuated airway hyperresponsiveness and mucus secretion in HDM-exposed Igf1r-deficient mice. *Allergy.* 2017;72: 1317-26.
13. Melgert BN, Postma DS, Kuipers I, Geerlings M, Luinge MA, van der Strate BW, et al. Female mice are more susceptible to the development of allergic airway inflammation than male mice. *Clin Exp Allergy.* 2005;35: 1496-503.
14. Lopez IP, Rodriguez-de la Rosa L, Pais RS, Pineiro-Hermida S, Torrens R, Contreras J, et al. Differential organ phenotypes after postnatal Igf1r gene

- conditional deletion induced by tamoxifen in UBC-CreERT2; Igf1r fl/fl double transgenic mice. *Transgenic Res.* 2015;24: 279-94.
15. Gregory LG, Causton B, Murdoch JR, Mathie SA, O'Donnell V, Thomas CP, et al. Inhaled house dust mite induces pulmonary T helper 2 cytokine production. *Clin Exp Allergy.* 2009;39: 1597-610.
 16. Cates EC, Fattouh R, Wattie J, Inman MD, Goncharova S, Coyle AJ, et al. Intranasal exposure of mice to house dust mite elicits allergic airway inflammation via a GM-CSF-mediated mechanism. *J Immunol.* 2004;173: 6384-92.
 17. Chu DK1, Llop-Guevara A, Walker TD, Flader K, Goncharova S, Boudreau JE, et al. IL-33, but not thymic stromal lymphopoietin or IL-25, is central to mite and peanut allergic sensitization. *J Allergy Clin Immunol.* 2013;131(1): 187-200.
 18. Vijayan A, Guha D, Ameer F, Kaziri I, Mooney CC, Bennett L, et al. IGFBP-5 enhances epithelial cell adhesion and protects epithelial cells from TGFbeta1-induced mesenchymal invasion. *Int J Biochem Cell Biol.* 2013;45: 2774-85.
 19. Nakae S, Komiyama Y, Yokoyama H, Nambu A, Umeda M, Iwase M, et al. IL-1 is required for allergen-specific Th2 cell activation and the development of airway hypersensitivity response. *Int Immunol.* 2003;15: 483-90.
 20. Nakae S, Lunderius C, Ho LH, Schafer B, Tsai M, Galli SJ. TNF can contribute to multiple features of ovalbumin-induced allergic inflammation of the airways in mice. *J Allergy Clin Immunol.* 2007;119: 680-6.
 21. Busse WW, Lemanske RF Jr. Asthma. *N Engl J Med.* 2001;344(5):350-62.
 22. Jacquet A. The role of innate immunity activation in house dust mite allergy. *Trends Mol Med.* 2011;17(10):604-11.
 23. Schulman ES, Pohlig C. Rationale for specific allergen testing of patients with asthma in the clinical pulmonary office setting. *Chest.* 2015;147(1):251-258.
 24. Makrinioti H, Toussaint M, Jackson DJ, Walton RP, Johnston SL. Role of interleukin 33 in respiratory allergy and asthma. *Lancet Respir Med.* 2014;2: 226-37.
 25. Prefontaine D, Nadigel J, Chouiali F, Audusseau S, Semlali A, Chakir J, et al. Increased IL-33 expression by epithelial cells in bronchial asthma. *J Allergy Clin Immunol.* 2010;125: 752-4.
 26. Raeiszadeh Jahromi S, Mahesh PA, Jayaraj BS, Madhunapantula SR, Holla AD, Vishweswaraiyah S, et al. Serum levels of IL-10, IL-17F and IL-33 in patients with asthma: a case-control study. *J Asthma.* 2014;51: 1004-13.
 27. Sjöberg LC, Gregory JA, Dahlén SE, Nilsson GP, Adner M. Interleukin-33 exacerbates allergic bronchoconstriction in the mice via activation of mast cells. *Allergy.* 2015;70: 514-21.
 28. Kearley J, Buckland KF, Mathie SA, Lloyd CM. Resolution of allergic inflammation and airway hyperreactivity is dependent upon disruption of the T1/ST2-IL-33 pathway. *Am J Respir Crit Care Med.* 2009;179: 772-81.
 29. Lopez IP, Pineiro-Hermida S, Pais RS, Torrens R, Hoefflich A, Pichel JG. Involvement of Igf1r in Bronchiolar Epithelial Regeneration: Role during Repair Kinetics after Selective Club Cell Ablation. *PLoS One.* 2016;11: e0166388.

30. Kouzaki H, Iijima K, Kobayashi T, O'Grady SM, Kita H. The danger signal, extracellular ATP, is a sensor for an airborne allergen and triggers IL-33 release and innate Th2-type responses. *J Immunol*. 2011;186: 4375-87.
31. Gaye B, Sikkema D, Lee TN. Development of an ultra-sensitive single molecule counting assay for the detection of interleukin-13 as a marker for asthmatic severity. *J Immunol Methods*. 2015;426: 82-5.
32. Tomlinson KL, Davies GC, Sutton DJ, Palframan RT. Neutralisation of interleukin-13 in mice prevents airway pathology caused by chronic exposure to house dust mite. *PLoS One*. 2010;5: e13136.
33. Justice JP, Shibata Y, Sur S, Mustafa J, Fan M, Van Scott MR. IL-10 gene knockout attenuates allergen-induced airway hyperresponsiveness in C57BL/6 mice. *Am J Physiol Lung Cell Mol Physiol*. 2001;280: L363-8.
34. Zhang YL, Luan B, Wang XF, Qiao JY, Song L, Lei RR, et al. Peripheral blood MDSCs, IL-10 and IL-12 in children with asthma and their importance in asthma development. *PLoS One*. 2013;8: e63775.
35. Wu D, Zhou J, Bi H, Li L, Gao W, Huang M, et al. CCL11 as a potential diagnostic marker for asthma? *J Asthma*. 2014;51: 847-54.
36. Ying S, Robinson DS, Meng Q, Rottman J, Kennedy R, Ringler DJ, et al. Enhanced expression of eotaxin and CCR3 mRNA and protein in atopic asthma. Association with airway hyperresponsiveness and predominant co-localization of eotaxin mRNA to bronchial epithelial and endothelial cells. *Eur J Immunol*. 1997;27: 3507-16.
37. Conroy DM, Williams TJ. Eotaxin and the attraction of eosinophils to the asthmatic lung. *Respir Res*. 2001;2: 150-6.
38. Sonar SS, Ehmke M, Marsh LM, Dietze J, Dudda JC, Conrad ML, et al. Clara cells drive eosinophil accumulation in allergic asthma. *Eur Respir J*. 2012;39: 429-38.
39. Ren X, Shah TA, Ustiyani V, Zhang Y, Shinn J, Chen G, et al. FOXM1 promotes allergen-induced goblet cell metaplasia and pulmonary inflammation. *Mol Cell Biol*. 2013;33: 371-86.
40. Sun L, Ren X, Wang IC, Pradhan A, Zhang Y, Flood HM, et al. The FOXM1 inhibitor RCM-1 suppresses goblet cell metaplasia and prevents IL-13 and STAT6 signaling in allergen-exposed mice. *Sci Signal*. 2017;10: eaai8583.
41. Swedin L, Ellis R, Kemi C, Ryrfeldt A, Inman M, Dahlen SE, et al. Comparison of aerosol and intranasal challenge in a mouse model of allergic airway inflammation and hyperresponsiveness. *Int Arch Allergy Immunol*. 2010;153: 249-58.

Figure legends

Fig 1. Protocol for acute HDM exposure and progressive accumulation of inflammatory cells in BALF of inbred C57BL/6 mice. (A) Eight- to 10-week-old (W8-10) inbred C57BL/6 female mice were intranasally challenged with daily consecutive doses of 40 µg of HDM extract in 20 µl of PBS (2 mg/ml) or equal volume of PBS. BALF and lungs were collected 24 h after the last exposure on days [D] 3, D5 or D7. (B-C) Representative images of BALF cytopsin preparations (scale bar: 20 µm) and total and differential cell counts in BALF from PBS- or HDM-treated inbred C57BL/6 mice at D3, D5 and D7. Data are expressed as mean ± SEM (n = 4 animals per group). * $p < 0.05$; ** $p < 0.01$; *** $p < 0.001$ (Dunn-Sidak multiple comparison test). HDM, house dust mite; PBS, phosphate buffered saline.

Fig 2. Progressive increase in airway inflammation and remodeling after acute HDM exposure in inbred C57BL/6 mice. Representative images of proximal airways showing inflamed lung areas (left) (scale bar: 0.5 mm), and airway thickness (orange bars in insets) (center left), mucus-producing cells per epithelium length (red arrowheads in insets) (center right) and collagen content (right) (scale bars: 50 µm) in PBS- or HDM-treated C57BL/6 mice at D3, D5 and D7. Bottom graphs represent quantification of the abovementioned parameters. Data are expressed as mean ± SEM (n = 4 animals per group). ** $p < 0.01$; *** $p < 0.001$ (Dunn-Sidak multiple comparison test). H&E, Hematoxylin and eosin; PAS, Periodic Acid Schiff; AW, airway; HDM, house dust mite; PBS, phosphate buffered saline.

Fig 3. Expression of airway inflammation and remodeling markers after acute HDM treatment in inbred C57BL/6 mice. (A) Lung tissue mRNA expression levels of dendritic cell activators (*Il33* and *Tslp*), T-lymphocyte marker (*Cd4*), Th2 cytokines (*Il4*, *Il10* and *Il13*), eosinophil (*Ccl11* and *Ccl5*), macrophage (*Ccl2*) and neutrophil

(*Cxcl1*) chemoattractants and Th1 cytokines (*Tnf* and *Il1b*); (B) bronchoconstriction (*Acta2*), goblet cell hyperplasia (*Muc5ac*) and collagen deposition (*Colla1*) markers, and (C) CCL11 protein levels in lung homogenates in PBS- or HDM-treated inbred C57BL/6 mice at D3, D5 and D7. Data are expressed as mean \pm SEM (n = 3-4 animals per group). * p <0.05; ** p <0.01; *** p <0.001 (Dunn-Sidak multiple comparison test). HDM, house dust mite; PBS, phosphate buffered saline.

Fig 4. Protocol for prophylactic induction of *Igf1r* deficiency and HDM treatment, bone marrow cell counts and circulating levels of allergy-related markers. (A) *Igf1r^{fl/fl}* (controls) and *UBC-CreERT2; Igf1r^{fl/fl}* female mice were treated with tamoxifen (TMX) for five consecutive days at four weeks of age (W4) to induce a postnatal *Igf1r* gene deletion [14]. Then, eight- to 10-week-old (W8-10) *Igf1r^{fl/fl}* and *UBC-CreERT2; Igf1r^{fl/fl}* female mice were intranasally challenged with seven daily consecutive doses of 40 μ g of HDM extract in 20 μ l of PBS (2 mg/ml) or equal volume of PBS. Bone marrow, serum, BALF and lungs were harvested 24 h after last dose on D7. (B-C) Representative images and total, neutrophil and eosinophil (red arrowheads) counts in bone marrow (BM) cytopsin preparations (Scale bar: 10 μ m; n = 4 animals per group) and (D-E) serum levels of IL10, IL13, IL33, CCL11 and IgE (n = 3-6 animals per group) in PBS- or HDM-exposed *Igf1r*-deficient vs. *Igf1^{fl/fl}* mice. Data are expressed as mean \pm SEM. * p <0.05; ** p <0.01; *** p <0.001 (Dunn-Sidak multiple comparison test). HDM, house dust mite; PBS, phosphate buffered saline.

Fig 5. *Igf1r* deficiency decreases airway inflammation and remodeling after HDM exposure. (A) Total and differential cell counts performed on cytopsin preparations of BALF (n = 8 animals per group) and (B) representative images of proximal airways showing inflamed lung areas (left) (scale bar: 0.5 mm); airway thickness (orange bars in insets) (center left), mucus-producing cells per epithelium length (red arrowheads in

insets) (center right) and collagen content (right) (scale bars: 50 μ m; n = 5-6 animals per group) in PBS- or HDM-exposed *Igf1r*-deficient vs. *Igf1^{fl/fl}* mice. Bottom graphs represent quantification of the abovementioned parameters. Data are expressed as mean \pm SEM * p <0.05; ** p <0.01; *** p <0.001 (Dunn-Sidak multiple comparison test). H&E, Hematoxylin and eosin; PAS, Periodic Acid Schiff; AW, airway; HDM, house dust mite; PBS, phosphate buffered saline.

Fig 6. Expression of IGF genes and airway inflammation and remodeling markers in HDM-exposed *Igf1r*-deficient lungs. Lung tissue mRNA expression levels of (A) IGF-system genes (*Igf1r*, *Igf1*, *Insr*, *Igfbp3* and *Igfbp5*); (B) dendritic cell activator (*Il33*), T-lymphocyte marker (*Cd4*), Th2 cytokines (*Il4*, *Il5* and *Il13*), eosinophil (*Ccl11*), macrophage (*Ccl2*) and neutrophil (*Cxcl1*) chemoattractants and Th1 cytokines (*Tnf* and *Il1b*); (C) bronchoconstriction (*Acta2* and *Ptgs2*), goblet cell hyperplasia (*Foxm1* and *Muc5ac*) and collagen deposition (*Colla1*) markers, and (D) IL10, IL13, IL33 and CCL11 protein levels in lung homogenates in PBS- and HDM-exposed *Igf1r*-deficient and *Igf1^{fl/fl}* mice. Data are expressed as mean \pm SEM (n = 5-6 animals per group). * p <0.05; ** p <0.01; *** p <0.001 (Dunn-Sidak multiple comparison test). HDM, house dust mite; PBS, phosphate buffered saline.

Fig 7. Protocol for therapeutic induction of *Igf1r* deficiency, HDM treatment and circulating levels of allergy-related markers. (A) Eight- to 10-week-old (W8-10) *Igf1r^{fl/fl}* and *UBC-CreERT2; Igf1r^{fl/fl}* female mice were intranasally challenged with seven (first set of animals non-treated with TMX and sacrificed at D7) or fourteen (second set of animals receiving five consecutive intraperitoneal TMX injections between D7 and D11 to induce *Igf1r* deletion in *UBC-CreERT2; Igf1r^{fl/fl}* mice to generate *CreERT2* mice) daily consecutive doses of 40 μ g of HDM extract in 20 μ l of PBS (2 mg/ml). Serum, BALF and lungs were collected 24 h after the last exposure. (B-

C) Serum levels of IL10, IL13, IL33, CCL11 and IgE (n = 3-4 animals per group) in HDM-exposed *CreERT2* vs. *Igf1^{fl/fl}* mice after the TMX treatment (D14) (+ TMX). Note that the *CreERT2* term used at D7 (- TMX) refers to *UBC-CreERT2*; *Igf1^{fl/fl}* mice. Data are expressed as mean \pm SEM. * $p < 0.05$; ** $p < 0.01$ (Mann-Whitney U and Dunn-Sidak multiple comparison tests). HDM, house dust mite; PBS, phosphate buffered saline; TMX, tamoxifen.

Fig 8. Therapeutic targeting of *Igf1r* reduces airway inflammation and remodeling features after HDM exposure. (A) Total and differential cell counts performed on cytospin preparations of BALF (n = 4-5 animals per group). (B) representative images of proximal airways showing inflamed lung areas (left) (scale bar: 0.5 mm) and airway thickness (orange bars in insets) (center left), mucus-producing cells per epithelium length (red arrowheads in insets) (center right) and collagen content (right) (scale bars: 50 μ m) in HDM-exposed *CreERT2* vs. *Igf1^{fl/fl}* mice non-treated with TMX (D7) (- TMX) or after the TMX treatment (D14) (+ TMX). Note that the *CreERT2* term used at D7 (- TMX) refers to *UBC-CreERT2*; *Igf1^{fl/fl}* mice. Bottom graphs represent quantification of the abovementioned parameters (n= 5 animals per group). Data are expressed as mean \pm SEM. * $p < 0.05$; ** $p < 0.01$; *** $p < 0.001$ (Dunn-Sidak multiple comparison test). H&E, Hematoxylin and eosin; PAS, Periodic Acid Schiff; AW, airway; HDM, house dust mite; PBS, phosphate buffered saline; TMX, tamoxifen.

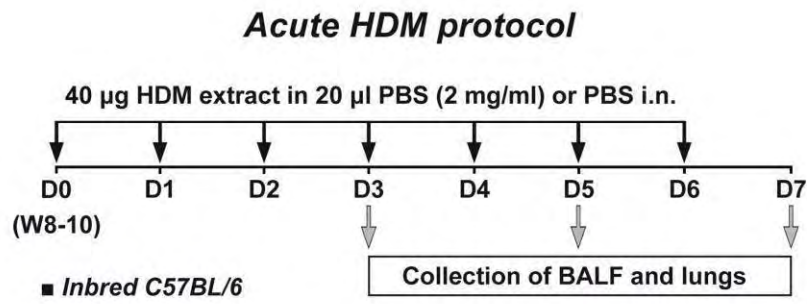
Fig 9. Therapeutic *Igf1r*-gene targeting diminishes expression of airway inflammation and remodeling-related markers after HDM exposure. Lung tissue mRNA expression levels of (A) Insulin-like growth factor 1 receptor (*Igf1r*), dendritic cell activator (*Il33*), T-lymphocyte marker (*Cd4*), Th2 cytokines (*Il4* and *Il13*), eosinophil (*Ccl11*), macrophage (*Ccl2*) and neutrophil (*Cxcl1*) chemoattractants and Th1 cytokines (*Tnf* and *Il1b*) and (B) bronchoconstriction (*Acta2* and *Ptgs2*), goblet cell

hyperplasia (*Scgb1a1* and *Muc5ac*) and collagen deposition (*Colla1*) markers, and (C) IL33, IL10, IL13 and CCL11 protein levels in lung homogenates (n = 3-5 animals per group). Quantifications were performed in HDM-exposed *CreERT2* vs. *Igf1^{fl/fl}* mice non-treated with TMX (D7) (- TMX) or after the TMX treatment (D14) (+ TMX). Note that the *CreERT2* term used at D7 (- TMX) refers to *UBC-CreERT2; Igf1^{fl/fl}* mice. Data are expressed as mean \pm SEM. * $p < 0.05$; ** $p < 0.01$; *** $p < 0.001$ (Dunn-Sidak multiple comparison test). HDM, house dust mite; PBS, phosphate buffered saline; TMX, tamoxifen.

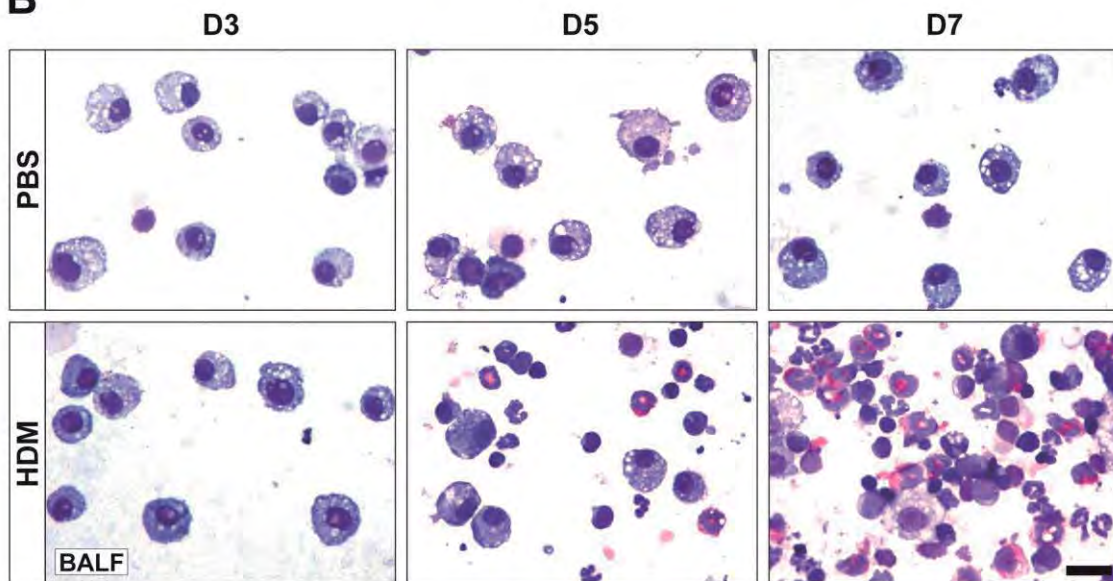
Fig 10. Proposed mechanism for reduced susceptibility to airway inflammation in *Igf1r*-deficient mice upon HDM-challenge. Following HDM exposure *Igf1r* deficiency counteracts collagen deposition, smooth muscle thickening and mucus secretion. The airway epithelium is known to be a major source of IL33 and its delayed differentiation by *Igf1r* deficiency could diminish IL33 levels after HDM treatment, reducing the induction of Th2 immunity and particularly IL13 expression. After HDM exposure, IL13 normally stimulates goblet cell differentiation in the airway epithelium which leads to goblet cell hyperplasia and mucus hyperproduction in addition to triggering the release of CCL11. Delayed differentiation of the airway epithelium caused by *Igf1r* deficiency together with diminished IL13 levels may inhibit differentiation of goblet cells and CCL11 production, reducing mucus secretion and eosinophil recruitment to the lung. Additionally, decreased eosinophilopoiesis in bone marrow of *Igf1r*-deficient mice can also substantially contribute to reduced eosinophil presence in the lung. The proposed mechanism illustrated in this figure is supported by results from the present study and additional reports [12,20,28,29,36,38].

Figures

A



B



C

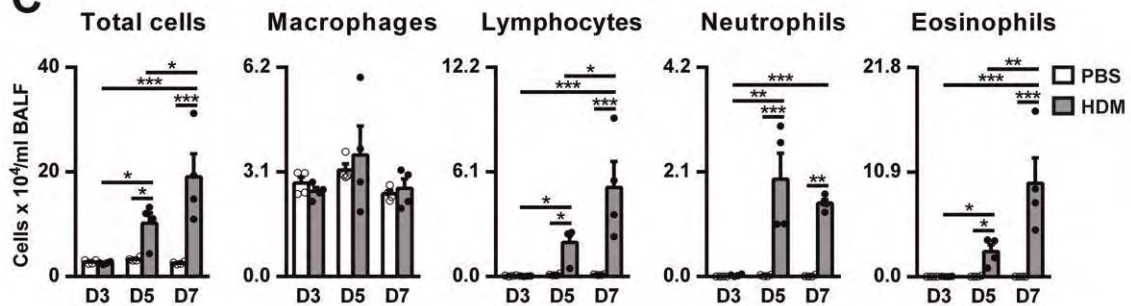


Figure 1

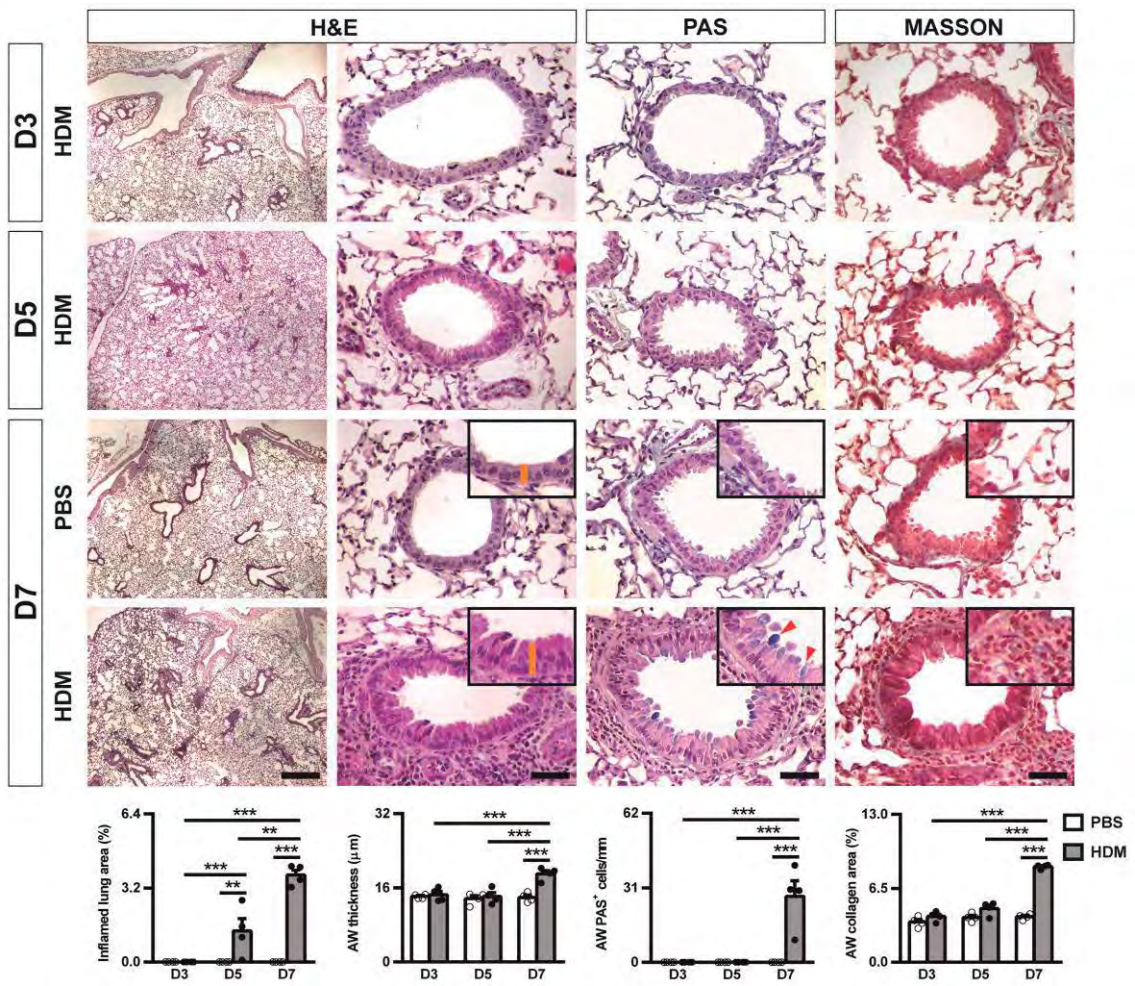


Figure 2

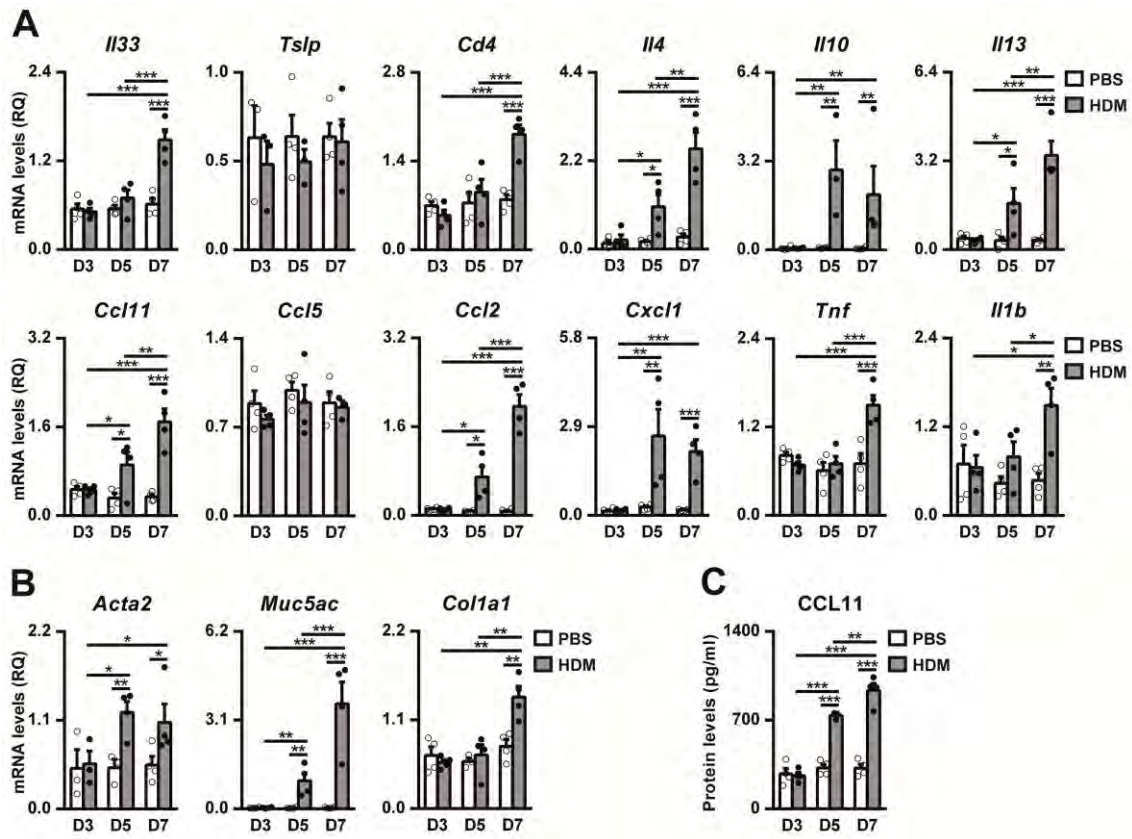
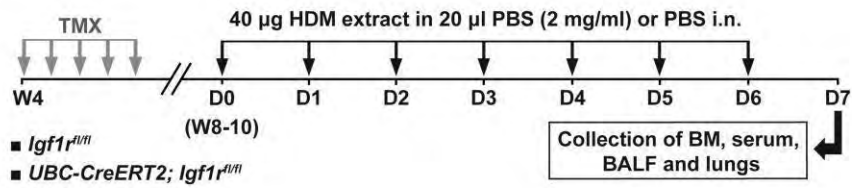
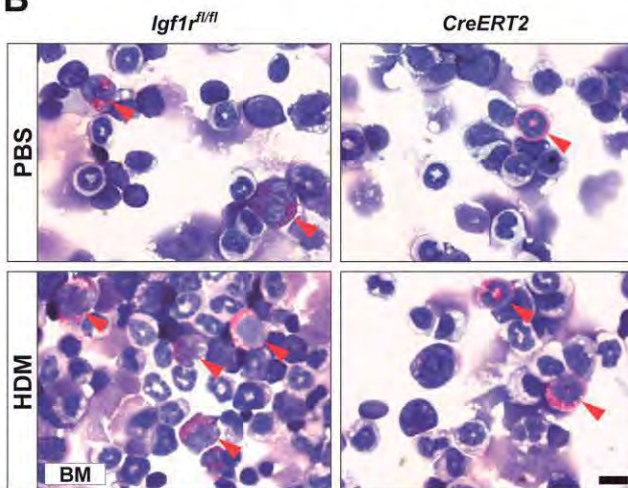
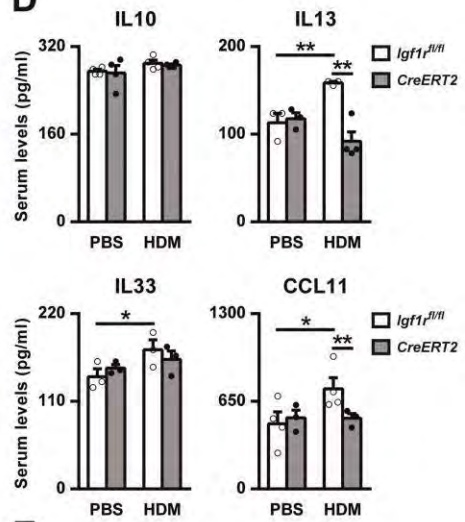
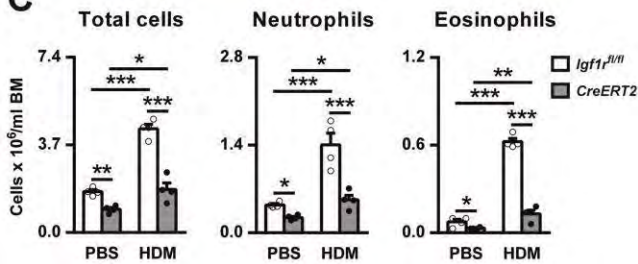
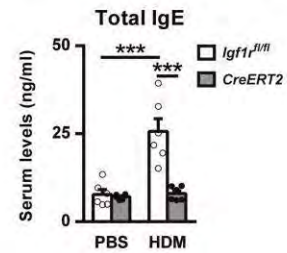


Figure 3

A**Prophylactic protocol****B****D****C****E****Figure 4**

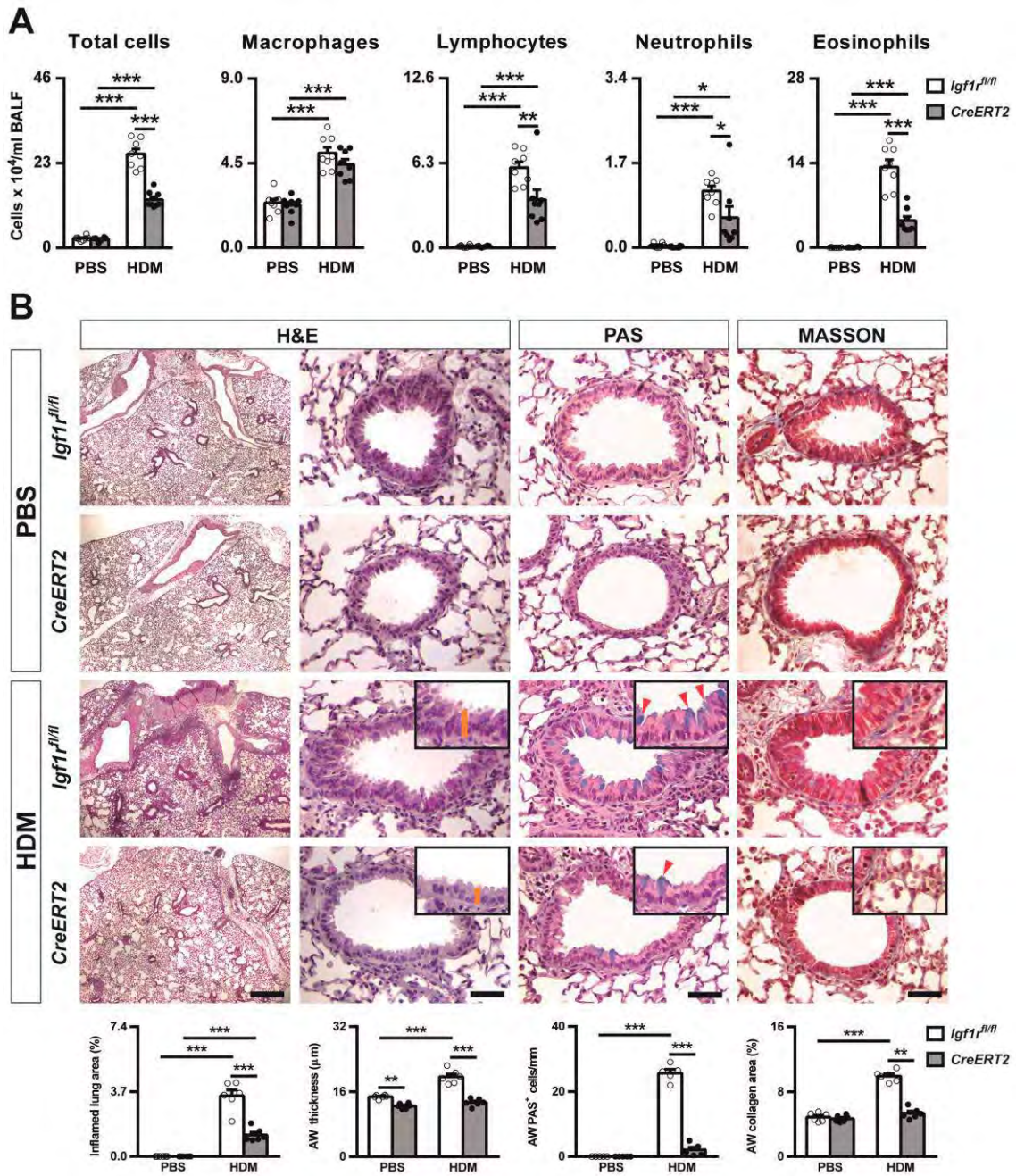


Figure 5

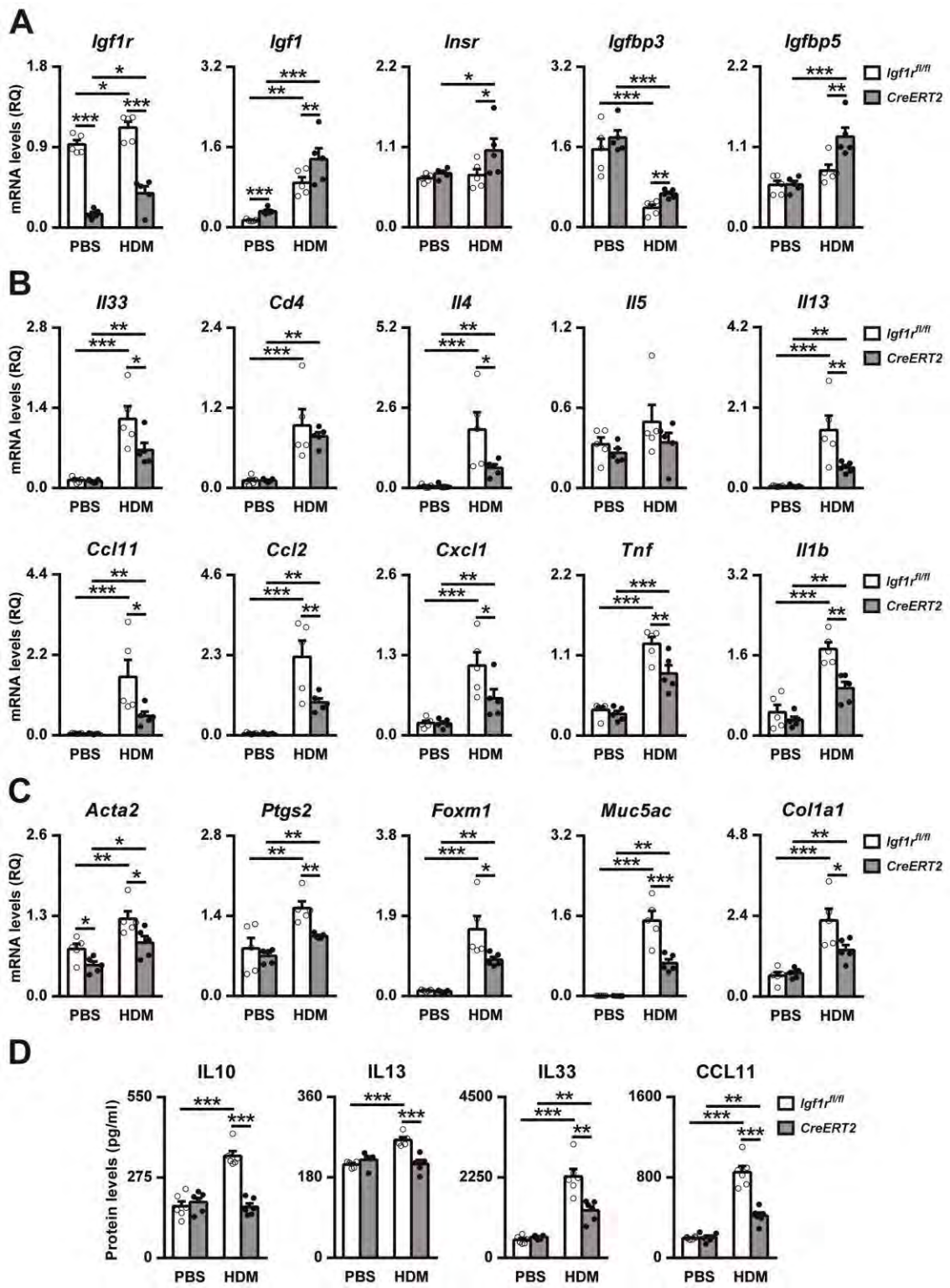


Figure 6

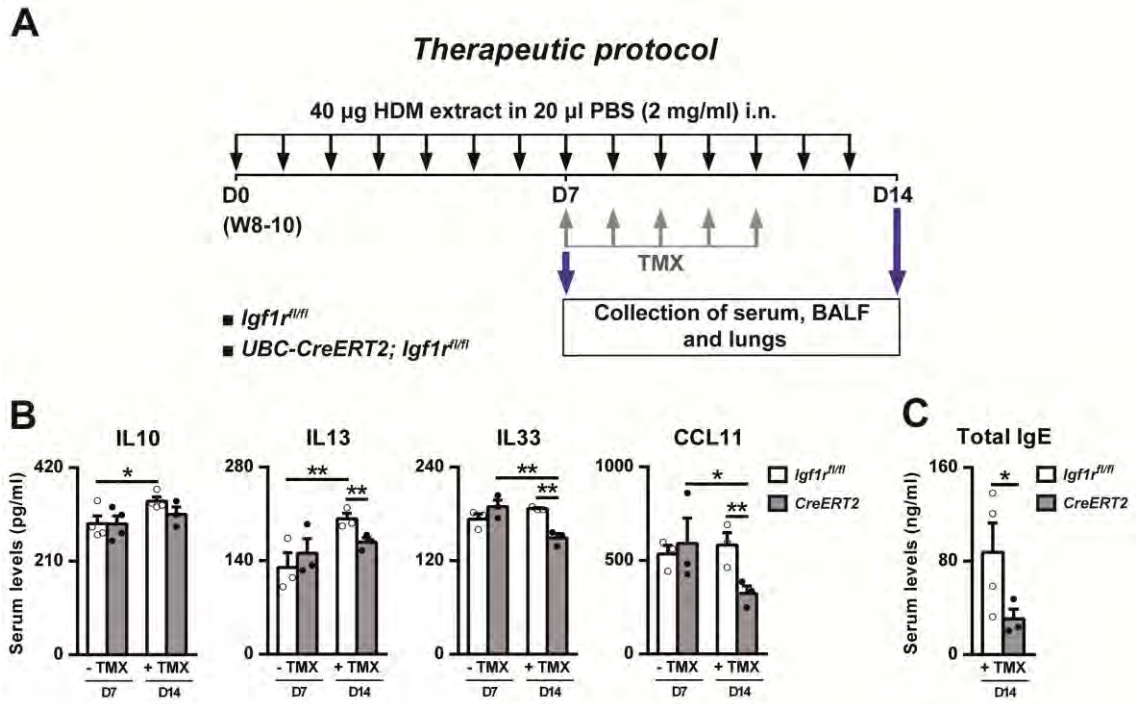


Figure 7

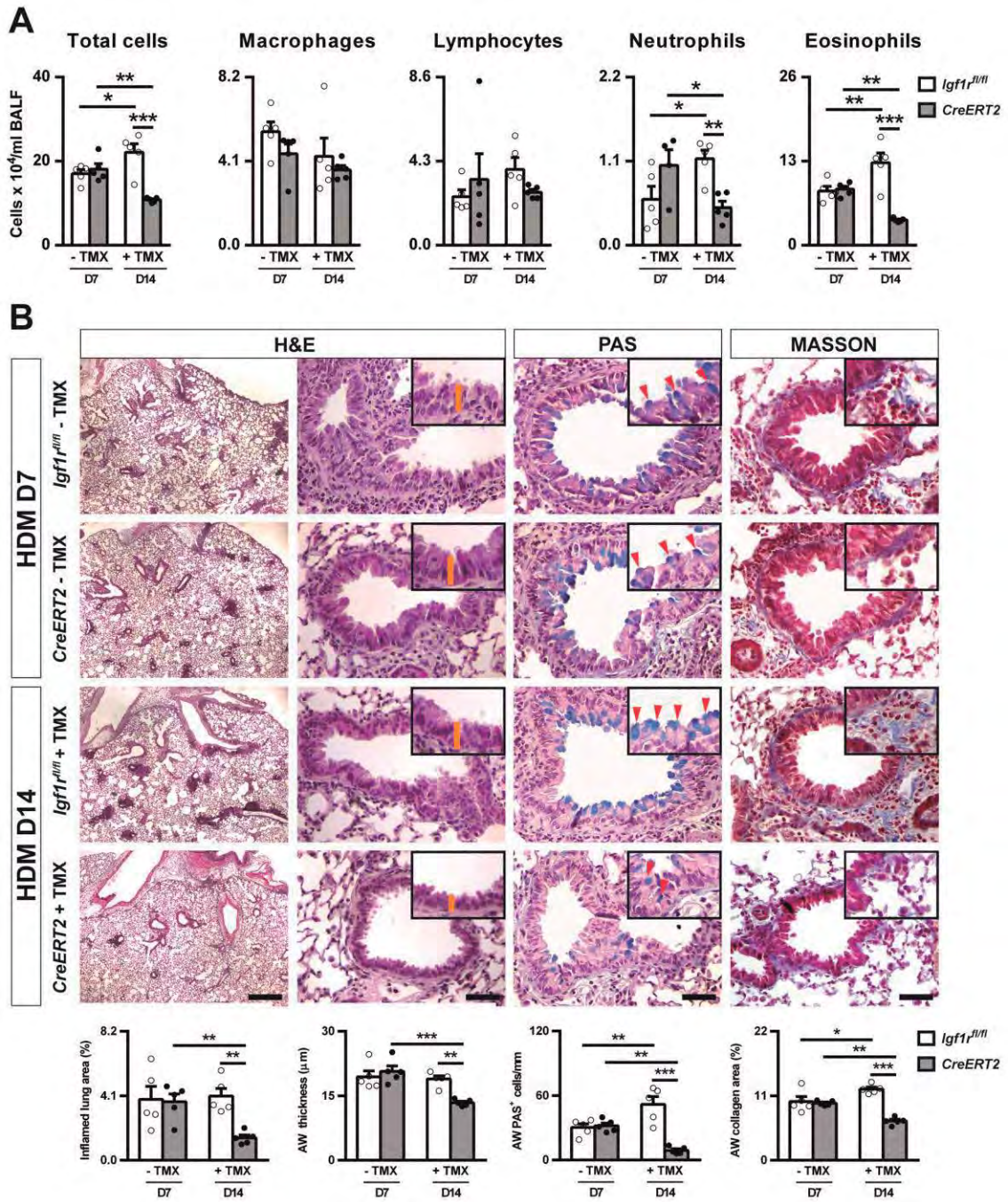


Figure 8

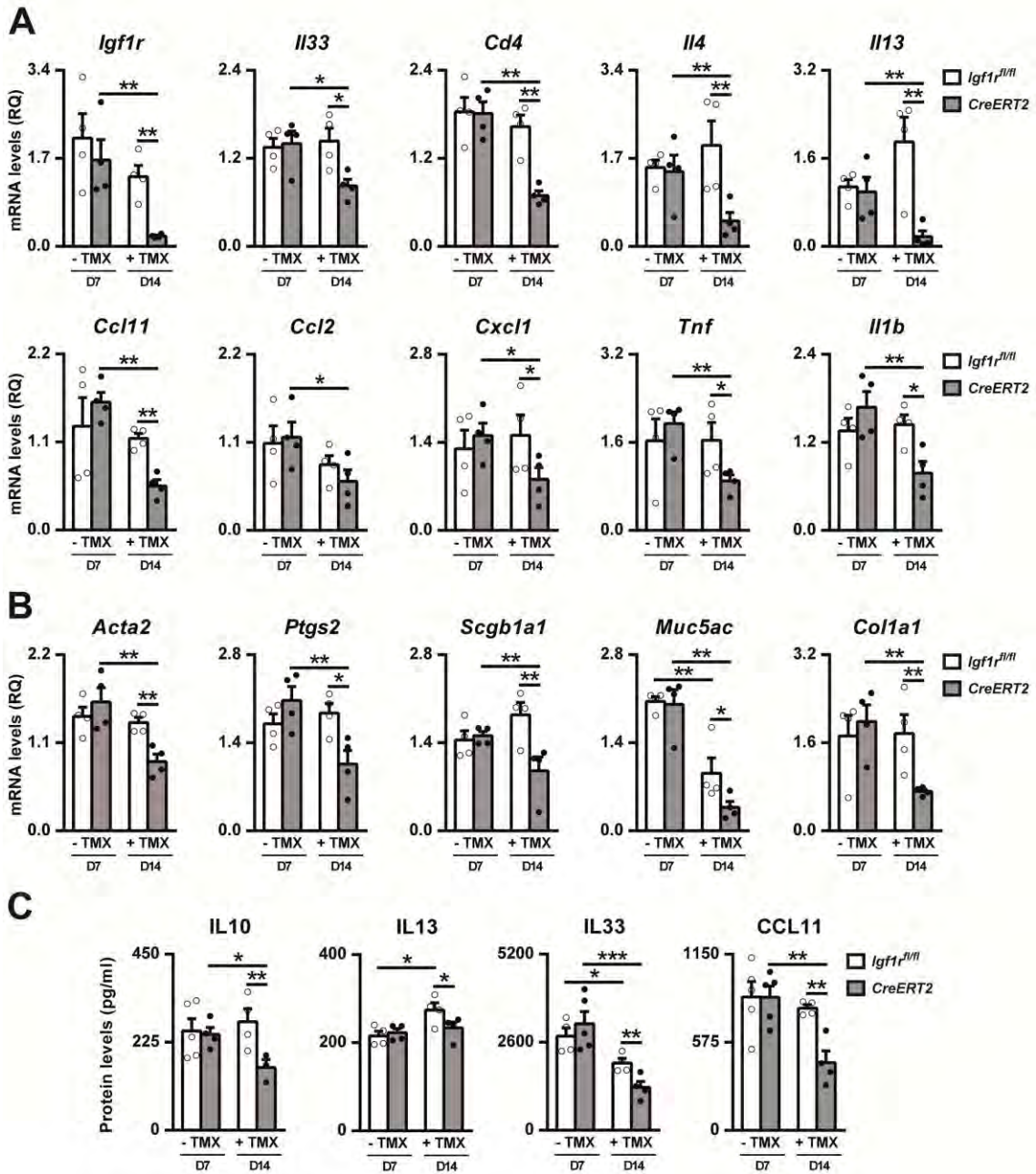


Figure 9

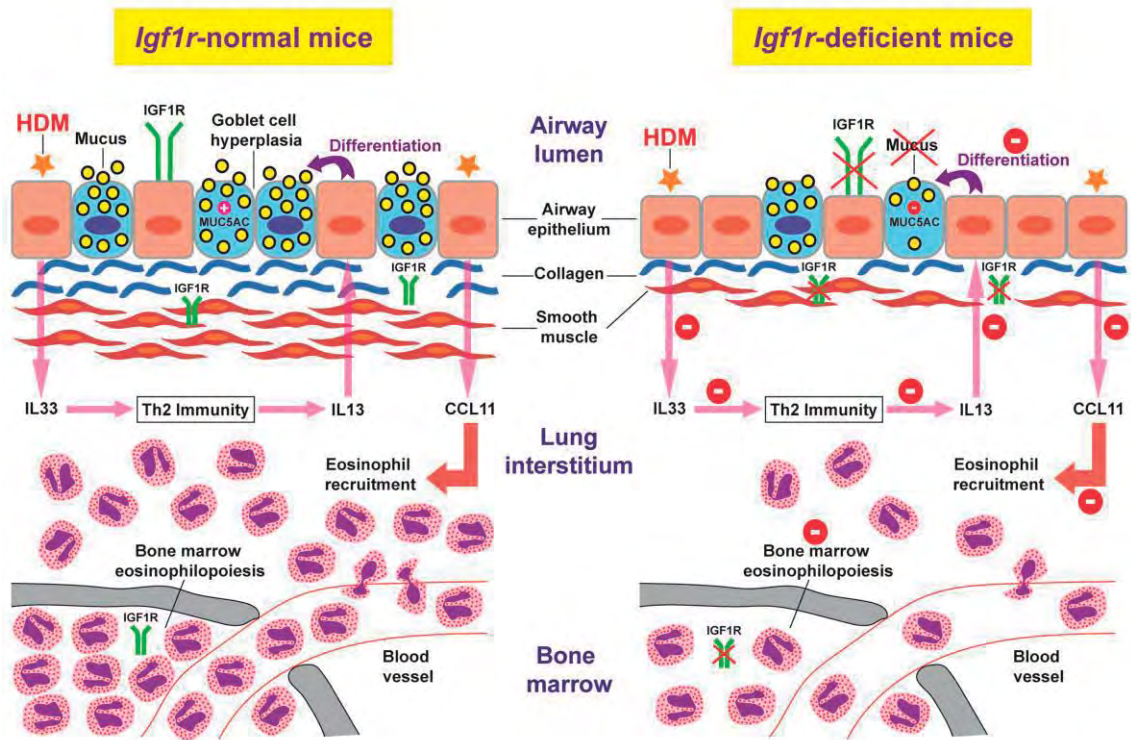


Figure 10

Supporting information for

Characterization of the acute inflammatory profile and resolution of airway inflammation after *Igflr*-gene targeting in a murine model of HDM-induced asthma

Sergio Piñeiro-Hermida¹, Elvira Alfaro-Arnedo¹, Joshua A. Gregory^{2#}, Raquel Torrens¹, Carlos Ruíz-Martínez³, Mikael Adner², Icíar P. López¹ and José G. Pichel^{1*}

¹Lung Cancer and Respiratory Diseases Unit, Centro de Investigación Biomédica de la Rioja (CIBIR), Fundación Rioja Salud, Logroño, Spain. ²Unit of Experimental Asthma and Allergy Research, Karolinska Institutet, Institute of Environmental Medicine (IMM), Stockholm, Sweden. ³Pneumology Service, Hospital San Pedro, Logroño, Spain.

[#]Current affiliation: Adlego Biomedical AB, Uppsala, Sweden.

*José G. Pichel, corresponding author.

Files included:

S1 Table. Primer sets used for qRT-PCR.

S1 Table. Primer sets used for qRT-PCR.

Gene	Accession No.	Forward primer (5'-3')	Reverse primer (5'-3')
<i>Acta2</i>	NM_007392.3	AATGGCTCTGGGCTCTGTAA	CTCTTGCTCTGGGCTTCATC
<i>Ccl2</i>	NM_011333.3	CACCAGCCAACTCTCACTGA	CGTAACTGCATCTGGCTGA
<i>Ccl5</i>	NM_013653.3	CCAACCCAGAGAAGAAGTGG	AGCAAGCAATGACAGGGAAG
<i>Ccl11</i>	NM_011330.3	GAGAGCCTACAGAGCCAGA	ACCGTGAGCAGCAGGAATAG
<i>Cd4</i>	NM_013488.2	ATGTGGAAGGCAGAGAAGGA	TGGGGTATCTTGAGGGTGAG
<i>Col1a1</i>	NM_007742.4	CGGAGAAGAAGGAAAACGAG	CAGGGAAACCACGGCTAC
<i>Cxcl1</i>	NM_008176.3	ATCCAGAGCTTGAAGGTGTG	GTCTGTCTTCTTCTCCGTTACTT
<i>Foxm1</i>	NM_008021.4	CCTGCTTACTGCCCTTTCCT	CACACCCATCTCCCTACACC
<i>Igfbp3</i>	NM_008343.2	GCCCTCTGCCTTCTTGATTT	TCACTCGGTTATGGGTTTCC
<i>Igfbp5</i>	NM_010518.2	GATGAGACAGGAATCCGAACAAG	AATCCT TTGCGGTACAGTTG
<i>Igf1</i>	NM_010512	CAGAAGCGATGGGGAAAAT	GTGAAGGTGAGCAAGCAGAG
<i>Igf1r</i>	NM_010513	ATGGCTTCGTTATCCACGAC	AATGGCGGATCTTCACGTAG
<i>Il1b</i>	NM_008361.3	GCAACTGTTTCTGAACTCAACT	ATCTTTTGGGGTCCGTCAACT
<i>Il4</i>	NM_021283.2	CCTCACAGCAACGAAGAACA	CGAAAAGCCCGAAAGAGTC
<i>Il5</i>	NM_010558.1	GAAGTGCTGGAGATGGAACC	GGATGAGGGGGAGGGAGTAT
<i>Il10</i>	NM_010548.2	GCACTACCAAAGCCACAAGG	TAAGAGCAGGCAGCATAGCA
<i>Il13</i>	NM_008355.3	GCCTCCCCGATACCAAAAAT	CTTCTCCTCAACCCTCCTC
<i>Il25</i>	NM_080729.3	AAGCCCTCCAAAGCCCTAC	TCTCCCAAGTCTCCATC
<i>Il33</i>	NM_133775.2	GCCTTGCTCTTTCCTTTTCTC	TCGGTTGTTTTCTGTTTTGTC
<i>Insr</i>	NM_010568.2	TCCTGAAGGAGCTGGAGGAGT	CTTTCGGGATGGCCTGG
<i>Muc5ac</i>	NM_010844.1	CACACACAACCACTCAACCA	TCTCTCTCCGCTCCTCTCAA
<i>Ptgs2</i>	NM_011198.4	GGAGGCGAAGTGGGTTTTA	TGATGGTGGCTGTTTTGGTA
<i>Rn18s</i>	NR_003278.3	ATGCTCTTAGCTGAGTGTCCTG	ATTCCTAGCTGCGGTATCCAGG
<i>Scgb1a1</i>	NM_011681	ATGAAGATCGCCATCACAATCAC	GGATGCCACATAACCAGACTCT
<i>Spdef</i>	NM_013891.4	GGCCAGCCATGAACTATGAT	GGTAGACAAGGCGCTGAGAG
<i>Tnf</i>	NM_013693.3	GCCTCTTCTATTCTGCTTG	CTGATGAGAGGGAGGCCATT
<i>Tslp</i>	NM_021367.2	AAATGGGAAATGAGCAATAGAC	GCAGGGGAGGTGAGAAAAGAC